

Development of Hydrophobic Inorganic-Organic hybrid Sol-gel Coatings on Aluminium using Nano- Particles

Submitted in partial fulfillment of the requirements

for the degree of

Doctor of Philosophy
of

Indian Institute of Technology, Bombay, India
and

Monash University, Australia
by

Ruchi Grover Wankhede

Supervised by

Prof. A. S. Khanna (IIT Bombay)
and

Prof. Nick Birbilis (Monash University)



*The course of study for this award was developed jointly by
the Indian Institute of Technology, Bombay and Monash University, Australia
and given academic recognition by each of them.*

*The programme was administered by the IITB-Monash Research Academy
(2013)*

DECLARATION

I declare that this written submission represents my ideas in my own words and where others' ideas or words have been included; I have adequately cited and referenced the original sources.

I also declare that I have adhered to all principles of academic honesty and integrity and have not misrepresented or fabricated or falsified any idea/data/fact/source in my submission. I understand that any violation of the above will be cause for disciplinary action by the Institute and can also evoke penal action from the sources which have thus not been properly cited or from whom proper permission has not been taken when needed.

Notice 1

Under the Copyright Act 1968, this thesis must be used only under the normal conditions of scholarly fair dealing. In particular no results or conclusions should be extracted from it, nor should it be copied or closely paraphrased in whole or in part without the written consent of the author. Proper written acknowledgement should be made for any assistance obtained from this thesis.

Notice 2

I certify that I have made all reasonable efforts to secure copyright permissions for third-party content included in this thesis and have not knowingly added copyright content to my work without the owner's permission.

(Ruchi Grover Wankhede)

Roll No. 10411404 (IIT Bombay)



Date:

Place: IIT Bombay, Mumbai

ACKNOWLEDGEMENTS

The work presented in this dissertation would not have been possible without the support of many people. Firstly, and most importantly, I would like to express my deep sense of gratitude to my PhD advisor Prof. A.S. Khanna for giving me the opportunity to study under his tutelage, for helping me to develop scientific skills and mindset of a scientist, and for opening my eyes to the vast and wonderful world of paints and coatings, both in academia and industry.

I wish to thank my advisor, Prof. Nick Birbillis, for giving me the opportunity to work in his lab in Monash University and offering invaluable assistance and guidance. His support, knowledge and encouragement made this research possible. I thank both of my guides for giving me abundant help and guidance in preparing paper work for publication during the course of my research work.

I would extend my sincere note of appreciation to my research committee members Prof. R.S. Raman and Prof. A.S. Panwar for helping me with any technical questions and editorial comments in reviewing my annual progress reports and providing valuable suggestions. I would also thank to IITB-Monash Research Academy for all the cooperative support throughout the tenure of my work.

I want to thank all of my colleagues Narayani, Garima, Swati, Vijay, Karan and Gunjan for providing help and support in their own way and providing a positive atmosphere that made it a pleasure to work every day.

But most of all I would like to thank my family, who without their support and encouragement throughout my life, I would not be where I am today. The unconditional love and support they have shown me is more important than anything else that has ever been given to me. I especially want to thank my parents, my husband Mr. Tushar Wankhede and my brother whose support is indispensable for the successful completion of my thesis.

At last but not least, would like to thank my little daughter Prisha for being sweet and cooperative during writing of this thesis.

ABSTRACT

Water-based inorganic-organic hybrid sol-gel coatings were developed on aluminium. The coatings were based upon epoxy-silane, glycidoxypyrtrimethoxysilane (GPTMS) and methyltrimethoxysilane (MTMS) as inorganic silane precursors crosslinked with the organic polymer, hexamethylmethoxymelamine (HMMM). The aim of the present work was to modify the hybrid sol-gel coating to obtain hydrophobic properties which could be achieved by either lowering the surface energy or increasing the surface roughness of the coatings. Lowering of surface energy was achieved by incorporating various fluoro-alkylsilanes (FASs) with two different chain lengths, of 3 and 17 fluorine atoms. The subsequent water contact angles achieved were 100° and 110° respectively for FAS modification. As a result, a commercial fluoro emulsion (FE) which was a water based six carbon atom perfluoro polymer, was employed as co-precursor. A substantial improvement in hydrophobicity was achieved with FE modification resulting in contact angle of 118° . Further, the surface roughness of the fluorinated sol-gel coating was enhanced by incorporating various nanoparticles with different size, surface area and surface chemistry, namely nano-Zinc Oxide (ZnO), hexadecyltrimethoxysilane (HDTMS) modified nano-silica, dichlorodimethylsilane (DDS) modified nano-silica and hexamethyldisilazane (HMDZ) modified nano-silica. Out of these HMDZ nano-silica modification resulted in maximum hydrophobicity with contact angle of 125° and sliding angle of 25° on aluminium surface. Furthermore an independent study was carried out on application of as developed composite coatings on chemically and mechanically roughened aluminium surfaces. It was found that contact angle increases up to 130° using techniques like chemical etching, plasma etching, sand blasting and grinding etc.

The as developed nano-composite coatings when applied on other non-metallic substrate such as glass, cotton, cardboard, paper, concrete and wood, it showed excellent hydrophobicity with a contact angle of $> 135^\circ$. Furthermore, all the substrates showed a sliding angle of about 15° .

The as developed coatings were characterised for their chemical and morphological structures, using techniques including FTIR, XPS, SEM and AFM. The wetting properties were analysed using contact angle goniometry. The performance of the as developed coatings

was evaluated by determining corrosion resistance, hardness, adhesion and scratch resistance properties.

Finally, the role of nano-particles distribution was studied in detail. It was found that maximum hydrophobic properties were achieved at optimum concentration of nano-particles.

TABLE OF CONTENTS

S.NO	PARTICULAR	Page no.
1	Chapter-1 Introduction	1
2	Chapter-2 Literature survey	7
2.1	Wettability and Contact Angle	7
2.2	Theoretical Background	8
2.2.1	Young's equation	8
2.2.2	Wenzel's equation	9
2.2.3	Cassie-Baxter Model	10
2.2.4	Contact angle hysteresis	11
2.2.5	Contact angle hysteresis	12
2.3	Various materials and fabrication procedures for developing water repellent hydrophobic coatings	13
2.3.1	Sol-gel Method	14
2.3.2	Hydrophobization	17
2.3.2.1	Hydrophobisation with fluorinated molecules	18
2.3.2.2	Hydrophobisation with alkyl molecules	22
2.3.3	Covalent layer-by-layer assembly	28
2.3.4	Polymer film roughening	30
2.4	Nano particles	31
2.4.4	Chemical vapor deposition	39
2.4.6	Hydrothermal synthesis	40
2.5	Common Industrial methods of introducing surface roughness	41
2.5.1	Texturing via stamp process	41
2.5.2	Structuring via sandblasting	42
2.5.3	Structuring via grinding	43
2.5.4	Chemical Etching	44
2.5.5	Chemical treatment of Aluminum using commercial Boehmite Powder	45
3	Chapter-3 Experimental Work	52
3.1	Materials and Reagents	53
3.2	Synthesis of Fluorine-based hydrophobic inorganic-organic sol-gel coatings	54
3.2.1	Synthesis of Neat Sol-gel	54
3.2.2	Synthesis of fluoro-alkylsilanes (FAS) modified sol-gel coatings	55
3.2.3	Synthesis of commercial Fluoro emulsion (FE) modified hydrophobic sol-gel coating	56
3.2.4	Incorporation of other commercial fluoro-additives	57
3.3	Synthesis of Nano-particles incorporated sol-gel coatings	57
3.3.1	Incorporation of Nano-ZnO (size 20-30nm) to optimised 30wt% FE modified sol-gel coating	58
3.3.2	Incorporation of various hydrophobically modified nano-silica to optimised 30wt% FE modified sol-gel coating	59
3.3.3	Synthesis of HDTMS Modified Fumed Silica particles.	60
3.4	Synthesis of Non-fluoro sol-gel coatings	61
3.5	Characterisation of as developed hydrophobic sol-gel coatings	62

3.5.1	Wettability of the coatings	62
3.5.2	Structural analysis of various modified sol-gel coatings	64
3.5.3	Surface Morphology of various modified sol-gel coatings	64
3.5.4	Corrosion resistance of various modified sol-gel coatings	65
3.5.5	Mechanical Properties of various modified sol-gel coatings	65
3.6	Characterisation of various nano-particles	66
3.7	Accelerated Life time tests for finally formulated hydrophobic sol-gel coating	66
4	Chapter 4- Result and discussions	67
4.1	Characterisation of GPTMS-MTMS-HMMM based neat sol-gel coating	67
4.1.1	Structural analysis of neat sol-gel coating	67
4.1.2	Wettability of neat sol-gel coating	68
4.1.3	Morphological Analysis of neat sol-gel coating	69
4.1.4	Corrosion resistance of neat sol gel	70
4.2	Characterisation of 3, 3-Trifluoropropyl-trimethoxysilane (3-FAS) incorporated sol-gel coatings	72
4.2.1	Wetting properties of 3-FAS modified sol-gel coatings	72
4.2.2	Morphological Analysis of 3-FAS modified sol-gel coatings	73
4.2.3	Structural Analysis	75
4.2.4	Corrosion resistance of 3-FAS modified sol-gel coatings	77
4.2.5	Mechanical Properties of various 3-FAS modified sol-gel coatings	79
4.3	Characterisation of 1H,1H,2H,2H perfluorodecyl-trimethoxysilane (17-FAS) modified sol-gel coatings	81
4.3.1	Contact Angle Measurements	81
4.3.2	Morphological characterisation of 17-FAS modified sol-gel coatings	82
4.3.3	Structural analysis of 17-FAS modified sol-gel coatings	85
4.3.4	Corrosion resistance analysis of 17-FAS modified sol-gel coatings	85
4.3.5	Mechanical characterisation of 17-FAS modified sol-gel coatings	88
4.4	Characterisation of commercial fluoro-emulsion (FE) modified sol-gel coating system	90
4.4.1	Wetting properties of FE modified sol-gel coatings	90
4.4.2	Morphological analysis of FE modified sol-gel coatings	91
4.4.3	Structural Analysis of FE-modified sol-gel coatings	95
4.4.4	Corrosion resistance of FE modified sol-gel coatings	97
4.4.5	Mechanical properties of FE modified sol-gel coatings	100
4.5	Comparative results of various fluoro modified sol-gel systems	101
4.6	Characterisation of nano-ZnO modified FE sol-gel coatings	108
4.6.1	TEM and BET analysis of nano-ZnO particles	108
4.6.2	Wetting properties of nano-ZnO modified FE sol-gel coatings	109
4.6.3	Morphological characterisation of nano-ZnO modified sol-gel coatings	111
4.6.4	Structural analysis of nano-ZnO modified sol-gel coatings	117
4.6.5	Corrosion resistance of nano-ZnO modified sol-gel coatings	118
4.6.6	Mechanical properties of nano-ZnO modified sol-gel coatings	120
4.7	Characterisation of HDTMS modified- fume silica sol-gel coatings	122
4.7.1	TEM and BET Analysis	122
4.7.2	Contact Angle and Sliding Angle Analysis	123
4.7.3	Morphological analysis of HDTMS modified FE-sol gel coatings	124

4.7.4	Structural Analysis of HDTMS-nanosilica modified sol-gel coatings	129
4.7.5	Corrosion resistance of HDTMS-nano-silica modified sol-gel coatings	130
4.7.6	Mechanical properties of HDTMS nano-silica modified sol-gel coatings	132
4.8	Characterisation of DDS nano- silica (Aerosil R-972) modified sol-gel coatings	134
4.8.1	TEM and BET surface area analysis	134
4.8.2	Wetting properties of DDS nano-silica modified sol-gel coatings	135
4.8.3	Morphological analysis of DDS nano-silica modified sol-gel coatings	137
4.8.4	Structural analysis of DDS modified sol-gel coatings	142
4.8.5	Corrosion resistance of DDS nano-silica modified sol-gel coatings	142
4.8.6	Mechanical Properties of DDS nano-silica modified Sol-gel coatings	145
4.9	Characterisation of HMDZ nano- silica (Aerosil R8200) modified Sol-gel coatings	147
4.9.1	TEM and BET surface area analysis of HMDZ nano-particles	147
4.9.2	Wetting properties of various HMDZ nano-silica modified sol-gel coatings	148
4.9.3	Morphological analysis of HMDZ nano-silica modified sol-gel coatings	150
4.9.4	Structural Analysis of HMDZ modified sol-gel coated samples	155
4.9.5	Corrosion resistance of HMDZ nano-silica modified sol-gel coatings	156
4.9.6	Mechanical Properties of HMDZ nano-silica modified sol-gel coatings	158
4.10	Comparative experimental results of all nano-particle incorporated sol-gel coatings	160
4.11	Accelerated lifetime study of HMDZ-FE composite nano-sol gel coatings	171
4.11.1	Self Life	171
4.11.2	Gel Time or Pot life	171
4.11.3	Salt Spray Exposure	171
4.11.4	U.V. exposure	173
4.11.5	Humidity exposure	175
4.11.6	Mechanical Strength	176
4.12	Effect of various surface roughness methods	176
4.12.1	Effect of Chemical Etching	176
4.12.2	Effect of Mechanical Roughening	177
4.12.3	Effect of Plasma etching	177
4.12.4	Effect of spraying	178
4.13	Effect of as developed hydrophobic coating on various non-metallic porous substrates	180
4.14	Characterisation of non-fluoro sol-gel coatings	183
4.14.1	Wetting properties of non-fluoro sol-gel coatings	183
4.14.2	Morphological analysis of non-fluoro sol-gel coatings	186
5	Chapter-5 General Discussion	191

List of figures

S.NO	PARTICULARS	Page no.
1.1	Superhydrophobic lotus leaf and water droplet on the leaf (inset). (B) Low magnification scanning electron microscope (SEM) image of the surface structures on the lotus leaf. (C) High-resolution SEM (HRSEM) image of a single papilla consisting of cilium-like nanostructures	1
1.2	Some typical cases in natural (lotus leaf, mosquito eye, rose petal, spider silks, butterfly wings, gecko feet, desert beetle and water strider and their potential applications	2
1.3	Chemical structure of a typical functional Organosilanes	4
1.4	Schematic for preparation of OIH coating based on metal alkoxide through sol-gel process	4
1.5	Sol-gel reactions	5
2.1	Surface wetting types	8
2.2	A water droplet on a smooth surface	9
2.3	A drop of liquid in the Wenzel state	9
2.4	A drop of liquid in Cassie state	10
2.5	(a) Contact angle hysteresis on a tilted surface, and (b) schematic illustration of advancing and receding contact angles on a flat surface via increasing and decreasing the volume of droplet, respectively	11
2.6	Sliding angle between substrate and a liquid droplet	12
2.7	A flowchart explaining the summary of various materials and fabrication procedures for developing hydrophobic coatings	14
2.8	SEM image of multiscale roughness structure obtained on cotton fabric at (a) low magnification and (b) high magnification	16
2.9	Examples of surface reactive molecules for low-surface-energy modification : (a) long alkyl chain with R1 groups; (b) long alkyl chain organic silanes with R2 groups; (c) long alkyl chain fluorinated silanes with R3 groups, in which R1 can be –SH, –OH, –COOH, –NH ₂ , etc, and R2 and R3 can be –Cl, –OCH ₃ , –OCH ₂ CH ₃ ; the length of these chains can be varied from C8 to C18; and (d) polymers based on polydimethylsiloxane, which can be bis-end-capped or mono-end-capped, where R4 is usually a 3-aminopropyl or glycidyl ether group	18
2.10	Reaction between metal substrate and hydrolysed FOTMS	19
2.11	Liquids on fluorinated silica nanoparticles film (a) 5 μ l water, (b) 5 μ l diiodomethane optical images of liquids, (c) water, (d) diiodomethane	20
2.12	Preparation of the fluorinated silica nanoparticles	20
2.13	variation of contact angle and contact angle hysteresis with UV exposure time	21
2.14	(A) SEM images of fluorinated silica nanoparticles of 119 ± 12 nm diameter deposited on aluminium substrates in three layers by spin coating; Inset of Figure 2 (A) shows the image of a water drop placed on this surface exhibiting a very high water contact angle of $\sim 152^\circ$, and (B) higher magnification image of (A)	22
2.15	Schematic representation of: (a) silanisation process of alkyltrichlorosilane molecules on a substrate covered with an oxide layer and formation of an	23

	alkylsiloxane monolayer and (b) well oriented (or close-packed) SAM molecules, pore, collapsed molecules and lying down monomers	
2.16	Proposed mechanism of the superhydrophobic surface formed by TEOS/MTES sol-gel derived coating	24
2.17	SEM image of the HDTMS modified film at low magnification and (b)high magnification	25
2.18	Formation of a Superhydrophobic Surface on Cotton Based on Silica Sol and HDTMS	26
2.19	Contact angles of glass substrates coated with SiO ₂ -sols with alkyltrialkoxysilanes of increasing chain lengths	27
2.20	a) SEM image, b) AFM image of 5% TMCS in hexane coated solgel glass panel	28
2.21	Steps used in the covalent layer-by-layer assembly of functional particles, with C groups and A groups on a substrate activated with A groups, for superhydrophobic surfaces. B groups are formed by the reactions of A groups with C groups	29
2.22	Preparation of superhydrophobic films based on covalent assembly yielding raspberry-like particles (reprinted with permission from)	30
2.23	SEM images of (a) porous membrane produced by solvent casting of polypropylene solution using methylethylketone as the nonsolvent; (b) superhydrophobic poly(vinyl chloride) film obtained by coating with a mixture ethanol and H ₂ O as the nonsolvent	31
2.24	Nano- particle-polymer composite coating for superhydrophobic surfaces	31
2.25	FESEM micrographs of (a) the unmodified silica nanoparticles with diameters of 167 nm and the vinyl-modified silica nanoparticles with different diameters: (b) 85 nm, (c) 167 nm, (d) 360 nm	33
2.26	SEM images of stearic acid-SiO ₂ coating: (a) low magnification, (b) High magnification; Stearic acid-CaCO ₃ coating (c) low magnification, (d) high magnification	36
2.27	Roughness profiles of the (a) sol–gel blank coating; (b) nano- composite coating with 16.58% fumed silica	37
2.28	Potentiodynamic polarisation behavior of the specimens coated with the sol-gel containing various wt% CeO ₂ nano-particles compared with the bare A2024-T3 alloy	38
2.29	Surface appearance of the coated specimens with different CeO ₂ nanoparticles contents after salt spray testing for 330 h: (a) without nanoparticles; (b) 7 wt. % CeO ₂ ; (c)14 wt. % CeO ₂ ; (d) 20 wt. % CeO ₂	38
2.30	Variation of contact angle with concentration of nano-silica particles in TEOS and MTEOS sol-gel coatings	39
2.31	Water droplets on the surface of a modified colored cotton fabric (a) and 3D atomic force microscopy image of the modified fiber surface (b)	40
2.32	Fabrication of superhydrophobic surfaces by hydrothermal growth of nanostructured surface and hydrophobization	41
2.33	Texturing by Stamp Process	42
2.34	SEM micrograph (left) and contact angle image of water (right) on becks etched aluminium specimen followed by surface fluorination	44
2.35	superhydrophobic surfaces on s copper alloy having water CA of 161° after	45

	etching	
2.36	Water contact angle on the surfaces plotted against the boehmite-ethanol ratio	46
2.37	Process for removing carbon black powder on the super-hydrophobic surface by water droplets: (a) carbon black spreading on the surface, (b) a droplet rolling through the surface, (c) all carbon black being removed by water droplets and (d) carbon black covering water droplet	47
2.38	Water droplets rolling off substrates with a normal hydrophobic surface (left) and a self-cleaning superhydrophobic surface (right) through dust particles	48
3.1	Work Schedule	53
3.2	Schematic of steps involved in preparation of fluorinated sol-gel coatings	55
3.3	Nano-ZnO powder (size 20-30nm) used in present work	58
3.4	Image of a) HDTMS nano-silica, b) DDS nano-silica and c) HMDZ nano-silica	59
3.5	Schematic formation of HDTMS modified hydrophobic nanosilica	61
3.6	Schematic diagram of (a) contact angle goniometer and (b) Movable platform for measuring SA	63
4.1	FTIR spectra of neat sol-gel coating	68
4.2	contact angle image of neat-sol gel coated Al substrate	69
4.3	a) SEM image and b) AFM image of neat sol-gel	70
4.4	Tafel plots of neat sol-gel, etched and unetched Al substrate	71
4.5	EIS plot of neat sol-gel, etched and unetched Al substrate.	72
4.6	Variation of contact angle with different concentrations of 3-FAS	73
4.7	SEM images of a) Neat, b) 1wt%, c) 2wt%, d) 3wt% and e) 5wt% of 3-F.A.S. modified sol-gel coated aluminium samples	74
4.8	AFM images of a) 0wt%, b) 1wt%, c) 2wt%, d) 3wt% and e) 5wt% of 3-F.S modified sol-gel coated aluminium samples	75
4.9	AFM images of a) 0wt%, b) 1wt%, c) 2wt%, d) 3wt% and e) 5wt% of 3-F.S modified sol-gel coated aluminium samples	76
4.10	Tafel plots of bare Al (etched), neat sol-gel and various 3-FAS modified sol-gel coated Al samples	78
4.11	Impedance plots of etched Al, neat sol and various 3-FAS modified sol-gel coated samples at initial period of immersion	79
4.12	Nano-indentation curve of neat and 2wt% 3FAS modified sol-gel coating	80
4.13	Variation of contact angle with different concentrations of 17-F.S.	82

4.14	The SEM images of various weight% of 17-F.A.S.coatings over aluminium substrate (a) Neat Sol-gel , (b) 0.5wt % (c) 0.75wt% (d) 2wt% (e) 3 wt%	83
4.15	AFM images of a) Neat Sol, b) 0.5wt% 17-FAS, c) 0.75wt% 17-FAS, d) 1wt% FAS and e)5wt% 17-FAS modified sol-gel coatings over Al surface.	84
4.16	FTIR spectra of neat and 17-FAS modified sol-gel coatings	85
4.17	Polarisation curves for neat and various 17-FAS modified sol-gel coated Al samples.	86
4.18	Bode plots of bare Al (etched), neat and various 17-FAS modified sol-gel coatings	88
4.19	Nano-indentation curves of neat and 17-FAS modified sol-gel coating	89
4.20	Variation of contact angle with different concentrations of FE	91
4.21	Scanning Electron Micrographs of Aluminium substrate coated with (a) Neat sol-gel, (b) 10 wt%, (c) 20 wt %, d) 30 wt % and (e) 50 wt % FE modified sol-gel coating	92
4.22	FEGSEM cross-sectional image of coating thickness of FE modified sol-gel coating	93
4.23	(ai) 2-D (bi) section profiles and (ci) 3-D AFM images of neat, 10, 20, 30 and 50wt% FE modified sol-gel coatings on aluminium substrate	94
4.24	FTIR plots of neat sol and 30wt% FE modified sol-gel coated aluminium samples	96
4.25	XPS plots of neat and various FE modified sol-gel coatings	97
4.26	Tafel plots of bare Al, neat and various FE modified sol-gel coatings	99
4.27	Bode plots of bare Al, neat sol and various wt % of FE modified sol-gel coatings	99
4.28	Nano-indentation of neat and FE modified sol-gel coating	100
4.29	XPS analysis of 3-FAS, 17FAS and FE modified sol-gel coating	102
4.30	SEM images of a)a') 3FAS, b)b')17-FAS and c)c')FE modified optimised sol-gel coatings at lower and higher magnifications respectively	103
4.31	AFM images of a) 3-FAS, b) 17-FAS and c) FE modified sol-gel coatings at optimum concentrations	104
4.32	Comparative Tafel plots of neat, 3-FAS, 17FAS and FE modified sol-gel coatings at optimised concentrations	105
4.33	Comparative bode plots of neat, 3-FAS, 17FAS and FE modified sol-gel coatings at optimised concentrations	106
4.34	Comparative nano-indentation curves of neat, 3-FAS, 17FAS and FE modified sol-gel coatings	107
4.35	TEM image of nano-ZnO particles	109
4.36	Variation of contact angle with concentration of nano-ZnO	110
4.37	Variation of sliding angle with concentration of nano-ZnO	110
4.38	SEM images of aluminium substrate coated with (a) 1wt % (b) 2wt % (c) 3 wt % and (d) 5 wt % nano-ZnO modified sol-gel coatings	112

4.39	EDX plots of 2wt % nano- ZnO modified sol- gel coating at point 1, 2 and 3	113
4.40	X-ray mapping at 2wt % nano- ZnO modified sol-gel coating	113
4.41	AFM images of (ai) 2D height and (bi) section profile of 1wt%, 2wt%, 3wt% and 5wt% nano-ZnO modified sol-gel coatings	115
4.42	AFM images of (ci) magnitude and (di) 3-Dimentional height of 1wt%, 2wt%, 3wt% and 5wt% nano-ZnO modified sol-gel coatings respectively	116
4.43	FTIR spectra of 2 wt % nano -ZnO modified sol gel coated sample	117
4.44	Potentiodynamic polarisation curves of bare Al and various wt % of nano- ZnO modified sol-gel coated samples	119
4.45	Bode plots of bare Al and various nano-ZnO modified sol-gel coatings	120
4.46	Load displacement curve of neat and nano-ZnO modified sol-gel coatings	121
4.47	TEM image of HDTMS modified nano-silica particles	122
4.48	Variation of contact angle with concentration of HDTMS nano-silica particles	123
4.49	Variation of sliding angle with concentration of HDTMS nano-silica concentration	124
4.50	SEM images of a) 0.5wt%, b) 1wt%, c) 3wt% and d)5wt% HDTMS nano-silica modified sol-gel coatings	125
4.51	AFM images of (ai) 2D height and (bi) section profile of 1wt%, 2wt% and 3wt% HDTMS nano-silica modified sol-gel coatings	127
4.52	AFM images of (ci) magnitude and (di) 3-Dimentional height of 1wt%, 2wt%, and 3wt% HDTMS nano-silica modified sol-gel coatings respectively	128
4.53	FTIR spectra of neat and HDTMS nano-silica modified sol-gel coating	129
4.56	Tafel plots of etched Al and various HDTMS-nano-silica modified sol-gel coated Al samples	130
4.57	Bode plots of bare Al and various HDTMS nano-silica modified sol-gel coatings	132
4.58	Nano-indentation curve of neat and 1wt% HDTMS nano-silica modified soll-gel coated sample	133
4.59	TEM image of DDS nano-silica particles	135
4.60	Variation of contact angle with concentration of DDS modified nano-silica particles	136
4.61	Variation of sliding angle with concentration of DDS nano-silica particles	137
4.62	SEM images of a) wt%, b) 2wt%, c) 3wt% and d) 5wt% DDS nano-silica modified sol-gel coated samples	138
4.63	AFM images of (ai) 2D height and (bi) section profile of 2wt%, 3wt% and 5wt% HD DDS nano-silica modified sol-gel coatings	140
4.64	AFM images of (ci) magnitude and (di) 3-Dimentional height of 2wt%, 3wt%, and 5wt% DDS nano-silica modified sol-gel coatings respectively	141
4.65	FTIR spectra of neat and DDS nano-silica modified sol-gel coating	142
4.66	Tafel plots of bare Al and various DDS nano-silica modified sol-gel coated samples	144
4.67	EIS plots of bare Al and various DDS nano-silica modified sol-gel coatings	145
4.68	Nano-indentation curve of neat and 2wt% DDS nano-silica modified sol-gel coating	146

4.69	TEM image of HMDZ nano-silica particles	147
4.70	Variation of contact angle with concentration of HMDZ nano-silica particles	149
4.71	Variation of sliding angle with concentration of HMDZ nano-silica particles	149
4.72	SEM images a) 2wt%, b) 3wt%, c) 5wt% and d) 10wt% of HMDZ nano-silica modified sol-gel coated samples	151
4.73	AFM images of (ai) 2D height and (bi) section profile of 1wt%, 2wt%, 3wt% and 5wt% HMDZ nano-silica modified sol-gel coatings	153
4.74	AFM images of (ci) magnitude and (di) 3-Dimensional height of 1wt%, 2wt%, 3wt% and 5wt% HMDZ nano-silica modified sol-gel coatings respectively	154
4.75	FTIR spectra of various HMDZ nano-silica modified sol-gel coated samples	155
4.76	Tafel plots of bare Al and various HMDZ nano-silica modified sol-gel coated samples.	157
4.77	EIS plots of bare Al and various HMDZ nano-silica modified sol-gel coated samples.	158
4.78	Nano indentation curves of neat and 3wt% HMDZ nano-silica modified sol-gel coating	159
4.79	The condensation reaction between (a) HDTMS and fume silica silanol group on the silica surface, (b) DDS and fume silica silanol group on the silica surface and (c) HMDZ and fume silica silanol group on the silica surface.	162
4.80	Comparative SEM images of a) neat sol, b) FE modified sol, c) nano-ZnO sol, d) HDTMS nano-silica modified sol, e) DDS nano-silica modified sol and f) HMDZ nano-silica modified sol	164
4.81	Comparative 2D AFM images of various sol-gel systems	165
4.82	Comparative 3D AFM images of various sol-gel systems	166
4.83	Comparative Tafel plots of various sol-gel systems	167
4.84	Comparative bode plots of various sol-gel systems	168
4.85	Comparative nano-indentation curves of various sol-gel systems	169
4.86	Comparative coating strength of various sol-gel systems	170
4.87	Variation of contact angle of HMDZ-FE composite coating upon salt spray exposure	172
4.89	Image of unexposed and salt spray exposed HMDZ-FE composite sol-gel coated Al panels	173
4.90	Image of unexposed and UV exposed HMDZ-FE composite sol-gel coated Al panels	174
4.91	Variation of contact angle of HMDZ-FE composite sol gel coated Al substrate upon UV exposure	174
4.92	Variation of a) change in color (ΔE) and (b) change in gloss (ΔG) after modification with nano-ZnO and HMDZ nano-silica particles	175
4.93	Contact angle image on hydrophobically coated a) glass, b) cardboard, c) wood, d) paper, f) concrete, g) epoxy coated surface and e) polyurethane coated surface	181
4.94	Variation of contact angle of different non-fluoro formulations coated aluminium samples etched with various reagents	185
4.95	a) SEM image, b) EDAX Spectra and c) AFM image of flat aluminium	186

	substrate coated with sol-gel formulation having GPTMS: HDTMS: TEOS ratio 2:2:6	
4.96	SEM images of specimens coated with sol-gel formulation having GPTMS:HDTMS:TEOS ratio of 2:2:6 after a) Krolles etching at magnification of 1000X and b) 5000 X , c) 10% NaOH etching at magnification of 1000X d) 5000 X and e)Becks etching at magnification of 1000X and(f)5000X	187
4.97	FE-SEM image of thickness of Sol gel coated (GPTMS: HDTMS: TEOS ratio 2:2:6) becks reagent etched aluminium sample	188
4.98	AFM images and RMS values of aluminium samples etched with a),d) Krolls reagent, b),e) 10% NaOH and c),d) Becks reagent followed by coating with sol-gel formulation having GPTMS:HDTMS:TEOS ratio 2:2:6 and ratio 1:3:6 respectively	189
5.1	Probable reaction mechanism of as developed hydrophobic sol-gel coating	192
5.2	The shape of a liquid droplet resting on a surface (yellow) is governed by the balance between liquid cohesion (red arrows) and interfacial adhesion (grey arrows)	193
5.3	The contact angle of a droplet at the triple phase contact point (red dot)	194
5.4	A droplet can occupy less geometric area on a surface with with increased roughness	194
5.5	A water droplet resting on a composite interface resulting in increased contact angle due to the presence of entrapped air	195
5.6	Surface morphology and nano-particle distribution of various sol-gel systems	196
5.7	Transition between various mixed states on a rough surface	198
5.8	Distribution of nano-particles at a) low concentration, b) high concentration and c) fluoro-composite nano-coating at optimised concentration	199
5.9	EDX analysis of HMDZ-FE composite coating at planner and bumpy surface	201
5.10	Proposed anti-corrosion mechanism of HMDZ-FE nano-composite sol-gel coating	202
5.11	Probable mechanism of reaction of GPTMS, TEOS and HDTMS	203

LIST OF TABLES

S.NO	PARTICULARS	Page no.
2.1	Corrosion resistance and Mechanical properties for various inorganic-organic systems	15
2.2	Various Electrochemical parameters for different concentrations of nano-Fe ₂ O ₃	34
2.3	Result of treated and coated samples with different sand blasting procedures	43
2.4	Result of treated and coated samples with different sand papers	43
3.1	Chemical Composition (wt %) of aluminium alloy used in present study	54
3.2	Composition of various concentrations of 3-FAS and 17FAS modified sol-gel	56
3.3	Physical properties of FE-2000 fluoro emulsion additive	56
3.4	Composition of various FE-modified sol-gel coatings	57
3.5	List of various commercial fluoro additives	57
3.6	Composition of various nano-particle modified sol-gel coatings	60
3.7	Specifications of DDS, HMDZ and HDTMS nano-silica particles	60
3.8	Various formulations of HDTMS, GPTMS and TEOS based sol-gel coatings	62
4.1	Potentiodynamic and EIS parameters of bare Al and neat sol-gel coating	70
4.2	Polarisation and EIS parameters of various 3-FAS modified sol-gel coatings	77
4.3	Crosshatch adhesion and pencil hardness results of various concentrations of 3-F.A.S. modified sol-gel coatings	80
4.4	Polarisation and EIS parameters of various FAS-17 modified sol-gel coatings	87
4.5	Crosshatch adhesion and pencil hardness results of various concentrations of 17-FAS modified sol-gel coatings	89
4.6	Effect of concentration of FE on contact angle and roughness of the sol-gel coatings	95
4.7	Polarisation and EIS parameters of various FE modified sol-gel coatings	98
4.8	Cross-hatch adhesion and pencil hardness results of various FE modified sol-gel coatings	101
4.9	Particle size BET surface area and Surface chemistry of nano-ZnO particles	108
4.10	Variation of surface roughness with nano-ZnO concentration	114
4.11	FTIR data corresponding to types of bands appearing in neat and nano-ZnO modified sol-gel coating	118
4.12	Polarisation and EIS parameters of various ZnO modified sol-gel coatings	119
4.13	Crosshatch adhesion and pencil hardness results of various wt % of nano - ZnO modified sol-gel coatings	121
4.14	Physical parameters of HDTMS nano-silica	122
4.15	RMS values of various HDTMS-nanosilica modified sol-gel coatings	128
4.16	Polarisation and EIS parameters of HDTMS-nano-silica modified sol-gel coatings	132
4.17	Cross-hatch adhesion and pencil hardness of HDTMS-nano-silica modified sol-gel coatings	134
4.18	Particle size and surface area of DDS nano-silica particle	135
4.19	Variation of surface roughness with concentration of DDS nano-silica	139

	particle	
4.20	Polarisation and EIS parameters of DDS modified sol-gel coatings	143
4.21	Crosshatch adhesion and pencil hardness results of DDS nano-silica modified sol-gel coatings	146
4.22	particle size and BET surface area of various nano-particles	147
4.23	Variation of surface roughness with concentration of HMDZ nano-silica particles	152
4.24	Polarisation and EIS parameters of HDMZ nano-silica modified sol-gel coatings	157
4.25	Pencil hardness and crosshatch adhesion results of various HMDZ modified sol-gel coated samples	159
	compiles the results of contact angle and sliding angle of various nano sol-gel systems	
4.25	Comparative particle size and surface area	163
4.26	Comparative SEM parameters of various nano-modified sol-gel coatings	163
4.27	Comparative RMS of various nano-modified sol-gel coatings	165
4.28	Comparative corrosion resistance results of various sol-gel systems	167
4.29	Comparative mechanical properties of various sol-gel systems	169
4.30	Effect of various surface roughness methods prior to hydrophobic sol-gel coating	179
4.31	Contact angle values on various non-metallic substrates	180
4.31	Gel-time and contact angle of various sols coated on un-etched aluminium substrate	183
4.32	Water contact angle of various formulations of non-fluoro sol-gel coatings developed on differentially etched aluminium specimens	184
4.33	Variation of sliding angle with different kind of etching on aluminium after coating with various hydrophobic sol-gel formulations	185

List of Abbreviations

MTMS	Methyl Trimethoxy silane
GPTMS	Glycidoxy Propyl Trimethoxy silane
TEOS	Tetra Ethyl Ortho Silicate
HMMM	Hexa Methyl Methoxy Melamine
pTSA	Pera Toluene Sulphuric Acid
3-FAS	3,3-Trifluoropropyl-trimethoxysilane
17-FAS	1H,1H,2H,2H perfluorodecyl-trimethoxysilane
FE	Fluoro Emulsion
HDTMS	Hexadecyl Trimethoxy Silane
DDS	Dichlorodimethylsilane
HMDZ	Hexamethyldisilazane
CA	Contact Angle
SA	Sliding Angle
FTIR	Fourier Transform Infrared Spectroscopy
XPS	X-ray Photon Spectroscopy
SEM	Scanning Electron Microscopy
AFM	Atomic Force Microscopy
EIS	Electrostatic Impedance Spectroscopy
UV	Ultra Violet
RMS	Root Mean Square
ASTM	American Standard Test Method
TEM	Transmission Electron Microscopy
EDAX	Energy Dispersive X-ray Analysis

Chapter 1

Introduction

Hydrophobic and water-repellent surfaces are desirable for various industrial applications such as reduction of ice and snow adhesion, surface self-cleaning, stain resistant textiles, corrosion prevention and anti-biofouling surfaces [1]. Such a surface can be achieved by a combination of low surface energy and micro- and/or nano-structured features, which can certainly reduce the contact area between the surface and the water droplet. The water droplets hence do not wet the surface and easily roll off to remove dirt and debris [2]. The best known example of a hydrophobic self-cleaning surface is the leaves of lotus plant (*Nelumbo nucifera*). Studies of lotus leaves by scanning electron microscopy (SEM), as shown in Fig. 1.1 revealed that the key features of the lotus leaf are a microscopically rough surface consisting of an array of randomly distributed micro papillae with diameters ranging from 5 to 10 μm . These micro papillae are covered with waxy hierarchical structures in the form of branch-like nanostructures with average diameter of about 125 nm. The water contact angle on a lotus leaf is higher than 160° with a rolling angle of about 2° , which would be considered a high performance superhydrophobic self-cleaning surface.

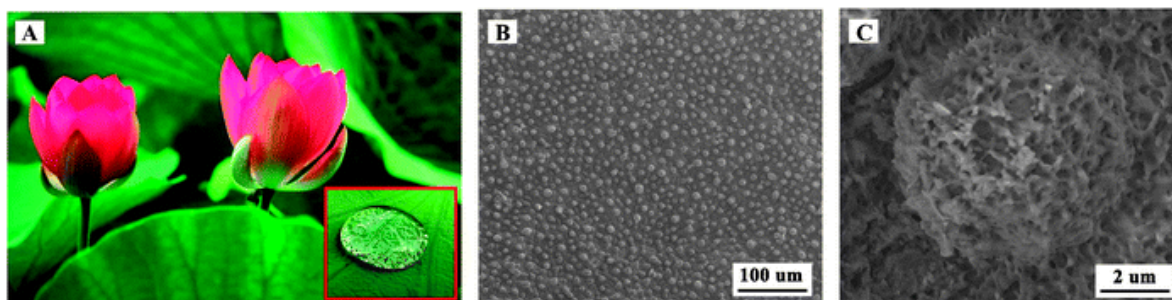


Figure 1.1: Superhydrophobic lotus leaf and water droplet on the leaf (inset). (B) Low magnification scanning electron microscope (SEM) image of the surface structures on the lotus leaf. (C) High-resolution SEM (HRSEM) image of a single papilla consisting of cilium-like nanostructures [3]

The other examples from nature in the area of hydrophobicity observed are mosquito eye, rose petal, spider silks, butterfly wings, gecko feet, desert beetle and water strider (Fig 1.2). The corresponding bio-inspired superhydrophobic surfaces have special wettability and solid-liquid adhesion that can be related to various potential applications like self-cleaning, drag reduction, anti-icing, water oil separation and friction reduction [4].



Figure 1.2: Some typical cases in natural (lotus leaf, mosquito eye, rose petal, spider silks, butterfly wings, gecko feet, desert beetle and water strider and their potential applications [4]

The ability of the hydrophobic surfaces to make water bead off completely and thereby wash off contamination very effectively, has been termed the “Lotus effect”. The lotus effect is based on the physical principle according to which low surface energy and micro-roughness reduces the surface area coming in to contact with water [5]. Inspired by “lotus-leaf effect”, lots of techniques have been developed to create water-repellent surfaces that mimic that of lotus-leaf. Majority of these approaches start by creating the roughness on the surface, by means like chemical etching, plasma patterning, electrochemical etching, template method,

vapor deposition and sol-gel method and ends up with deposition of low surface energy materials on rough surfaces [5-9]. It is well known that the maximum contact angle that can be attained on a flat surface by lowering the surface energy does not exceed 120° . However, the addition of roughness to the surface can increase the contact angle of water without altering the surface chemistry [10]. The commonly used reactive molecules for low surface-energy modification are mainly long alkyl chain thiols, alkyl or fluorinated organic silanes, per-fluorinated alkyl agents, long alkyl chain fatty acids, polydimethylsiloxane-based polymers or other polymers, or their combinations [11]. Moreover, surface roughness can be enhanced by introducing nano-particles such as nano-ZnO, nano-TiO₂, nano-SiO₂ and nano-ZrO₂. However, most of the fluoro-chemicals used for hydrophobisation are non-biodegradable, expensive and potentially harmful to human health and the environment, which limits their potential applications [12]. Therefore, developing a simple, non-toxic approach to obtain an industrially feasible hydrophobic surface is important and necessary [13, 14]. The present study investigates both fluoro and non-fluoro approaches of developing water based hydrophobic inorganic-organic hybrid coatings on aluminium via sol-gel route with incorporation of different nano-particles.

Inorganic-organic hybrid coatings combine the best properties of organic coatings (flexibility, low density and toughness) and inorganic coatings (surface hardness, high modulus, thermal stability and low coefficient of thermal expansion). Such coatings have been recognized as barrier coatings to obtain low permeation which lead to better protection of underlying substrate from environmental degradations [15]. It is interesting to know that the commercial applications of inorganic-organic hybrids, at present, are in the field of protective coatings of metallic and non-metallic substrates such as iron, steel, aluminium, magnesium, copper, plastic, glass, wood, fabric and concrete. The sol-gel reaction makes possible to incorporate the organic polymer entity in the network matrix of inorganic materials. The high homogeneity of the hybrid suggests that the organic polymer segments and inorganic one are blended at the nano-meter level. The organic polymer nano-hybrids can thus be considered not only as the combination of organic polymer and inorganic materials, but as quite new material. Silanes are hybrid molecules containing functional organic groups, such methoxy or ethoxy groups, on inorganic silicon atoms. Some silane types also contain other types of functional groups, such as chloride, amine, sulphur or epoxy. The latter silane types are so-called organosilanes (Fig 1.3) where the additional functional group promotes adhesion with

overlaying organic films such as paints coatings. The ethoxy or methoxy groups are hydrolysed when adding water to the system, and the resulting silanol groups –Si-OH can react with metal hydroxide groups on the substrate surface, thus forming a –Si-O-M covalent bonded metal/film interface.

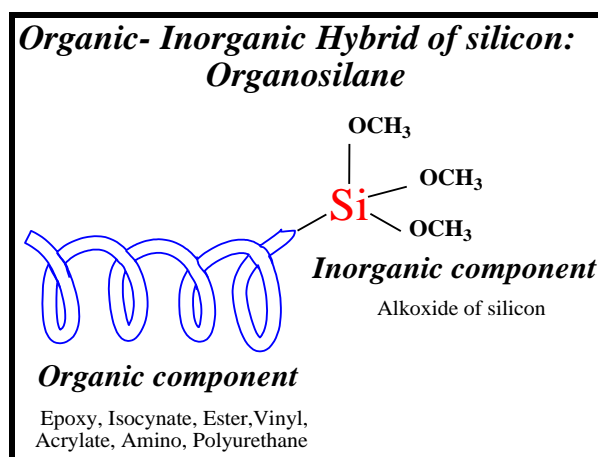


Figure 1.3: Chemical structure of a typical functional Organosilanes [14]

The sol-gel method, as is shown in Fig 1.4, is made of the elemental reactions of hydrolysis of silicate followed by condensation reaction of silanol group, and resulting in three-dimensionally cross-linked silica gel matrix with Si-O-Si bonds as the unit of repetition. By incorporating an organic polymer simultaneously in this sol-gel reaction, it is possible to synthesize an inorganic-organic hybrid polymer [14].

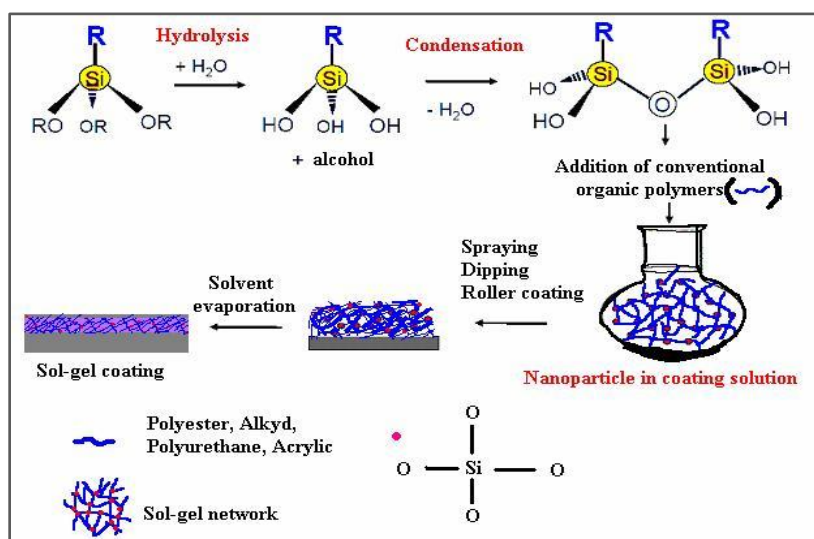


Figure 1.4: Schematic for preparation of OIH coating based on metal alkoxide through sol-gel process [14]

Sol-gel process [1-2] takes place in a two-step acid or base catalysed reaction, starting with a metal alkoxide in acidic or basic medium (Fig. 1.5).

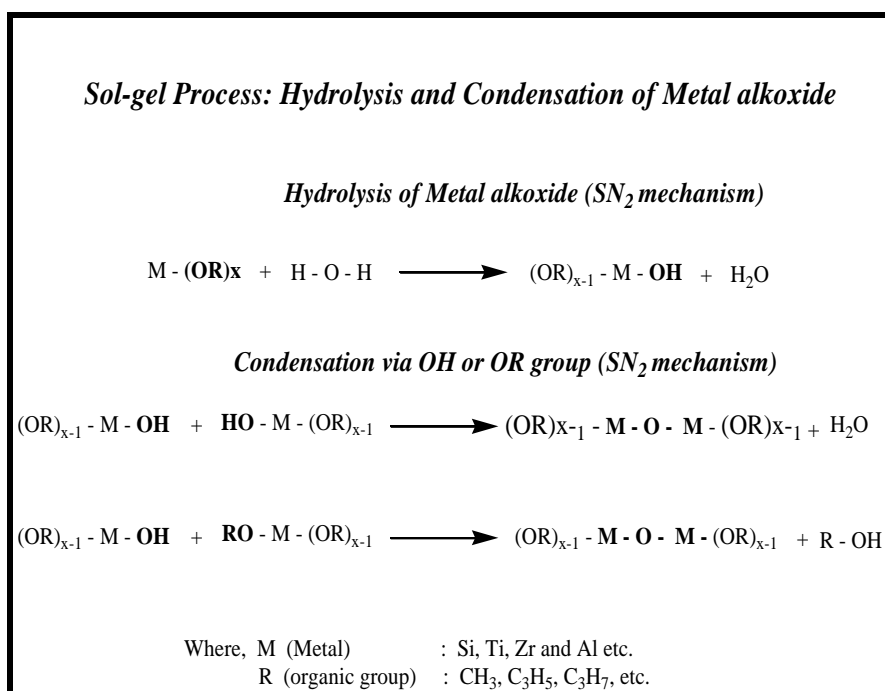


Figure 1.5: Sol-gel reactions [14]

Further these species undergo a stepwise hydrolysis and poly-condensation reactions involving both hydroxyl and alkoxy groups with the formation of a metal oxide three-dimensional network. Silicon alkoxide, commonly known as silane, is frequently used in preparation of corrosion resistant coatings for ferrous and non-ferrous alloys (iron, steel, aluminium, galvanized steel, magnesium), adhesion promoters and corrosion inhibitors in conventional organic coatings. Silanes hydrolyze in a water/alcohol mixture and form silanol groups (Si-OH) which are adsorbed on the metal surface and form metallosiloxane (M-O-Si) bonds. Formation of metallosiloxane and hydrophobic nature of the film make silane suitable for corrosion resistance. Also, due to the hybrid character, they possess high optical transparency, superior weathering resistance, excellent abrasion and impact resistance, low

surface energy and better adhesive properties than the traditional organic and inorganic coating [14].

Deposition of sol-gel film on the substrate requires curing of the silane layer which results in crosslinking and branching and formation of dense inorganic-organic hybrid sol-gel network which restricts the access of corrosive electrolyte to the underlying metal and hence forming an effective barrier, against corrosive attack. Organosilanes are also relatively environmentally friendly. Coatings can be applied by simple deposition techniques such as dipping, spinning or spraying.

Present work aims at development of hybrid sol-gel coatings using various organo-silanes crosslinked with organic polymers. Hydrophobic properties were achieved by introducing low energy fluoro-alkyl groups of various chain lengths to the coating backbone and incorporating various nano-particles resulting in enhanced surface roughness.

Chapter 2

Literature Survey

2.1 Wettability and Contact Angle

A surface is said to be wetted if a liquid spreads over the surface evenly without the formation of droplets. When the liquid is water and it spreads over the surface without the formation of droplets, the surface is said to be hydrophilic. In terms of energetics, this implies that the forces associated with the interaction of water with the surface are greater than the cohesive forces associated with bulk liquid water [16]. Water droplets form on hydrophobic surface, implying that cohesive forces associated with bulk water are greater than the forces associated with the interaction of water with the surface (Fig 2.1).

Practically, hydrophobicity and hydrophilicity are relative terms. If the contact angle of water is less than 90° , the surface is designated as hydrophilic since the forces of interaction between water and the surface nearly equal the cohesive forces of bulk water, and water does not cleanly drain from the surface. If water spreads over a surface, and the contact angle at the spreading front edge of the water is less than 10° , the surface is often designated as super-hydrophilic provided that the surface is not absorbing the water, dissolving in the water or reacting with the water. Surfaces with contact angles greater than 90° are designated as hydrophobic. The theoretical maximum contact angle that can be achieved for water on a smooth surface is 120° . Micro-textured or micro-patterned surfaces with hydrophobic

asperities can exhibit apparent contact angles exceeding 150° and are associated with superhydrophobicity and the “lotus effect” [16].

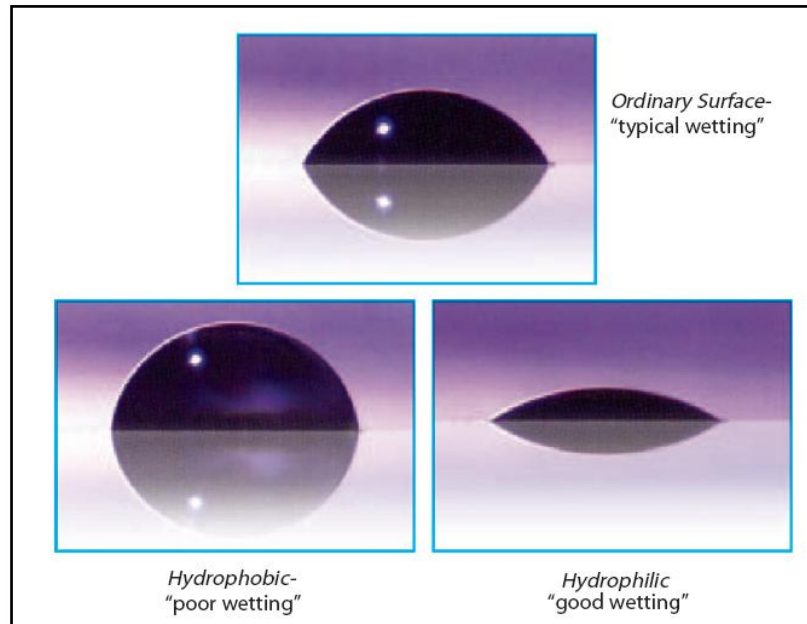


Figure 2.1: Surface wetting types [16]

2.2 Theoretical Background:

The principles of super hydrophobicity were first outlined by Wenzel in 1936 and then by Cassie and Baxter in 1944. Both models put emphasis on the geometrical structure of solid surfaces as an important factor in determining the wettability. Following are the proposed theories on superhydrophobicity.

2.2.1 Young’s equation

When a drop is deposited onto a solid surface, it forms a so-called contact angle. The contact angle of a liquid on a perfectly smooth and chemically homogeneous solid surface is given by Young’s equation (Fig 1.2) [17].

$$\cos \theta = \frac{\gamma_{SV} - \gamma_{SL}}{\gamma_{LV}} \quad (2.1)$$

Where γ_{SV} , γ_{SL} and γ_{LV} are the interfacial tensions of the solid-vapor, solid-liquid and the liquid-vapor interface respectively. Wetting of realistic surfaces which are rough and chemically heterogeneous is more complex. The earliest work on the effect of surface roughness on contact angle was done by Wenzel [18] and Cassie & Baxter [19] many years ago.

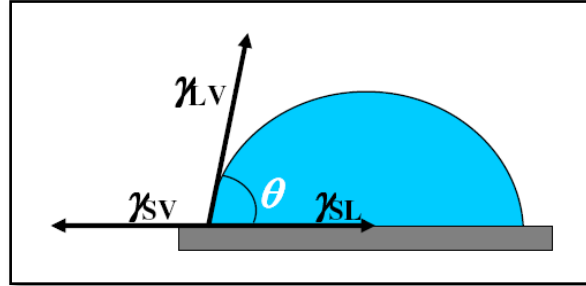


Figure 2.2: A water droplet on a smooth surface [18]

2.2.2 Wenzel's equation

Wenzel developed a model where the liquid may completely penetrate into the roughness grooves (fig 2.3), and the contact angle on rough surfaces is given by the following equation [18]

$$\cos \theta_w = r \cos \theta \quad (2.2)$$

In this equation, θ_w is the contact angle on a rough surface, θ is the Young's contact angle on a similar smooth surface, and r is the surface roughness factor, defined as the ratio between the actual and projected surface area ($r = 1$ for a perfectly smooth surface, and $r > 1$ for a rough one). The Wenzel equation predicts that wetting is enhanced by roughnesses, when θ is $< 90^\circ$; and lessened by roughness, when θ is $> 90^\circ$

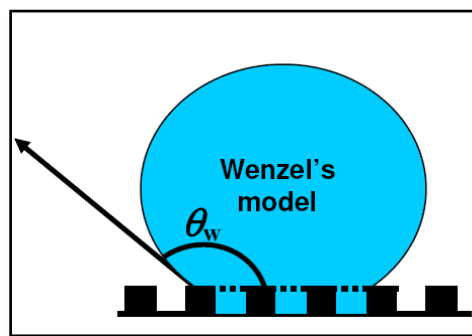


Figure 2.3: A drop of liquid in the Wenzel state

However when $\theta > 90^\circ$, under some roughness condition, air bubbles may be trapped in the rough grooves. In this case, the drop is actually situated on a composite surface, and the wetting behavior is described by Cassie & Baxter [19].

2.2.3 Cassie-Baxter Model

The Cassie-Baxter state [19], also known as the composite or heterogeneous state, is a wetting state unlike Wenzel's state, which considers that the grooves under the droplet are filled with vapor instead of liquid, as schematically shown in Fig 2.4. In this case, the liquid-surface interface is actually an interface consisting of two phases, namely a liquid-solid interface and a liquid-vapor interface. And the apparent contact angle is the sum of all the contributions of the different phases as described below:

$$\cos \theta_c = f_1 \cos \theta_1 + f_2 \cos \theta_2 \quad (2.3)$$

Where θ_c is the apparent contact angle, f_1 and f_2 are the surface fractions of phase 1 and phase 2, respectively; θ_1 and θ_2 are the contact angles on phase 1 and phase 2, respectively. This equation is the general form, which also applies when there is no roughness. When one of these surfaces is the air-liquid interface, f is the solid fraction, defined as the fraction of the solid surface that is wetted by the liquid. Then the air fraction is $(1-f)$. With $\theta = 180^\circ$ for air, the resulting contact angle can be calculated by the following equation:

$$\cos \theta_c = f \cos \theta + (1-f) \cos 180 = f \cos \theta + f - 1 \quad (2.4)$$

The parameter f ranges from 0 to 1, where at $f = 0$ the droplet does not touch the surface at all and at $f = 1$ the surface is completely wetted, similar to behavior of a flat surface.

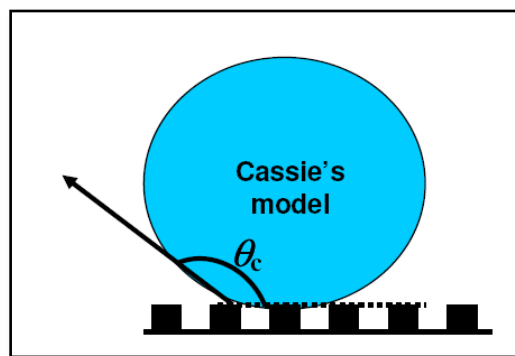


Figure 2.4: A drop of liquid in Cassie state [3]

When a droplet is in the Cassie state, the small contact area between the droplet and solid surface allows the droplet to roll easily over the surface.

2.2.4 Contact angle hysteresis

The contact angle we mentioned above is the static contact angle, which defines the energetically most favorable state of a droplet on a solid surface. However, different contact angles can coexist along the contact line due to chemical heterogeneity, surface roughness or surface recognition upon its contact with a probe liquid [20]. A small droplet of water can remain immobile on a tilted surface; the water contact angle at the back of the droplet is smaller than that at the front of the droplet, as shown in Fig 2.5.

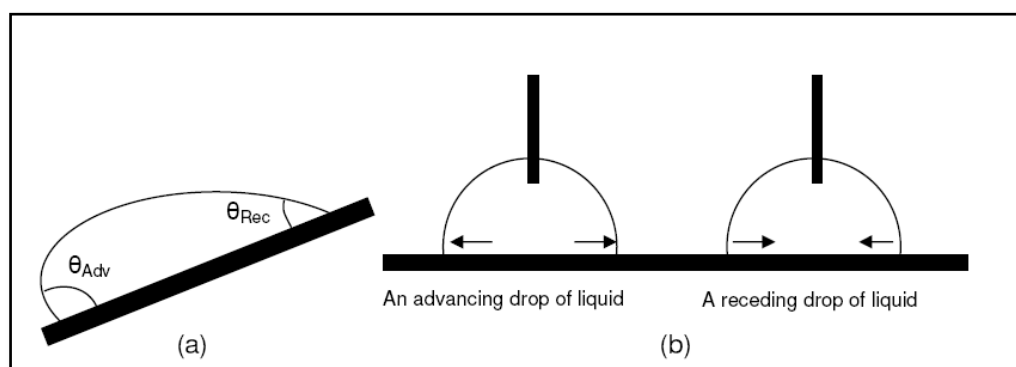


Figure 2.5: (a) Contact angle hysteresis on a titled surface, and (b) schematic illustration of advancing and receding contact angles on a flat surface via increasing and decreasing the volume of droplet, respectively [20]

The two different contact angles can also be observed when more water is added to and withdrawn from the droplet. When water is added into a water droplet, the contact angle will increase until the contact line starts to move forward; this contact angle is called advancing contact angle. On the other hand, when water is withdrawn from a water droplet, the contact angle will decrease until the contact line starts to recede; this contact angle is called receding contact angle (Fig 2.5 b). The difference between advancing and receding contact angles is defined as the contact angle hysteresis. The contact angle hysteresis is a measure for how well a drop of liquid sticks to the surface. It is therefore important that a self-cleaning surface has a low contact angle hysteresis.

Most researchers relate hydrophobicity to a high contact angle. However, the contact angle is not the only parameter that defines liquid-solid interactions. An additional parameter, the

sliding angle, related to the adhesion between the liquid drop and the solid surface is also important in cases where liquid sliding is involved, such as self-cleaning applications. In this work, it is postulated that wetting which is related to the contact angle, and interfacial adhesion, which is related to the sliding angle, are interdependent phenomena and have to be considered simultaneously. A variety of models that relate the sliding angle to forces developed along the contact line between a liquid drop and a solid surface have been proposed in the literature [21].

2.2.5 Sliding angle is defined as the critical angle at which a drop of certain weight spontaneously starts to slide down an inclined surface. It is commonly employed as a criterion for assessing the dynamic hydrophobicity of a solid surface. Fig 2.6 shows a typical sliding angle between the hydrophobic substrate and liquid droplet.

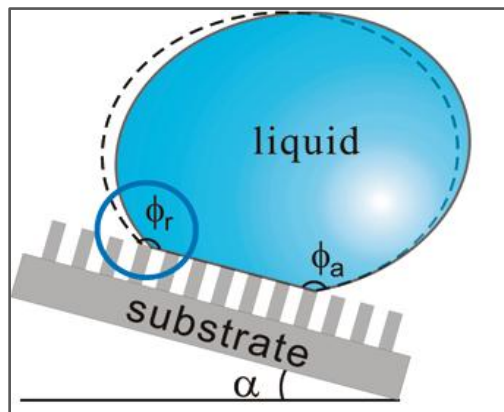


Figure 2.6: Sliding angle between substrate and a liquid droplet [21]

Wolfram et al. [21] have proposed an empirical equation describing the sliding angle of droplets on smooth surfaces of various materials.

$$\sin \alpha = k \frac{2r\pi}{mg}$$

Where R is the sliding angle, r is the radius of the contact circle, m is the weight of the droplet, g is the gravitational acceleration, and k is proportionality constant. Hence, while the contact angle of water has been commonly used as a criterion for the evaluation of

hydrophobicity of the surface, this alone is insufficient for the evaluation of the sliding properties of water droplets on surfaces. A surface with a high contact angle does not always show a low sliding angle, which is defined as the critical angle where a water droplet with a certain weight begins to slide down the inclined plate. For example, *Murase et al.* demonstrated that a fluoro-polymer with a water contact angle of 117° showed a higher sliding angle than a poly- (dimethylsiloxane) with a water contact angle of 102° . They have proposed that this phenomenon was due to a negative excess entropy caused by the rigidity of fluoropolymer segments and the enhancement of an ice- like molecular arrangement in water. Therefore, when we discuss hydrophobicity, the sliding property of water droplets should be evaluated separately from the contact angle [22].

2.3 Various materials and fabrication procedures for developing water repellent hydrophobic coatings

In order to create a hydrophobic surface, two requirements must be met. First, the surface should have low surface energy (in other words, it should be initially hydrophobic). Second, the surface should be roughened. Surface roughness has a complicated effect on wetting. It increases the surface area so that the same solid-liquid contact area can be achieved for a liquid drop sitting on a rough solid surface with a higher CA than on a smooth surface. More importantly, roughness combined with hydrophobicity often results in air pockets being trapped between the solid and liquid (the composite solid-liquid-air interface), leading to a significant decrease in the solid-liquid adhesion and an increase of the CA [18].

Many techniques to roughen the surfaces have been published in literature, including anodic oxidation, plasma treatment, chemical vapor deposition, spraying, colloidal sediment, and so on. The other aspect to improve water- repellency of a solid surface is to modify the surfaces with chemical groups that exhibit low surface free energy. Surface energy for some commonly used groups has an order $-\text{CF}_3 < -\text{CF}_2 < -\text{CH}_3 < -\text{CH}_2$, indicating that use of fluorinated compounds is beneficial for the enhancement of water- repellency. To date, some groups showed that the surfaces can be obtained by coating trifluoromethyl ($-\text{CF}_3$) groups on them [23-27]. With the scope, artificial water-repellency can be achieved by modifying a rough surface by chemical composition with a low surface free energy and roughening the

surface using various physical and chemical etching methods and incorporation of nano-particles. Fig 2.7 shows a flowchart explaining the summary of various methods and materials for developing hydrophobic coatings out of which sol-gel process is mainly focused to develop the same.

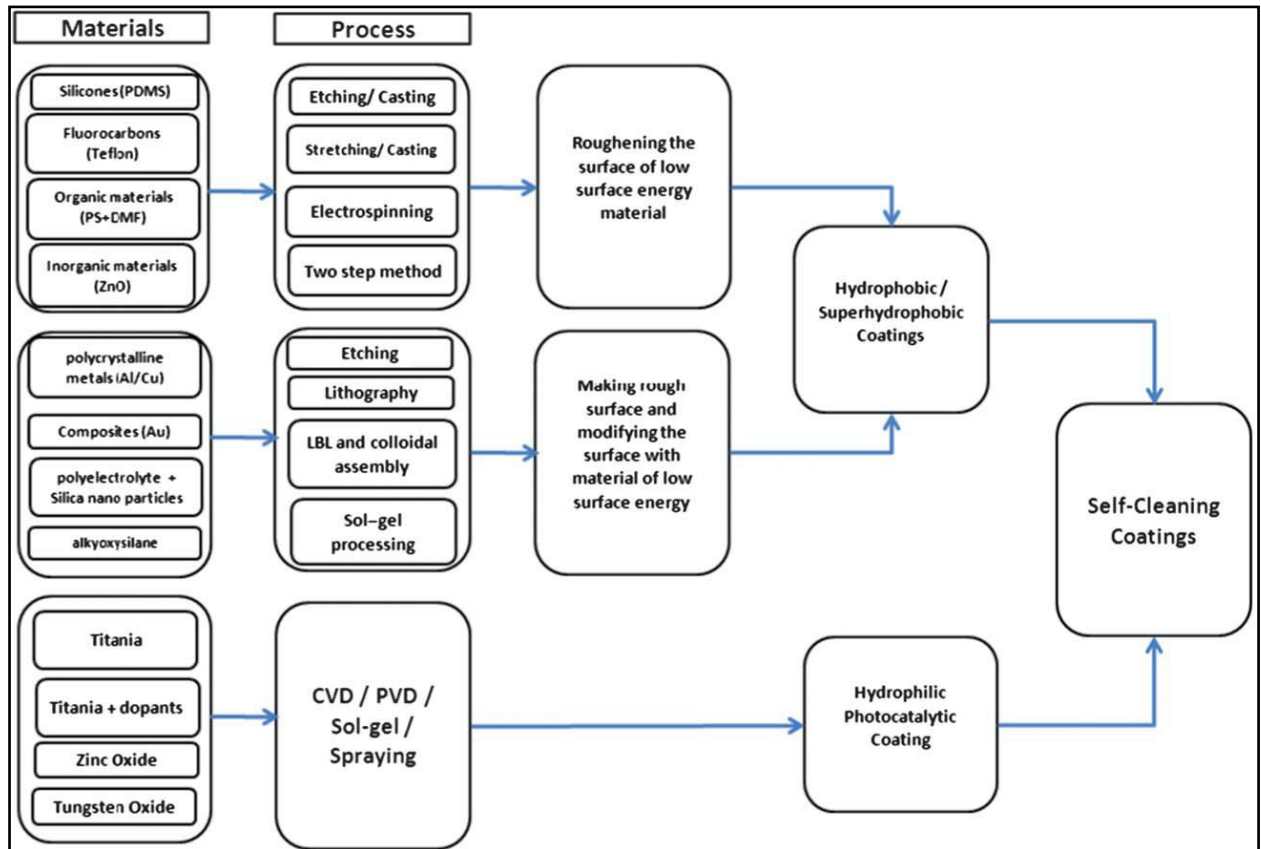


Figure 2.7: A flowchart explaining the summary of various materials and fabrication procedures for developing hydrophobic coatings. [28]

2.3.1 Sol-gel Method:

Surface modification with hydrophobic properties using the sol-gel method has been investigated during recent years. This has been particularly true for the preparation of hybrid inorganic-organic nano-composite materials. Although simple sol-gel reactions usually result in the formation of amorphous materials, self-organisation of organosilanes molecules offers an opportunity to create ordered hybrid materials with hydrophobic properties [29].

Pathak et al. [30] developed various inorganic-organic hybrid coating systems using different organic polymers like melamine resin (HMMM), polyester, amines, polyurethanes and alkyds. They developed waterborne ormosil coating systems, based on Hexamethoxymethylmelamine (HMMM) as a crosslinking agent by sol-gel process for aluminium alloy. Coatings were found uniform, continuous and crack free. Electrochemical experiments and immersion test confirmed that the ormosil coatings, acted as an efficient barrier to corrosive electrolytes (such as water, oxygen and chlorides) and reduced corrosion current by one order of magnitude compared to the bare aluminium alloy. However, highest corrosion resistance and hydrophobicity was found for 20–30 wt% HMMM crosslinked coatings. Further, the coatings were found stable up to 300°C and their pencil hardness was above 6H. Therefore, these coatings had unique properties and can be used as protective as well as multifunctional coatings [30].

Pathak et al. also developed waterborne hybrid silicone-polyurethane coatings (SiPU coating). It was found that the silicone modification increased the corrosion resistance of blank polyurethane resin significantly with decrease in corrosion current from (3.1×10^{-6} A) for PU to (7×10^{-7} A) for SiPU. Improvement in corrosion resistance was attributed to the formation of aluminium-oxygen-silicon (Al O-Si) bond which acted as barrier layer against the migration of chloride ions and water, towards the substrate. A summary of work carried out is given in Table 2.1 [31].

Table 2.1: Corrosion resistance and Mechanical properties for various inorganic-organic systems [30-32]

Sr. no	Hybrid System	Corrosion Current A/cm ²	Pencil Hardness
1.	Silane-melamine resin(HMMM)	7×10^{-7}	6H
2.	Silane-Polyurethane resin	$1.21-2.71 \times 10^{-6}$	6H
3.	Silane-Polyester resin	$4.6-13.1 \times 10^{-7}$	6H
4.	Silane- Alkyd	3.34×10^{-8}	6H

The pencil hardness of neat PU coating was found to be 2H while it was enhanced to a 6H for SiPU hybrid sol-gel coatings. Furthermore, the presence of siloxane (Si-O-Si) moieties in

SiPU coatings made them flexible and robust enough to sustain the mechanical stresses during service [32]. They also developed thermal-cured, sol–gel derived, waterborne organosilane–polyester coatings (SiE) using MTMS, GPTMS and polyester resin for corrosion protection of aluminium AA6011. Results from polarisation studies have shown that the SiE coated substrate ($4.6\text{--}13.1 \times 10^{-7} \text{ A/cm}^2$) provided a better corrosion protection than the polyester coated substrate ($7.8 \times 10^{-6} \text{ A/cm}^2$) due to formation of aluminium–oxygen–silicon covalent bond at aluminium–coating interface. Furthermore, SiE coatings provided better hydrophobicity and hardness than the polyester coating [33].

Apart from metal surface, fabrication of hydrophobic coatings is being reported on various other substrates like cotton fabric, glass, plastic etc. Daoud et al [34] prepared transparent and durable superhydrophobic surfaces on woven cotton substrates using a modified silica sol, which was produced via cohydrolysis and polycondensation of a mixture of hexadecyltrimethoxysilane, tetraethoxyorthosilicate and 3-glycidoxypyltrimethoxysilane

Similar work was reported by *Hoefnagels et al.* [35], *Leng et al.* [36], *Gan et al.* [37], *Li et al.* [38] and *Bae et al.* [39]. They reported the fabrication of superhydrophobic textiles based on multiscale structure obtained on cotton fabric. When fluoro compounds were used for the surface modification, hydrophobic textiles were obtained with a static contact angle of about 140° and a roll-off angle of 24° . The multiple length scales of the roughness originated from the woven structure having two additional layers of silica particles (microparticles and nanoparticles), which were covalently bonded to the fiber as schematically shown in Fig. 2.8 (a) and (b)

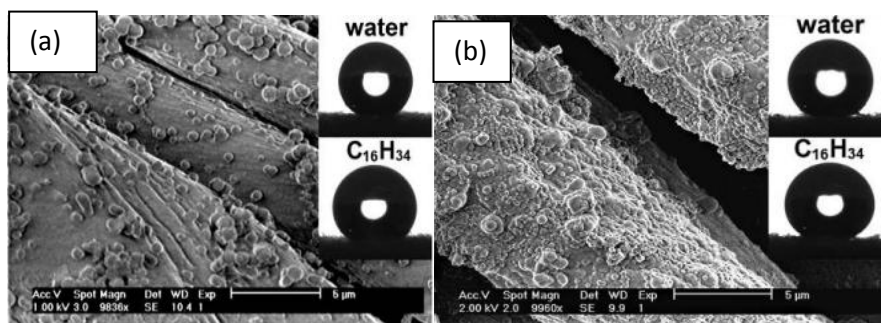


Figure 2.8: SEM image of multiscale roughness structure obtained on cotton fabric at (a) low magnification and (b) high magnification [35]

Latthe et al. [40] described the synthesis of superhydrophobic silica films on glass substrates using trimethylethoxysilane as a co-precursor. The coating sol was prepared by keeping the molar ratio of tetraethoxysilane precursor, methanol and water at 1:38.6:8.68, using 2 M NH_4OH throughout the experiments, and the molar ratio (M) of trimethylethoxysilane to tetraethoxysilane was varied from 0 to 1.1. The hydrophobicity of the films increased with increasing M value; however, the optical transmission decreased from 88 to 82% in the visible range. Silica films with a static water contact angle as high as 151° and a sliding angle of 8° have been produced from a sol with an M value of 1.1. The hydrophobic silica films retained their hydrophobicity up to 275°C . These films were transparent and stable to high temperature and humidity. By modifying silica sols with trimethylethoxysilane, sol-gel coatings could be prepared on glass substrates at room temperature. The coatings had excellent water-repelling properties without any addition of fluorine containing compounds.

Wang et al. [41] have produced stable superhydrophobic surfaces with water contact angles over 170° and sliding angles below 7° by simply coating a particulate silica sol solution of cohydrolyzed tetraethoxysilane/fluorinated alkyl silane with $\text{NH}_3\cdot\text{H}_2\text{O}$ on various substrates, including textile fabrics (e.g. polyester, wool and cotton) and electrospun nano-fibers mats. The superhydrophobic coatings obtained through the sol-gel treatment of substrates with hydroxyl groups were quite stable owing to the formation of covalent bonds between the coating and substrate by condensation in the sol-gel process followed by dehydration in the curing process resulting in robust sol-gel coating system.

2.3.2 Hydrophobisation

It is necessary to lower the surface energy of the roughened surfaces. The commonly used reactive molecules for low-surface-energy modification are shown in Fig 2.9, which are mainly long alkyl chain thiols, alkyl or fluorinated organic silanes, perfluorinated alkyl agents, long alkyl chain fatty acids, polydimethylsiloxane-based polymers or other polymers, or their combinations. Among others, commercially available products such as water repellents and poly (acrylate-g-siloxane) textile finishing agent can also be used.

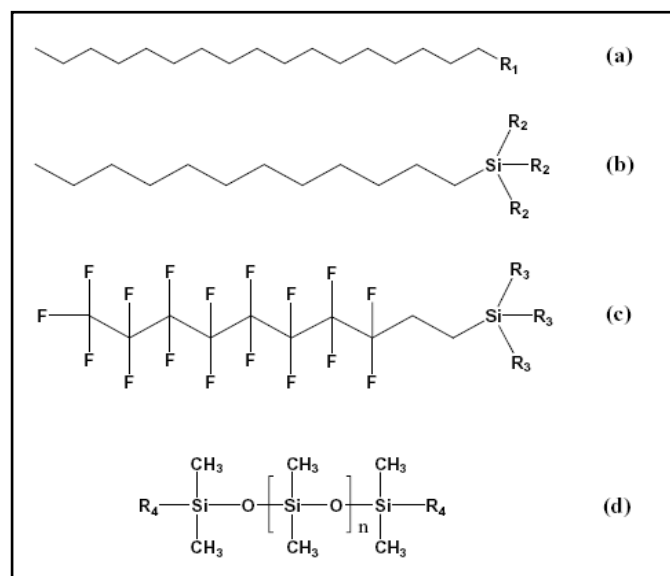


Figure 2.9: Examples of surface reactive molecules for low-surface-energy modification : (a) long alkyl chain with R_1 groups; (b) long alkyl chain organic silanes with R_2 groups; (c) long alkyl chain fluorinated silanes with R_3 groups, in which R_1 can be $-\text{SH}$, $-\text{OH}$, $-\text{COOH}$, $-\text{NH}_2$, etc, and R_2 and R_3 can be $-\text{Cl}$, $-\text{OCH}_3$, $-\text{OCH}_2\text{CH}_3$; the length of these chains can be varied from C8 to C18; and (d) polymers based on polydimethylsiloxane, which can be bis-end-capped or mono-end-capped, where R_4 is usually a 3-aminopropyl or glycidyl ether group [42]

2.3.2.1. Hydrophobisation with fluorinated molecules:

The most commonly used chemicals for hydrophobisation are fluoro alkylsilanes owing to their extremely low surface free energy and the simple reaction of the silane groups with the hydroxyl groups on coatings [42]. Also, most superoleophobic surfaces are created by the hydrophobisation of a per fluorinated material. It is well known that a fluorinated polymer has a low wettability due to its low surface energy. Therefore, it is an ideal building block to develop a superhydrophobic coating. On the other hand, the low wettability is basically a surface property, so it is unnecessary to have fluorine in the bulk. Surface segregation provides an excellent strategy to create a coating with a fluorine-rich surface. In such an approach, due to its low surface energy, the fluorinated species would migrate toward the air/film interface to minimize the interfacial energy. Thus, only a very small quantity of

fluorinated species is needed to provide a surface with low surface energy. The surface segregation process is demonstrated in Fig. 2.10 [43]

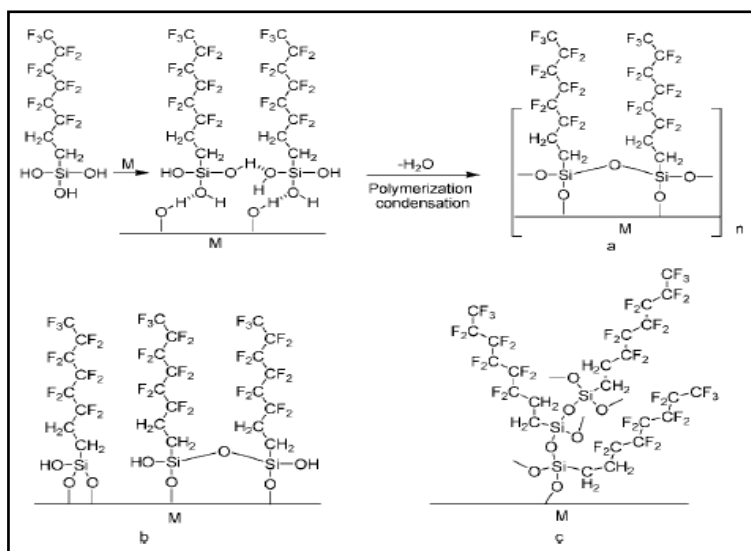


Figure 2.10: Reaction between metal substrate and hydrolysed FOTS [43]

The incorporation of fluorine atoms, which have a small atomic radius and high electronegativity, could achieve low surface energy. However, this method to increase hydrophobicity is limited. The maximum contact angle that can be reached by coating fluorinated methyl groups onto a flat solid surface is only 120°, which can be hardly called superhydrophobic [43].

Bravo et al. created a transparent superhydrophobic film by applying dual-size silica nanoparticles (20 nm, 50 nm) on a glass substrate. Subsequently, the film was treated with 1*H*, 1*H*, 2*H*, 2*H*-perfluorooctyltrichlorosilane to obtain superhydrophobicity [44].

Wenguo Xu obtained superhydrophobic surface on copper and galvanised iron substrates by means of a simple solution immersion process i.e. immersing the clean metal substrates into a methanol solution of hydrolysed 1*H*, 1*H*, 2*H*, 2*H* perfluorooctyltrichlorosilane for 3-4 days at room temperature and then heated at 130 °C in air for 1 hour. Both of the surfaces resulted in water contact angle of larger than 150° as well as a small sliding angle of less than 5° [45].

Superoleophobic surfaces possessing static contact angles greater than 140° with organic liquids are extremely rare. A simple approach has been developed by *Hsin Chu et al.* to fabricate an extremely superamphiphobic coating material based on fluorinated 1H,1H,2H,2H-perfluorodecyltriethoxysilane (PFTS) silica nanoparticles resulting contact angles of water and diiodomethane at 167.5° and 158.6° , respectively. The contact angle of diiodomethane of 158.6° was founded substantially higher than the highest literature reported value known of at 110° . In addition, this developed film also possessed extremely high contact angles with other organic liquids such as soybean oil (146.6°), decahydronaphthalene (142.5°), diesel fuel (140.4°), and xylene (140.5°) as shown in Fig 2.11. The root-mean-square roughness of this fluorinated silica nanoparticles film was found to be 280.1 nm as measured from AFM technique. Fig 2.12 shows the probable mechanism of formation of fluorinated silica nanoparticles [46].

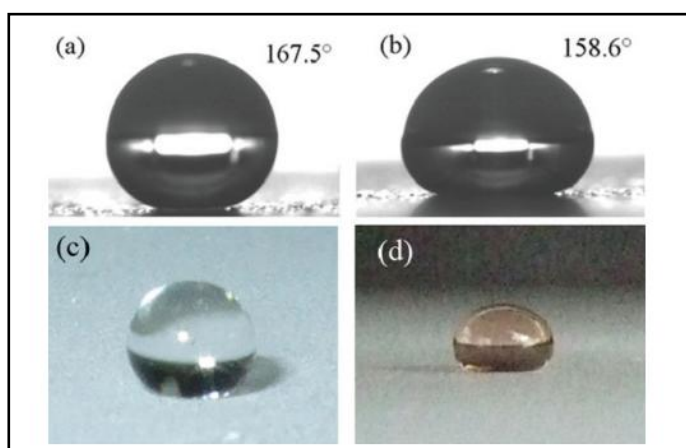


Figure 2.11: Liquids on fluorinated silica nanoparticles film (a) 5 μl water, (b) 5 μl diiodomethane optical images of liquids, (c) water, (d) diiodomethane [31]

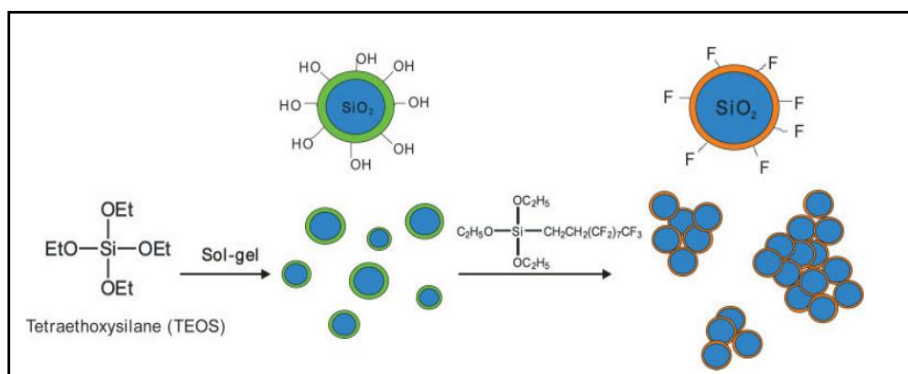


Figure 2.12: Preparation of the fluorinated silica nanoparticles [31]

Lakshmi et al. developed hydrophobic sol-gel coatings by incorporating optimum amount of commercially available perfluoroalkylmethacrylic copolymer, Zonyl 8740 (FP) in a hybrid sol-gel matrix containing fumed silica particles. The fabricated fluoro-based sol-gel nano coatings revealed highly porous structure with contact angle of about 135°. According to this work the improved hydrophobicity was attributed to the combined effect of low surface energy due to the FP and roughness created by the random distribution of silica aggregates [47].

Yonghao et al. fabricated UV resistant low surface energy silica coatings using tetraethoxysilane and trifluoropropyltrimethoxysilane as precursors. According to him when trifluoropropyltrimethoxysilane was incorporated into silica, hydrophobic tri-fluoropropyl groups were present on the surface, yielding hydrophobicity. In order to measure the surface hydrophobicity retention of the silica surfaces under UV irradiation, UV accelerated aging tests were conducted according to ASTM D 4329. The coated samples showed excellent UV stability with respect to contact angle and contact angle hysteresis for a test time of 1000 h due to the strong Si-(CH₂)₃CF₃ bond, which suggests possible outdoor applications where UV exposure is prevalent. Fig 2.13 shows the variation of contact angle and contact angle hysteresis with UV exposure time [48].

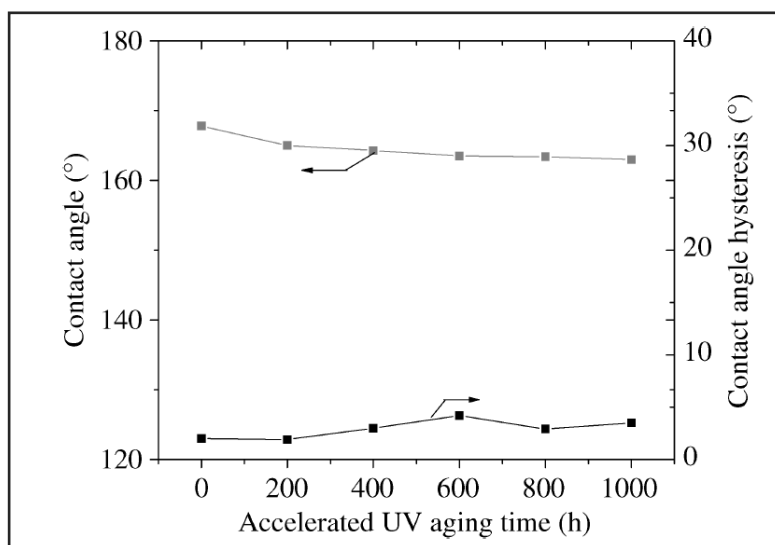


Figure 2.13: variation of contact angle and contact angle hysteresis with UV exposure time [33]

Brassard et al. developed fluorine based superhydrophobic coatings on aluminium for corrosion resistance, biofouling and water and air drag reduction applications. This work emphasis on synthesis of mono-dispersive silica nanoparticles of ~120 nm diameter via Stöber process and further functionalised using fluoroalkylsilane (FAS-17) molecules to incorporate the fluorinated groups. The synthesised fluorinated silica nanoparticles were spin coated on flat aluminium alloy, silicon and glass substrates. The contact angle achieved was about 150° with a critical roughness value of ~0.70 µm. Fig 2.14 shows the SEM image at lower and higher magnification of fluorinated nano-particles developed in this work [49].

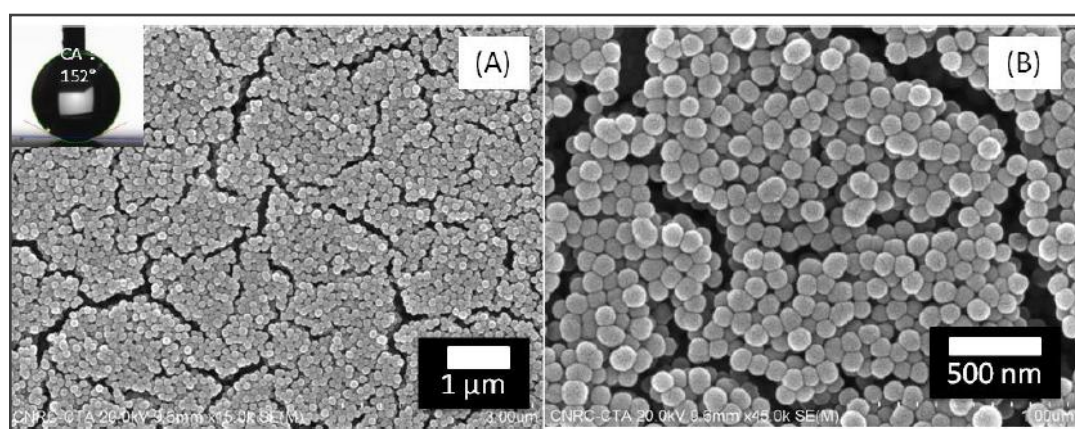


Figure 2.14: (A) SEM images of fluorinated silica nanoparticles of 119 ± 12 nm diameter deposited on aluminium substrates in three layers by spin coating; Inset of Figure 2.14 (A) shows the image of a water drop placed on this surface exhibiting a very high water contact angle of ~152°, and (B) higher magnification image of (A) [49]

2.3.2.2. *Hydrophobisation with alkyl molecules*

Fluoroalkyl compounds have several economical and ecological disadvantages, such as high cost and potential risk for human health in case of skin contact and for the environment in case of emission of fluorine compounds during and after the coating process. Hence, some producers have stopped their production of water-repellent fluorine-containing compositions during the past few years. In addition to the environmental hazards associated with their production and application, a high-temperature process is usually required for their production. Therefore, the formation of non-fluorinated superhydrophobic surfaces at low

temperatures is important for the fabrication of environmentally friendly coatings on substrates with low heat resistance.

According to S.A. Kulinich and M. Farzaneh, self-assembled organic monolayers (SAMs) on solid substrates provide an interesting approach to tailor-designed surfaces with controlled physical and chemical properties. A class of widely used SAMs is based on n-alkyltrichlorosilane precursor molecules which through hydrolysis and polymerization, produce self-assembled alkylsiloxane films with low free surface energy as shown in fig 2.15. Hydrophilic surfaces can be made hydrophobic through the self-assembly of molecules with hydrophobic ‘tail groups’ such as n-alkyltrichlorosilanes. Octadecyltrichlorosilane (OTS), as the most common model compound, self-assembles into a robust monolayer on almost any high-energy surface. By virtue of their hydrolysable functional groups, OTS molecules can be covalently bound to substrate hydroxyl groups, as well as cross-linked within the octadecylsiloxane layer [50]

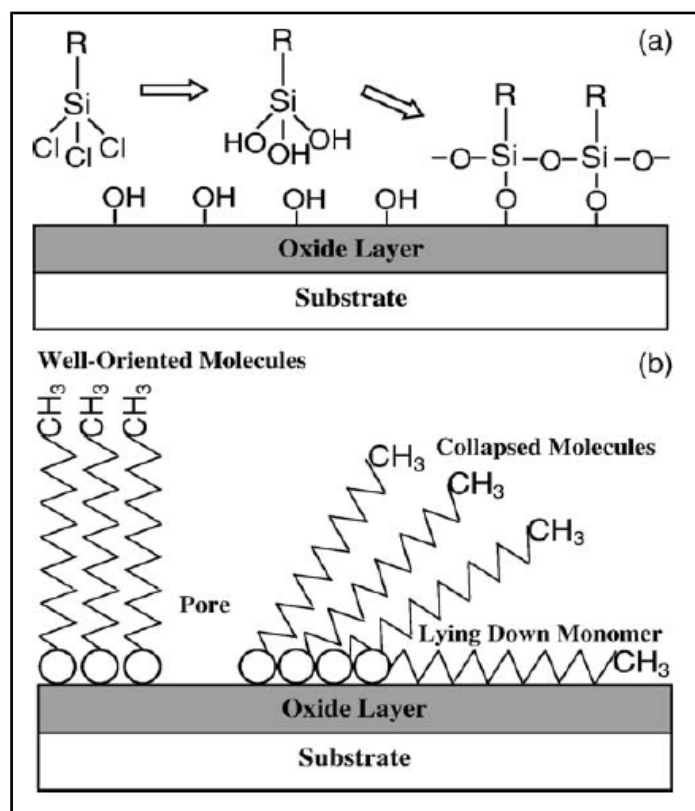


Figure 2.15: Schematic representation of: (a) silanisation process of alkyltrichlorosilane molecules on a substrate covered with an oxide layer and formation of an alkylsiloxane monolayer and (b) well oriented (or close-packed) SAM molecules, pore, collapsed molecules and lying down monomers [50]

Another appreciable work was done by *Sheen et al.* [51] who have successfully developed a simple approach to fabricate an extremely superamphiphobic coating material by the TEOS/MTES sol-gel derived materials. It was found that optimum TEOS/MTES composition had the contact angles of 149.8° and 133.1° for water and CH_2I_2 , respectively. It exhibited both super-hydrophobicity and super-oleophobicity, i.e., superamphiphobicity, resulted from the rough TEOS-derived surface and hydrophobic MTES-derived surface. Also, it had relatively low-surface energy (1.38 mJm^{-2}) considerably lower than that of F-silane-coated surface with 39.3 mJm^{-2} . Thus the study supported that superamphiphobic surface could be achieved by non-fluorinated sol-gel derived silica materials. Figure 2.5 shows the proposal mechanism of the superhydrophobic surface formed by TEOS/MTES sol-gel derived coating.

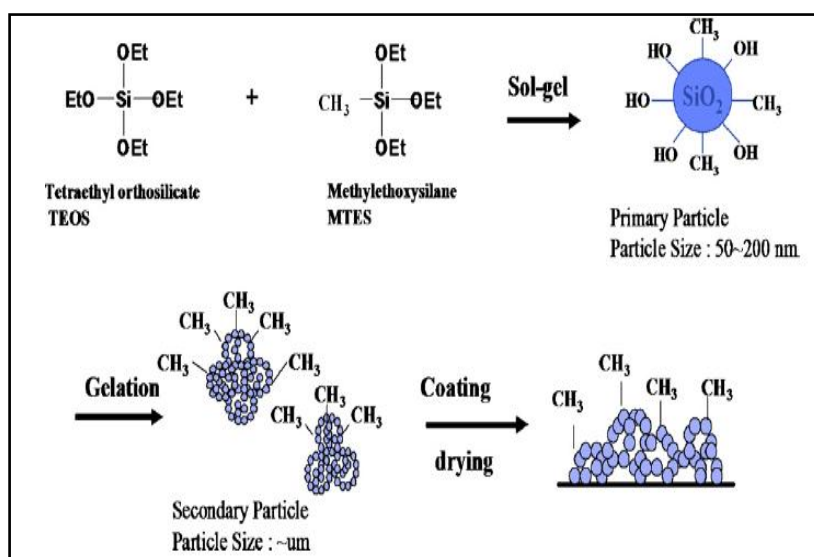


Figure 2.16: Proposed mechanism of the superhydrophobic surface formed by TEOS/MTES sol-gel derived coating [51]

The hydrophilicity of silica films was due to the presence of a large number of Si-OH groups on the surface of the films. Replacement of the Hs from the Si-OH groups by the hydrolytically stable Si-R groups through the oxygen bonds prevents the adsorption of water and hence results in hydrophobic silica surfaces. *Daoud et al.* [52] successfully prepared transparent and durable superhydrophobic silica-coating films on cotton substrates at low temperatures via cohydrolysis and polycondensation of hexadecyltrimethoxysilane

(HDTMS), tetraethoxyorthosilicate (TEOS), and 3 glycidyloxypropyltrimethoxysilane (GPTMS) mixture. HDTMS reacts with hydroxyl in the inorganic substrates or atmospheric moisture to form stable covalent bonds, thereby generating the active ingredient while liberating alcohol. The active ingredients greatly increase the water contact angle and oil wettability of the treated substrates, providing water-repellant, dustproof, anti-stiction, and hydrophobicity effect.

Latthe et al. [53] have also used HDTMS as a co-precursor and synthesised macroporous hydrophobic silica films by the two step sol–gel process using the dip coating technique. The maximum contact angle obtained was of 125 °. It was observed that the water contact angle value on the HDTMS modified films remained stable at 125° after heat treatment up to 235 °C. However, the water contact angle value decreased to 52° in the case of unmodified films, indicating the improvement in the thermal stability using HDTMS as a co-precursor. The hydrophobic silica films retained their hydrophobicity up to a temperature of 235 °C and above this temperature the films became hydrophilic. Fig 2.17 shows SEM images of HDTMS modified silica film at different magnifications.

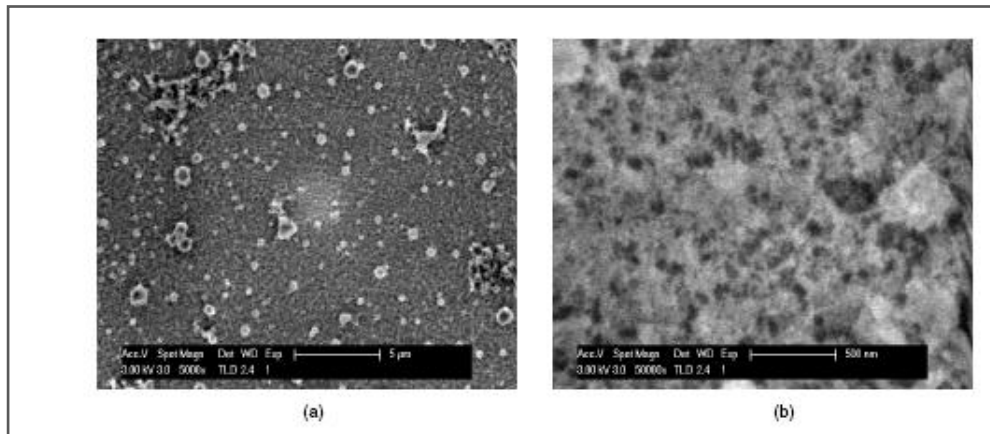


Figure 2.17: (a) SEM image of the HDTMS modified film at low magnification and (b) high magnification [53]

Gao et al. [37] in his research, studied the formation of highly hydrophobic surfaces on polyester fabrics using silica sol formed by hydrolysis and subsequent condensation of tetraethoxysilane under alkaline conditions followed by hydrophobisation using hydrolysed hexadecyltrimethoxysilane (HDTMS). The textile fabrics thus treated showed excellent water

repellency with a water contact angle as high as 143° on polyester. The high hydrophobicity of the treated fabrics was due to the presence of hydrophobic HDTMS as well as the increase in roughness by silica sol on the surfaces of the treated fabrics which are two factors responsible for water repellency. The scheme for forming a superhydrophobic surface on cotton fabric using silica sol and HDTMS is described in Fig 2.18.

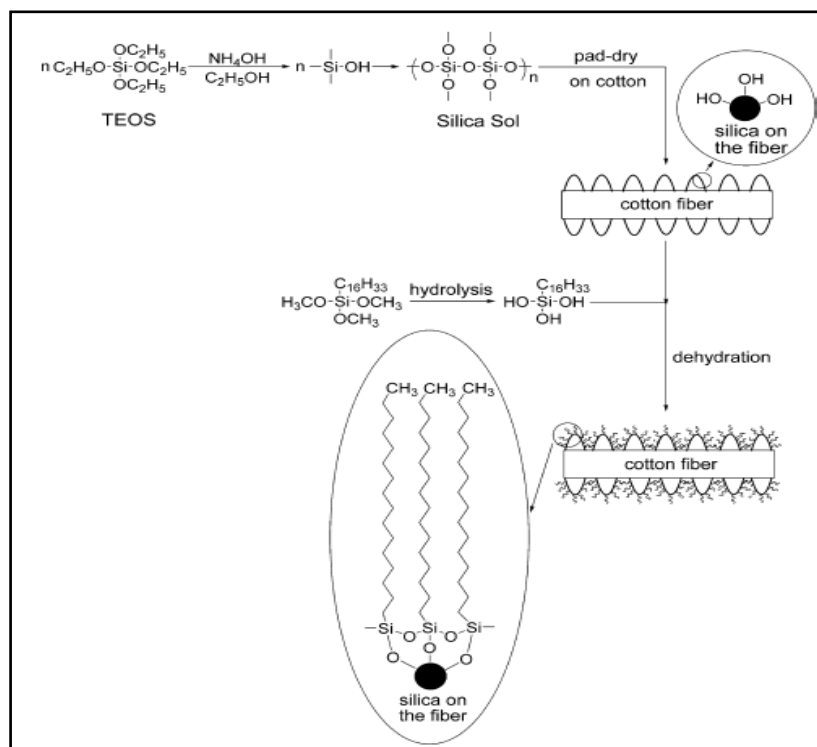


Figure 2.18: Formation of a Superhydrophobic Surface on Cotton Based on Silica Sol and HDTMS [37]

Similar work has been reported by *Textor et al.* [54] according to which hydrophobic sol-gel based coatings can be prepared by combining, e.g., simple TEOS-based sols with minor amounts of hydrophobic additives like alkyltrialkoxysilanes, as methyltrimethoxysilane (C1), butyltrimethoxysilane (C4), octyltrimethoxysilane (C8), dodecyltrimethoxysilane (C12), hexadecyltrimethoxysilane (C16) and octadecyltrimethoxysilane (C18). Driven by the differences in the surface tension of the components, the hydrophobic components enrich at the solid/ air interface during the coating and drying process yielding low surface energy while the bulk of the coating was found to be less hydrophobic. The experiment aimed at preparation of simple TEOS based alcoholic sol-gel by acidic hydrolysis followed by testing with different aliphatically modified alkoxy silane additives. The alkoxy silanes were

modified with linear alkyl chains of increasing chain length. The different sols were applied to glass by a simple dipping process before drying. Roughly estimated the water repellence was higher, the longer the alkyl chain of the additive used (Fig 2.19).

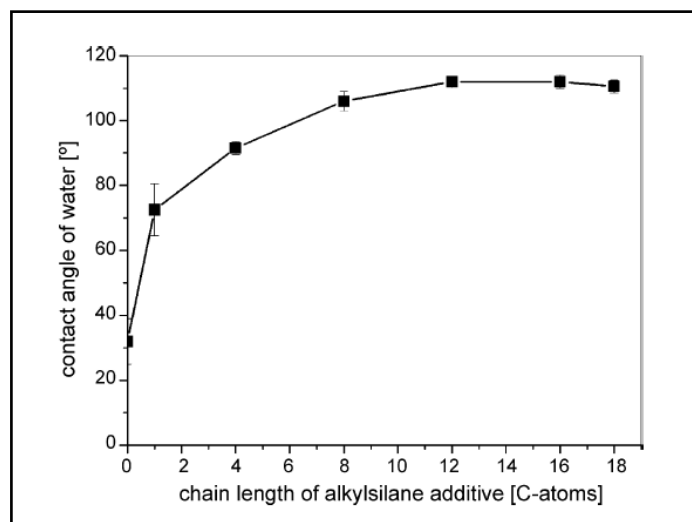


Figure 2.19: Contact angles of glass substrates coated with SiO_2 -sols with alkyltrialkoxysilanes of increasing chain lengths [54]

Similar type of work is reported by *Mahadik et al.* [22]. According to his work also initially prepared silica films contain a large number of hydroxyl and alkoxy groups which are responsible for the hydrophilic character of the film surface. However after using TMCS in the sol-gel processing, the $-\text{OH}$ groups were replaced by hydrolytically stable $-\text{O}-\text{Si}-(\text{CH}_3)_3$ groups. The coatings surface becomes super hydrophobic because of the hydrolytic stability of $\text{Si}-\text{C}$ bond having a water contact angle of 161° and sliding angle of 9° .

Venkateswara Rao et al. [26] reported the preparation of the MTMS based hydrophobic surface ($\text{CA} > 90^\circ$) and then conversion of the hydrophobic surface to super hydrophobic ($\text{CA} > 150^\circ$) by TMCS derivatisation and in ultrahydrophobic ($\text{CA} > 120^\circ$) by HMDZ derivatisation. According to the work, the coating solution was prepared under basic condition from the MTMS, CH_3OH , and H_2O in with 5 M NH_4OH and coated over glass substrate by dip coating process. After the films were thermally cured, they were soaked in solution of 5% HMDZ and 5% TMCS in hexane for 2 h at 50°C . Both the HMDZ and TMCS

modified films were thermally cured at 100 and 150 °C for 1 h resulting in superhydrophobic surface after thermal curing. Fig. 2.20 shows the SEM and AFM image of rough micro-profile of TMCS modified sol-gel coated glass panel. In principle, the HMDZ and TMCS react with hydroxyl groups on the silica surface and could be represented by the following chemical reactions:

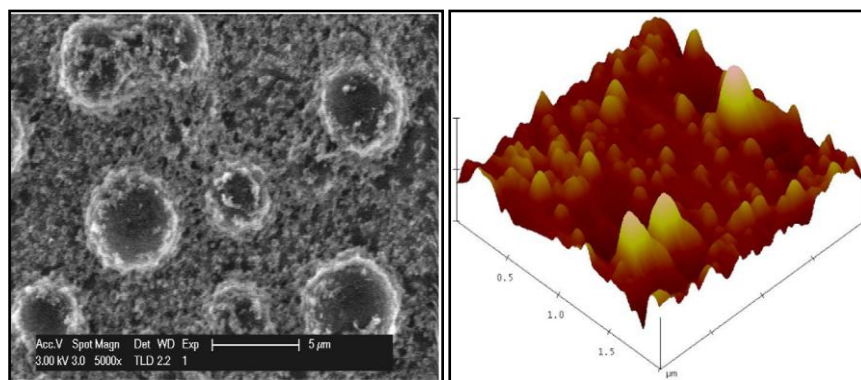
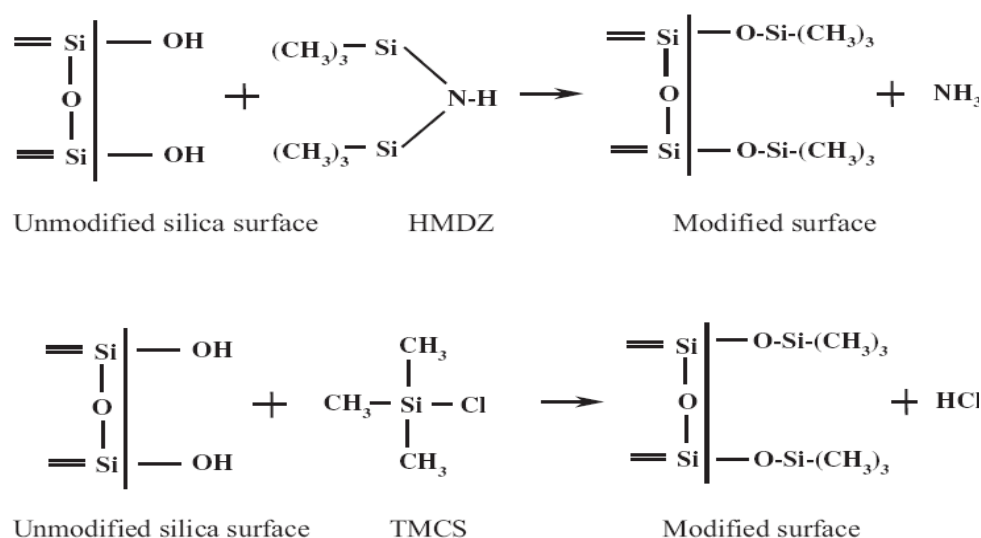


Figure 2.20: a) SEM image, b) AFM image of 5% TMCS in hexane coated sol-gel glass panel [26]

2.3.3 Covalent layer-by-layer assembly

Layer-by-layer assembly is a versatile way to construct thin-film nano-composites [55]. It is most commonly used to fabricate an interface involving a multilayer ionic assembly of polyelectrolytes. However, some ionic assemblies are of limited applicability because of the weak interaction between the substrate and the layers. This review focuses on layer-by-

layer assembly approaches that use covalent bonds to form multilayer grafts, which are durable, stable and practical. As shown in Fig. 2.21, the design of chemical reactions between layers is very important since it affects the stability of the formed coating as well as the feasibility of the process.

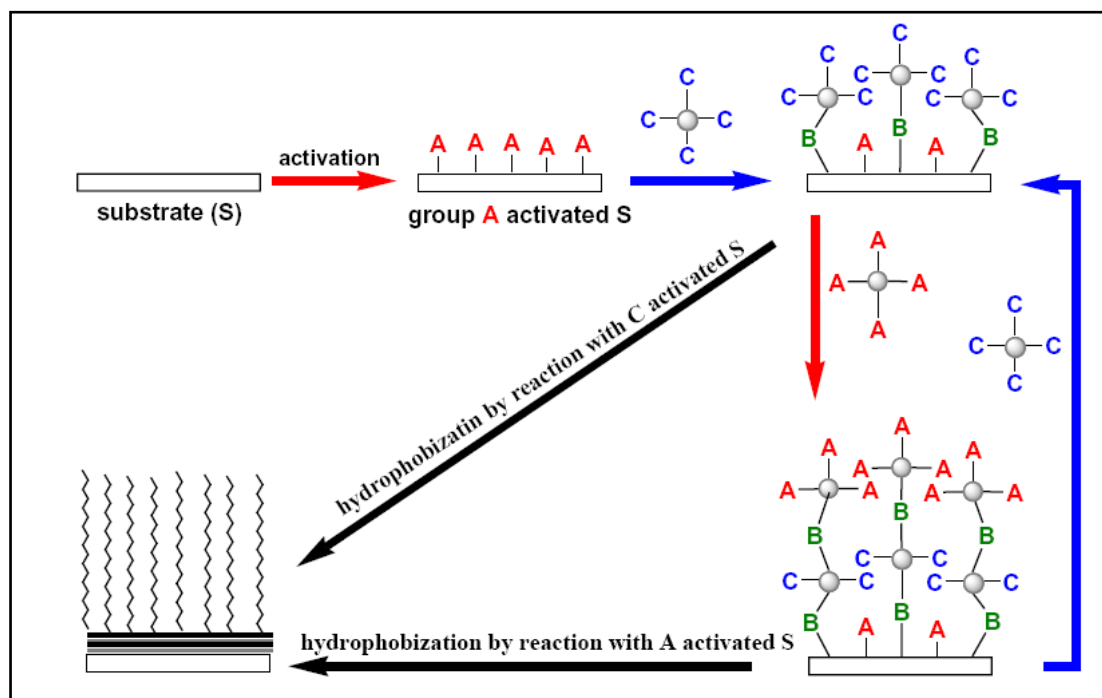


Figure 2.21: Steps used in the covalent layer-by-layer assembly of functional particles, with C groups and A groups on a substrate activated with A groups, for super-hydrophobic surfaces. B groups are formed by the reactions of A groups with C groups [55]

Usually, functionalised nanoparticles facilitate the production of rough surfaces on a substrate simply by controlling the nanoparticles layers. To enhance the interaction between the first layer and the substrate, the substrate should usually be activated. After layer-by-layer assembly, the outer surface usually contains residual functional groups, marked by letters A and C in figure 2.21, which can be utilised to react with low-surface-energy agents for covalent hydrophobization.

Ming *et al* [56] reported a simple and robust procedure for preparing superhydrophobic films

with a dual-size hierarchical structure originating from well-defined raspberry-like particles. Firstly, a conventional cross-linked film based on an epoxy–amine system was prepared with unreacted epoxy groups available for further surface grafting. Secondly, raspberry-like silica particles with an amine-functionalised surface were chemically deposited onto the epoxy films, generating roughness with two characteristic length scales. Finally, a layer of monoepoxy-end-capped poly (dimethylsiloxane) was grafted onto the raspberry-like particles to render the film surface hydrophobic. (Fig 2.22)

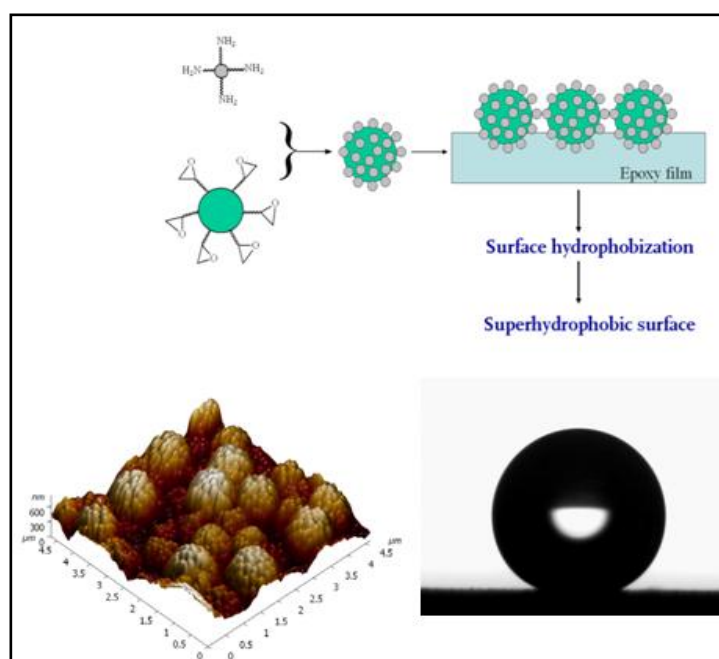


Figure 2.22 Preparation of superhydrophobic films based on covalent assembly yielding raspberry-like particles (reprinted with permission from [56])

2.3.4 Polymer film roughening

Polymer-based rough surfaces can be formed by the phase separation of a multicomponent mixture [57]. If a stable mixture becomes unstable owing to changes such as cooling or solvent evaporation, it will begin to separate into two phases, one of which might be a solid or become solid at some point in the process. This creates a solid porous structure, as shown in Fig 2.23 (a), or a lotus-like structure with micro- and nanopapillae, as shown in Fig 2.23 (b). The size of the pores or papillae in the formed solid structures can be

controlled if the rate of phase separation can be altered relative to the rate of solidification. Phase separation has received great interest for the fabrication of superhydrophobic surfaces owing to its low cost, ease of production and the possibility of creating substrates with various shapes by casting and coating.

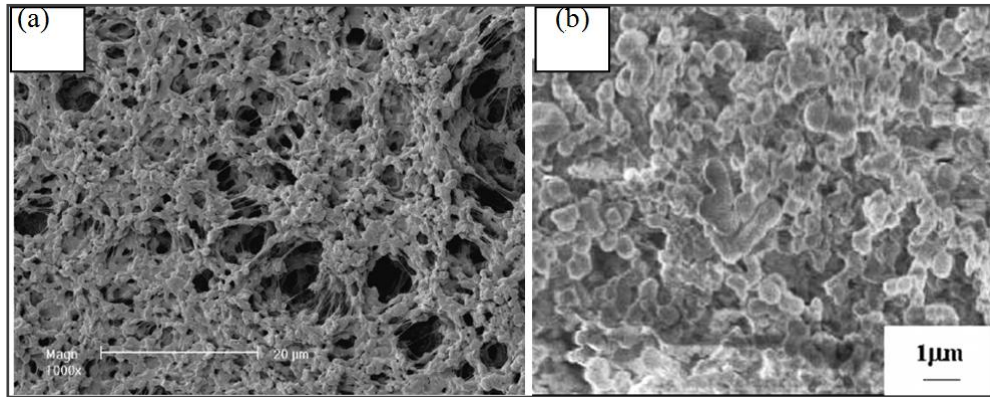


Figure 2.23: SEM images of (a) porous membrane produced by solvent casting of polypropylene solution using methylethylketone as the nonsolvent; (b) superhydrophobic poly(vinyl chloride) film obtained by coating with a mixture ethanol and H₂O as the nonsolvent [57]

2.4 Nano particles : Another method of producing rough polymer films uses incorporation of inorganic nanoparticles, in which the polymer acts as a binder with low surface energy. Thus, durable superhydrophobic surfaces can be obtained even without post-hydrophobisation as shown in Fig.2.24.

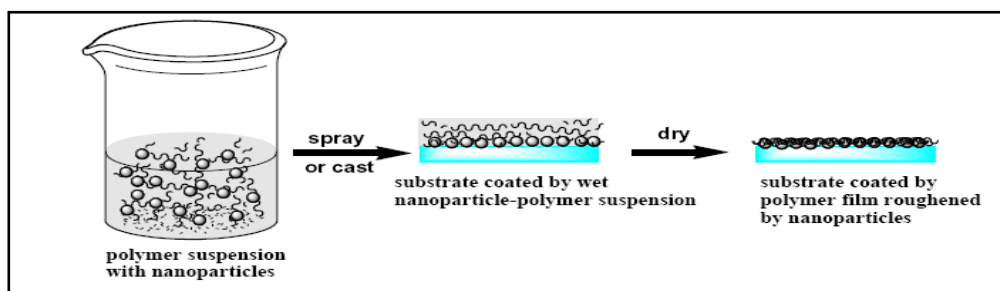


Figure 2.24: Nano- particle-polymer composite coating for superhydrophobic surfaces [58]

Steele et al. [58] described a technique for fabricating superoleophobic coatings by spray-casting nanoparticles-polymer suspensions. The method used ZnO nanoparticles blended with a waterborne perfluoroacrylic polymer emulsion and cosolvents to produce self-assembling nanocomposite slurries that form hierarchical nano-textured morphology upon

curing. The resulting surface attained high contact angles and low contact angle hysteresis. The coatings could be easily applied to large and/or flexible substrates by spray coating and required no additional surface treatment by commonly used hydrophobic molecules such as fluorosilanes.

Manoudis et al. [59] fabricated superhydrophobic surfaces for the enhanced protection of stone by adding silica nanoparticles into a commercial siloxane composition, thereby enhancing its protective efficiency. The extent of surface hydrophobisation depended on the nano-particle concentration and reached a maximum value of 160° at 1% w/v of nanoparticles for white Greek marble treated with the modified composition.

Kamps et al. [60] tried to introduce roughness into the coating; metal oxide particles with a size of 50nm to 100nm were dispersed into the basic coating solution. After spraying the solution onto the substrate, a defined roughness was generated by a random arrangement of the metal oxide particles in the coating. The particle size and particle amount was varied and the surface roughness was evaluated. An increase in the particle concentration led to an increase in the surface roughness until a maximum was reached. Using 50 nm particles alone improvement was not much whereas the coating prepared with 1 μm particles was completely destroyed. However a combination (1 μm / 50nm) of particles gave excellent results. Samples prepared from 1 μm (or 50 nm) particles showed a water contact angle of about 140° while the ones prepared from the mixture reached 152° .

Kulinich and Farzaneh [3] incorporated ZrO_2 nanopowder in a perfluoroalkylmethacrylic copolymer based sol-gel formulation of different diameters. It was found that after the ZrO_2 suspension of sol-gel was sprayed over substrate and heat treating at 120°C produced a superhydrophobic surface with contact angle of more than 150°

Xue et al. [61] in his work fabricated super-hydrophobic surfaces ($\text{CA} \sim 169 \pm 2^\circ$) composed of vinyl modified silica nanoparticles (V-SiOx-NPs). The influence of diameter of V-SiOx-NPs on super-hydrophobicity was also investigated. The V-SiOx-NPs films with diameters ranging from 167 to 1600 nm had the same CA of about 166° , while the film of 85nm V-SiOx-NPs had the lowest CA of about 158° . The packing manner of V-SiOx-NPs determined the air fraction on the film surface and then the CA. The rough surfaces, which were composed of microstructures of disordered V-SiOx-NPs rather than the chemical

composition, primarily account for the super-hydrophobicity. Fig. 2.25 shows the FESEM micrographs of unmodified and vinyl-modified silica nanoparticles with different diameters.

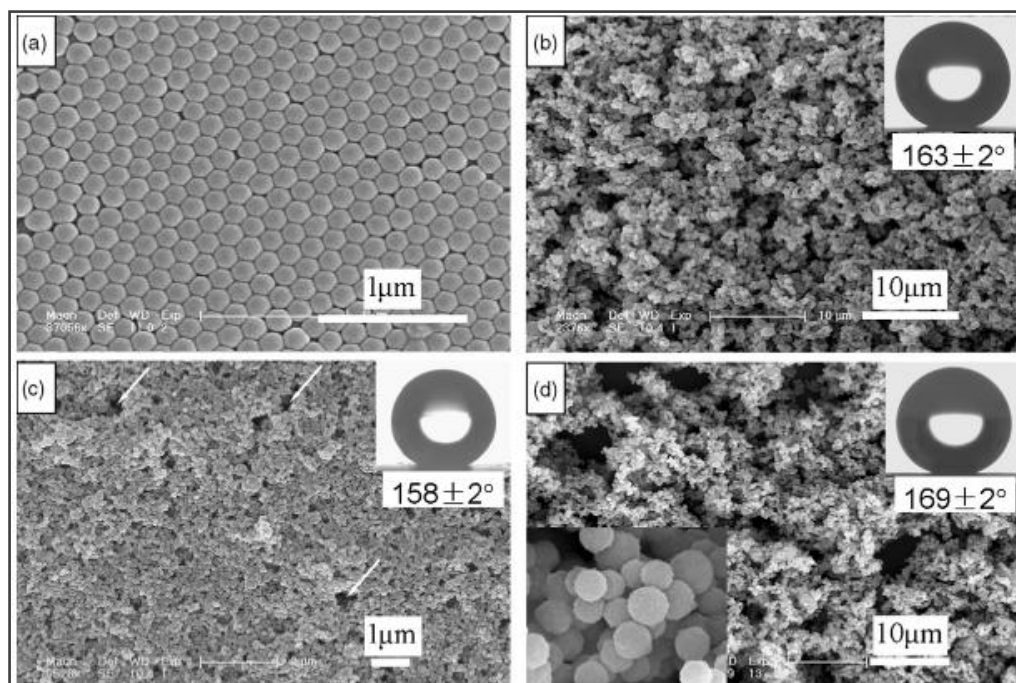


Figure 2.25: FESEM micrographs of (a) the unmodified silica nanoparticles with diameters of 167 nm and the vinyl-modified silica nanoparticles with different diameters: (b) 85 nm, (c) 167 nm, (d) 360 nm [61]

Dhoke et al. also published lots of work on waterborne coatings, where various nano-particles like nano-Alumina, nano- Zinc oxide and nano iron oxide particles were incorporated in base matrix of various waterborne polymers to achieve improved U.V resistance, corrosion resistance, better adhesion, scratch and mar resistance properties. In one of such study, a modification in the alkyd based waterborne coating was studied with the addition of 0.05%, 0.1%, 0.2%, and 0.3% nano- Al_2O_3 . Corrosion performance of the nano-composite coatings was evaluated when applied on mild steel substrate. The results showed that, with an increase in the concentration of nano- Al_2O_3 there was an improvement in the corrosion resistance, UV resistance, and mechanical properties of the coatings indicating the positive effect of addition of nano- Al_2O_3 particles in the coatings [62].

They also incorporated nano-ZnO into alkyd based waterborne coating using HMMM as the crosslinking agent at different concentrations. It was found that the heat-resistance and mechanical properties such as scratch resistance and taber resistance of the coatings improved significantly as a function of nano-ZnO addition [63].

Dhoke *et al.* [64] also incorporated nano-Fe₂O₃ and studied the corrosion behavior of waterborne alkyd resin as function of various concentrations of nano-Fe₂O₃. These modified coatings showed delay in corrosion process as evident from the *R*_{po} and *C*_c values after the 30 days of exposure. Among the different concentrations studied, coatings modified with lower concentration of nano-Fe₂O₃ (0.05 wt. %, 0.1wt. % and 0.2 wt. %) showed moderate corrosion resistance, which may be attributed to the inadequate concentration of nano-particle in the coating matrix. The improvement in the corrosion resistance of the nano-Fe₂O₃ modified coatings was much significant at higher loading level (0.3%). The improvement in the corrosion resistance can be attributed to their smaller size and large surface area, which reduces the transport paths for permeation of corrosive environment through the coating film. This suggested the positive effect of nano-pigments addition on alkyd based waterborne coatings. Following Table 2.2 summarizes the electrochemical data of neat and nano-Fe₂O₃ incorporated alkyd based waterborne coatings after 30 days of immersion. It can be clearly seen that corrosion resistance increases with increase in concentration of nano-particles.

Table 2.2: Various Electrochemical parameters for different concentrations of nano-Fe₂O₃ [53]

Coating system	OCP	<i>R</i> _{po} (Ω cm ⁻²)	<i>C</i> _c (Fcm ⁻²)
Neat	-0.620	371.8	3.11 × 10 ⁻⁷
0.05% nano-Fe ₂ O ₃	-0.512	552.3	4.18 × 10 ⁻⁹
0.1% nano-Fe ₂ O ₃	-0.497	617.8	3.20 × 10 ⁻⁹
0.2% nano-Fe ₂ O ₃	-0.458	1213.1	2.68 × 10 ⁻⁹
0.3% nano-Fe ₂ O ₃	-0.397	1354.0	2.48 × 10 ⁻⁹

Fumed silica particles have an extremely large surface area per unit weight and numerous silanol groups (Si-OH) on the surface. The structure consists of microscopic droplets of amorphous silica fused into branched, chainlike, three-dimensional secondary particles which then agglomerate into tertiary particles. The resulting powder has an extremely low bulk density and high surface area. Its three-dimensional structure results in viscosity-increasing, thixotropic behavior when used as a thickener or reinforcing filler. Primary particle size of

fumed-silica is 5–50 nm Owing to these characteristics; the fumed silica shows hydrophilicity and exhibits a very high surface energy leading to the aggregates and particle-particle interaction of filler in non-polar liquids. Thus, the silanol groups on its surface can be chemically modified into various methyl-silyl groups to reduce Si-OH from silica surface to form hydrophobic surface from hydrophilic one, thereby reducing the surface energy without changing its fundamental nature [44].

Xu et al. prepared methyl-modified silica sols with the polymer of methyltriethoxysilane (MTES), the polymer of dimethyldiethoxysiloxane (DDS), and hexamethydisilazane (HMDS) as mono-, di-, and tri-methyl modifiers respectively. By comparing the size and the shape of clusters in three different methyl-modified silica sols, the special nature of the sol was found to be the key to the property of films. Different modal modification of methyl to silica particles led to different cluster fractal structures that influenced the morphology, the porosity of films and consequently the hydrophobic characteristics. It was found that using mono- or di-methyl modified silica sol the film water contact angles were less than 120°, but reached 165° using tri-methyl-modified silica sol. Therefore, as a result of the comparative study, tri-methyl-modified silica sol was found to be more suitable to prepare hydrophobic films [65].

Non-fluorinated, hydrophobic silica coatings were generated by *Jeevajothi et al.* using dimethyldiethoxysilane (DMDEOS), tetraethoxysilane (TEOS) and a silylating agent hexamethyldisilazane (HMDS) using sol-gel process. To improve the mechanical properties of the coating, epoxy modified nano-silica particles were added to various developed sols. It was found that an optimised coating composition of nano-silica particles and sol synthesised from DMDEOS, TEOS and HMDS yielded coatings that exhibited a water contact angle of 125° with pencil scratch hardness of 5B [66].

Hydrophobic surfaces were prepared using a very simple spray coating method by *Jafari et al.* A high static water contact angle of about 154° was obtained by deposition of stearic acid on an aluminium alloy. The hydrophobicity was further increased by incorporating nanoparticles of SiO₂ and CaCO₃ in stearic acid resulting in contact angle of 162°. It was said that such excellent resulting hydrophobicity is attributed to the synergistic effects of micro/nano

roughness and low surface energy. Fig 2.26 shows the SEM images of stearic acid- SiO_2 and stearic acid- CaCO_3 coatings [67].

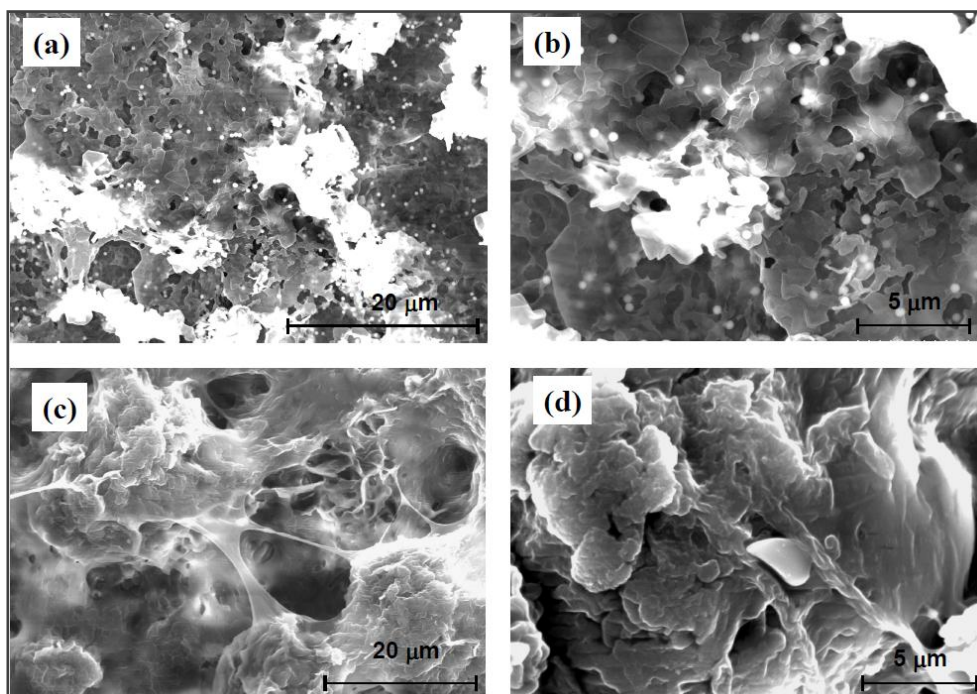


Figure 2.26: SEM images of stearic acid- SiO_2 coating: (a) low magnification, (b) High magnification; Stearic acid- CaCO_3 coating (c) low magnification, (d) high magnification [67]

Gao et al. [68] has reported their recent work of fabricating superhydrophobic surfaces made from SiO_2 -PDMS films. Silica nanoparticles of 7-nm and 14-nm were dispersed in PDMS solutions with variable concentrations respectively to prepare nanoparticles suspensions for application. The measurement showed the contact angle would increase with the concentration of nanoparticles in solution. The composite films based on the SiO_2 -PDMS nano-suspensions resulted in a contact angle greater than 150° attributed to the hierarchical structure resulting in micro and nano scale roughness which played an important role in prompting the superhydrophobic (water-repelling) properties.

A similar kind of work was reported by *Bharathibai et al.* [69] based on incorporation of fumed silica nano-particles in methyltriethoxysilane (MTEOS) sol-gel coatings resulting in enhanced hydrophobicity with improved hardness. Fumed silica particles of size 25–30 nm

were incorporated in the sol and the mixture was spray-coated on glass substrate. It was found that water contact angle (WCA) of the composite coating increased with increase in silica content of the sol mixture with maximum contact angle of 162.5° and a pencil hardness of 5H. Fig 2.27 shows the roughness profile of sol-gel blank and 16.5wt% nano-silica composite coating indicating the increase in height and depth of peaks and valleys after nano-silica incorporation.

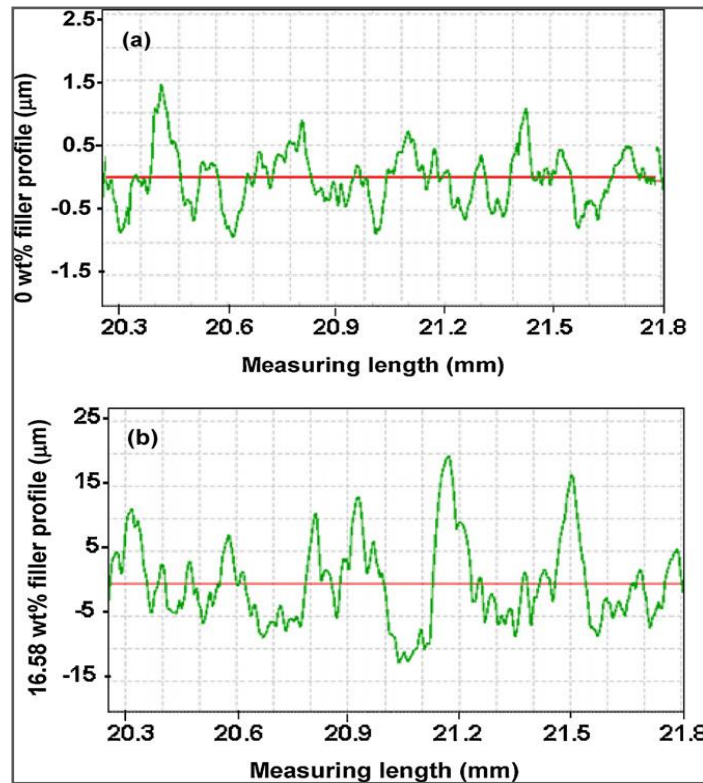


Figure 2.27: Roughness profiles of the (a) sol–gel blank coating; (b) nano- composite coating with 16.58% fumed silica [69]

Schem et al. [70] studied the effect of incorporation of CeO_2 nano-particles in sol–gel coatings, synthesised from organic/inorganic precursors fabricated on the treated AA2024-T3 alloy. Incorporation of 7 or 14 wt. % nanoparticles reduced the anodic current density by 7 orders of magnitude compared with the uncoated alloy during polarisation in chloride solution (Fig 2.28). The nanoparticles-filled coatings did not reveal any pits after polarisation, whereas the passive region for unfilled coatings did not exceed 100 mV from E_{corr} . The coatings containing 7 wt. % CeO_2 nanoparticles resisted exposure in the neutral salt spray test

for more than 2000 h without general corrosion, and reduced corrosion compared with the unfilled coating at an artificial scratch (Fig 2.29).

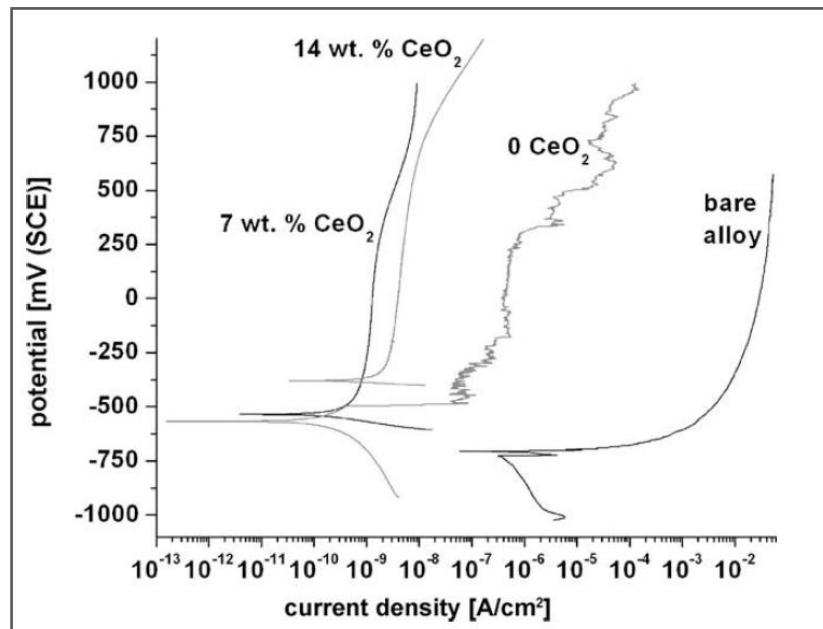


Figure 2.28: Potentiodynamic polarisation behavior of the specimens coated with the sol-gel containing various wt% CeO₂ nano-particles compared with the bare A2024-T3 alloy [70]

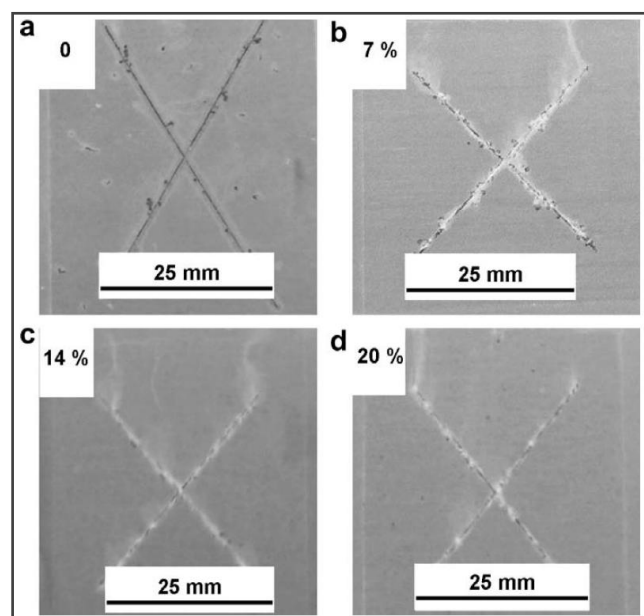


Figure 2.29: Surface appearance of the coated specimens with different CeO₂ nanoparticles contents after salt spray testing for 330 h: (a) without nanoparticles; (b) 7 wt. % CeO₂; (c) 14 wt. % CeO₂; (d) 20 wt. % CeO₂ [70]

Aruna et al. [71] obtained binary micro-nano-structured superhydrophobic coatings by incorporating hydrophobically modified silica nanoparticles in sol–gel matrices prepared with TEOS and MTEOS. The sol–gel processing parameters and the concentration of silica particles in the coating were optimised to prepare superhydrophobic surfaces. The composite coatings showed maximum WCA of 166° and roll-off angle of 2°. The excellent hydrophobicity achieved for nano-composite coatings was attributed to combined effects of multi-scale roughness and hydrophobic nature of methyl groups on HMS-silica particles. Fig 2.30 shows the variation of contact angle with concentration of nano-silica particles in TEOS and MTEOS sol-gel coatings [61].

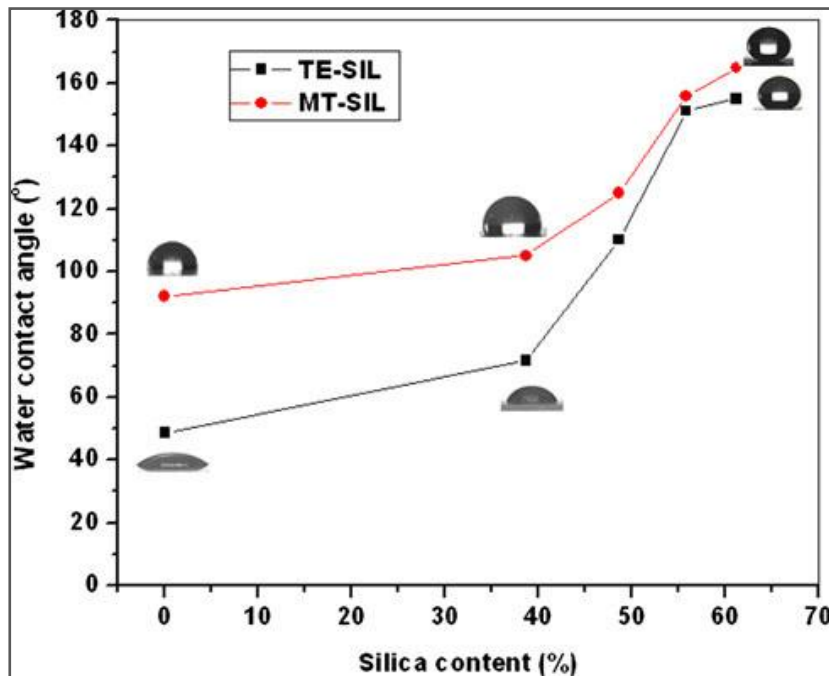


Figure 2.30: Variation of contact angle with concentration of nano-silica particles in TEOS and MTEOS sol-gel coatings [71]

2.4.4. Chemical vapor deposition

Chemical vapor deposition is a technique whereby gaseous reactants can be deposited onto a substrate to form a nonvolatile solid film. The film morphology is mostly dependent on the surface morphology of the substrate, which is usually used as a template. However, through selection of the gaseous reactants and adjustment of the reaction conditions, different

morphologies can be realised on the substrate. Li *et al.* [72] transformed hydrophilic cellulose into superhydrophobic cellulose via chemical vapor deposition followed by hydrolysis and polymerization. First, a sheet of cotton fabric was ultrasonically cleaned in ethanol and in water and dried. Then it was placed in a sealed chamber and exposed to a saturated atmosphere of trichloromethylsilane. Next, the fabric was immersed at room temperature into an aqueous solution of pyridine to hydrolyze the remaining Si–Cl bonds. The fabric was carefully washed with water to remove the excess reagents. Finally, it was treated in an oven at 150 °C for 10 min. Subsequent polymerisation of the Si–OH groups resulted in a nanoscale silicone coating tightly attached to the surface with no changes in morphology and color of the original cotton fabric, as shown in Fig 2.31.

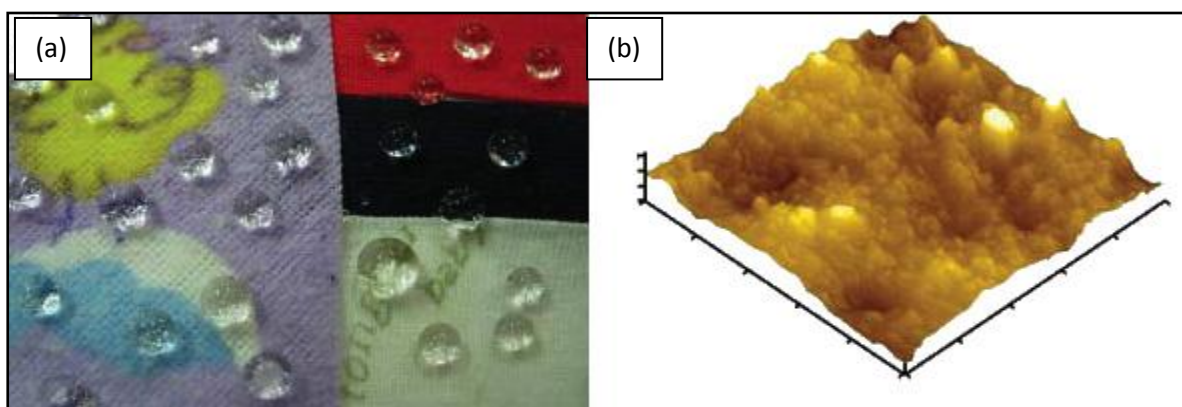


Figure 2.31: Water droplets on the surface of a modified colored cotton fabric (a) and 3D atomic force microscopy image of the modified fiber surface (b) [72]

2.4.6. Hydrothermal synthesis:

Hydrothermal synthesis is a well-known method for the fabrication of micro-scale materials. There has been considerable research on the growth of ZnO materials with different structures on substrates to fabricate superhydrophobic surfaces. As shown in Fig 2.32, this method usually includes two steps. First, ZnO micro/nanostructures are grown in a basic solution of Zn^{2+} on the target substrate, which might have been pretreated by ZnO seeding. Then the as-prepared rough surface is hydrophobised by a layer of polymers or small molecules to obtain a superhydrophobic surface. This wet chemical route could be

applied to a variety of substrates, such as silicon wafers, glasses and even polymer surfaces, regardless of their irregular shapes or curved surfaces. This advantage makes this process favorable for practical applications such as aircrafts, ships and some special decorations [42].

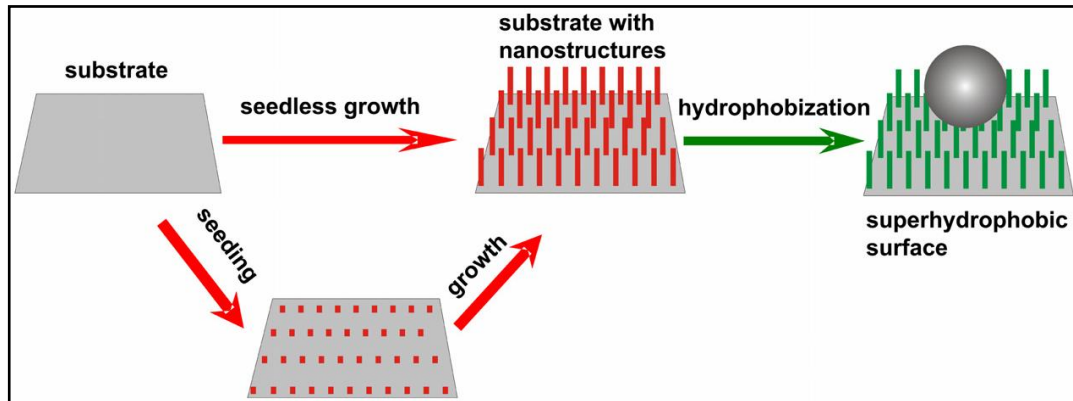


Figure 2.32: Fabrication of superhydrophobic surfaces by hydrothermal growth of nanostructured surface and hydrophobisation [42]

2.5. Common Industrial methods of introducing surface roughness:

Common industrial processing procedures have been used to introduce surface roughness into hydrophobic surfaces. In this paper, four different concepts (stamping, spraying, grinding and sandblasting) are evaluated regarding their applicability for large-scale production of hydrophobic surfaces [60].

2.5.1 Texturing via stamp process:

Several silicone stamps were prepared by casting sandpapers with different roughnesses with liquid silicone (step 1). After curing, the silicon was removed and showed the inverted surface structure of the sandpaper (step 2). By pressing this custom made stamp onto the surface of a previously coated sample a define structure was transferred into the hydrophobic coating (step 3). After curing, a water contact angle of about 125° was measured (Fig 2.33).

After wiping with a paper towel the contact angle retained unchanged. This process can be easily upscale for producing silicon stamps of large size for transferring surface roughnesses into coatings. For roll-to-roll applications, where laminating and lining processes are used, these silicon stamps could be applied onto heatable rolls, allowing surface structuring and curing of the coating in one step.

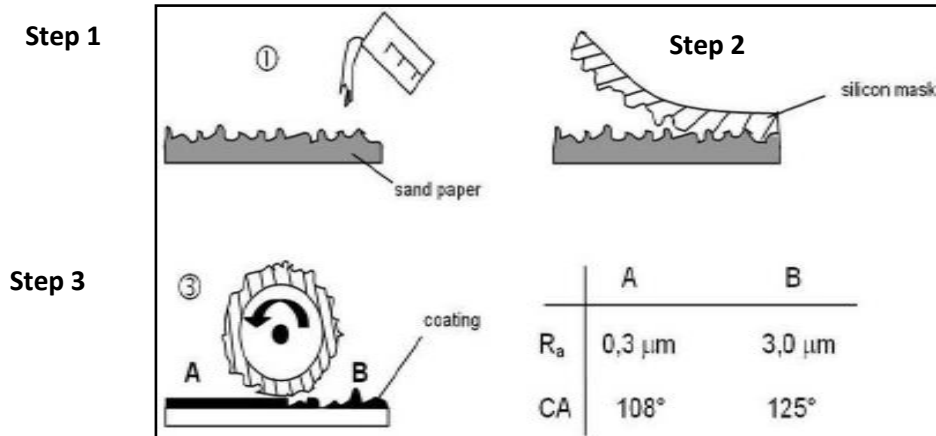


Figure 2.33: Texturing by Stamp Process [60]

2.5.2 Structuring via sandblasting:

Sandblasting is often used to clean large areas from rust or colors and can also use for more geometrically complex shaped substrates. Aluminium substrates and steel substrates were treated with a sandblasting machine. A sand type (ST) of splintered sand, $d(0,9) = 500 \mu\text{m}$ (ST-1) was used. Afterwards the hydrophobic coating was applied by spray coating. The type of sand (ST-1 / ST-2) used the operating pressure (p), distance to substrate and residence time generates characteristic sandblasting structures, which can be used to improve the hydrophobicity of a water-repellent coating. Table 2.3 shows result of treated and coated samples with different sand blasting procedures.

Table 2.3: Result of treated and coated samples with different sand blasting procedures [60]

Substrate	ST	p[bar]	Ra [μm]	CA
Aluminium	1	2	2,5	140°
	1	4	4,5	141°
	1	6	6,0	151°
Steel	1	2	1,0	130°
	1	4	2,5	140°
	1	6	3,5	150°
Aluminium	2	2	1,2	121°
	2	4	2,4	122°
	2	6	3,5	121°
Steel	2	2	0,3	119°
	2	4	0,7	118°
	2	6	1,2	119°

2.5.3 Structuring via grinding:

Grinding is often used to level out surface defects like welding seams or ridges. Steel and aluminium substrates were treated with a grinding machine. Different roughness was obtained by using differently grained sandpapers. Subsequently, the hydrophobic coating was applied by a dip coating process. The roughness and water contact angle of different substrates treated with sandpaper is given in Table 2.4.

Table 2.4: Result of treated and coated samples with different sand papers [60]

Substrate	Sand Paper	Ra [μm] sandpaper	Ra [μm] substrate	CA
Aluminium	-			118°
	1200	5	0,4	117°
	500	7,1	0,6	120°
	120	24,0	2,2	130°
	80	30,0	2,5	130°
Steel	-		0,1	112°
	1200	5	0,4	120°
	500	7,1	0,5	121°
	120	24,0	2,0	125°
	80	30,0	2,2	125°

Using more coarse grained sandpaper a stronger roughening of the substrate was obtained up to 25 μm and a higher water contact angle up to 130°. The same roughness was measured before and after applying the coating material. The same substrate coated by spray coating also did not show any deviation of surface roughness before and after applying the coating solution. Both application methods are suitable for this procedure.

2.5.4 Chemical Etching:

Superhydrophobic surfaces on engineering materials can be prepared via a convenient solution-immersion method. The binary geometric structures at the micro- and nanometer scale bestow superhydrophobic properties on the surfaces [51]. *Mengnan et al.* [73] etched aluminium specimens by immersing in Beck's dislocation etchant. The etchant was prepared by mixing 40 ml of 37 wt % HCl, 12.5 ml of H₂O, and 2.5 ml of 40 wt % HF. The etching time was varied from 5 to 15 s. After etching, the specimens were immediately rinsed ultrasonically with water and dried at 80 °C in air. Etched samples were then subjected to surface fluorination using a solution of fluoroalkylsilane tridecafluorooctyltriethoxysilane, C₈F₁₃H₄Si (OCH₂CH₃)₃ in 3 fold molar excess of water at room temperature for 1 hour at room temperature, and then heat treated at 130 °C for 1 h. The key to the etching technique was the use of a dislocation etchant that preferentially dissolves the dislocation sites in the grains. The etched metallic surfaces, when hydrophobised with fluoroalkylsilane, exhibited superhydrophobic properties with water contact angles of larger than 150°, as well as roll-off angles of less than 10°. Figure 2.13 shows SEM micrograph and contact angle image of water on becks etched aluminium specimen followed by surface fluorination.

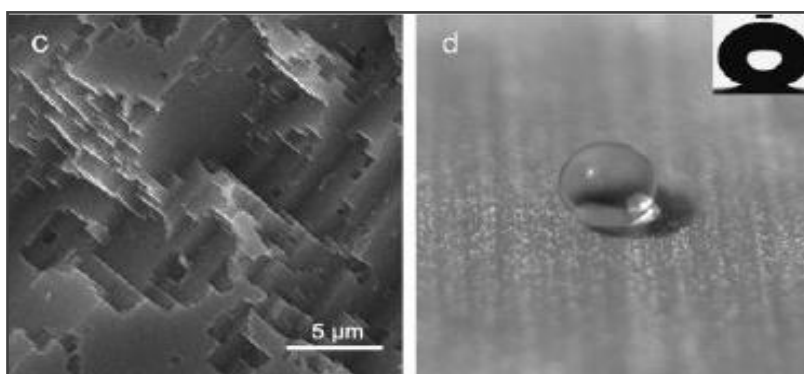


Figure 2.34: SEM micrograph (left) and contact angle image of water (right) on becks etched aluminium specimen followed by surface fluorination [73]

Baitai Qian and *Ziqiu Shen* [74] used nitric acid and hydrogen peroxide mixed-solution system as the etching reagent on the engineering materials to obtain the rough surfaces. Fluoroalkylsilane was used as a hydrophobic material to reduce the surface free energy. The blocks of steel and copper alloy were immersed in the etching solution for several minutes, followed by washing and immersion in a methanol solution of fluoroalkylsilane. After etching and fluorination, the as prepared superhydrophobic surfaces on steel and copper alloy have water CA of $161^\circ \pm 1^\circ$ and $158^\circ \pm 1^\circ$, respectively, as shown in Fig 2.35.

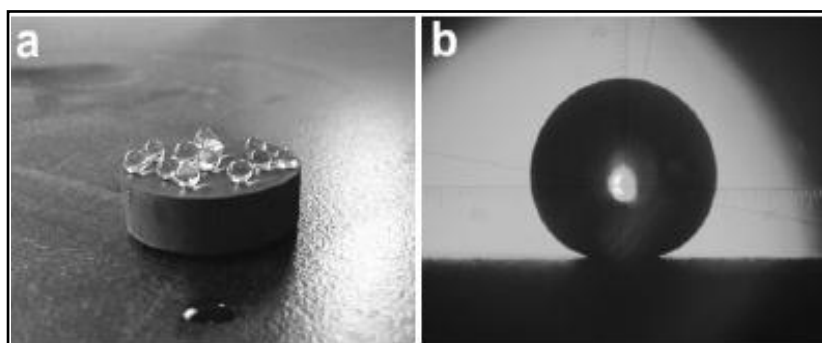


Figure 2.35: superhydrophobic surfaces on s copper alloy having water CA of 161° after etching [74]

2.5.5. Chemical treatment of Aluminium using commercial Boehmite Powder:

Masashi et al. [21] prepared hydrophobic surfaces by use of a method utilizing the sublimation of aluminium acetylacetonate (AACA, $\text{Al}(\text{C}_5\text{H}_7\text{O}_2)_3$). The surface structures were easily varied by changing the composition of the starting materials by this method. According to their work commercial boehmite powder (AlOOH , DISPAL 18N4) and reagent-grade AACA were mixed with ethanol with varying ethanol to boehmite ratios. The suspension was sonicated for 20 min, resulting in the dissolution of AACA into ethanol. The sonicated suspension was coated on pyrex glass plates by spin-coating at 1000 rpm for 10 s and were calcined at 500°C for 20 s. White smoke was generated, and the boehmite films were roughened by the sublimation of AACA during calcination. These coating and calcination procedures were repeated five times to coat the glass plates completely with boehmite. Heptadecafluorodecyltrimethoxysilane was used as a water-repellent agent. The flat glass plate coated with FAS-17 showed a water contact angle of 105.4° (average). The

contact angles on the prepared surfaces were plotted against the boehmite-ethanol ratio (Fig 2.36). It was observed when the boehmite ethanol ratio decreases, the contact angle first increases gradually from 147.1° to 160.9° , became almost constant, and then started decreasing sharply.

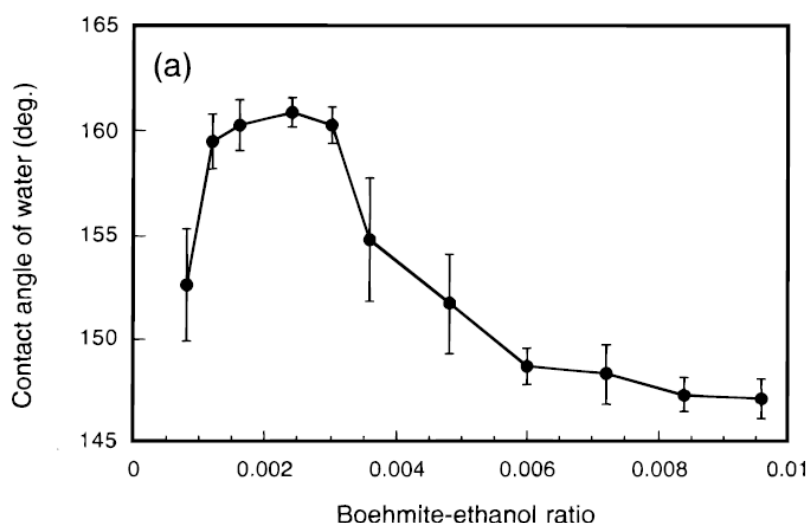


Figure 2.36: Water contact angle on the surfaces plotted against the boehmite-ethanol ratio [21]

Applications of water repellent coatings:

A number of products using the lotus effect are already commercially available or in the process of development. In addition, many patents have been granted for various possible applications of self-cleaning surfaces. Most of these applications use the self-cleaning effect, especially of glasses (for architecture, automotive, optical sensor and other applications), roof tiles and other architectural materials. Additionally, sprays and paints that create clean surfaces (e.g. graffiti-resistant) have been proposed, as well as water-repellent textiles [20].

The prospect of producing surfaces that repel water suggests huge opportunities in the areas of corrosion inhibition for metal components, chemical and biological agent protection for clothing, antifouling of marine vehicles and many other applications. Given their strong water repulsion properties, superhydrophobic coatings are ideal for slowing the breakdown of the native metal oxide layer of metal substrates, and thus the corrosion of the aluminium layer underneath [75]. Due to strong water repellent properties, hydrophobic coatings are ideal for protection of various metals and alloys like copper, zinc, magnesium and aluminium. The development of superhydrophobic aluminium surfaces continues to attract attention because

of the potential anti corrosion properties imparted [76-80], fluid drag reduction [49], no-loss transportation [81], semiconductors, electrical and optical devices [82], air conditioning [80] and marine engineering [83]

Superhydrophobic and self-cleaning coatings have numerous potential applications. Self-cleaning coatings on the satellite dishes, solar energy panels, exterior architectural glass and green houses can be cleaned by an occasional rain shower. The low friction between superhydrophobic surfaces and liquid offers potential applications on piping and boat hulls. The superhydrophobic surfaces also show their applications on antifouling on boats and antisticking of snow for antennas and windows [1]. *Wang et al.* fabricated anti-frosting hydrophobic coatings based upon nano CaCO_3 particles modified by low energy heptadecafluorodecyl trimethoxysilane embedded in ordinary polyacrylate resin. The modification resulted in self-cleaning properties as shown in Fig 2.37 with contact angle of about 155° [84].

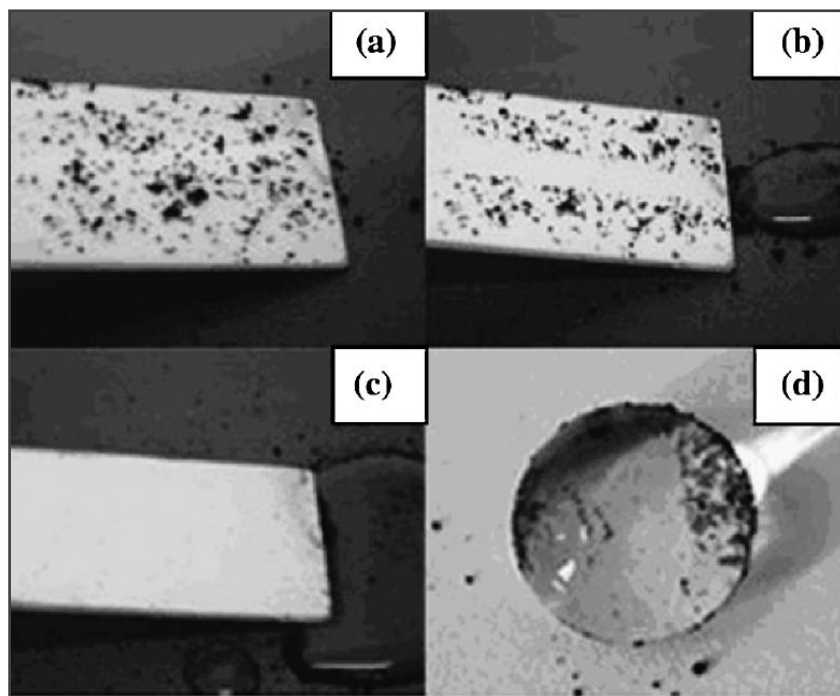


Figure 2.37: Process for removing carbon black powder on the super-hydrophobic surface by water droplets: (a) carbon black spreading on the surface, (b) a droplet rolling through the surface, (c) all carbon black being removed by water droplets and (d) carbon black covering water droplet [84]

The ability of super hydrophobic surfaces to retain air when immersed in water leads to a number of potential applications. One area of application is related to the drag reduction of an underwater vessel (e.g., a submarine). The no-slip boundary condition that states that fluid velocity next to a solid surface is a standard assumption in hydrodynamic problems. It has been argued recently that slip may be present in many microfluidics systems, in particular, due to the presence of an adsorbed layer of nano bubbles. Liquid slip reduces resistance to flow very significantly. Roughness increases the ability of a surface to retain air and form the composite interface and thus reduces water friction with the walls of a channel [4]. Water droplets coming in contact with a super hydrophobic surface (contact angle $>150^\circ$) form nearly spherical beads. The contaminants, either inorganic or organic, on such surfaces are picked up by water droplets or adhere to the water droplet and are removed from the surface when the water droplets roll off, as illustrated in Fig 2.38 [27].

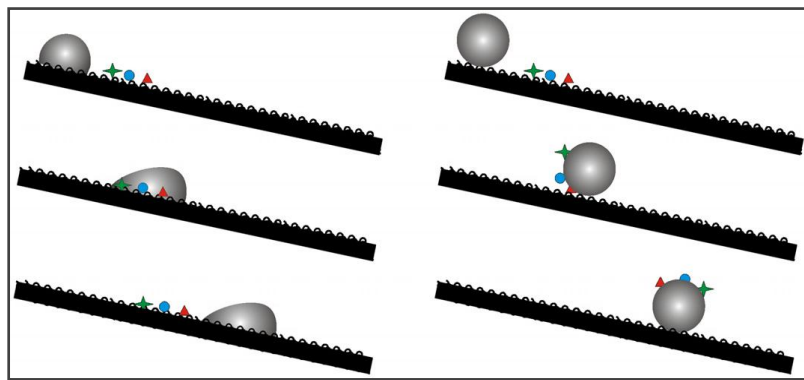


Figure 2.38: Water droplets rolling off substrates with a normal hydrophobic surface (left) and a self-cleaning superhydrophobic surface (right) through dust particles [27].

However, very few products with superhydrophobic surfaces have been developed for the real applications in our daily life. There are many problems to be solved. The first one is the wear resistance. The natural superhydrophobic surfaces such as lotus leaves can be easily repaired, for example, epicuticular wax is secreted by the leaf continuously. However, for most artificial superhydrophobic surfaces, the nano-and micro-textures on them are fragile, and are easily destroyed by impacts, or even by simply rubbing them with a tissue paper [27].

There has been considerable research on superhydrophobic surfaces. However, there have been few reports on the robustness of superhydrophobic coatings and the durability of

superhydrophobicity. There is still much work to be done for superhydrophobic surfaces to be incorporated into commercial products. Besides durability, issues such as large-area production and the availability and price of raw materials should also be taken into consideration. In the future, superhydrophobic surfaces based on novel materials, such as carbon nano-tubes, fullerenes, gold and carbon fibers, might also be produced at a large scale once the price of these materials is reduced. For self-cleaning surfaces, many publications focus only on removing dust by water, which is a complex problem. Firstly, the contamination could contain various components such as fly ash, water slurry, kitchen oil, etc. In this case, washable or oil repellent surfaces are preferable. Secondly, the surface might be contaminated with a smudge and might not function properly until it is removed. A lotus leaf repairs itself after it has been scratched because it has tiny wax crystals on the surface that regenerate. Self-healing materials have been prepared in other fields. In future, the practical applications of self-cleaning or contaminant-free surfaces and the fabrication of self-cleaning surfaces with self-healing superhydrophobicity might be possible. Finally, environmental issues should be taken into account when preparing superhydrophobic surfaces for everyday use. It has been recognised that some fluoro-chemicals and organic solvents have potential risks to human health and the environment and their use should be minimised. Therefore development of non-fluorine eco-friendly self cleaning coatings are focused [27]

After detailed literature survey there appeared to be several gaps which are summarized as follows:

1. Studies reported fabrication of sol-gel coatings using various solvents, whereas in present work focus upon development of water based sol-gel coatings.
2. Shelf life of the coating is the time available to preserve the sol-gel solution before application. Pot life is the time available immediately after mixing the base and hardener. Present work reports the long term shelf life and pot life of the as developed hydrophobic inorganic-organic sol-gel coatings.
3. Though lots of work has been reported to fabricate superhydrophobic aluminium surface using various etchants, corrosion resistance studies of etched aluminium samples after hydrophobic coating application is not reported in several papers. Present work deals with detail corrosion testing of as developed coatings on aluminium surface etched with 10% NaOH solution.

4. Fabrication of hydrophobic aluminium surface requires roughening of aluminium surface prior to hydrophobic coating application. Apart from chemical etching, several sophisticated and expensive methods like laser lithography, plasma etching, ion beam irradiation, PVD and CVD techniques are reported in most of the work to achieve the same. Present work reports various laboratory scale methods like sand paper grinding, sand blasting along with chemical etching to achieve rough aluminium surface.
5. A detailed study is reported on distribution of nano-particles using surface probe microscopy images and a probable mechanism is deduced. Also a clear explanation of mixed state is covered in present work.
6. Multiple utility of the single hydrophobic formulation is not reported in literature. Whereas hydrophobic sol-gel coatings developed on aluminium in present work can be used on various non-metallic substrates like cotton, wood, concrete, glass, paper and cardboard apart from aluminium.
7. Along with multiple utility, multiple application methods are reported in present work. As developed coatings can be applied using any of the application technique like brush coating, dip coating or spray coating to achieve the reproducible results.
8. Robustness of the superhydrophobic coatings fabricated on various substrates in terms of adhesion, nano-indentation, scratch resistance etc is not focused in present work.
9. Hydrophobic coatings are developed keeping the large scale commercial aspect in mind. Hence various commercially viable raw materials are used to develop them. Additives like BYK 333 and BYK 349 were added to the final formulation to improve the applicability and thixotropic properties of the as develop coatings.

Aim and Objective:

The objective of this thesis is to develop hydrophobic inorganic-organic hybrid coatings by water-based sol-gel process which can be achieved by

1. Modification and optimisation of initially developed hydrophilic sol-gel composition by Pathak et.al based upon GPTMS-MTMS-HMMM precursors by various fluoro-alkyl silanes of different chain lengths to achieve low surface energy.

2. Incorporation and optimisation of nano-particles with different surface chemistry, size and surface area to the optimised fluorinated sol-gel system in order to enhance surface roughness of the coatings
3. Creating micro-nano roughness on aluminium using various physical and chemical methods prior to the application of nano-modified fluorinated sol-gel coatings
4. Application of as developed hydrophobic sol-gel nano coatings on various non-metallic substrates
5. Fabrication of non-fluoro sol-gel coating system using long chain hydrophobic alkyl silane to achieve low surface energy followed by application on differentially etched aluminium surface.
6. Structural and morphological characterisation of as developed coatings using FTIR and XPS techniques.
7. Morphological characterisation of as developed coatings using SEM, FEGSEM, EDAX and AFM techniques.
8. Performance evaluation in terms of corrosion resistance of as developed coatings using potentiodynamic polarisation and EIS spectroscopy techniques.
9. Mechanical testing of as developed coatings using nano-indentation, pencil hardness and crosshatch adhesion tests.
10. Life time study of final formulated hydrophobic sol-gel coating using accelerated salt spray, UV weatherometer and humidity exposure tests.

The work mainly focus on obtaining uniform, crack free hydrophobic thin films on aluminium surface followed by various characterizations to ensure the durability and sustainability of as developed coatings concluding with proposed mechanism to deeply understand the role of nano-particle distribution in obtaining enhanced hydrophobic and water repellent properties.

Chapter 3

Experimental Methods

In the present work, GPTMS-MTMS-HMMM based inorganic-organic hybrid sol-gel coatings, developed by *Pathak et al.* [32] were modified to improve their hydrophobic and water repellent properties. Various hydrophobic sol-gel systems were developed on aluminium using combinations of fluoro-silanes of different chain lengths and nano-particles of different sizes in order to achieve coatings with low energy and rough surface respectively. Also non-fluorine sol-gel system was developed using long chain alkyl silane precursor and applied over differentially etched aluminium surfaces. Further effect of roughness on hydrophobic properties of as developed coatings was studied by application of coating on various other rough substrates apart from aluminium.

As developed coatings were applied using brush coating method and cured at optimum temperature for adequate period. Hydrophobicity of various coated systems was determined using contact angle analysis. Structural analysis and surface morphology of coated substrates were analysed using FTIR spectroscopy, SEM and AFM techniques. Corrosion resistance of the coatings was evaluated using potentiodynamic polarisation and impedance spectroscopy. Further coatings were evaluated for their mechanical properties using nano-indentation, crosshatch adhesion and pencil hardness. Fig 3.1 lists the step by step work schedule followed in present work

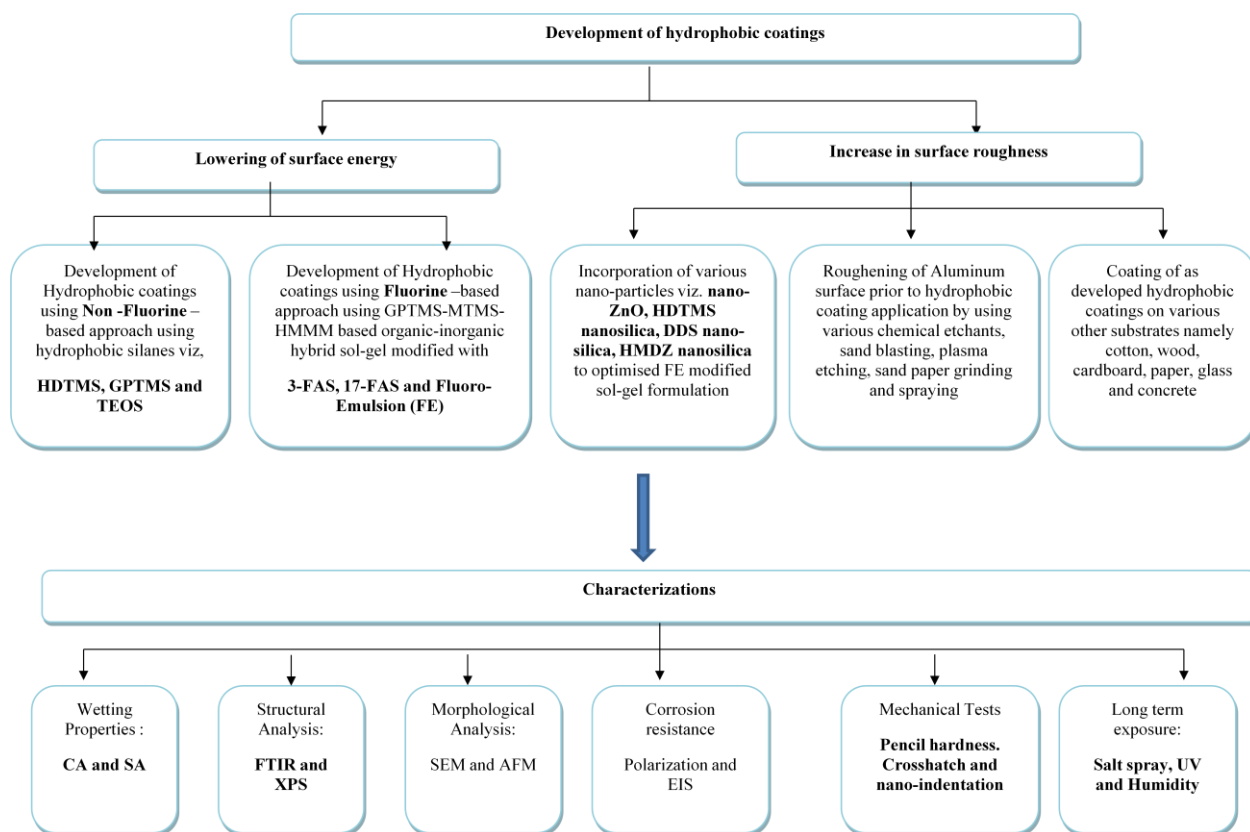


Figure 3.1: Work Schedule

3.1 Materials and Reagents:

Various organo-silanes viz. glycidoxypyriltrimethoxysilane (GPTMS), methyltrimethoxysilane (MTMS), hexadecyltrimethoxysilane (HDTMS) 3,3-Trifluoropropyl-trimethoxysilane (3-FAS), 1H,1H,2H,2H perfluorodecyl-trimethoxysilane (17-FAS) and glacial acetic acid were procured from Sigma Aldrich. Hexamethylmethoxymelamine resin (HMMM) and p-toluene sulphuric acid (p-TSA) were purchased from Cytec Chemicals. BYK 349 was supplied by BYK chemicals. Fluoro emulsion (FE-2000) was commercially procured from Chemguard. Hydrophobically modified nano-silicas namely R972 (DDS –nanosilica) and R-8200 (HMDZ –nanosilica) were purchased from Evonik Degussa. Nano-ZnO and HDTMS modified nano-silica particles were prepared in corrosion Laboratory, Dept of MEMS, IIT Bombay. Aluminium panels used in the present study were purchased from local market and the composition was determined by Inductively Coupled Plasma Optical Emission Spectroscopy (ICP-OES) as shown in table 3.1. Aluminium panels were polished by emery papers of 400

and 600 grit sizes. Cleaned, dried and then etched in 10% NaOH solution for 5 to 10 minutes. Etched samples were washed with running tap water and acetone. Dried and then coated with as prepared sol-gel coating

Table 3.1 Chemical Composition (wt %) of aluminium alloy used in present study

Al	Mn	Si	Cu	Ti	Zn	Fe	Mg
98.37	0.049	0.83	0.060	0.019	0.037	0.60	0.022

3.2 Synthesis of Fluorine-based hydrophobic inorganic-organic sol-gel coatings :

3.2.1 Synthesis of Inorganic-organic hybrid sol-gel coating

GPTMS and MTMS were mixed in a flask in molar ratio of 2:1. To the above mixture 85% of 0.05M acetic acid solution was added. The pH of the above solution measured was neutral. The above mixture was stirred for 3 days continuously at speed of 900 rpm. In this process several condensation and substitution reactions takes place between silanol groups of GPTMS and MTMS resulting in Si-O-Si network formation. To this thick and sticky sol, 30wt% of HMMM of initial silane content was added followed by addition of 1wt% p-TSA which acts as a catalyst to prevent self condensation reaction of HMMM. This resulted in epoxy ring opening reaction and further crosslinking to form 3-dimentional inorganic-organic hybrid network. The mixture was allowed to stir under high shear till a transparent homogenous primary sol was obtained. This prepared sol designated as neat sol was applied on pre-treated aluminium samples using a thin brush and cured at 120°C for 40 min to obtain thin crosslinked sol-gel film with thickness of about 2µm. Fig 3.1 depicts the experimental set up for carrying out the synthesis. A simple flask and stirrer assembly is required for preparation of the coatings developed in the study at laboratory scale.

3.2.2 Synthesis of fluoro-alkylsilanes (FAS) modified sol-gel coatings

The neat sol obtained was hydrophilic when applied on aluminium sample with C.A. of about 70° and was further subjected to hydrophobic modification by blending fluoro-alkylsilanes of different chain length to the neat sol before crosslinking with HMMM. Fig 3.2 shows the schematic diagram of various steps involved in the synthesis of fluorinated sol-gel coatings. Various percentages of 3-FAS and 17-FAS were added to the neat sol-gel and stirred for 15 to 20 minutes to obtain clear transparent coating solution. These fluoro-alkyl groups migrate towards the surface due to their low energy resulting in hydrophobicity. Coatings were applied uniformly on pretreated aluminium samples using a flat thin brush and then cured at 120°C for 40 minutes. Table 3.2 lists various concentrations of fluoro-alkylsilanes used.

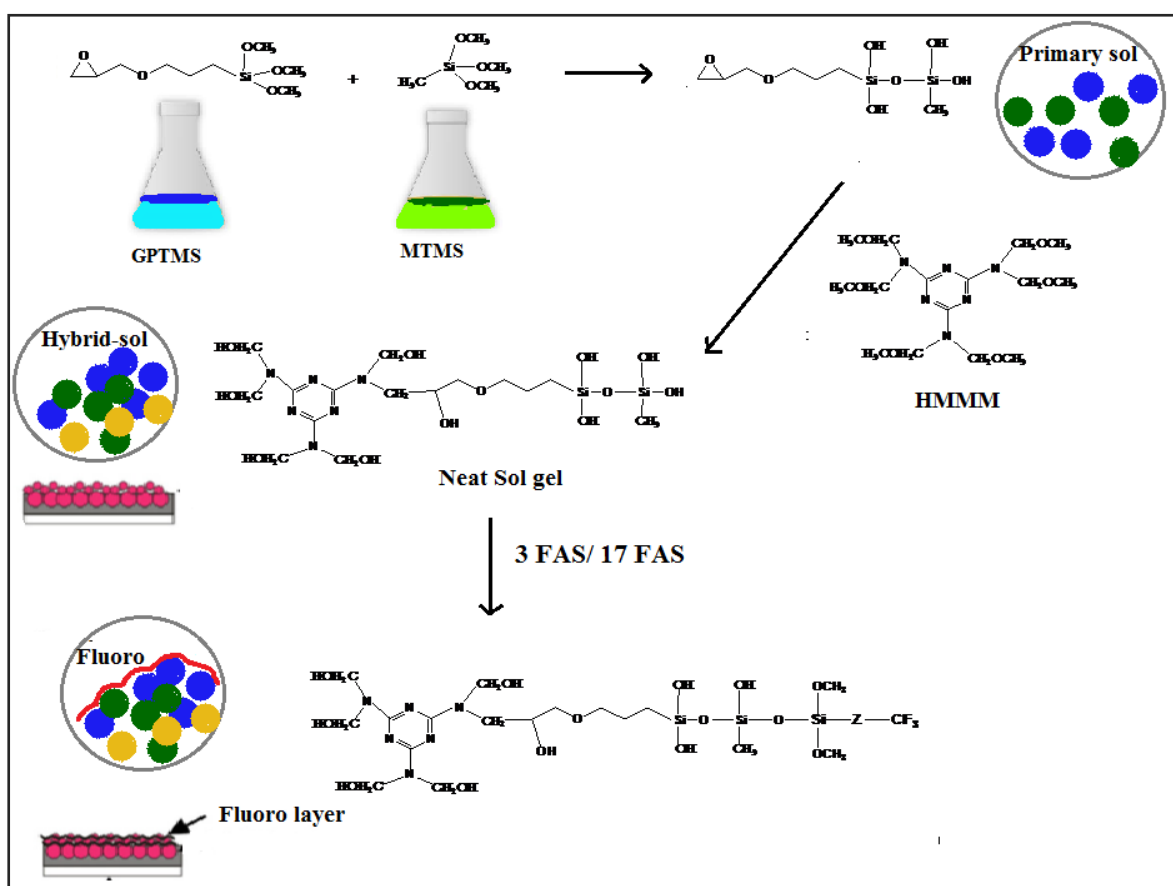


Figure 3.2: Schematic of steps involved in preparation of fluorinated sol-gel coatings

Table 3.2: Composition of various concentrations of 3-FAS and 17FAS modified sol-gel coatings

GPTMS:MTMS (molar ratio)	Concentration of HMMM	Concentration 3- FAS	Concentration of 17-FAS
1:2	30wt%	1wt%	0.5wt%
1:2	30wt%	2wt%	0.75wt%
1:2	30wt%	3wt%	1wt%
1:2	30wt%	5wt%	2wt%

3.2.3 Synthesis of commercial Fluoro emulsion (FE) modified hydrophobic sol-gel coating:

To achieve FE modified sol-gel coatings, FE was chosen as third precursor along with GPTMS and MTMS to obtain a primary sol which was further crosslinked with HMMM. Various concentrations of FE were added to GPTMS and MTMS mixture in molar ratio of 2:1 followed by addition of 0.05M acetic acid solution. The mixture was allowed to stir for 3 days to obtain a hazy whitish solution. After that 30wt% HMMM was added and the mixture was vigorously stirred to obtain a homogenous sol. To this homogenous sol, 0.005 wt% of BYK 349 was added drop-wise under constant stirring. Coatings obtained were then applied uniformly on pretreated aluminium samples using a flat thin brush and then cured in oven at 120°C for 60 minutes. Table 3.3 lists physical properties of the additive supplied by the vendor. Table 3.4 lists various compositions of FE modified sol-gel coatings.

Table 3.3: Physical properties of FE-2000 fluoro emulsion additive

Appearance	Liquid, white dispersion
Ionic Character	Weakly cationic
Density	1.1g/ml at 25°C
Solids Content	35%
pH	3.5-4.5
Flash Point	>220°F, TCC
Odour	Mild
Water Solubility	Dispersible

Table 3.4: Composition of various FE-modified sol-gel coatings

GPTMS:MTMS (molar ratio)	Concentration of HMMM	Concentration of FE
1:2	30wt%	10wt%
1:2	30wt%	20wt%
1:2	30wt%	30wt%
1:2	30wt%	50wt%

3.2.4 Incorporation of other commercial fluoro-additives

To several other commercial fluoro additives were also tried to see their effect on hydrophobicity. Table 3.5 shows the list of various fluoro additives with their optimum concentrations to achieve highest contact angle. It was found that FE-2000 resulted in maximum hydrophobicity with contact angle of 118° and hence was chosen to be best choice for further studies.

Table 3.5: List of various commercial fluoro additives

S.No	Fluoro-Emulsion/Polymer	Wt%
1	FEE-2000 (perfluoro polymer)	30
2	FEE-5000	30
3	Chemguard S-764P	5
4	Chemguard S-550-100	5
5	DuPont Capstone ST-300	15
6	DuPont Capstone ST-200	15
7	Teflon Dispersion	10

3.3 Synthesis of Nano-particles incorporated sol-gel coatings:

After finalizing the fluoro modification with 30wt% commercial fluoro-emulsion (FE), the maximum contact angle achieved was about 118°, which could be attributed to the

substitution of hydrophilic surface –OH groups of neat sol-gel matrix by low energy perfluoro groups. In order to further improve the hydrophobic properties various nano-modified sol-gel coatings were fabricated by incorporation of nano-particles of different size, surface area and surface chemistry to the fluorinated system. This resulted in enhanced surface roughness and therefore, superior hydrophobic and water repellent properties.

3.3.1 Incorporation of Nano-ZnO (size 20-30nm) to optimised 30wt% FE modified sol-gel coating

Nano-ZnO powder used in present study was developed in our own laboratory and consisted of 20-30 nm of size. After obtaining GPTMS-MTMS-FE crosslinked sol, previously stirred for 3 days, different concentrations of nano-ZnO viz 1wt%, 2wt%, 3wt% and 5wt% of total silane content were added to the sol. To achieve maximum dispersion the nano-ZnO powder was grinded thoroughly before adding to the sol. The grinded nano-powder was then ultrasonicated for 15 to 20 min, while keeping the sol in an ice bath. Ice bath is mandatory to dissipate the heat generated during the ultrasonication. This heat can lead to extensive gelling of the sol resulting in wax like sticky solution which is difficult to apply on the Al surface. After that, 30wt% HMMM was added and stirred vigorously to obtain a homogenous thin and whitish sol-gel. As fabricated nano-ZnO –FE composite sol-gel coatings were then applied on pre-treated Al panels by brush coating and cured at 120°C for 40 min. The nano-particles after curing of the coating were supposed to enhance the surface roughness of the coatings which is being discussed ahead in the report. Fig 3.3 shows the image of nano-ZnO powder used in present study.



Figure 3.3: Nano-ZnO powder (size 20-30 nm) used in present work

3.3.2 Incorporation of various hydrophobically modified nano-silica to optimise d 30wt% FE modified sol-gel coating:

After using nano-ZnO particles, optimised FE coating formulation were modified by incorporation of three types of hydrophobically modified fumed-silica particles (Fig 3.4)

1. Hexadecyltrimethoxysilane (HDTMS) modified fumed silica
2. Dichlorodimethylsilane (DDS) modified fumed Silica
3. Hexamethyldisilazane (HMDZ) modified Fumed silica

GPTMS-MTMS-FE sol was obtained as described earlier. Various nano-silica particles were ultrasonicated at different loading levels (table 3.6) to the fluorinated sol in order to achieve high surface roughness. Due to the hydrophobic modification the nano-silica particles exhibited non-polar behaviour and were sparingly soluble in water-based sol. Hence, the small amount of dispersing agent namely BYK 333 was added which helped in emulsification of non-polar silica nano-particles. Ultrasonication was carried out from 20 min to 40 min depending upon the size and concentration of the nano-silica particle. The ice bath was required to dissipate the heat generated during the ultrasonication. Further the addition of 30wt% HMMM leads to homogenous thin and whitish sol. As fabricated nano-silica –FE composite sol-gel coatings were then applied on pre-treated Al panels by brush coating and cured at 120°C for 40 min. Table 3.7 lists the physical properties of commercially procured DDS nano-silica and HMDZ nano-Silica particles. However, HDTMS nanosilica particles were prepared in our own laboratory.



Figure 3.4: Image of a) HDTMS nano-silica, b) DDS nano-silica and c) HMDZ nano-silica

Table 3.6: Composition of various nano-particle modified sol-gel coatings

GPTMS:MTMS (molar ratio)	Concentration of HMMM	Concentration of FE	Concentration of HDTMS nano-silica (20nm)	Concentration of DDS nano- silica (15nm)	Concentration of HMDZ nano-silica (7nm)
1:2	30wt%	30wt%	0.5wt%	1wt%	1wt%
1:2	30wt%	30wt%	1wt%	2wt%	2wt%
1:2	30wt%	30wt%	1.5wt%	3wt%	3wt%
1:2	30wt%	30wt%	2wt%	5wt%	5wt%

Table 3.7: Specifications of DDS, HMDZ and HDTMS nano-silica particles

Characteristic properties	DDS nanosilica	HMDZ nano-silica	HDTMS nano-silica
Nature	Hydrophobic	Hydrophobic	Hydrophobic
BET surface area (m ² /g)	115±10	160±25	85±20
Primary particle size (nm)	16	7	20
Colour	White	White	White
Odour	Odourless	Odourless	Odourless
pH	3.6-5.5	>=5	4-5
Tapped density (g/cm ⁻³)	Approx. 50	Approx. 150	-
Water solubility	Insoluble	Insoluble	insoluble

3.3.3. Synthesis of HDTMS Modified Fumed Silica particles:

4 gm of hydrophilic fumed silica namely Aerosil 200 was dispersed in toluene and ultrasonicated for about 30 min till the transparent solution was obtained. 1 gm HDTMS was added drop-wise at 80°C under magnetic stirring. Subsequently the mixture was refluxed at 110 °C for 6 h. Finally, the product was obtained when centrifuged and washed repeatedly in toluene and dried under vacuum overnight at 80 °C. The synthesis of hydrophobic silica involves functionalizing of nanosilica with hexadecyltrimethoxysilane (HDTMS) as described in Fig. 4.21. The excess amount of HDTMS was used to obtain complete encapsulation of silica nano-particles with HDTMS. This ensures the silanol groups of nano-silica were completely reacted with the alkoxy-silane groups of HDTMS.

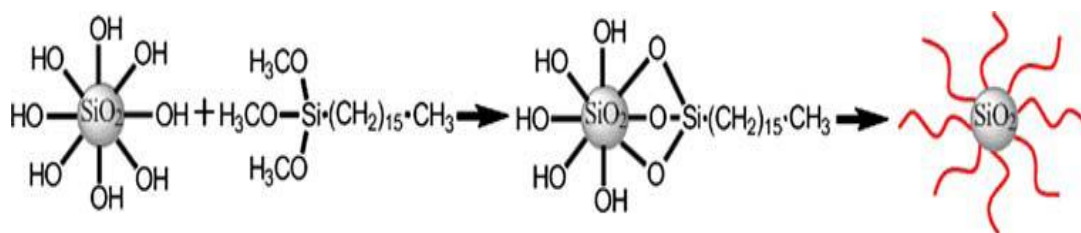


Figure 3.5: Schematic formation of HDTMS modified hydrophobic nanosilica [85]

3.4 Synthesis of Non-fluoro sol-gel coatings

Various formulations of sol-gel coatings were made with different concentrations of GPTMS, HDTMS and TEOS. These were represented as Sol A, B, C, D and E as given in Table 3.8 which also lists various concentrations of HDTMS, GPTMS and TEOS. Ethanol was added to this mixture and allowed to stir for 10 minutes at speed of 400 rpm. After 10 minutes, 18 ml of 50 % acetic acid was added drop wise to adjust the pH upto 3. Further, the stirring was continued for 8 hours till a slight hazy solution was obtained. All these preparation were carried out at room temperature. Aluminium panels, with smooth finish were used and were etched using various chemical etchants to create surface roughness. This was followed by the application of HDTMS modified sol-gel coatings using brush, followed by baking at 120°C for one hour. Details of various etchants used are as follows:

a) **10% NaOH solution** - Aluminium panels were first prepared by polishing with emery papers of 400 and 600 grades, cleaned, dried and then etched in 10% NaOH solution for 5 to 10 minutes. Etched samples were washed with running tap water and acetone, dried and then brush coated with as prepared sol-gel coatings.

b) **Krols reagent** - Krolles reagent was prepared by mixing 40 ml of water, 5 ml nitric acid, 3ml hydrochloric acid and 2 ml hydrogen fluoride. Bare aluminium panels were dipped in the as prepared Krols reagent for 1 minute. Etched samples were washed with water and acetone and brush coated with various HDTMS sols.

c) **Becks reagent** - Becks reagent was prepared by mixing 40 ml hydrochloric acid, 12.5 ml water and 2.5 ml hydrogen fluoride. Bare aluminium panels were etched for 5 seconds and brush coated with various HDTMS sol.

Table 3.8: Various formulations of HDTMS, GPTMS and TEOS based sol-gel coatings

Formulations	GPTMS (ml)	HDTMS (ml)	TEOS (ml)
Sol A	0.5	1.5	8
Sol B	1	3	8
Sol C	1	3	6
Sol D	2	2	6
Sol E	1	3	12

3.5 Characterisation of as developed hydrophobic sol-gel coatings:

3.5.1: Wettability of the coatings:

The hydrophobicity was measured by determining *water contact angle* (WCA) and *sliding angle* (SA) of water droplet placed on various coated substrates. WCA was measured using the contact angle goniometer equipped with CCD camera (Model OCA15EC, make: Dataphysics) at room temperature. A water droplet of volume approx. 5 μ L was allowed to fall on the coated surface using a micro-syringe and the contact angle θ was measured using Laplace fitting correction software.

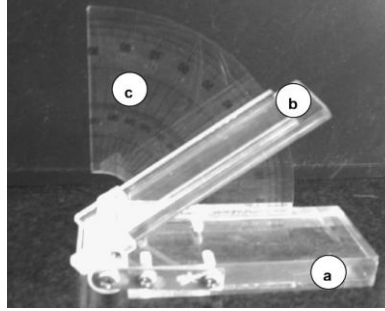
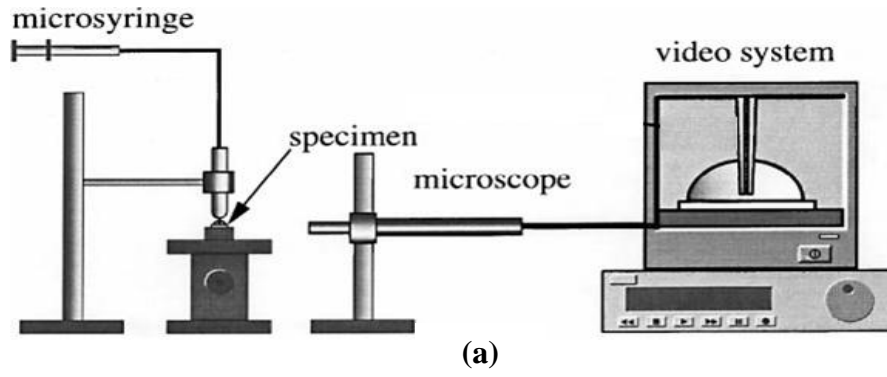


Figure 3.6: Schematic diagram of (a) contact angle goniometer and (b) Movable platform for measuring SA [86]

The contact angle was measured at 4 different spots on each sample and the average value was reported as contact angle. The sliding angle (SA) was determined, placing a droplet of about 15 μ L volume on a tiltable horizontal platform. The angle, where the droplet started sliding defined the SA of the coating. Fig 3.6 shows the schematic diagram of apparatus for measuring WCA and SA.

Theoretically the contact angle can be measured using Young's equation

$$\gamma_{SL} = \gamma_{SV} - \gamma_{LV} \cos \theta$$

Where,

γ_{SL} is the interfacial free energy between the bare/coated Al and the water,

γ_{SV} is the surface free energy of the bare/coated Al in equilibrium with water vapour

γ_{LV} is the surface tension of the water in equilibrium with its own vapour and

θ is the contact angle

3.5.2 Structural analysis of various modified sol-gel coatings:

Fourier transform infrared (FTIR) spectroscopy was used to characterize the structure of the neat sol-gel and various modified sol-gel coatings, using a Perkin Elmer ATR spectrum 100 FTIR spectrometer, at a resolution of 4 cm^{-1} for 32 scans. It was one of the useful technique to qualitatively determine the extent of hydrophobic modification by comparing the $-\text{OH}$ spectra of modified and unmodified sol-gel systems. Also the extent of crosslinking was indicated by comparing the IR spectra corresponding to Si-O-Si bonds.

X-ray photoelectron spectroscopy (XPS) analysis was performed with a MULTILAB from Thermo VG Scientific ESCA spectrometer using the Al K α X-ray source. The calibration of the binding energy of the spectra was performed with the C 1s (284.6 eV) peak. This technique helped in quantitatively measuring the extent of low surface energy fluoro-groups on the coated surface by comparing the F 1s and F KL₂₃L₂₃ bands.

3.5.3 Surface Morphology of various modified sol-gel coatings:

The microstructure of various films was closely observed by using *scanning electron microscopy* (SEM) (Model no.S3400, Hitachi). The technique proved to be a useful tool in studying the distribution mechanism of various nano-particles and therefore correlating with various hydrophobicity models. Since the as deposited coatings were very thin, the approximate thickness of the film was determined using *Field Emission scanning electron microscopy* (FEGSEM), which is more sophisticated and advance technique than conventional SEM and closely magnify the nano-scale structures in the film. *Electron Diffraction X-ray* (EDAX) analysis was carried where elemental distribution is assessed by using X-rays. This technique helped in determining the elemental distribution of groups like fluorine, Zn and Si on the coated surface.

Atomic force microscopy (AFM) (Model Smart SPM 1000, make: AIST-NT) was used to examine the surface topography along with surface roughness (RMS) in tapping mode. Images were further analysed using software AIST 3.3.60 and Ipro 3.0.3 to obtain roughness parameters like section profiles, height and depth of several protrusions and magnitude of

agglomeration. These parameters helped in proposing a suitable mechanism of distribution of various nano-particles used in present study.

3.5.4 Corrosion resistance of various modified sol-gel coatings

Potentiodynamic polarisation and *Electrochemical Impedance Spectroscopy (EIS)* was carried out using potentiostat (Autolab-Metrohm) to evaluate the protective properties of various sol-gel coatings. A three-electrode system was used, in which the coated sample acted as the working electrode, a saturated calomel electrode (SCE) was used as the reference electrode and a platinum electrode as the counter electrode. 1cm² of the coated substrate was exposed in 3.5 % sodium chloride (NaCl) aqueous solution for 30min allowing the system to be stabilised. Potentiodynamic polarisation curves were subsequently measured with respect to the OCP in range of -2V to 2V at scan rate of 2mV/s. The EIS test was performed in the frequency range from 0.1Hz to 10⁶ Hz, with a sinusoidal AC perturbation of 10 mV amplitude coupled with the open circuit potential. All samples were immersed in 3.5% NaCl solution for 30 min before all the impedance measurements.

3.5.5 Mechanical Properties of various modified sol-gel coatings:

Adhesion of the coating layer with the substrate was assessed according to the ASTM D3359 standard test method using *Cross Hatch Cutter*. In this test, eleven cuts were made in two directions using the cutter at right angles to each other to form a grid of small squares. A pressure-sensitive adhesive tape was applied over the lattice and removed by pulling in a single smooth action. Adhesion was then assessed by comparing the fraction of coating removed from grid of squares against the ASTM standard ratings. Hardness and scratch resistance of the coating were measured using *Pencil Hardness Tester* according to ASTM D 1522. The pencil hardness test is a constant-load scratch test. It uses pencil leads of different hardness grades as the scratch stylus. The hardest pencil grade that does not cause damage to the coated specimen is considered as the pencil hardness of the coating.

To measure the hardness of the coatings *nano-indentation* tests were carried out for various modified sol-gel coated panels using a Hysitron Inc Minneapolis USA (Model no. TI-900). While indenting the coated surface a load vs. displacement graph was recorded. The

measurements were conducted in displacement-controlled mode; i.e., a certain indentation depth was set, and the required indentation force was measured as function of indentation depth. The maximum displacement was set in the range from 50 to 1000 nm.

3.6 Characterisation of various nano-particles:

Various nano-powders were investigated by *Transmission Electron Microscopy* [TEM, Philips CM200 electron microscope] to determine the average particle size followed by determination of *BET surface area*

3.7 Accelerated Life time tests for finally formulated hydrophobic sol-gel coating

Al samples coated with final sol-gel formulation were exposed in *salt spray* conditions as per ASTM B117 specifications i.e. the coated substrates were exposed to a salt fog chamber having 3.5wt% aqueous NaCl solution at temperature of 35 ± 1.7 °C. Salt spray test provides information about the nature of failures like blisters, rusting or cracking and delamination of film. Accelerated weathering of coated specimen was carried out to simulate outdoor weathering using combination of UV light and water condensation (ASTM-G63). The coated panels exposed in *UV-weatherometer* were characterised for color change (dE) and gloss retention (dG) using a spectrometer (BYK-Gardener Spectrometer equipped with Color-Lab Quality Control software. Further coated sample was exposed in *Humidity chamber* as per ASTM to study the effect of humid environment on water-repellent nature of the coatings.

Chapter 4 - Part I

Results and Discussions

This chapter consists of a few important characterisation reproduced for GPTMS-MTMS-HMMM based coating on Al, designated as neat sol, which was developed by *Pathak et al.* [32] using sol-gel process. Further, the obtained neat sol was modified for achieving superior hydrophobic properties by either lowering of surface energy or increasing surface roughness. Lowering of surface energy was achieved by modification of neat sol with various fluorine based compounds differing in number of fluorine atoms. Hydrophobicity of fluorinated coatings was further enhanced by incorporating various nano-particles varying in size, surface area and surface chemistry which is discussed in part II of this chapter. Furthermore, non-fluorine based sol-gel composition was also developed on differentially etched Al surfaces and discussed in part III. Hence, following sections consist of detailed characterisation results for various fluoro and non fluoro based sol-gel coating systems modified with various nano-particles followed by general discussion about various theories and probable mechanisms of hydrophobic behavior of as developed hydrophobic hybrid nano-composite coatings.

4.1 Characterisation of GPTMS-MTMS-HMMM based neat sol-gel coating

4.1.1 Structural analysis of neat sol-gel coating

The chemical structure of neat sol-gel coating was deduced with the help of *FTIR spectroscopy*. The absorbance spectra as shown in Fig 4.1 consists of all the major peaks contributing to GPTMS, MTMS and HMMM moieties confirming the effective crosslinking

of the precursors [30-32]. The broad peak around 3524 cm^{-1} is attributed to surface -OH groups which are mainly responsible for the hydrophilic nature of the neat sol-gel coating. The dual peaks around 2945 cm^{-1} and 2845 cm^{-1} are probably due to -CH_3 and -CH_2 stretching vibrations coming from GPTMS, MTMS and HMMM moieties. A sharp band appearing at 1562 cm^{-1} is attributed to C-N stretching associated with HMMM structure. The small bands appearing near 1484 and 1342 cm^{-1} can be associated with -CH_2 bending vibrations and -CH stretching vibrations due to epoxide ring of GPTMS. Further the peak at 1020 cm^{-1} is due to Si-O-CH_3 bonds coming from MTMS and GPTMS. Hence, from the FTIR spectra of the neat sol-gel a crosslinked inorganic-organic sol gel structure was confirmed.

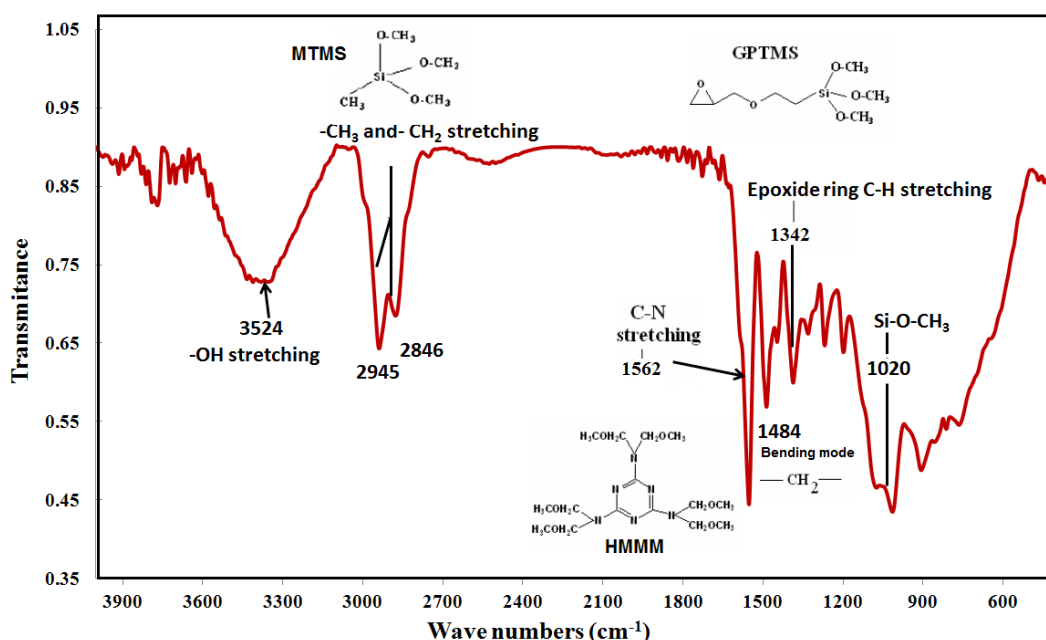


Figure 4.1: FTIR spectrum of neat sol-gel coating

4.1.2 Wettability of neat sol-gel coating

The neat sol-gel coated aluminium substrate was found to be hydrophilic with average contact angle of about $70\text{-}75^\circ$ (Fig 4.2). As discussed earlier, hydrophilicity could be attributed to presence of polar -OH groups on the surface of the coating which were responsible for high surface energy and attraction of water molecules. Due to the acidic hydrolysis of -OCH_3 groups followed by several condensation reactions, large number of $\text{-$

Si-OH groups were generated below and above the sol-gel matrix [30-32]. The –Si-OH groups below the matrix formed covalent bridges with the metal-OH groups and imparted excellent adhesion to the coatings. However, OH groups above the sol-gel matrix were responsible for increasing the surface energy which resulted in spreading of water droplet when poured on it. The high surface tension of the precursors used could be another probable reason for hydrophilicity of neat sol gel coating. The critical surface tension values reported for MTMS and GPTMS are 22.5 dyne/cm² and 42.5 dyne/cm² respectively, which are much higher to obtain hydrophobic properties. Further the curing of GPTMS with HMMM resulted in opening of epoxy ring and additional –OH groups responsible for hydrophilicity. Hence, the neat sol-gel was hydrophobically modified by replacing surface hydroxyl groups with low energy groups using fluoro -alkylsilanes, per-fluoro polymers and long chain alkyl silanes.

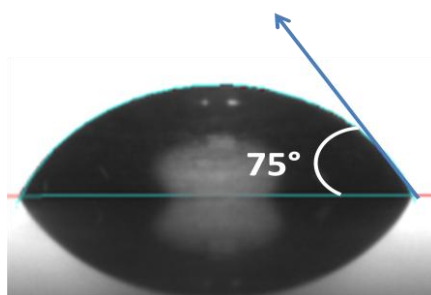


Figure 4.2: Contact angle image of neat-sol gel coated Al substrate

4.1.3 Morphological Analysis of neat sol-gel coating

As seen from Fig 4.3 (a), the *SEM* image of neat sol gel coated sample consisted of smooth profile which is responsible for the spreading of water. This smooth profile was due to small surface roughness of 3nm obtained from AFM technique, according to which the surface topography of neat sol-gel consisted of small protrusions attributed to its three dimensional inorganic-organic hybrid structure (Fig 4.3 (b)). These protrusions probably consist of –OH groups responsible for generating high energy surface. Hence, both the smooth profile with low value of surface roughness and high surface energy confirmed the hydrophilic behavior of the neat sol-gel coating with contact angle of ~75°.

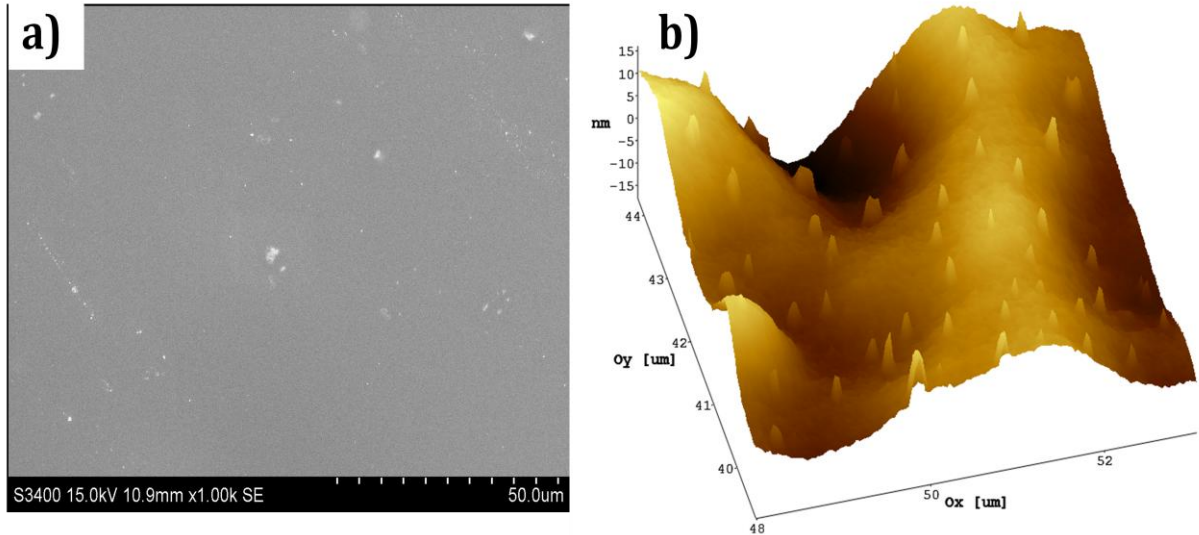


Figure 4.3: a) SEM image and b) AFM image of neat sol-gel

4.1.4 Corrosion resistance of neat sol gel

The corrosion resistance analysis of the neat sol-gel coated substrate was carried out using potentiodynamic polarisation and EIS studies. The coating was applied on Al substrate etched in 10% NaOH solution for better anchoring and adhesion of the coating. As per Fig 4.4, the unetched Al showed the characteristic passive window and sustained lower current density of about $2 \times 10^{-5} \text{ Acm}^{-2}$ as compared to etched specimen with E_{corr} value of -1.2 V (Table 4.1). Etched specimen showed unusual polarisation behavior, with current density rapidly increasing at potentials above its respective E_{corr} by one order of magnitude.

Table 4.1: Potentiodynamic and EIS parameters of bare Al and neat sol-gel coating

Substrate	E_{corr} (V)	Current Density (A/cm^2)	Impedance (Ωcm^2)
Pure Al	-1.19	2.42×10^{-5}	2.76×10^3
Etched Al	-1.34	2.15×10^{-4}	1.02×10^3
Neat sol-gel	-0.89	3.05×10^{-5}	7.74×10^3

Hence the alkaline treatment effectively destroyed the passive window of the bare Al resulting in drastic decrease in corrosion resistance. The influence of neat sol-gel coating upon etched samples was obvious, with a positive shift in E_{corr} value upto -0.89 V arising as a

result of the stifling of the anodic reaction kinetics. The corrosion resistance of the neat sol-gel coating was attributed to the dense inorganic-organic hybrid structure of the coating which provided effective barrier protection from the corrosive electrolyte[87].

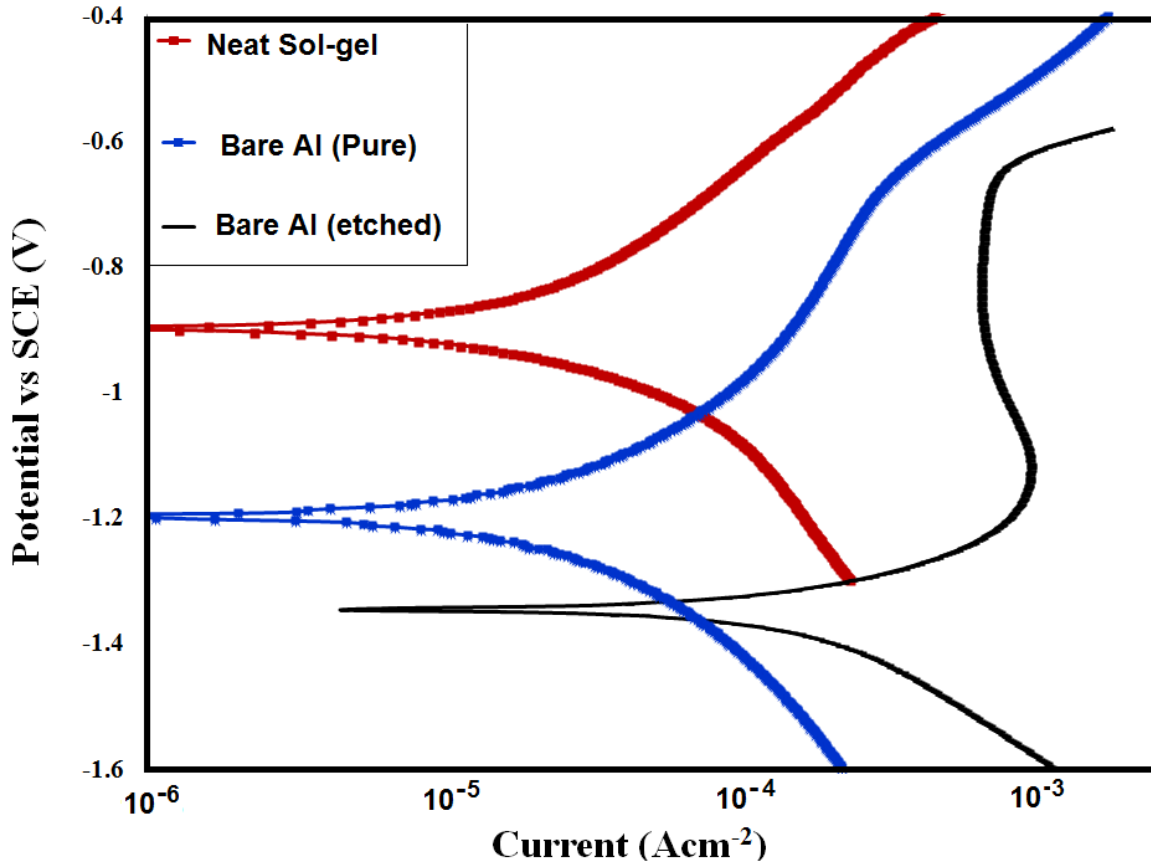


Figure 4.4: Tafel plots of neat sol-gel, etched and unetched Al substrate.

Similar trend was obtained from the EIS analysis as shown in Fig 4.5. The Neat sol gel coating showed higher impedance $|Z|_{0.01\text{Hz}}$ value of $7.74 \times 10^3 \Omega\text{cm}^2$ than both unetched and etched specimens with impedance value of 2.76×10^3 and $1.02 \times 10^3 \Omega\text{cm}^2$ respectively, indicating corrosion protection efficiency of the neat sol-gel coating. Since the neat sol-gel and as developed various modified sol gel coatings were applied on etched specimens, polarisation and bode plots of etched Al were used as reference in further studies. Following sections consist of detailed results and discussion of various modified sol-gel coatings and their hydrophobic behavior.

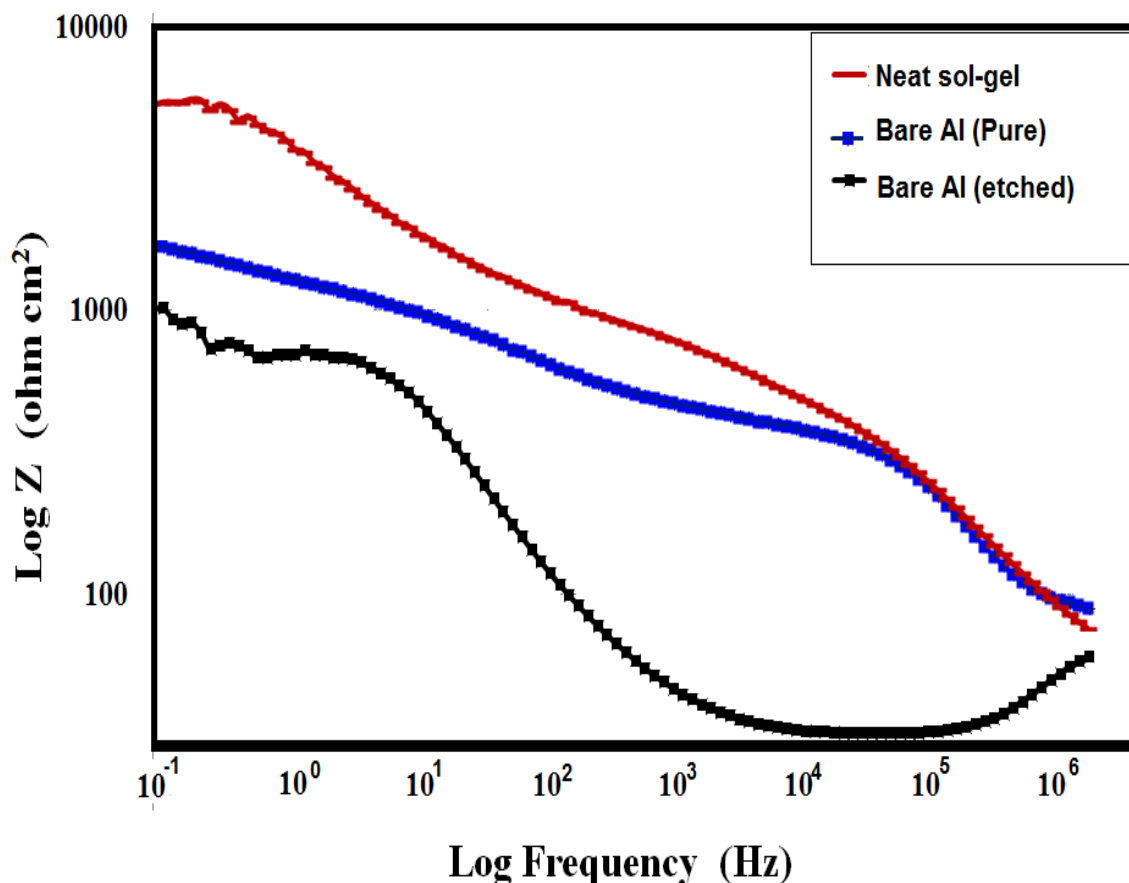


Figure 4.5: EIS plot of neat sol-gel, etched and unetched Al substrate

4.2 Characterisation of 3, 3-Trifluoropropyl-trimethoxysilane (3-FAS) incorporated sol-gel coatings:

4.2.1 Wetting properties of 3-FAS modified sol-gel coatings:

Hydrophobicity of the coatings was determined using WCA analysis. Fig 4.6 shows the variation of contact angle with various concentrations of 3-FAS. It was found that contact angle increases drastically with incorporation of 3-fluoro-silane as hydrophobic additive. This could be attributed to lowering of surface energy due to migration of fluorinated species toward the air/film interface and thereby increasing the hydrophobicity of the coatings [49]. The neat sol-gel coated substrate showed a contact angle value of only 70° indicating the hydrophilic nature of the sol-gel network formed from GPTMS-MTMS and HMMM due to large number of polar OH- groups on the surface responsible for attraction of water. However

after modification of the neat sol with 3-FAS some of the surface hydroxyls groups were replaced by electronegative $-\text{Si}-\text{CF}_3$ groups leading to decrease in interfacial energy and increase in water repelling properties. The fact was supported by FTIR spectra of neat and 3-FAS fluorinated system. Contact angle value of 100° was obtained for 2wt% modification whereas the higher concentrations of 3-FAS showed decrease in contact angle attributed to lower surface roughness at higher loading level which is discussed under SEM and AFM characterizations section.

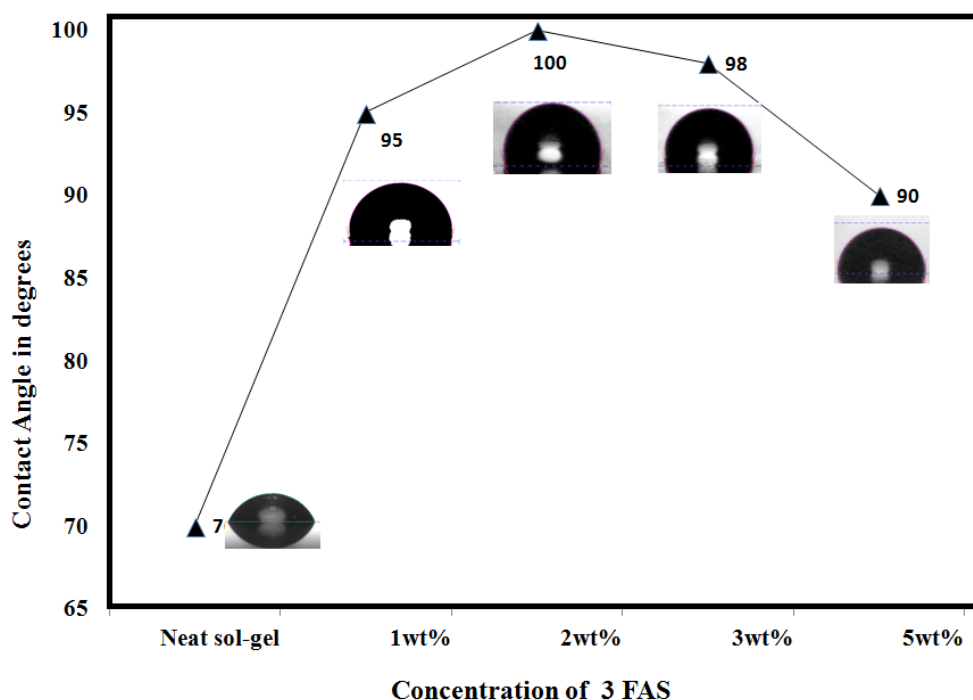


Figure 4.6: Variation of contact angle with different concentrations of 3-FAS

4.2.2 Morphological Analysis of 3-FAS modified sol-gel coatings

Surface roughness is another important factor along with low energy for achieving hydrophobic properties. *SEM* images of different percentages of 3-FAS modified sol-gel coatings are shown in Fig. 4.7. The smoother surface of neat sol-gel coated sample as compared to modified ones was responsible for spreading of water droplets resulting in hydrophilic contact angle of 70° . However, the SEM micrographs of 2wt% and 3wt% 3-FAS formulation resulted in uniformly distributed microspheres of diameter ranging between $5\mu\text{m}$ - $10\mu\text{m}$. Such micro-scale roughness supported the higher value of contact angle of $98-100^\circ$ at 2wt% and 3wt%. Further the higher surface roughness is supported quantitatively by

determination of root mean square (RMS) roughness values using AFM analysis. At higher percentages the micro-sphere profile diminishes leading to poor hydrophobicity and wetting of the surface supporting the decrease in contact angle value.

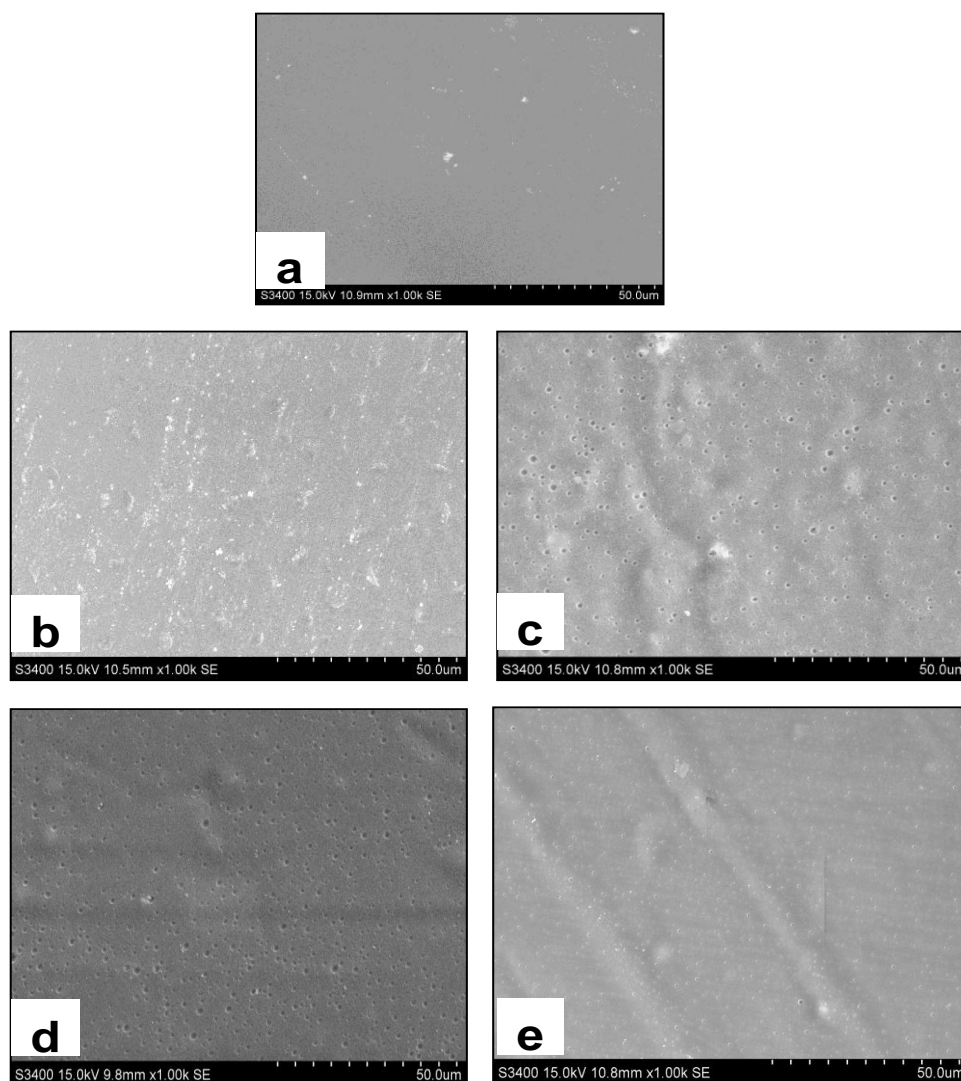


Fig. 4.7: SEM images of a) Neat, b) 1wt%, c) 2wt%, d) 3wt% and e) 5wt% of 3-F.A.S. modified sol-gel coated aluminium samples

AFM technique was further used to study the topography of the surface in tapping mode. Fig 4.8 shows the three dimensional height images of neat and various 3-FAS modified sol-gel coated samples. Neat sol-gel coated sample showed RMS value of about 3nm with relatively smoother profile as compared to 3-FAS modified samples. Fluorinated samples showed protruding peaks throughout the surface with maximum RMS value of about 10 nm for 2wt% concentration. It was found that the water droplets tend to stick to the surface with no sliding

at all indicating that the hydrophobicity lied in the Wenzel state, where the peaks and valleys prevent the spreading of water on the coated surface, but droplet get stuck within the roughness grooves resulting in beading up with contact angle of about 100°. Hence much higher surface roughness was required to enhance the hydrophobic properties of the present system for which long chain fluoro-alkyl silane i.e. 17 fluoro-atoms silane was used further.

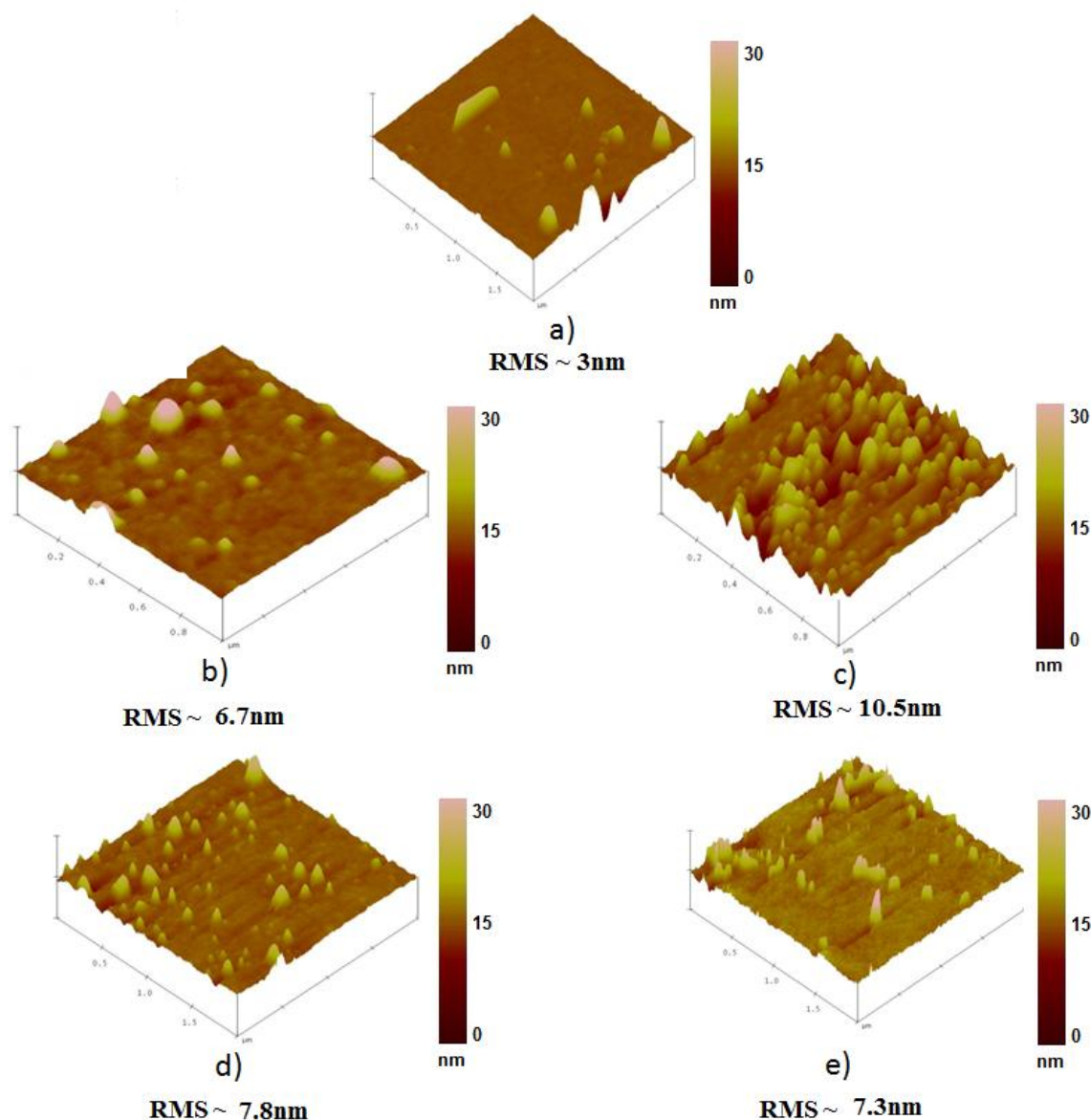


Figure 4.8: AFM images of a) 0wt%, b) 1wt%, c) 2wt%, d) 3wt% and e) 5wt% of 3-F.S modified sol-gel coated aluminium samples

4.2.3 Structural Analysis:

Structural characteristics of 3-FAS coatings and there interaction with aluminium substrate were observed using FT-IR spectroscopy as shown in Fig. 4.9. Various bands appeared were

related to the vibrations of both, inorganic and organic structural units. Broad band at around 3367cm^{-1} in neat sol-gel spectrum is attributed to the OH stretching indicating the presence of hydroxyl groups responsible for the hydrophilic nature of the unmodified sol. However the intensity of -OH band decreases in fluorinated system probably due to replacement of surface hydroxyls with low energy fluoro groups resulting in enhanced hydrophobic properties. The intensive band, at about 1090 cm^{-1} , is attributed to the asymmetric stretching vibrations of the Si-O-Si of cyclic silicate structure. Also the presence of peak at 906 cm^{-1} indicated the network formation between aluminium substrate and sol-gel coating. The sharp peak at 1550 cm^{-1} is attributed to C-N stretching vibrations.

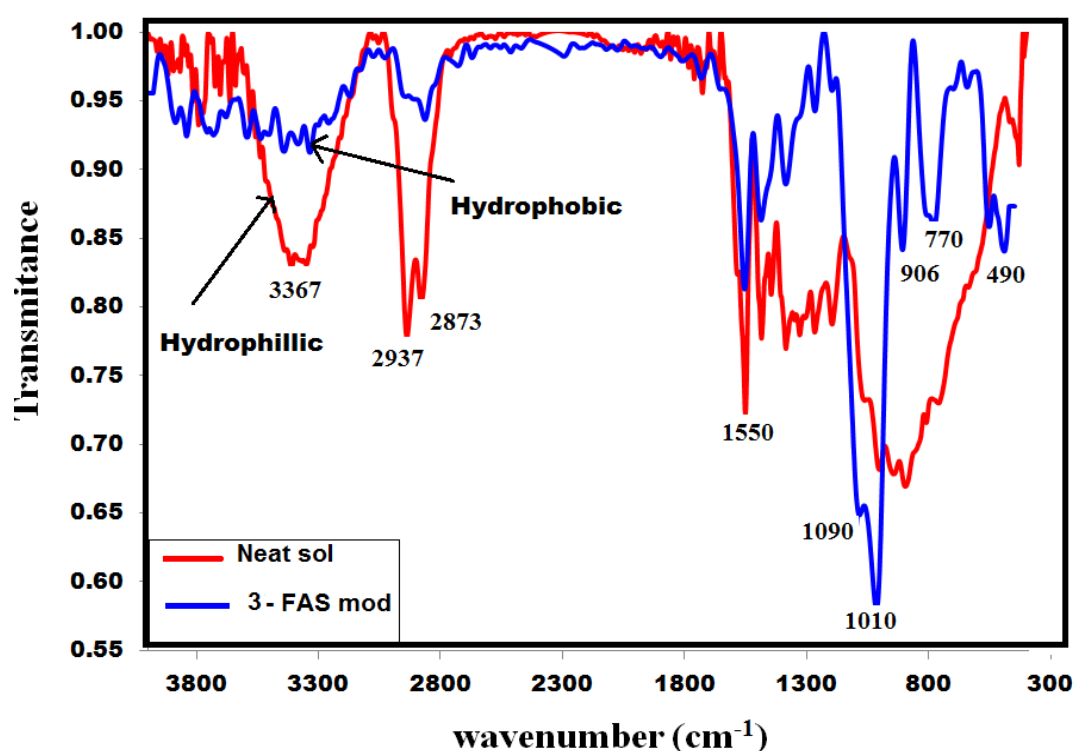


Figure 4.9: FTIR spectra of neat and 3-FAS modified sol gel coated Al sample

The strong adsorption bands appearing at 2942 and 2887 cm^{-1} correspond to asymmetric stretching vibration of C-H bonds in both neat and fluorinated sol-gel coated systems. Peak at 1010 cm^{-1} in 3FAS modified system corresponds to stretching vibrations of C-F bonds anticipated because of fluorination of hydroxyl groups by $-\text{CF}_3$ group. Also the presence of additional new peak around 770 cm^{-1} in 3-FAS modified system confirms the existence of C-

F bonds in the form of CF_3 , indicating the presence of lower energy fluoro groups on the surface.

4.2.4 Corrosion resistance of 3-FAS modified sol-gel coatings

Potentiodynamic polarisation and *Electrostatic Impedance Spectroscopy (EIS)* were used to determine the corrosion resistance of neat sol-gel and various 3-FAS modified sol-gel coated samples. Table 4.2 lists various polarisation parameters for different sol-gel compositions. The polarisation curve of bare Al after etching in 10% NaOH solution has been included as reference data to compare the corrosion efficiency of the various fluorinated systems. It was found that the alkaline treatment effectively destroyed the passive window of aluminium alloy resulting in $I_{\text{corr}} \sim 2 \times 10^{-4} \text{ A/cm}^2$. When the etched specimen was coated with hydrophilic neat sol-gel coating, the corrosion resistance was increased by one order of magnitude with I_{corr} value of about 3×10^{-5} . This could be attributed to crosslinked inorganic-organic sol-gel network which provides efficient barrier from corrosive electrolytes and water and influencing the anodic kinetics [77, 87]. Finally when various 3-FAS modified hydrophobic sol-gel coatings were applied on etched Al, corrosion resistance was further increased by an order with current density of about $7 \times 10^{-6} \text{ A/cm}^2$ for 2wt% FAS modification. Hence, tuning the surface wettability from hydrophilic to hydrophobic resulted in improvement in corrosion resistance properties.

Table 4.2: Polarisation and EIS parameters of various 3-FAS modified sol-gel coatings

Sol-gel composition	E_{corr} (V)	Current Density (A/cm^2)	Impedance (Ωcm^2)
Etched Al	-1.34	2.15×10^{-4}	1.02×10^3
Neat sol-gel	-0.89	3.05×10^{-5}	7.74×10^3
1wt%FAS-3	-0.93	2.08×10^{-5}	8.86×10^3
2wt% FAS-3	-0.88	3.13×10^{-6}	1.25×10^4
3wt% FAS-3	-0.85	2.09×10^{-6}	1.09×10^4
5wt%FAS-3	-0.97	2.089×10^{-5}	9.43×10^3

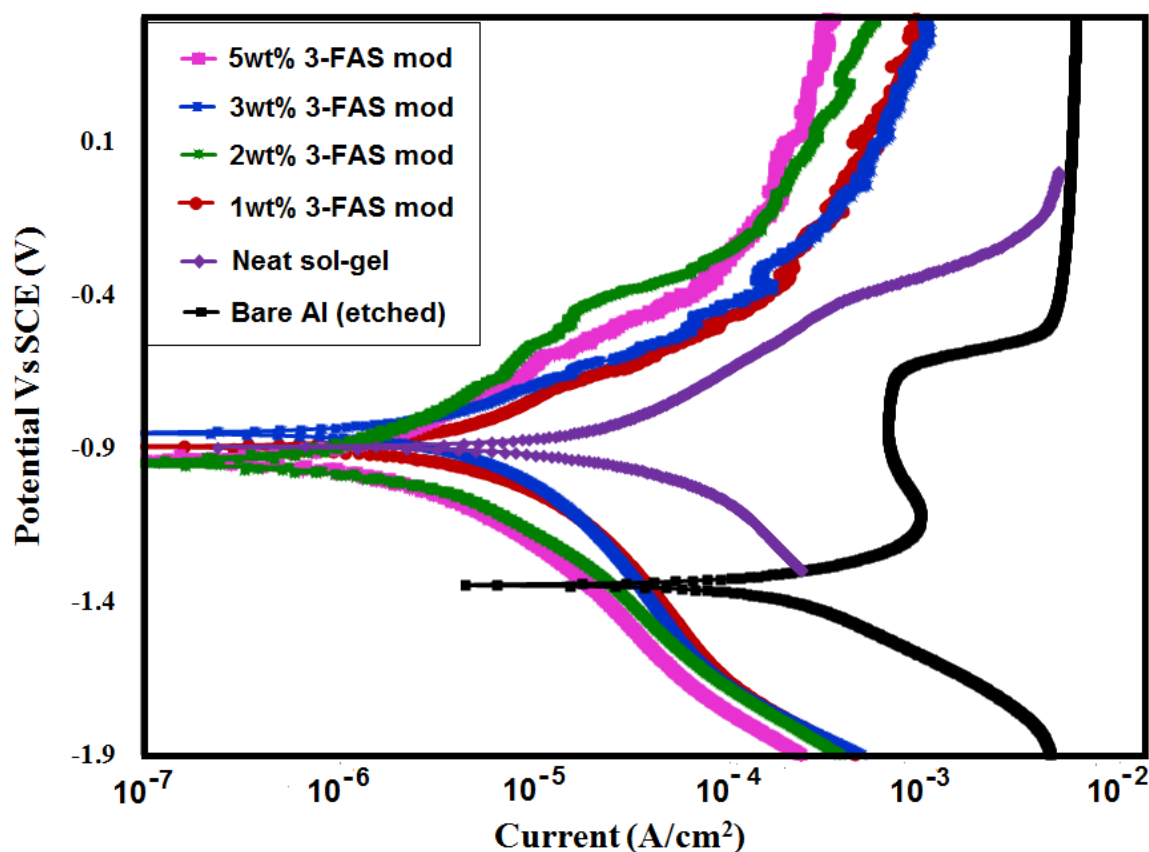


Fig 4.10: Tafel plots of bare Al (etched), neat sol-gel and various 3-FAS modified sol-gel coated Al samples

Fig 4.11 shows the impedance behavior of etched Al, neat sol-gel and various modified sol-gel coated samples at initial period of immersion in 3.5% NaCl. The impedance value $|Z|_{0.1}$ of etched Al was found to be $2 \times 10^3 \Omega \text{ cm}^2$, whereas both neat and fluorinated sol-gel coated samples showed an increase in impedance value of $|Z|_{0.1} \sim 10^4$ which is one order of magnitude higher than the uncoated one. Hence, the potential to protect the substrate is associated with both low wettability and the inorganic-organic hybrid structure of sol-gel network which acted as physical diffusion barrier to corrosive environment. The coatings were further tested for various mechanical properties like adhesion, pencil-hardness and resistance to nano-indentation in the following section.

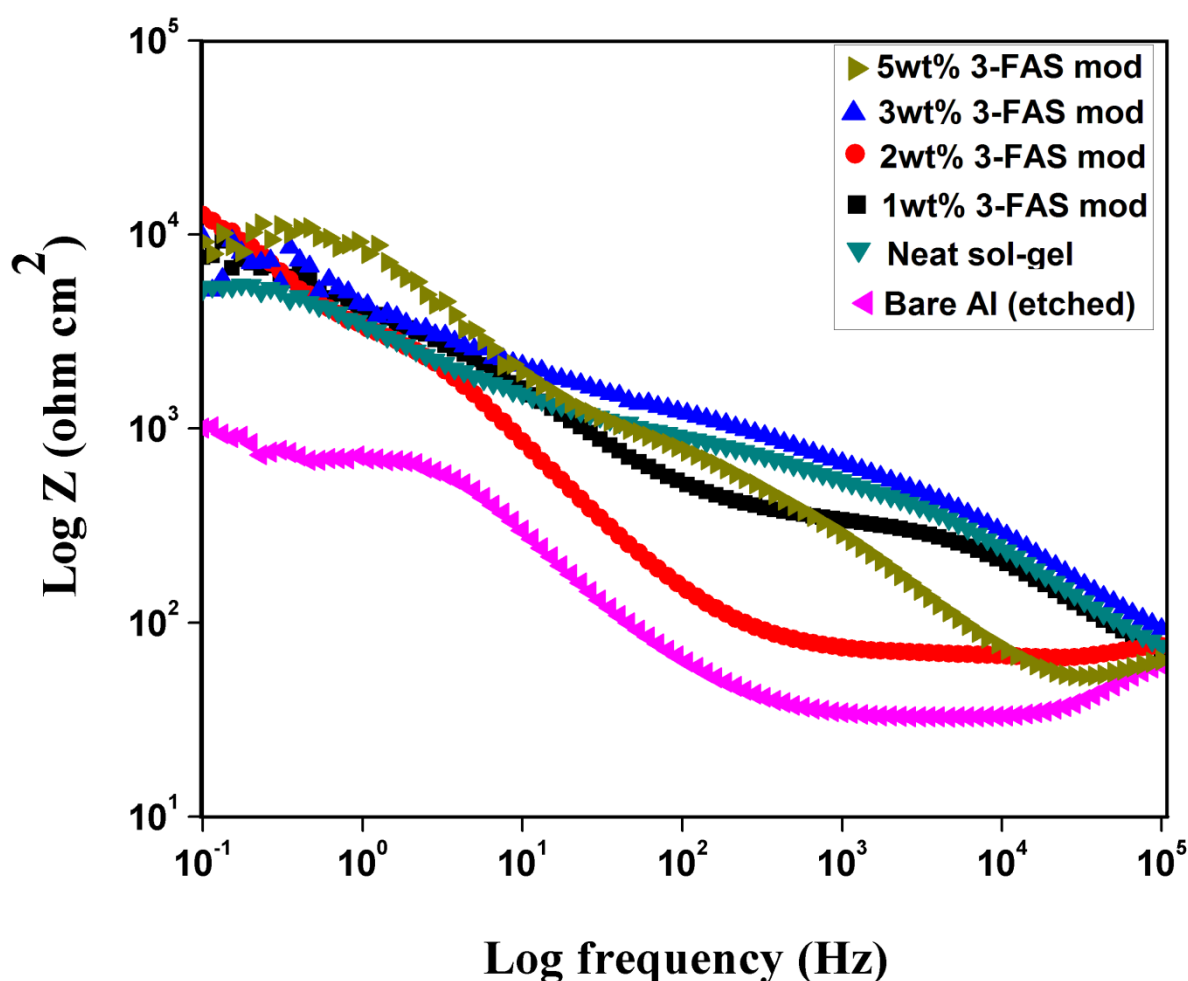


Figure 4.11: Impedance plots of etched Al, neat sol and various 3-FAS modified sol-gel coated samples at initial period of immersion

4.2.5 Mechanical Properties of various 3-FAS modified sol-gel coatings

Since thickness of the obtained films ranges between few microns, compression or tension tests could not be performed. Nano-indentation is a powerful method to characterize thin films or polymers in nanoscale range. Typical force curve of neat so-gel and 2wt% 3-FAS modified sol-gel coated samples were obtained from nano-indentation measurements (Fig.4.12). The maximum penetration depth for neat sol-gel and 2wt% 3-FAS modified coating was found to be about 1000 nm and 770 nm respectively. Hence there was a significant increase in hardness of the coating after hydrophobic modification which could be attributed to more crosslinked sol-gel network due to addition of fluorosilane groups. The average hardness value for 3FAS modified coatings was found to be 0.07 GPa whereas neat sol-gel showed hardness of 0.05 GPa only.

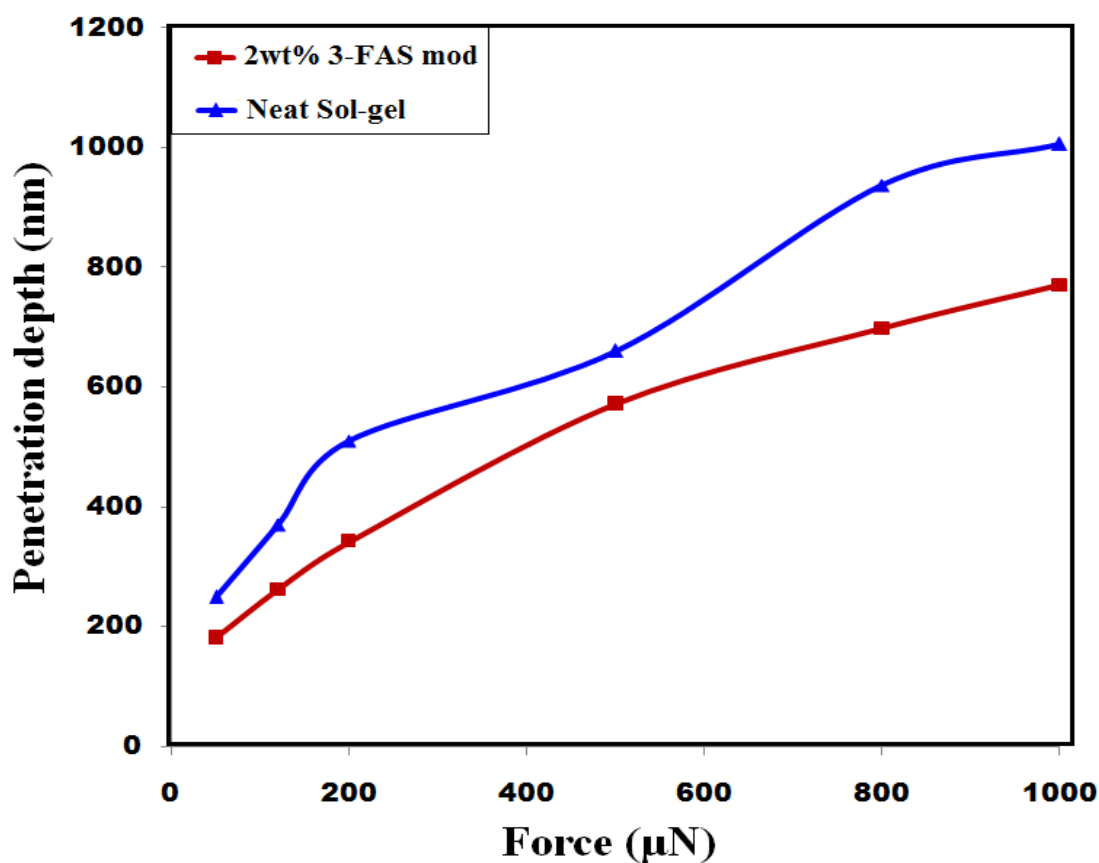


Figure 4.12: Nano-indentation curve of neat and 2wt% 3FAS modified sol-gel coating

Further adhesion and scratch resistance of the neat and 3FAS modified coatings were determined by cross-hatch technique as per ASTM D3359 and pencil hardness test as per ASTM D 1522. The results are shown in Table 4.3. It was found that addition of 3 FAS showed strong adhesion with the substrate with cross-hatch value of 5B at all concentrations. Pencil hardness showed an improvement from value of 4H for neat sol-gel to 5H for 2wt% modification and higher concentrations.

Table 4.3: Cross-hatch adhesion and pencil hardness results of various concentrations of 3-F.A.S. modified sol-gel coatings

Concentration of 3-FAS (Wt %)	Cross-hatch adhesion	Pencil Hardness
Neat Sol	5B	4H
1	5B	4H
2	5B	5H
3	5B	5H
5	5B	5H

4.3: Characterisation of 1H, 1H, 2H, 2H perfluorodecyl-trimethoxysilane (17-FAS) modified sol-gel coatings:

Modification of hydrophilic neat sol-gel system with optimised amount of 3-FAS helped in achieving a contact angle of about 100° only. In order to further enhance the hydrophobic properties 17 fluorine atoms alkyl silane (17-FAS) was used. The long chain fluoro modification helped in achieving both lower energy as well as increased surface roughness as compared to short-chain fluoro alkyl silane modification.

4.3.1 Contact Angle Measurements:

Variation of contact angle with various concentrations of 17-FAS formulations is shown in Fig 4.13. The effective contact angle for 17-FAS modification was found to be around 110° for 0.75wt% formulation. Higher value of contact angle for 17-FAS modification than 3-FAS modified one is attributed to much more lowering of energy due to increase in number of electronegative fluorine groups which migrate to the surface and hence minimize the interfacial energy. At slightly higher concentrations the fluorinated coatings showed wetting problem due to large difference of surface tension between the substrate and the coating. Also at higher fluoro contents the coatings showed orange peel effect after curing i.e. the films were not uniformly obtained everywhere and consisted of several craters or gaps with accumulated coating particles at different places. Such defect is clearly seen in SEM images shown in following section. Like 3-FAS modification, 17-FAS modification also resulted in only beading up of water droplets which stick to the surface even if the panel was tilted perpendicular. Hence it can be said that the hydrophobicity achieved completely lied in Wenzel state as the water droplet was found stuck within the roughness grooves with restricted sliding behavior due to high coefficient of friction [82]. Contact angle values were further justified by morphological studies of the coated samples.

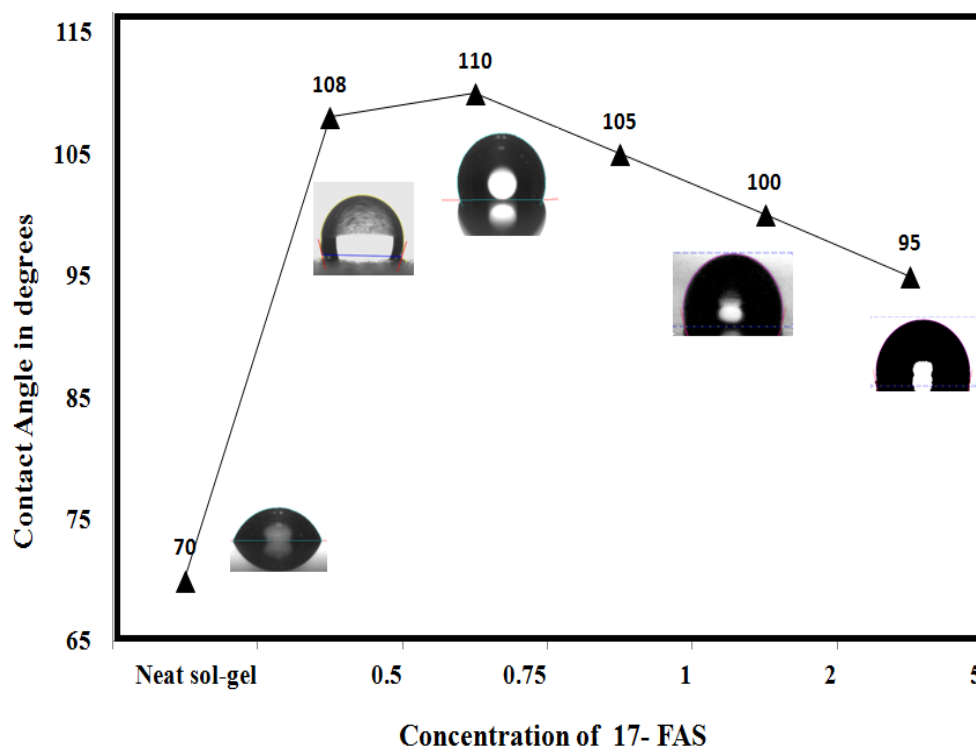


Figure 4.13: Variation of contact angle with different concentrations of 17-FAS

4.3.2. Morphological characterisation of 17-FAS modified sol-gel coatings

The SEM micrographs of various 17-FAS coated aluminium samples are shown in Fig 4.14. As seen from the images, only lower percentage upto 0.75wt% for 17-FAS resulted in micro-grooves supporting high value of contact angle of about 110°. The microgrooves obtained had diameter ranging between 10µm-20 µm which were bigger in size than 3-FAS one, supporting the high surface roughness and hence high hydrophobicity. Beyond 0.75wt%, for 17 FAS, the contact angle decreases as surface energy of the coating decreases drastically due to long chain fluorine backbone leading to poor wetting of the surface by the coating. Accumulation of coating particles was observed after curing of the coating as seen from Fig 4.14 d) and e). Hence at higher percentage of 17-F.S. the microspheres profile diminishes leading to flatter surface and poor contact angle. Overall, even modification with long chain fluoro-alkyl silane did not resulted in self cleaning properties as the roughness obtained was capable of beading water droplet by WCA of 110° only and residing in Wenzel regime [88]. Hence further a short chain six carbon atom per-fluoro water based emulsion was used to enhance the hydrophobic behaviour of the coatings.

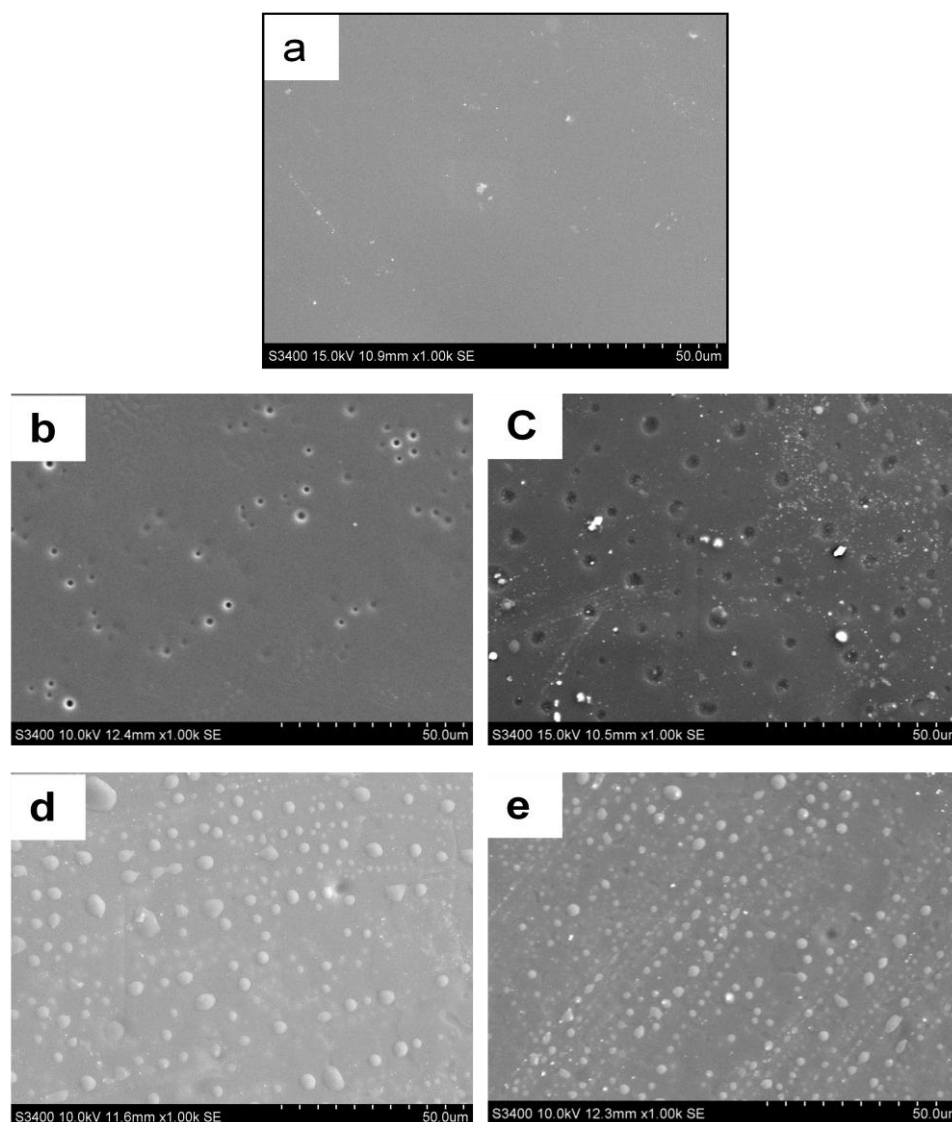


Figure 4.14: The SEM images of various weight% of 17-FAS coatings over aluminium substrate (a) Neat Sol-gel , (b) 0.5wt % (c) 0.75wt% (d) 2wt% (e) 3 wt%

AFM technique being the successful tool in closely examining the surface topography was used again for 17-FAS modification. Fig 4.15 shows three dimensional topographical images of neat and various 17-FAS modified sol-gel coated samples. The increase in surface roughness in form of several peaks and valleys was clearly visible with 17-FAS modification. At 0.75wt% modification maximum roughness of about 15 nm was achieved whereas in case of 3-FAS modification maximum roughness achieved was only about 10nm. Hence the quantitative increase in surface roughness again supported the higher value of WCA achieved with 17- FAS modification over 3- FAS modification. Still the surface roughness achieved resulting in “peaks” and “valleys” pattern, was not capable of entrapping sufficient air below

them, required to reduce the coefficient of friction between the surface and water. Hence, the state of hydrophobicity achieved lied in Wenzel regime with sliding angle $>90^\circ$. Hence after exploring the effect of fluoro-alkylsilanes of various chain lengths, various commercial fluoro polymers/additives were incorporated in the coating backbone to achieve enhanced water repellency maintaining the coating's mechanical properties.

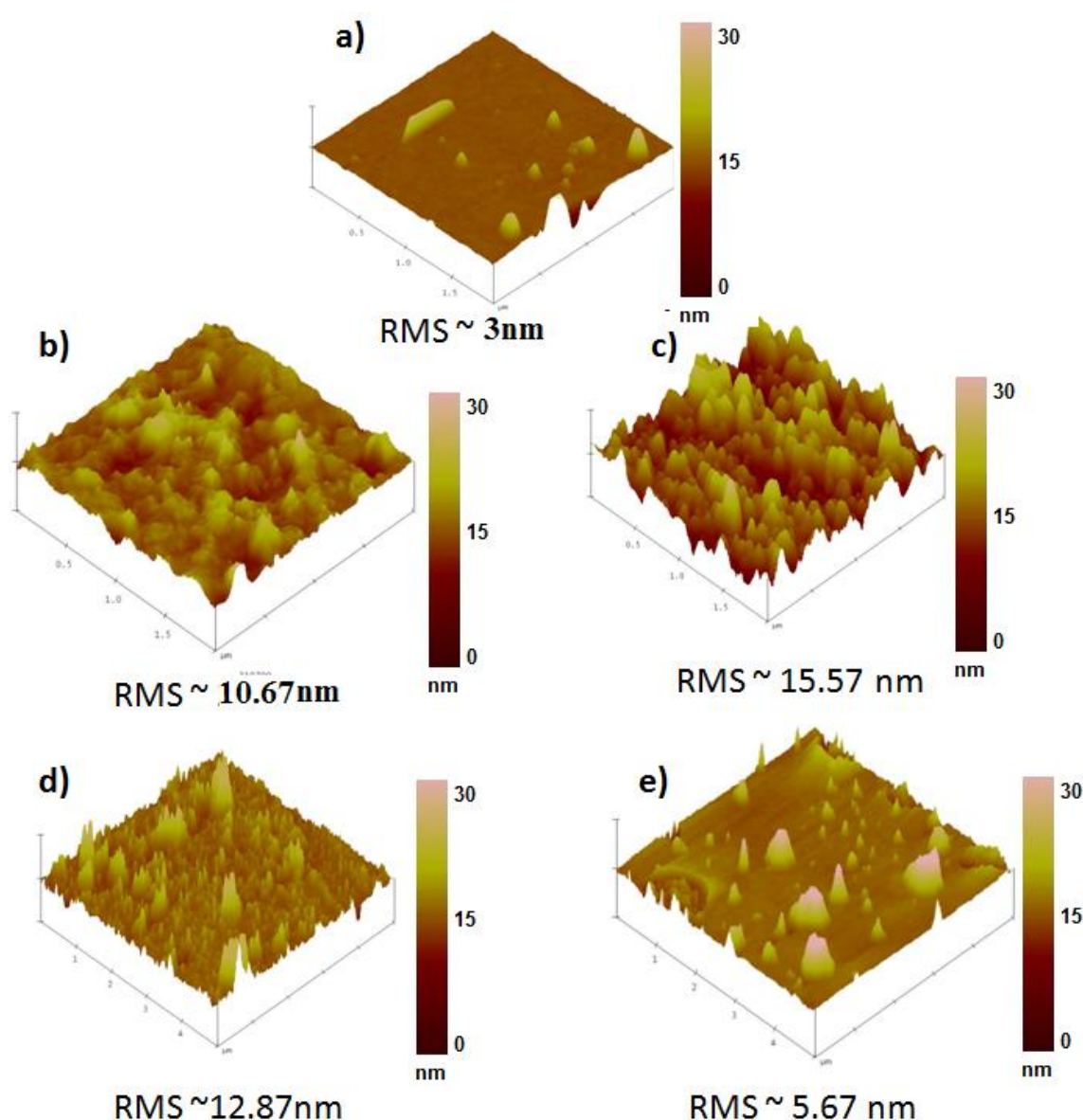


Figure 4.15 AFM images of a) Neat Sol, b) 0.5wt% 17-FAS, c) 0.75wt% 17-FAS, d) 1wt% FAS and e) 5wt% 17-FAS modified sol-gel coatings over Al surface.

4.3.3 Structural analysis of 17-FAS modified sol-gel coatings

In order to study the changes taking place in the surface chemistry FTIR analysis was performed on optimised 17-FAS sol-gel coating (Fig 4.16). The fluorinated spectrum was found similar to 3-FAS modification with broader OH- band around 3367cm^{-1} in neat sol spectrum indicating hydrophilic nature and narrower OH-bond in 17-FAS modifies spectrum indicating hydrophobic nature of the coating surface. A sharp peak at 550 cm^{-1} , in addition to 490 cm^{-1} and 1010 cm^{-1} , in 17-FAS modification is indicative of fluorine bonds in the form of C-F_2 along with C-F and C-F_3 bonds coming from long chain structure [89]. Other peaks such as 1090cm^{-1} and 906cm^{-1} are attributed to Si-O-Si linkages within the sol-gel network and between Al substrate and sol-gel coating respectively. Also the strong adsorption bands appearing at 2942 and 2887 cm^{-1} correspond to asymmetric stretching vibration of C-H bonds in both neat and fluorinated sol-gel coated systems [90].

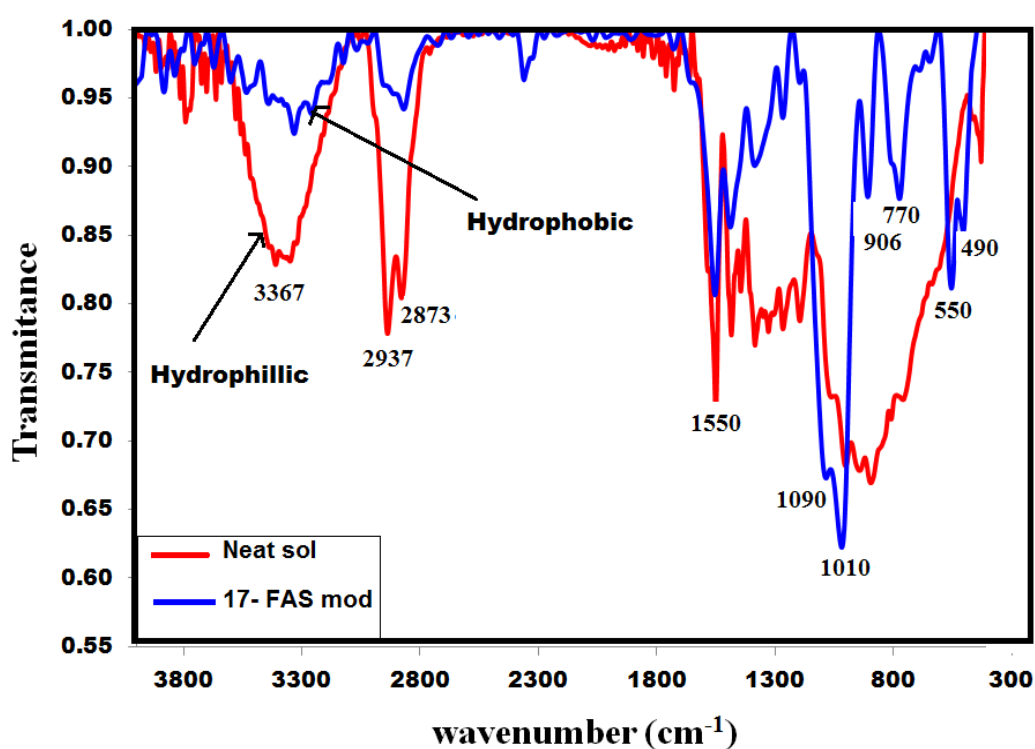


Figure 4.16 FTIR spectra of neat and 17-FAS modified sol-gel coatings

4.3.4 Corrosion resistance analysis of 17-FAS modified sol-gel coatings

The potentiodynamic polarisation curves of 17-FAS coatings were compared with neat sol coated and etched aluminium alloy to find the extent of reduction in corrosion current due to

hydrophobic modification. Fig 4.17 shows the results of potentiodynamic polarisation curves, and Table 4.4 lists the electrochemical parameters derived. The bare etched Al alloy showed active dissolution and pitting behavior due to intense alkaline etching while the neat sol-gel coated substrate showed lower current densities than the bare material. This is an indication that the coating is inhibiting the anodic process and acting as a barrier to the electrolyte by impeding its contact with the metal surface. Finally when various 17-FAS modified hydrophobic sol-gel coatings were applied on etched Al, corrosion resistance was further increased by an order with current density of about $5.06 \times 10^{-6} \text{ A/cm}^2$ for 0.75wt% modification. Also a positive shift in E_{corr} values was observed for the hydrophobic modification of sol-gel coatings from $-1.3 \text{ V}_{\text{SCE}}$ for bare Al to $-0.68 \text{ V}_{\text{SCE}}$ for 0.75wt% FAS-17 modification. Though 17-FAS modified coatings exhibited current densities in similar range of 3-FAS modified coatings, they showed a gradual shift in E_{corr} values in noble direction indicating superior potential to protect the substrate from corrosive environment.

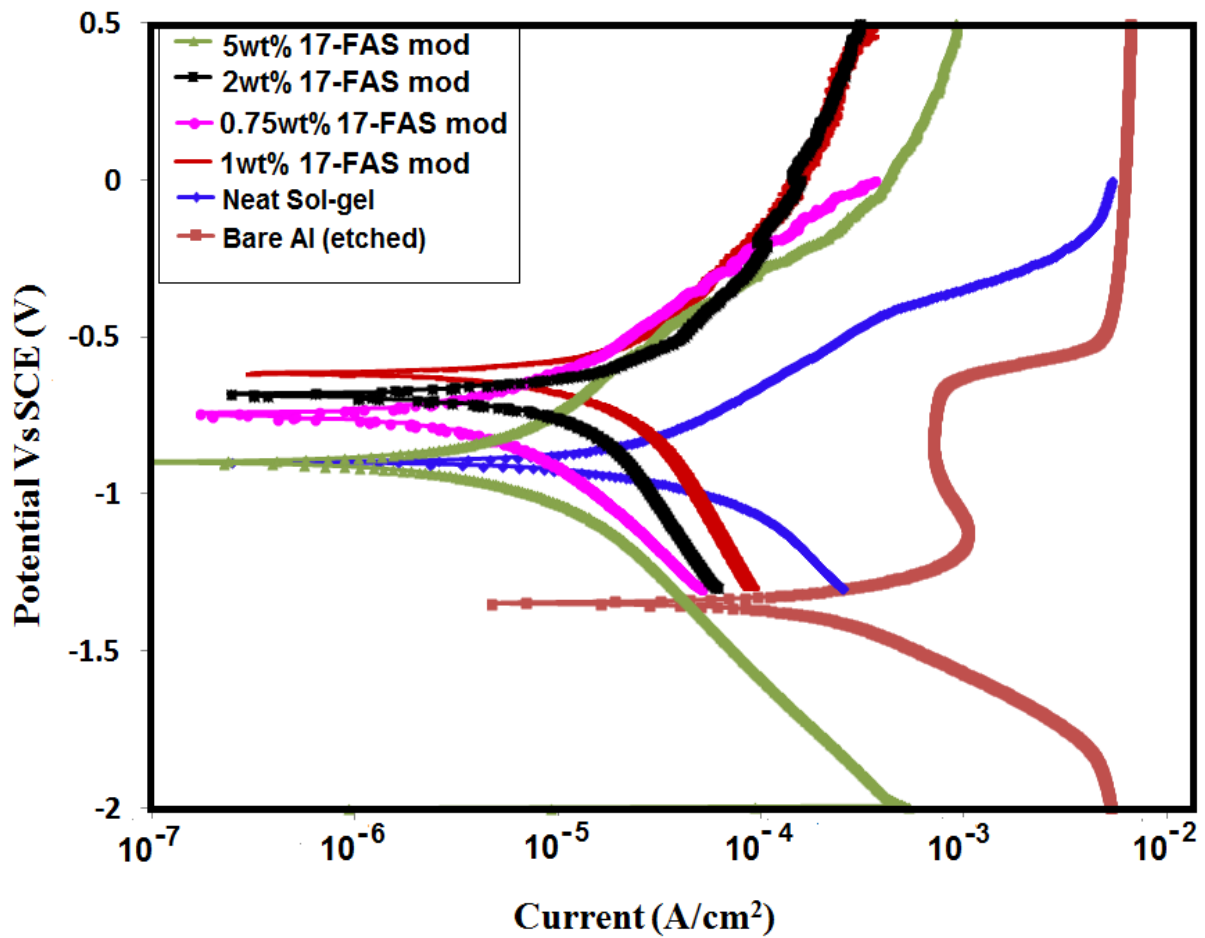


Figure 4.17: Polarisation curves for neat and various 17-FAS modified sol-gel coated Al samples.

Table 4.4: Polarisation and EIS parameters of various 17-FAS modified sol-gel coatings

Sol-gel composition	E_{corr} (V)	Current Density (A/cm²)	Impedance (Ωcm^2)
Etched Al	-1.34	2.15×10^{-4}	1.02×10^3
Neat sol-gel	-0.89	3.05×10^{-5}	7.74×10^3
0.75 wt%FAS-17	-0.68	5.06×10^{-6}	5.24×10^4
1wt% FAS-17	-0.65	9.98×10^{-6}	3.28×10^4
2wt%FAS-17	-0.61	1.95×10^{-5}	2.45×10^4
5wt%FAS-17	-0.91	6.48×10^{-6}	1.02×10^4

Further electrostatic impedance measurements were carried on various 17-FAS coated samples and compared with neat sol-gel and etched Al substrates (Fig 4.18). 17-FAS modified coatings showed impedance $|Z|_{0.1\text{Hz}}$ of about 10^4 which is one order higher in magnitude than bare Al substrate i.e. $|Z|_{0.1\text{Hz}} \sim 10^3$. The 17FAS modified coatings showed a small increase in impedance value from neat sol-gel with maximum value achieved for 0.75wt% modification, though the difference is not significant on the $\log |Z|$ scale. Hence, the hydrophobic modification had minuet effect on impedance value for both 3-FAS and 17-FAS modified systems. Therefore, it can be said that any loss in corrosion resistance properties due to micro-sized pores through which the corrosive electrolytes could penetrate was balanced by the water repellent nature and barrier properties of the hydrophobic sol-gel coating. After corrosion resistance analysis these coatings were further subjected to various mechanical characterisations discussed in following section.

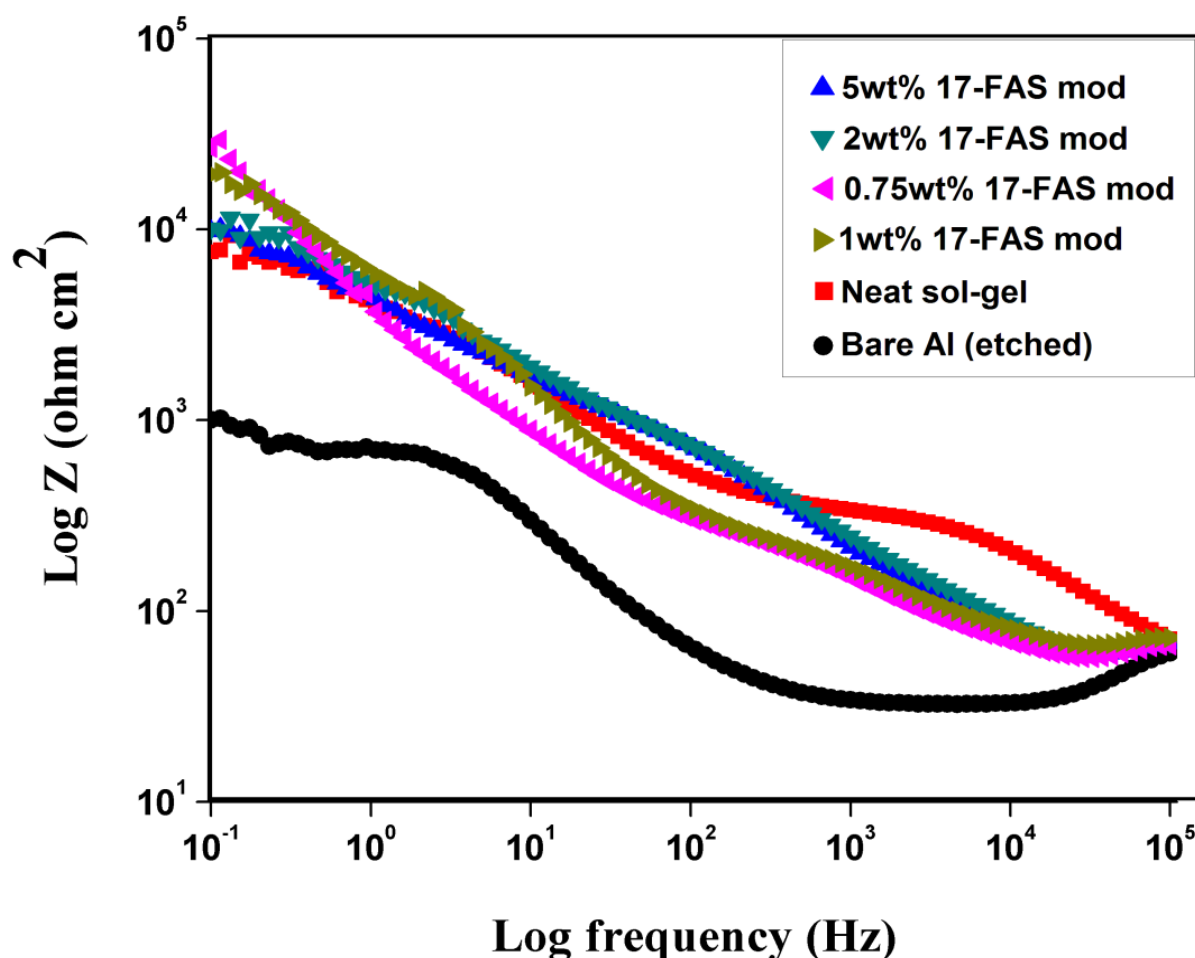


Figure 4.18: Bode plots of bare Al (etched), neat and various 17-FAS modified sol-gel coatings

4.3.5 Mechanical characterisation of 17-FAS modified sol-gel coatings

As reported earlier the maximum penetration depth achieved for load of 1000 μ N in case of neat sol-gel was about 1000 nm. After modification with 17 FAS groups the hardness of the coatings was found to be enhanced with penetration of about 785nm (Fig 4.19) and strength of 0.07 GPa. Other mechanical tests like cross hatch adhesion and pencil hardness of 17FAS coatings were also performed as listed in Table 4.5. The modification did not showed much improvement in adhesion or scratch resistance as compared to 3- FAS coatings. The probable reason could be the steric hindrance of Si-O-Si bond formation due to long chains resulting in interference of both cohesive and adhesive properties of the coatings.

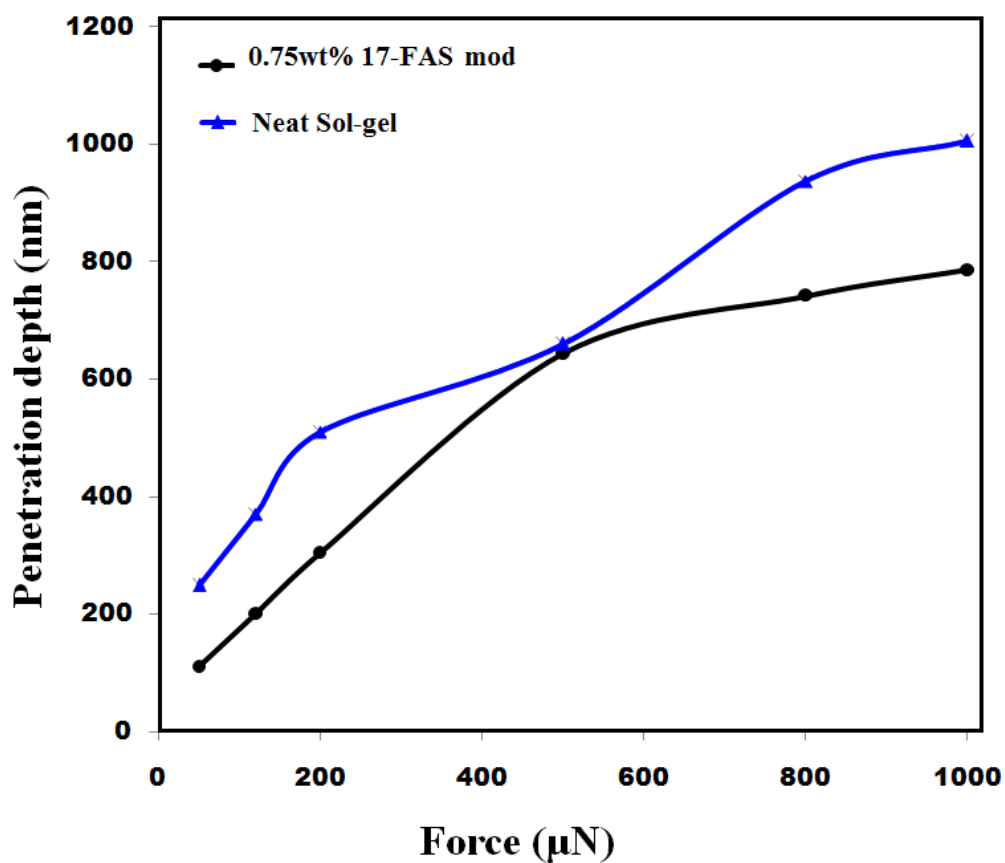


Figure 4.19: Nano-indentation curves of neat and 17-FAS modified sol-gel coating

Table 4.5: Crosshatch adhesion and pencil hardness results of various concentrations of 17-FAS modified sol-gel coatings

Wt% of 17- F.S	Cross-hatch adhesion	Pencil Hardness
0.75	5B	4H
1	5B	4H
2	5B	4H
3	5B	3H

4.4 Characterisation of commercial fluoro-emulsion (FE) modified sol-gel coating system:

To achieve further lowering of surface energy, a commercially available fluoro- emulsion (FE) was used which is a short chain water based per-fluoro polymer consisting of 6 carbon atoms. FE was incorporated at various percentages, ranging from 10wt % to 50 wt% on the solid resin content, along with GPTMS and MTMS and various hydrophobic properties were compared with neat sol-gel coating

4.4.1 Wetting properties of FE modified sol-gel coatings:

Hydrophobic nature of coatings was investigated by contact angle measurement using goniometer. Fig 4.20 shows variation of contact angle with different concentrations of FE modified sol-gel coated aluminium samples. The surface of the neat sol-coated sample was found to be hydrophilic with C.A. of about 70°. However, using perfluoro emulsion as hydrophobic co-precursor in the sol-gel process resulted in larger contact angles with maximum value of 118°-120° for 30wt% FE modification attributed to lowering of interfacial energy due to replacement of hydrophilic surface –OH groups of sol-gel matrix by electronegative perfluoro groups [87]. It was found that contact angle increases with increase in FE percentage upto 30wt% and further decreases at higher percentages. This could be attributed to either increase in surface energy or decrease in surface roughness at higher concentrations. Both the factors are discussed in detail in the report. Another interesting parameter to which the extent of hydrophobicity could be linked was improved sliding behavior of FE modified hydrophobic coatings. The coatings exhibited sliding angle of 70° for 10μL of water droplet at 30wt% modification. This indicated the transition from Wenzel state towards Cassie state with formation of air pockets within the roughness grooves leading to significant decrease in coefficient of friction between the coated surface and water droplet [91, 92]. Therefore it can be said that FE modification resulted in both enhanced surface roughness and lowering of energy as compared to 3-FAS and 17-FAS modification.

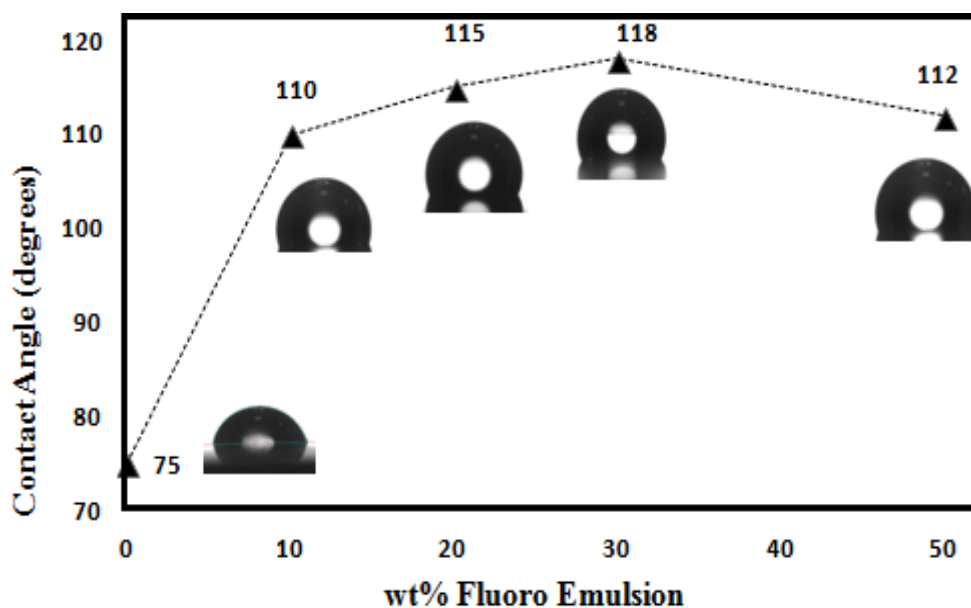


Figure: 4.20: Variation of contact angle with different concentrations of FE

4.4.2 Morphological analysis of FE modified sol-gel coatings

The SEM images of various concentration of FE modified sol-gel coated aluminium samples at magnification of 1000x are shown in Fig 4.21. As seen from SEM micrographs, perfluoro modified sol-gel coatings showed micro porous morphology throughout the surface resulting in enhanced surface roughness which is another important requirement along with low interfacial energy for achieving hydrophobic character. It was found that 30wt% FE formulation showed maximum porous structure with craters having outer diameter ranging from 20 to 30 μm , evenly dispersed in film surface. These micro grooves tend to entrap air in the pores of the film contributing to the beading up and easy rolling of water droplet over the protrusions and hence resulting in increased water repellency with contact angle of about 118° and sliding angle of 70° for $10\mu\text{L}$ water droplet. Hence it can be attributed that perfluoro modification of neat sol-gel system resulted in strong hydrophobic properties derived from both low surface energy and enhanced micro scale roughness. Coating thickness of various formulations was measured by carrying out cross-sectional SEM analysis as shown in Fig 4.22. It was found that average thickness of the as developed coatings was approximately 1.5-2 μm .

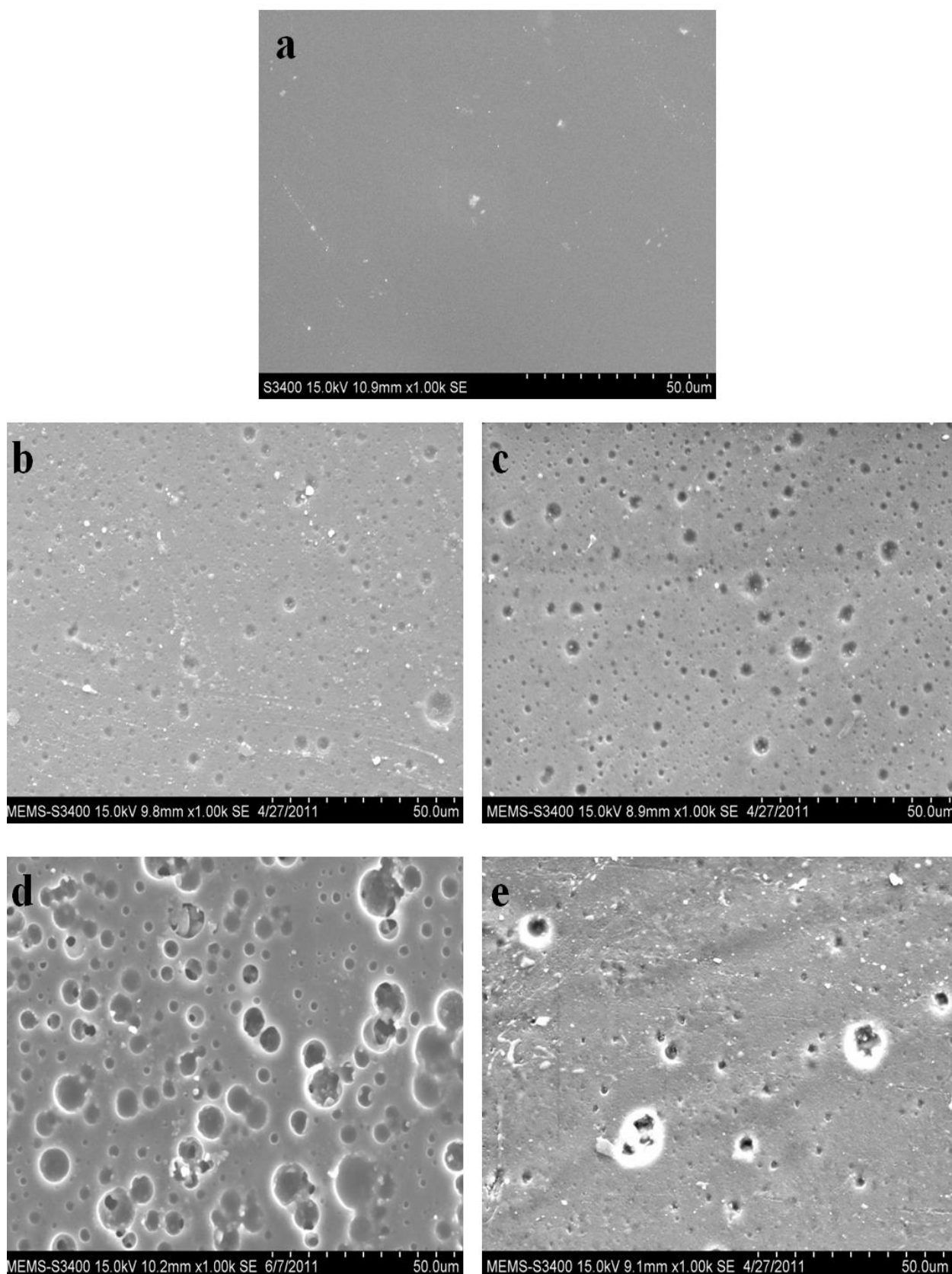


Figure 4.21: Scanning Electron Micrographs of Aluminium substrate coated with (a) Neat sol-gel, (b) 10 wt%, (c) 20 wt %, (d) 30 wt % and (e) 50 wt % FE modified sol-gel coating.

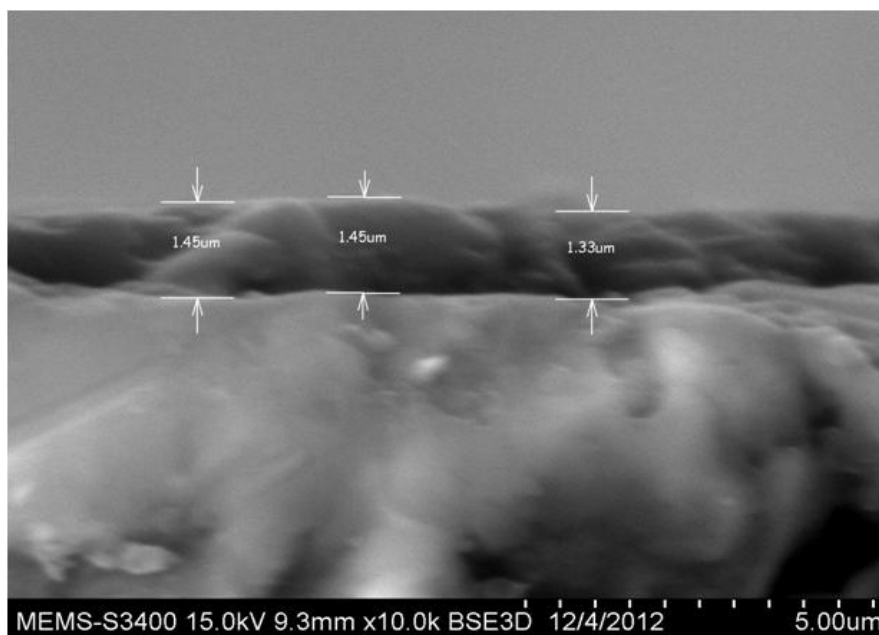


Figure 4.22: FEGSEM cross-sectional image of coating thickness of FE modified sol-gel coating

In order to further characterize the microstructure of the as developed inorganic-organic hybrid organic coatings, AFM analysis was performed on aluminium samples coated with sol-gel coatings with various concentrations of fluoro emulsion. From Fig 4.23 (ai) and (ci) of different samples, the micro-scale and nano- scale roughness can be seen clearly. Number of peaks with “maximum height” increased with increase in concentration of FE content from neat to 30 wt%, beneficial for the increase in hydrophobicity, with highest value of 37 nm for 30wt% FE concentration. Maximum peak was found at $2.58\mu\text{m}$ and the minimum valley was calculated at $2.32\mu\text{m}$ relative to average crossline. From the section profiles in Fig. 4.23 (bi) the number of different protrusions, “hills” were increasing with increase in concentration of FE upto 30wt% .This allows entrapment of enough air to prevent the penetration of the water into the grooves thereby reducing the contact area of the water drops with the surface leading to beading up of water and hence enhancing water repellent properties. As such, the terminal perfluoro groups in the polymer emulsion contribute to both the enhancement of surface roughness of the film and the lowering of surface energy [78-80]. Further 50wt% FE concentration showed broader section profile due to smoothening of protrusions and hence decreasing the surface roughness. Also from Table 4.6, it was observed that the contact angle increases with increase in surface roughness (RMS) of the films which can be explained by the Wenzel’s equation according to which the WCA of the surface increases with increasing surface roughness when the surface is composed of hydrophobic materials [82, 88].

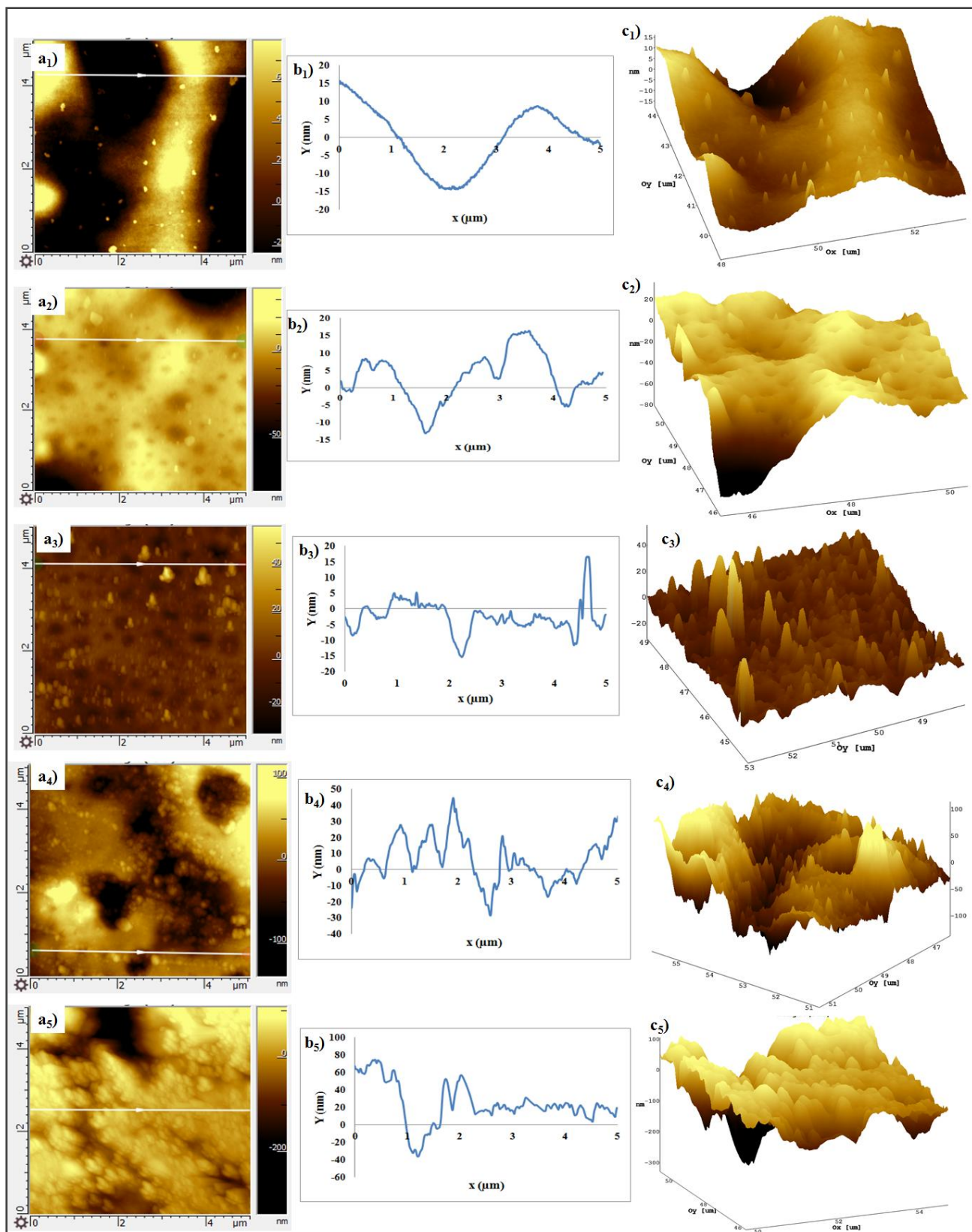


Fig. 4.23: (a_i) 2-D (b_i) section profiles and (c_i) 3-D AFM images of neat, 10, 20, 30 and 50wt% FE modified sol-gel coatings on aluminium substrate

Table 4.6: Effect of concentration of FE on contact angle and roughness of the sol-gel coatings

Concentration	Average Contact Angle	Average RMS (nm)
Neat Sol	75°	3
10wt%	108°	11
20wt%	115°	25
30wt%	120°	37
50wt%	112°	14

4.4.3 Structural Analysis of FE-modified sol-gel coatings

FTIR spectra of the neat sol without any fluoro modification and 30wt% FE modified so-gel coated sample are seen in Fig 4.24. As seen from the spectra, –OH peak appearing around 3400 cm^{-1} in neat sol-gel system was found broader than modified fluorinated system indicating hydrophilic nature of the neat sol-gel film [82]. Also the development of sharp band around 912 cm^{-1} , in FE modified system is attributed to rocking vibrations of Si-C bond which indicate surface modification of silica film due to replacement of surface OH's by –Si-(CF₃) groups resulting in enhanced hydrophobicity of the modified fluorinated film [89, 91]. The peak appearing at 1079 cm^{-1} , in fluorinated spectra is associated with the vibrational mode corresponding to the asymmetric stretching of Si-O-Si linkage which confirms the formation of a cross-linked siloxane network structure inside the film [49, 89]. The strong adsorption bands appearing at 2942 and 2887 cm^{-1} [82, 90], correspond to asymmetric stretching vibration of C-H bonds in both neat and fluorinated sol-gel coated systems. Band at 1014 cm^{-1} in 30wt% FE modified system corresponds to stretching vibrations of C-F bonds as anticipated because of fluorination of hydroxyl groups by perfluoro groups [80, 82, 93]. Also, the presence of additional new peak at 779 cm^{-1} in FE modified system confirms the existence of C-F bonds, indicating the presence of lower energy fluoro groups on the surface and hence responsible for enhancing hydrophobicity [90]. The characteristic stretching peak of the NH group was found to be strong at 1730 cm^{-1} in both the spectra due to HMMM moiety [32].

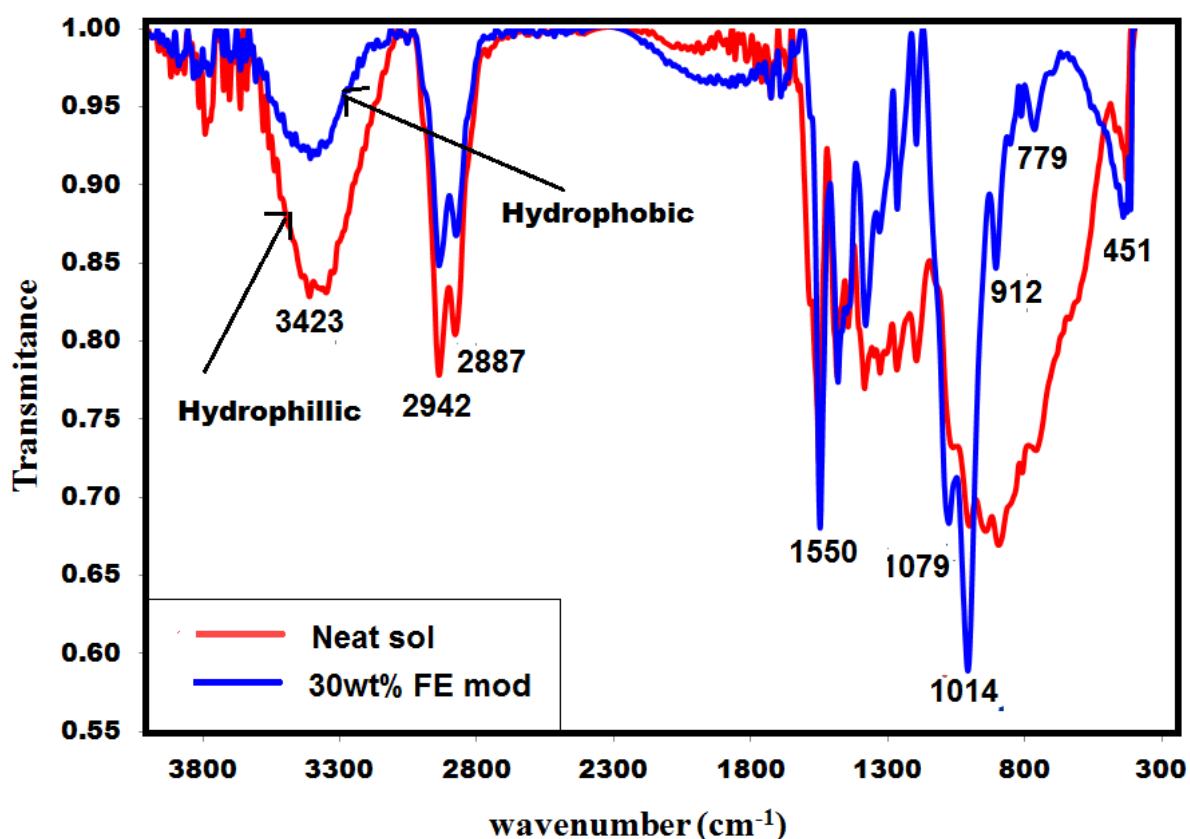


Figure 4.24: FTIR plots of neat sol and 30wt% FE modified sol-gel coated aluminium samples

Further XPS analysis was carried out to analyse chemical states and composition of elements present in the film surface. The presence of low energy fluorine groups on surface was confirmed by comparing the XPS results of neat sol-gel and various FE modified sol-gel coated samples (Fig 4.25). Peaks located near 680 eV and 830 eV in Fe modified system correspond to the strong fluorine F 1s and F $KL_{23}L_{23}$ bands [73, 82, 83, 92], which were absent in neat sol. It was found that the extent of fluorination increases with increase in FE content resulting in lowering of surface energy required for achieving hydrophobic properties. Peaks appearing at 99 eV and 151 eV correspond to Si 2p and Si 2s respectively [82, 94, 95]. It was seen that O 1s peak at 530 eV in fluorinated spectra had reduced intensity as compared to neat sol-gel spectra which is again attributed to replacement of large amount of hydrophilic OH groups by perfluoro-groups supporting the hydrophobic nature of the fluorinated system [95].

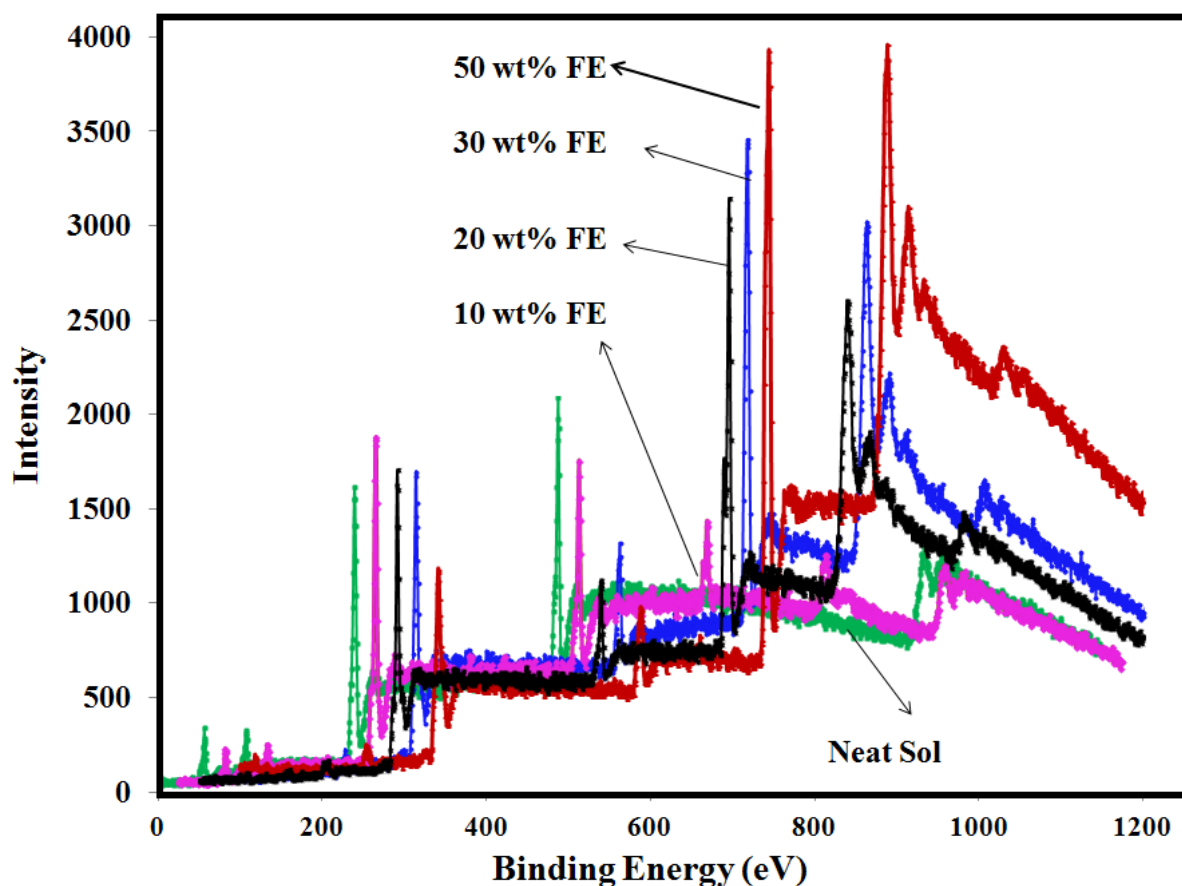


Figure 4.25: XPS plots of neat and various FE modified sol-gel coatings

4.4.4 Corrosion resistance of FE modified sol-gel coatings

Potentiodynamic polarisation plots and Bode plots from EIS analysis of the bare and various sol-gel coated aluminium samples are shown in Fig.4.25 and Fig.4.26 respectively. The polarisation curves of bare Al in the un-etched and the etched condition have been included as reference / benchmark data for which the efficacy of the coatings can be contrast. The unetched Al showed the characteristic passive window and sustained very high current densities above $\sim -0.70V_{SCE}$. The etched specimen interestingly shows rather unusual polarisation behavior, with current rapidly increasing at potentials above its respective E_{corr} , and the alkaline treatment effectively destroys the passive window (for the particular alloy being tested). The influence of sol-gel coating upon samples is obvious, with a positive shift in E_{corr} values (upto $-0.69 V_{SCE}$ for 30wt% FE modification) arising as a result of the stifling of the anodic reaction kinetics. This stifling of the anodic kinetics occurs by just the coating

with the neat sol, and is enhanced by the further addition to 30wt% FE (and slightly compromised with further FE modification). From the many replicate tests conducted in this work, the cathodic kinetics upon Al was not notably influenced by the coating or the coating modifications, and the electrochemical differences were dominated by alterations in anodic kinetics. The corrosion current density for hydrophobically modified sol-gel coated sample was lowered by about 3 orders of magnitude i.e. from an average value of $\sim 2 \times 10^{-4} \text{ A/cm}^2$ for the etched Al, to $\sim 9 \times 10^{-7} \text{ A/cm}^2$ for 30wt% FE modified sol-gel coated sample. This indicates that the hybrid fluoropolymer films are somewhat effective at imparting corrosion resistance from a barrier effect, and also aided by the presence of non-polar perfluoro groups on the surface which can contribute to repelling water and Cl^- ions to reach the base metal due to low surface tension as well as air entrapped within the micro-scale grooves [78, 79, 96-98]. The densely crosslinked structure of organic–inorganic matrix resulting in enhanced adhesion strength, also supports the improved corrosion protection due to strong chemical bonding of the silica groups to the metal substrate [77, 87]. Table 4.7 lists the polarisation and EIS parameters of various FE modified sol-gel coatings.

Table 4.7: Polarisation and EIS parameters of various FE modified sol-gel coatings

Sol-gel composition	E_{corr} (V)	Current Density (A/cm^2)	Impedance (Ωcm^2)
Etched Al	-1.34	2.15×10^{-4}	1.02×10^3
Neat sol-gel	-0.89	3.05×10^{-5}	7.74×10^3
10wt% FE	-0.71	4.59×10^{-6}	1.68×10^4
30wt%FE	-0.70	9.89×10^{-7}	3.73×10^4
50wt%FE	-0.61	1.00×10^{-5}	1.03×10^4

From EIS measurements it was observed that impedance increases by an order of magnitude for 30wt% FE modification ($3.73 \times 10^4 \Omega\text{cm}^2$) as compared to uncoated specimen ($1.02 \times 10^3 \Omega\text{cm}^2$), again suggesting that corrosion resistance afforded is associated with both low wettability and the inorganic-organic hybrid structure of the grafted-fluoropolymer films which act as a physical diffusion barrier due to entrapment of air between the roughness protrusions [97].

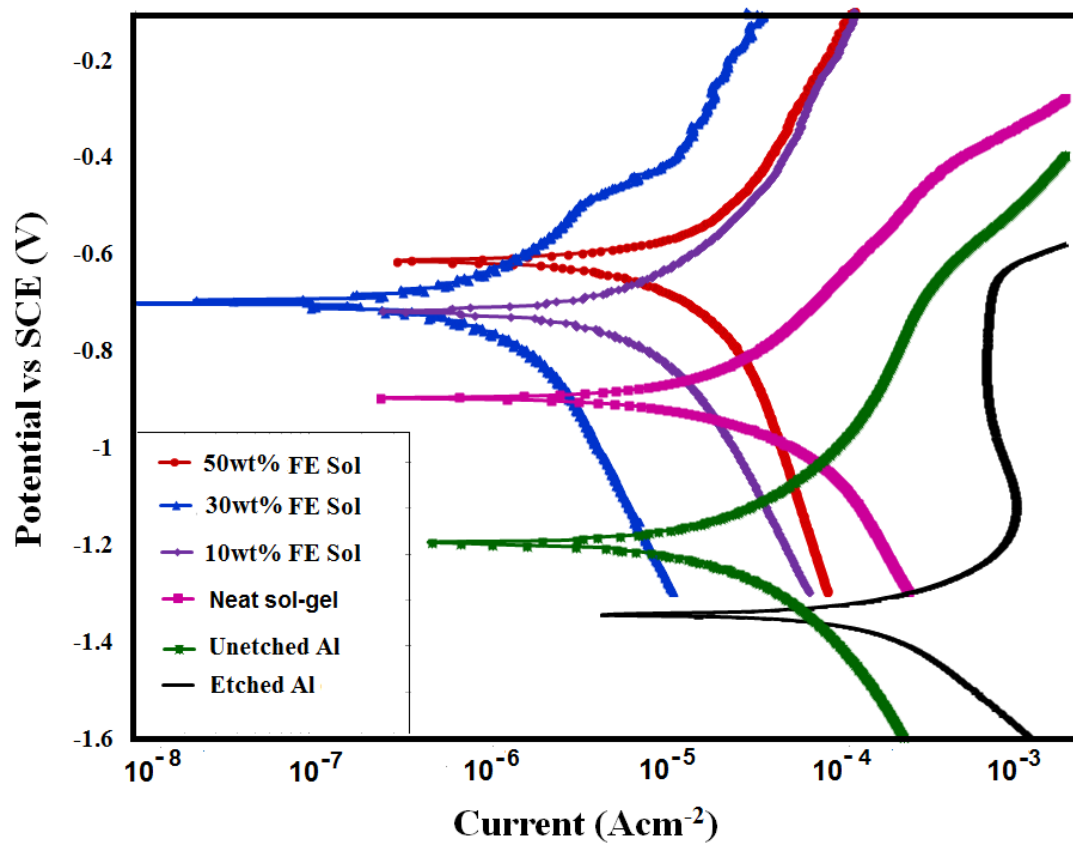


Figure 4.26: Tafel plots of bare Al, neat and various FE modified sol-gel coatings

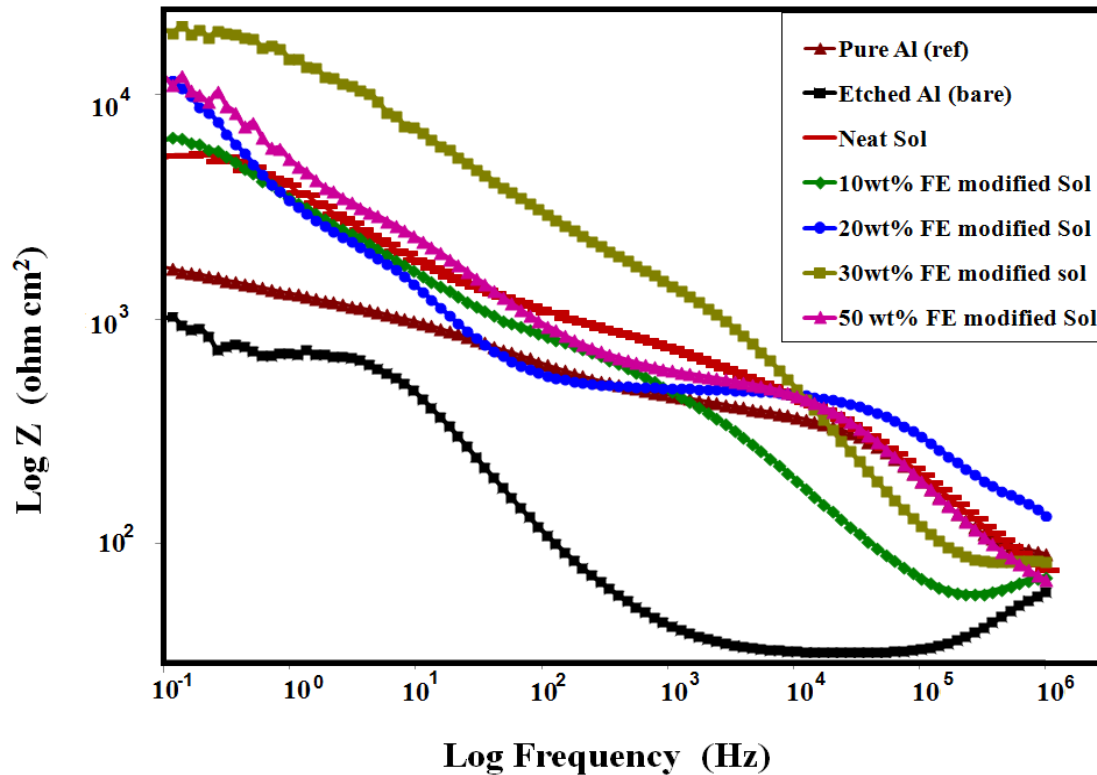


Figure 4.27: Bode plots of bare Al, neat sol and various wt % of FE modified sol-gel coatings

4.4.5 Mechanical properties of FE modified sol-gel coatings

A typical force curve of 30wt% FE modified sol-gel coated sample was obtained from nano-indentation measurements (Fig 4.27). The maximum penetration depth was found to be about 490nm which is quite less compared to the film thickness (2 μ m). The average nano hardness value was found to be 0.18 GPa using load of 1000 μ N. The scratch resistance and pencil hardness of the coatings were determined and compared in accordance with ASTM D3363-92a (Table 4.8) [71]. It was found that the pencil hardness of perfluoro modified sol-gel coatings was 4H. Adhesion of the coatings was determined in accordance with ASTM D3359. The coatings showed strong adhesion with measure of 5B at 30wt% corresponding to the most adhesive rating, with the edges of the cuts completely smooth and none of the squares of the lattice detached. The superior mechanical properties of the as developed coatings can be attributed to the excellent elasticity of CF_x layer and rigid inorganic-organic hybrid polymer network [23].

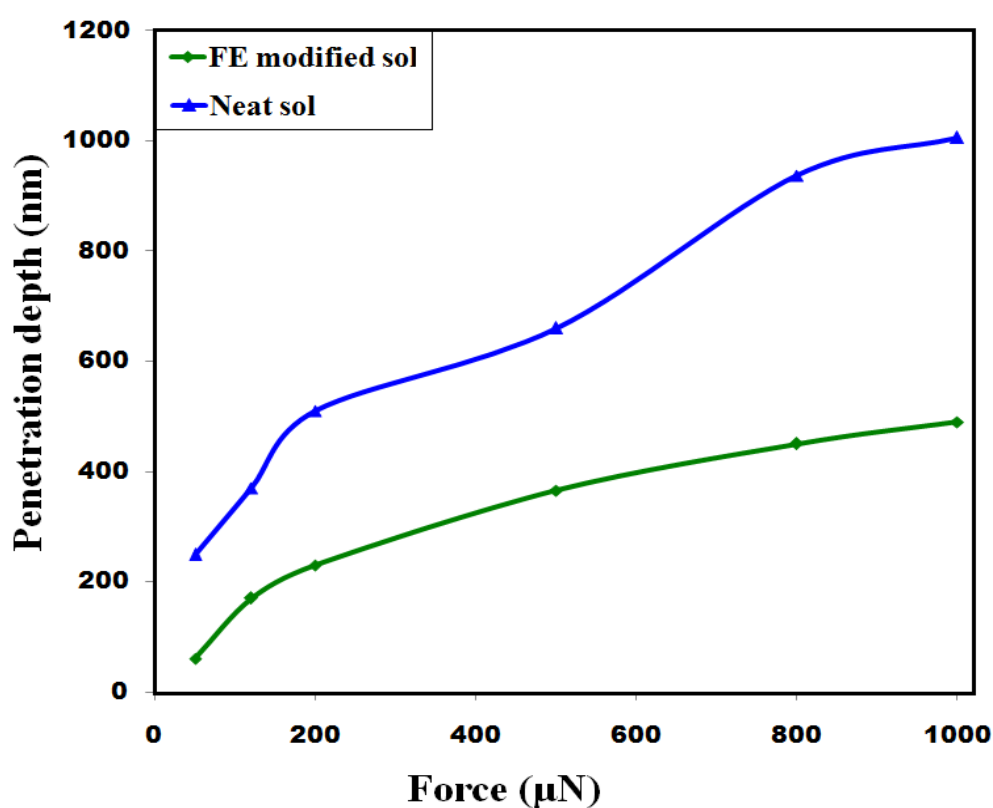


Figure 4.28: Nano-indentation of neat and FE modified sol-gel coating

Table 4.8: Cross-hatch adhesion and pencil hardness results of various FE modified sol-gel coatings

Wt% of FE	Cross-hatch adhesion	Pencil Hardness
10	4B	4H
20	5B	4H
30	5B	4H
50	3B	4H

4.5 Comparative results of various fluoro modified sol-gel systems

GPTMS-MTMS-HMMM hybrid, hydrophilic sol-gel coatings were modified with low energy fluoro-alkyl groups using fluoro-silanes of 3- fluorine atoms (3-FAS), 17- fluorine atoms (17-FAS) and a commercial 6 carbon atom perfluoro polymer (FE). Various parameters were measured to determine the hydrophobic properties after different modifications. As per WCA measurements 3-FAS and 17-FAS modification resulted in contact angle of about 100° and 110° respectively. However FE modification at optimized concentration of 30wt% concentration showed enhanced contact angle of about 118°. Increase in hydrophobicity shown by FE modification could be attributed to either decrease in surface energy or increase in surface roughness. In order to closely examine the difference in surface energies, XPS of all the three optimized fluoro-systems was carried out (Fig 4.28). It was found that the FE modified sol-gel coatings showed strong fluorine peaks, located near 680 eV and 830 eV, corresponding to F1s and FKL₂₃L₂₃ bands [73, 82, 83, 92] as compared to other two fluoro-systems. These fluoro-peaks clearly indicated the extent of surface fluorination, which was found much higher in FE modification than other fluoro-systems, supporting the superior hydrophobicity in the FE modified system.

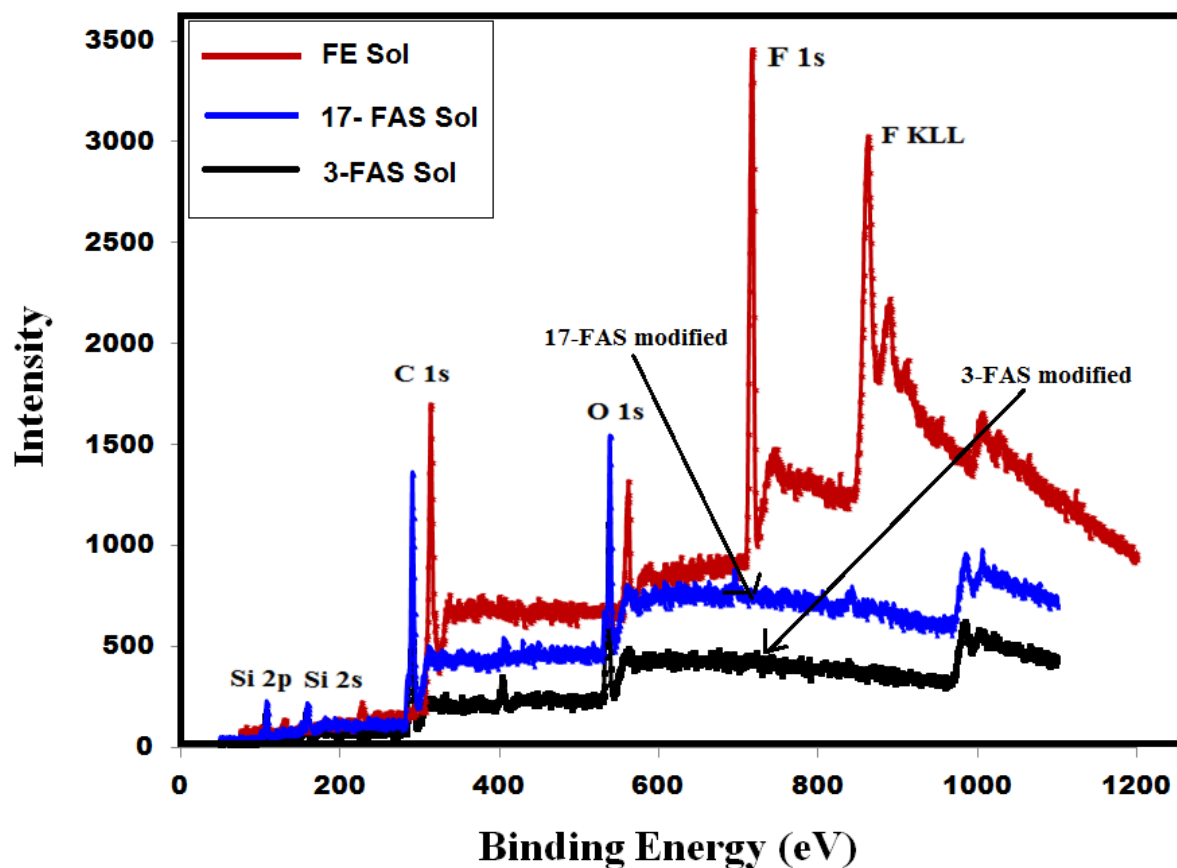


Figure 4.29: XPS analysis of 3-FAS, 17-FAS and FE modified sol-gel coating

The second factor responsible for enhancing the hydrophobicity i.e. the surface roughness was compared by using SEM and AFM analysis. As per SEM studies (Fig 4.29), FE modified coating showed micro-spheres of size ranging in diameter of 20 μ m to 30 μ m whereas 3-FAS and 17 FAS coatings were composed of smaller micro-spheres of size with diameter ranging from 5-10 μ m and 10-20 μ m respectively.

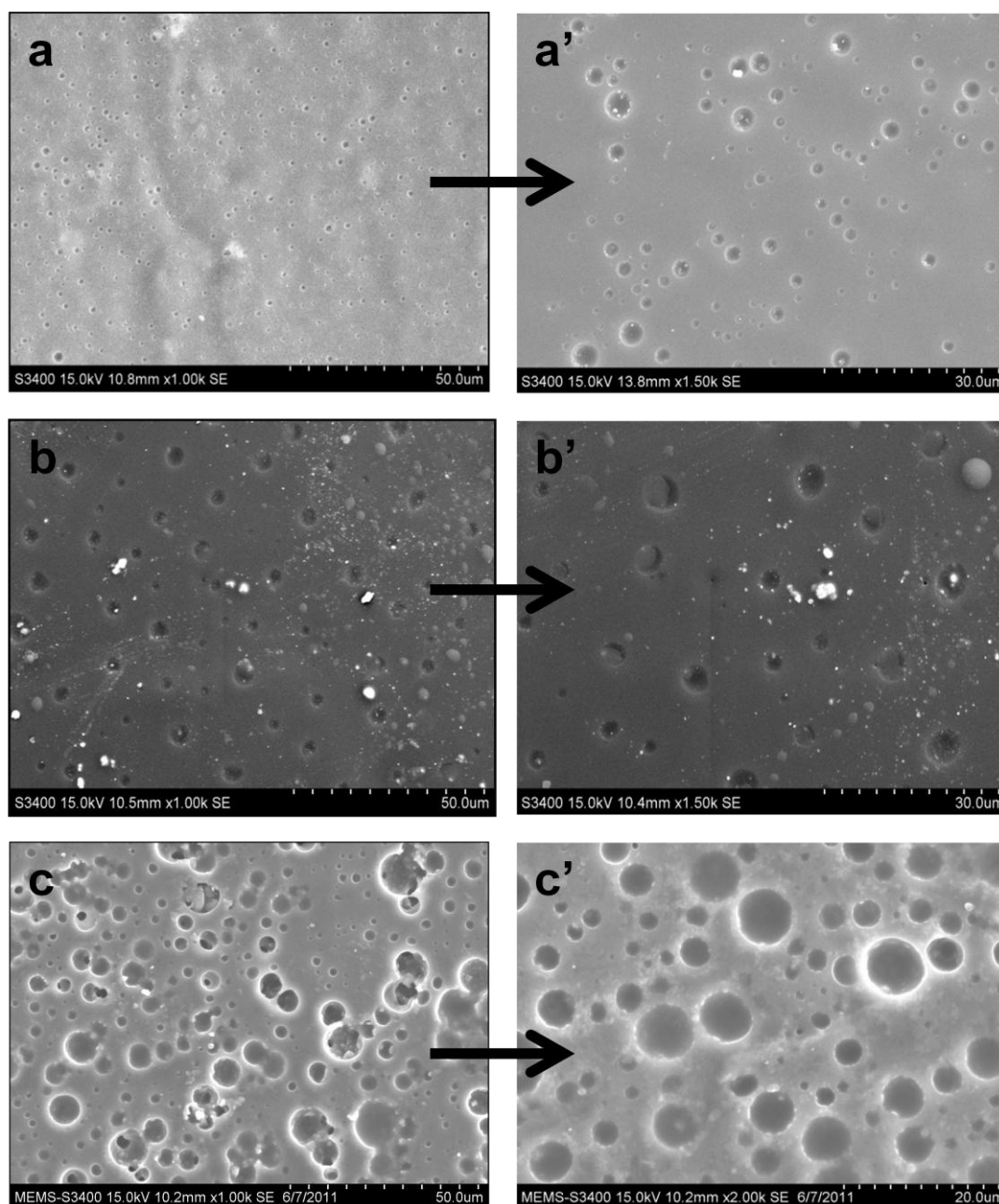


Figure 4.30 : SEM images of a)a') 3FAS, b)b')17-FAS and c)c')FE modified optimized sol-gel coatings at lower and higher magnifications respectively

When 3D AFM images were compared similar trend was observed. FE modified sol-gel coated substrate consisted of peaks much larger in magnitude as compared to other two fluoro-modifications. As seen from the Fig 4.30, maximum “height” achieved in FE modified image was 100 nm whereas in other two systems the maximum height achieved was about 50 nm only. Also the RMS values lied in the same trend with maximum value of 37 nm for FE modification as compared to 10 nm and 15 nm achieved for 3-FAS and 17-FAS modification

respectively. Hence both surface energy and surface roughness factors supported higher contact angle value and hydrophobicity of FE-modified sol-gel coatings. Another parameter which is also considered a measure of hydrophobicity is sliding angle. Both 3-FAS and 17-FAS modification did not showed any sliding behavior, indicating that the state of hydrophobicity lied in perfect Wenzel state whereas FE modification resulted in significant improvement in sliding angle $\sim 70^\circ$. Therefore, it can be said that state of hydrophobicity slightly shifted from Wenzel state to Cassie state resulting in formation of air-pockets and hence facilitating sliding of water droplets [2].

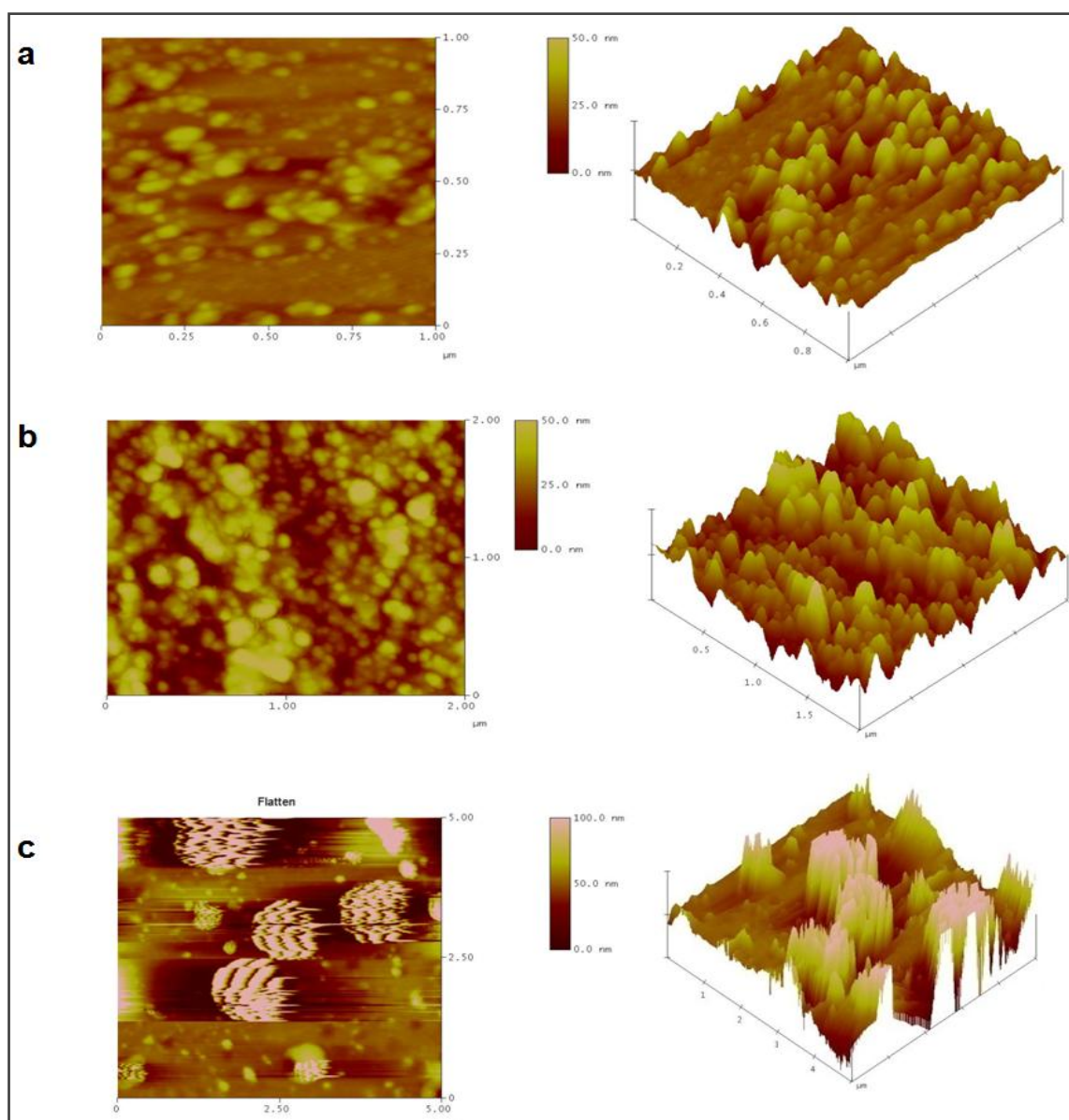


Figure 4.31: AFM images of a) 3-FAS, b) 17-FAS and c) FE modified sol-gel coatings at optimum concentrations

Further comparative potentiodynamic polarisation and EIS measurements (Fig 4.31 and Fig 4.32) revealed that FE modified sol-gel coating showed better corrosion resistance than 3-FAS and 17-FAS coatings with E_{corr} value of about 9×10^{-7} A/cm² for 30wt% FE modification. FE coatings also showed higher impedance supporting the superior water repellence nature of the FE modified coating.

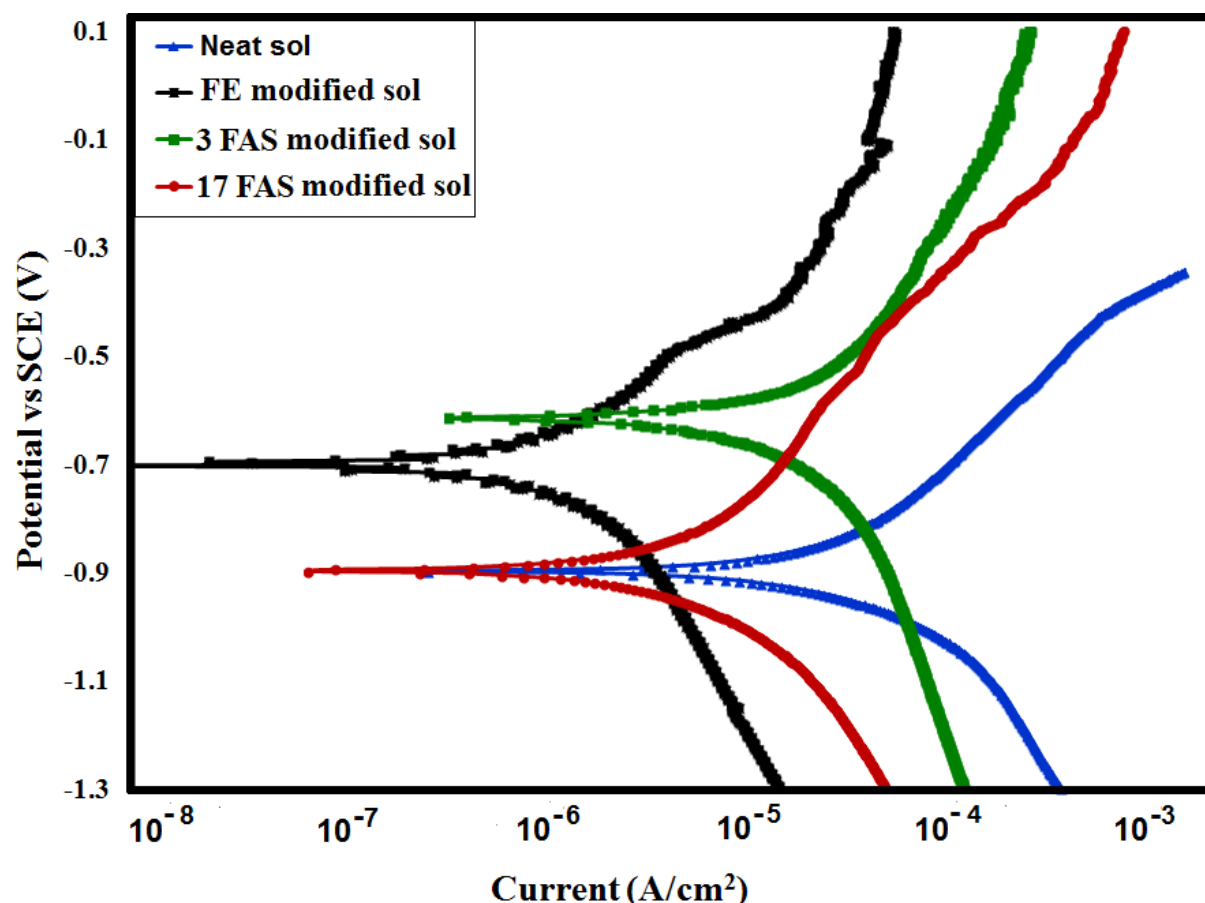


Figure 4.32: Comparative Tafel plots of neat, 3-FAS, 17FAS and FE modified sol-gel coatings at optimised concentrations

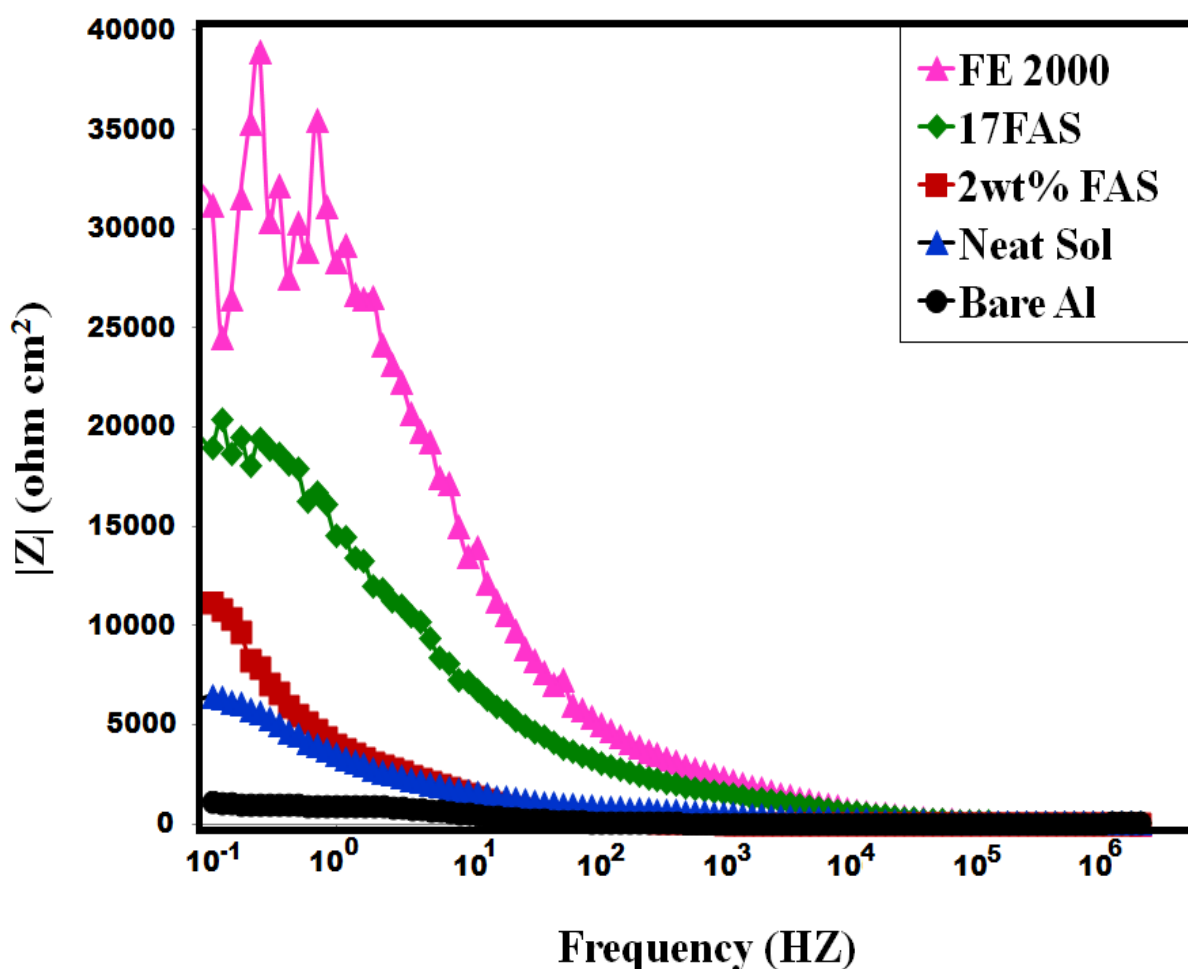


Figure 4.33: Comparative bode plots of neat, 3-FAS, 17FAS and FE modified sol-gel coatings at optimised concentrations

Finally, as per comparative nano-indentation plots (Fig 4.33), FE modification showed maximum hardness and minimum penetration depth of 490 nm for load of 1000 μ N. Also the 30wt% FE modified sol-gel coating showed strong adhesion of 5B pencil hardness of 4H.

Apart from these three fluoro-silanes, several other commercially available fluoro-additives were blended with primary inorganic-organic GPTMS-MTMS-HMMM hybrid sol. Based on the entire experimental results 30wt% FE modification was found to have better degree of hydrophobicity and water repellency as compared to others with contact angle of about 118° on aluminium. Therefore it was chosen for the final commercial formulation followed by incorporation of various nano-particles to further increase the surface roughness which ultimately resulted in excellent sliding of water droplets as the substrate was slightly tilted. After obtaining initial hydrophobicity by chemical modification of MTMS-GPTMS neat sol by 30wt% low energy FE-additive a contact angle value of about 118° and sliding angle of

70-75° for 10 μ l droplet was achieved. In order to further enhance the hydrophobic properties, FE modified formulation was further subjected to incorporation of various nano-particles with different surface chemistry, size and surface area. Nano-particles because of their unique properties resulted in the improved corrosion resistance, surface roughness, scratch resistance, and water repellency etc. at optimised concentrations. Following is the detailed analysis of nano-particles addition to present coating system.

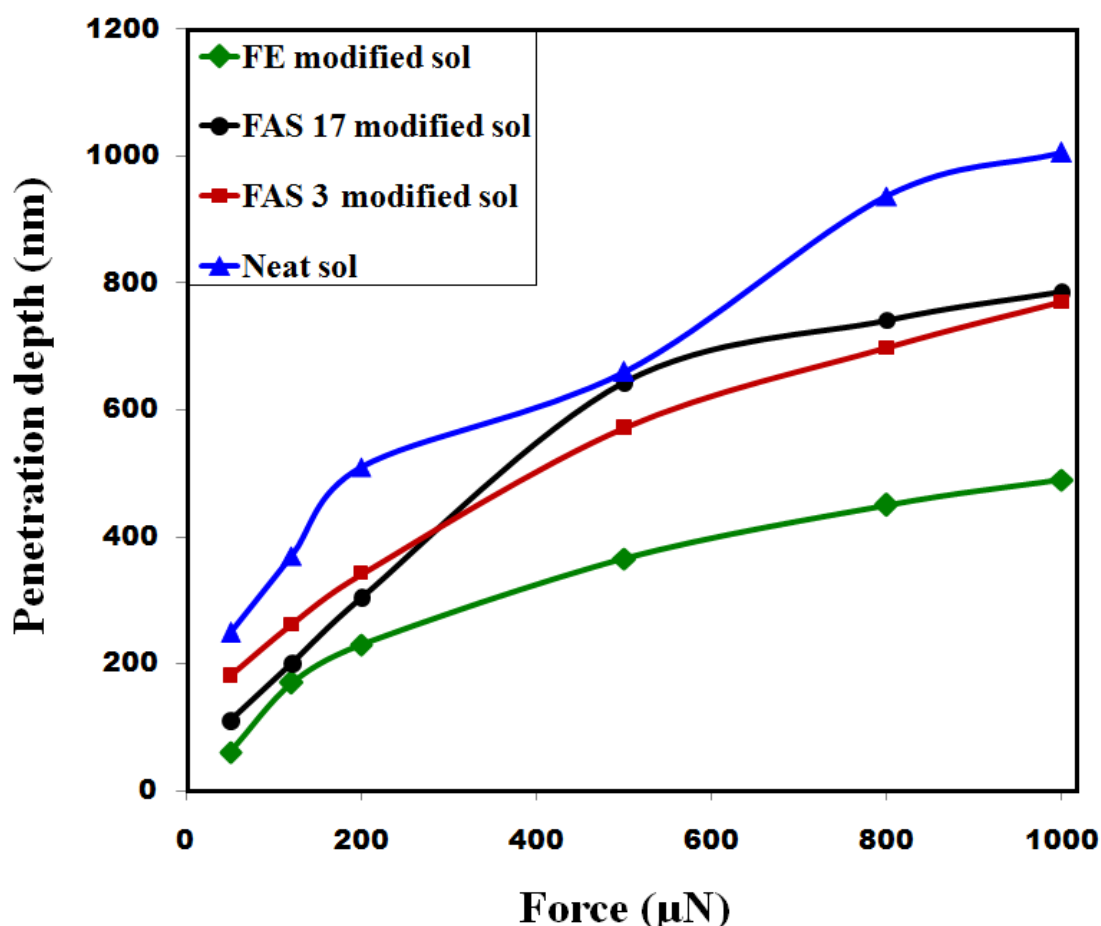


Figure 4.34: Comparative nano-indentation curves of neat, 3-FAS, 17FAS and FE modified sol-gel coatings

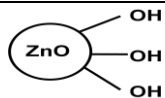
Result and Discussion –Part II

4.6 Characterisation of nano-ZnO modified FE sol-gel coatings:

4.6.1 TEM and BET analysis of nano-ZnO particles:

The nano-ZnO particles used were developed in our own laboratory were subjected to TEM and BET surface area analysis to determine the particle size and surface area. Fig. 4.35 shows the TEM image of nano-ZnO particles according to which the average diameter was found to be ~ 30 nm and consist of hydrophilic surface chemistry. Since nano-ZnO particles used consisted of large amount of surface hydroxyls, they were capable of forming larger agglomerates in aqueous medium due to particle-particle interaction between them [99, 100]. According to BET analysis, the surface area of the nano-ZnO particles was found to be quite high with value of $45 \pm 20 \text{ m}^2/\text{g}$ due to large size of nano-particles. Table 4.9 lists the summarized results.

Table 4.9: Particle size BET surface area and Surface chemistry of nano-ZnO particles

Nano-particle	Particle Size (nm)	BET surface area (m^2/g)	Surface chemistry
Nano-ZnO	30-40 nm	45 ± 20	

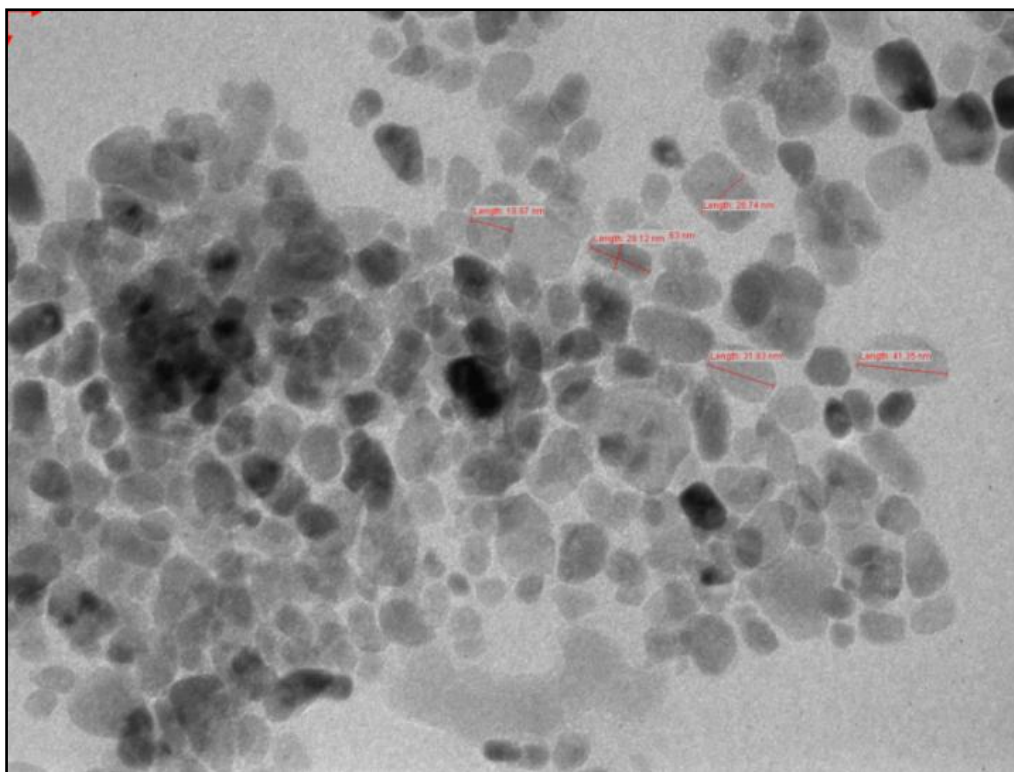


Figure 4.35: TEM image of nano-ZnO particles

4.6.2 Wetting properties of nano-ZnO modified FE sol-gel coatings:

In order to improve the hydrophobic properties further, FE modified formulation was subjected to incorporation of nano-ZnO particles (size ~30nm) at various loading levels of 1wt%, 2wt%, 3wt% and 5 wt%. The maximum contact angle achieved using nano-ZnO was about 120° at 2wt% concentration and decreases at higher loading levels (Fig 4.36). This could be explained as agglomeration of nano-particles takes place at higher concentrations due to particle-particle interaction between the surface hydroxyls groups present on the surface of nano-ZnO particles. These agglomerates due to low surface to volume ratio tend to accumulate leading to smoothening of the hydrophobic profile [101]. The hydrophilic nature of the nano-ZnO particles also supported much less increase in contact angle. Further, the hydrophobicity was defined in terms of sliding angle.

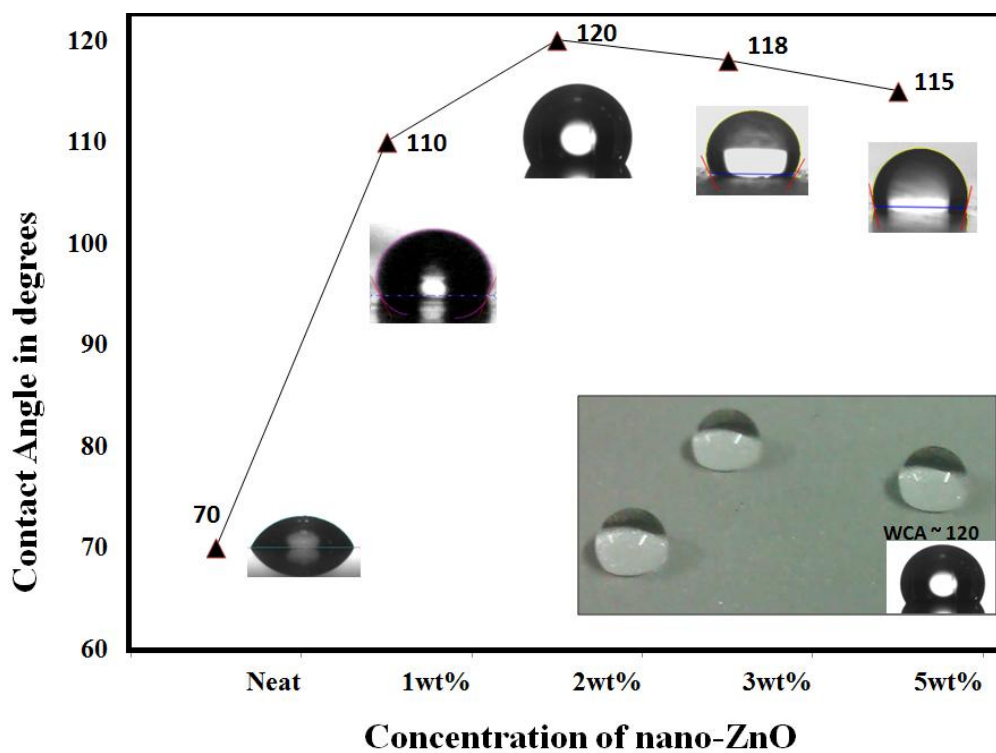


Figure 4.36: Variation of contact angle with concentration of nano-ZnO

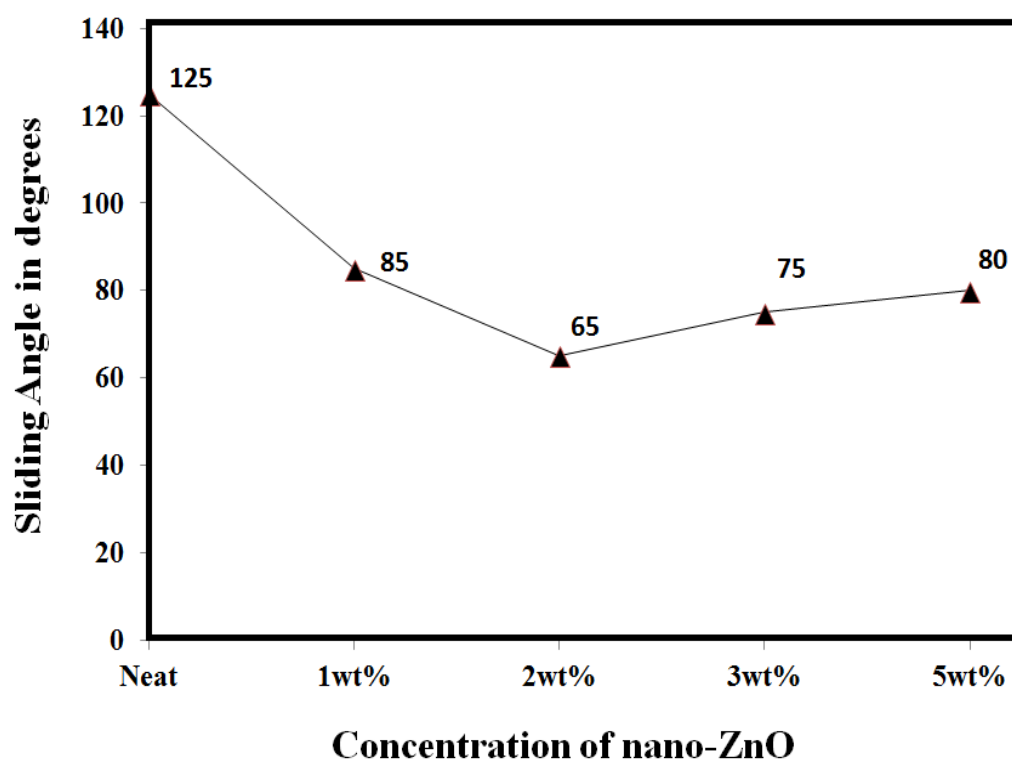


Figure 4.37: Variation of sliding angle with concentration of nano-ZnO

Fig 4.37 shows the variation of sliding angle with various percentages of nano-ZnO. Minimum value of S.A. achieved for nano-ZnO modification was 65° for 10 μ L water droplet. Therefore, the hydrophobicity achieved was sufficient to bead up water droplet, but still the water tend to stick to the surface even if tilted with high angles. This was probably due to penetration of water within the peaks and valleys (Wenzel state). Therefore in order to allow water to slide down, it should lie in Cassie-Baxter state, according to which air is trapped below the water droplet inside the pockets and does not allow water droplet to stick to the surface therefore allowing water droplet to slide off easily [102, 103]. Hence in order to achieve superior hydrophobicity by nano particles, they can be hydrophobically treated with various hydrophobic precursors and then used in coating formulation. Hence, in present work various hydrophobically modified nano-silica particles were used further.

4.6.3 Morphological characterisation of nano-ZnO modified sol-gel coatings:

The main purpose of incorporating nano-particles to FE modified sol-gel system was to achieve dual-scale roughness. FE modification resulted in microscale-roughness with craters of diameter 20-30 μ m. Further addition of nano-ZnO particles were expected to form second scale of roughness. Such hierarchical pattern tends to entrap more fraction of air and helps in achieving Cassie state [59, 104-106]. The SEM images of various concentrations of nano-ZnO modified sol-gel coated aluminium samples at different magnifications are shown in Fig 4.38. As per SEM analysis 2wt% nano-ZnO modified formulation showed maximum rough profile as compared to other percentages which supported the maximum value of contact angle for 2wt % nano-ZnO modification. The average diameter size ranged from 5 μ m-10 μ m for 2wt% modification and increases upto ~ 30 μ m at 5wt% concentration which is similar to roughness created by FE modification. Hence at higher concentration the dual scale roughness was lost due to agglomeration, leading to flattening of hydrophobic profile. The fact was closely examined by detail AFM analysis at various concentrations of nano-ZnO particles.

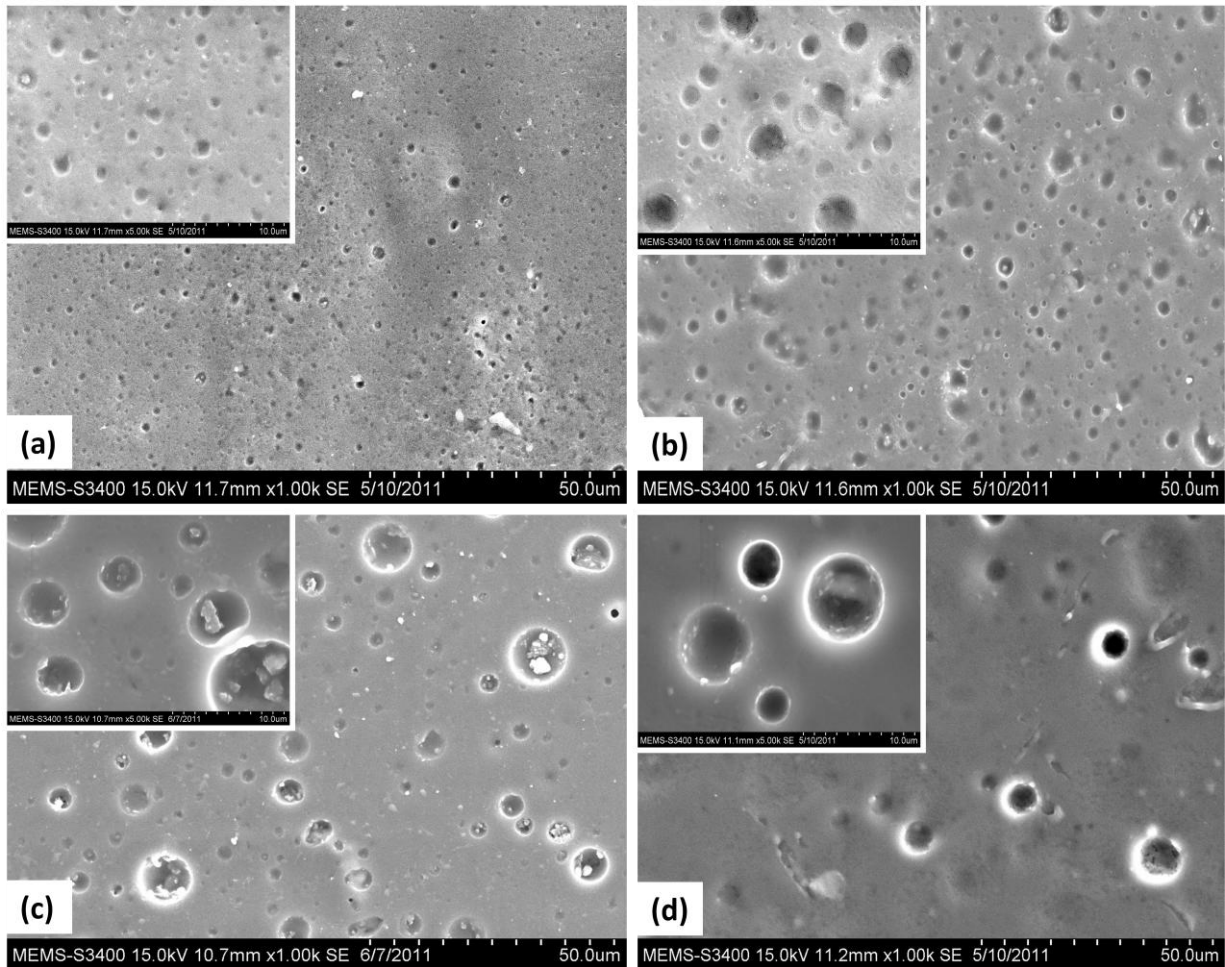


Figure 4.38 SEM images of aluminium substrate coated with (a) 1wt % (b) 2wt % (c) 3 wt % and (d) 5 wt % nano-ZnO modified sol-gel coatings

Fig 4.39 shows EDX analysis of 2wt % modified ZnO sol gel coated samples at various points. Similar diffraction pattern was obtained at all the three points indicating the presence of uniform hydrophobic profile. Further in X-ray mapping mode also (Fig 4.40), uniform distribution pattern of ZnO nano-particles all over the sample was observed at 2wt% concentration, which accounts for effective hydrophobicity.

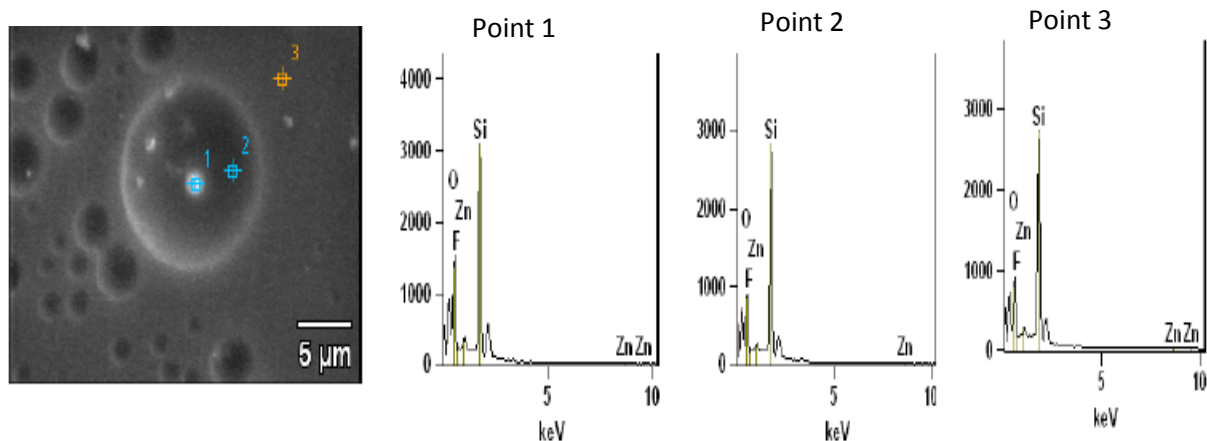


Figure 4.39: EDX plots of 2wt % nano- ZnO modified sol- gel coating at point 1, 2 and 3

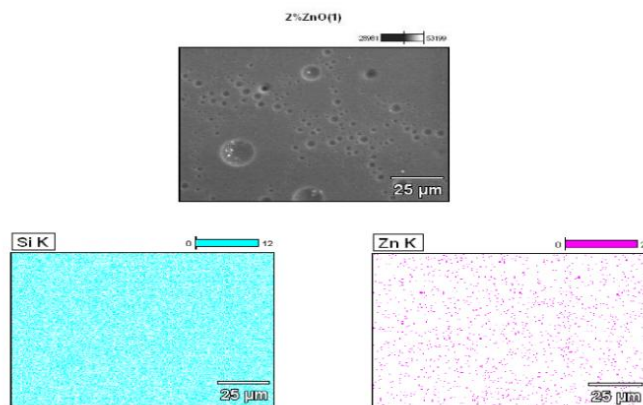


Figure 4.40: X-ray mapping at 2wt % nano- ZnO modified sol-gel coating

In order to further characterize the surface topography of the nano-ZnO modified sol-gel coatings detailed SPM analysis was performed on aluminium samples coated with sol-gel coatings with different nano-ZnO contents. Fig 4.41 shows (ai) two dimensional height images, (bi) section profile and Fig 4.42 shows (ci) magnitude profiles and (di) three dimensional topographic images obtained from SPM software aist-3.3.60 and i-apro-3.0.3 respectively. As seen from the 2D and 3D images, the number of peaks with “maximum height” increases upto 2wt% concentration of nano-ZnO and further decreases at higher concentrations due to significant agglomeration of the nano-particles. The maximum height achieved for 2wt% modification was ~ 200 nm with maximum magnitude of $\sim 10,000$ nm. Also the root mean square roughness (RMS) increases accordingly with value of 45 nm for 2wt% nano-ZnO (Table 4.10). From the section profiles in Fig 4.36 (bi), the number of peaks and valleys increases with respect to base line with increase in concentration of nano-ZnO

upto 2wt%, which implies formation of more multiscale structures than that of lower concentrations attributing to uniform distribution of nano-particles throughout the surface. Further 5wt% nano-ZnO section profile showed broad peaks indicating enhanced agglomeration at higher loading level and hence decreased surface roughness. More important, the magnitude images as seen from Fig 4.8 (ci) highlighted the nano-particle distribution pattern. The magnitude of nano-clusters increases with increase in nano-ZnO content with uniform and dense distribution of nano-particles at particles at 2wt% concentration. Hence enhanced surface roughness of 105nm was achieved after nano-ZnO modification resulting in higher contact angle of 120° and SA of 65°. The increase in hydrophobicity was not much as expected due to hydrophilic surface hydroxyl groups of nano-ZnO particles responsible for increasing the surface energy and hence reducing the overall effect of increase in surface roughness. Hence in order to achieve lower surface energy along with surface roughness nano particles must be hydrophobically modified.

Table 4.10: Variation of surface roughness with nano-ZnO concentration

Concentration of nano-ZnO	Average Surface Roughness,Rms (nm)
1	75
2	105
3	95
5	65

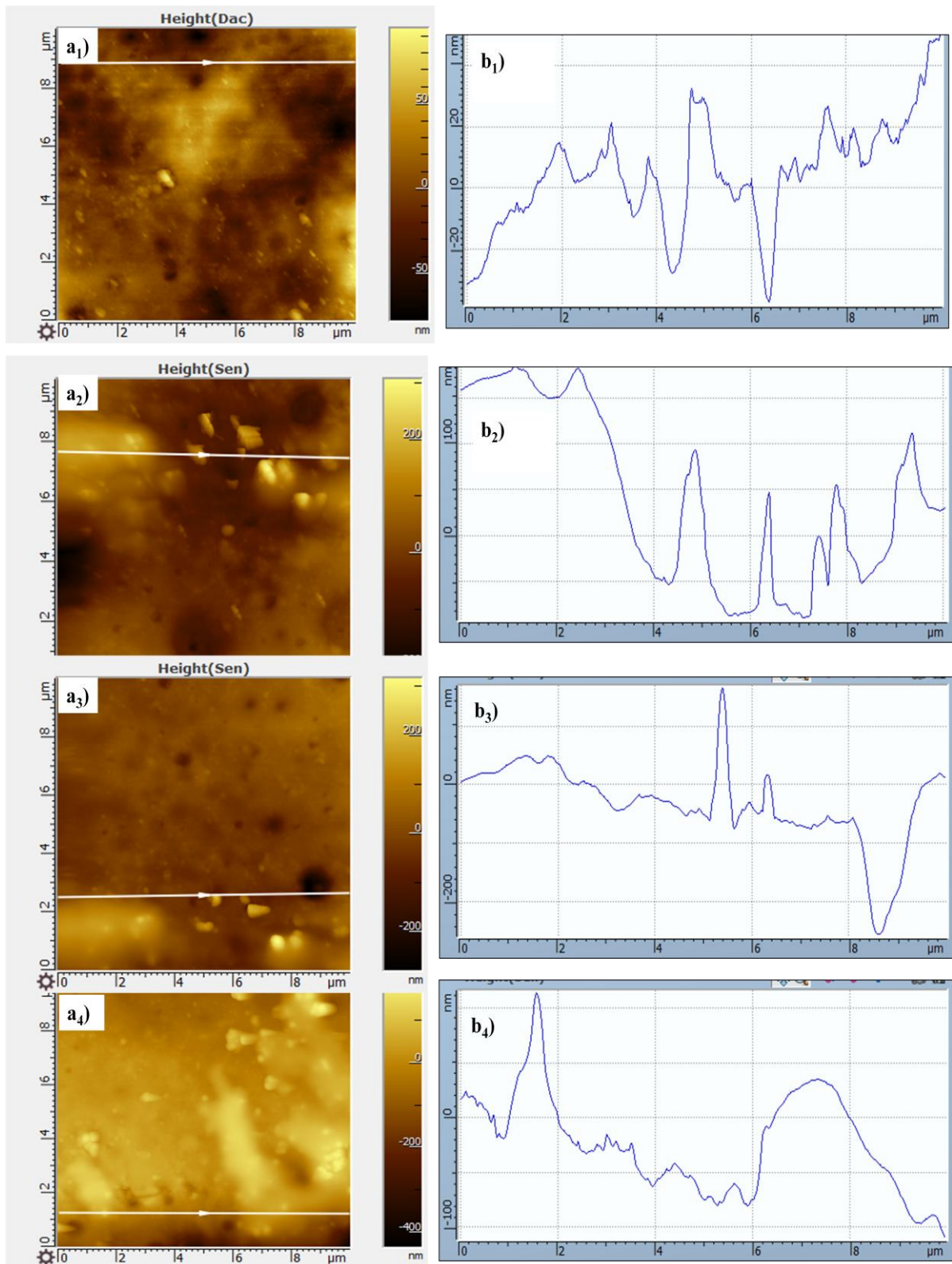


Figure 4.41: AFM images of (ai) 2D height and (bi) section profile of 1wt%, 2wt%, 3wt% and 5wt% nano-ZnO modified sol-gel coatings

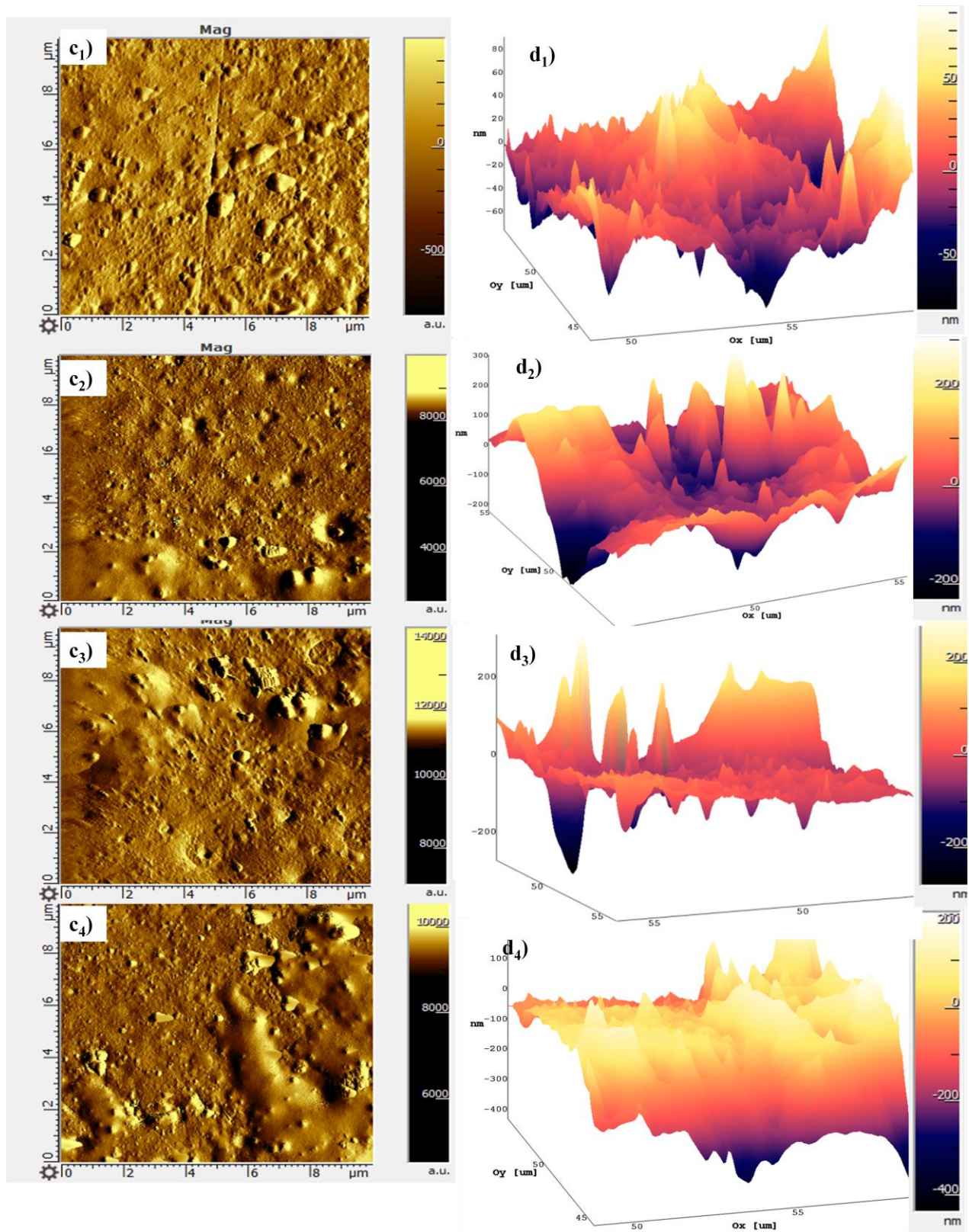


Figure 4.42: AFM images of (ci) magnitude and (di) 3-Dimensional height of 1wt%, 2wt%, 3wt% and 5wt% nano-ZnO modified sol-gel coatings respectively.

4.6.4 Structural analysis of nano-ZnO modified sol-gel coatings

Fig. 4.43 shows the FTIR spectra for Nano-ZnO modified sol gel coated samples which consisted of all the characteristic peaks of MTMS, GPTMS, HMMM and Nano-ZnO indicating a fine crosslinked structure of nano – ZnO hybrid sol gel coating. A small peak was observed due to Zn-O stretch near 650 cm^{-1} [100]. The most important fact to be discussed here is that nano-ZnO modified spectrum showed broader -OH stretch near 3423 cm^{-1} than the neat sol-gel, confirming the presence of hydroxyl groups on surface of nano-ZnO responsible for increasing the surface energy of the modified coatings. Table 4.11 lists various frequency bands obtained from both the systems.

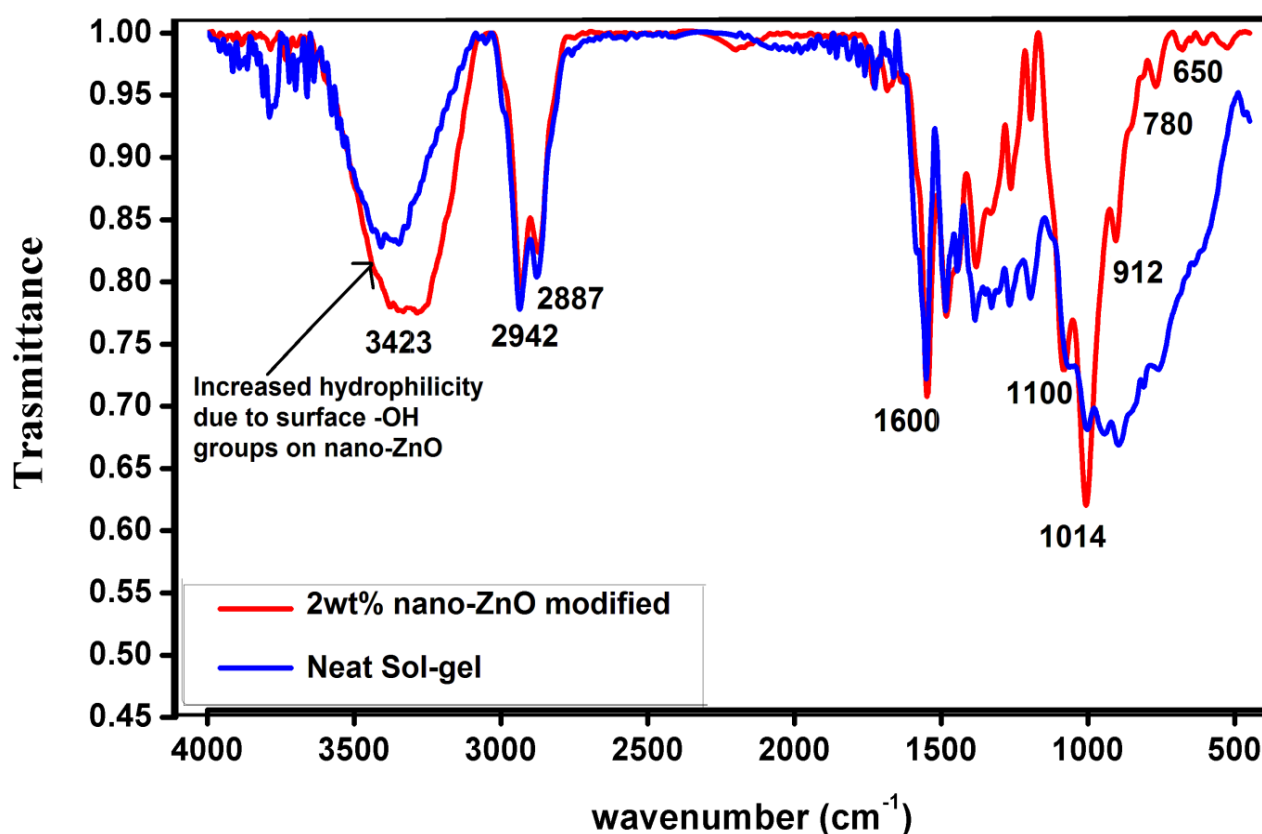


Figure 4.43: FTIR spectra of 2 wt % nano -ZnO modified sol gel coated sample

Table 4.11: FTIR data corresponding to types of bands appearing in neat and nano-Zno modified sol-gel coating

S.No.	Types of bonds	Frequency (in cm^{-1})
1.	Alkyl C-H stretch	2950 -2850
2.	Al-O-Si stretch	1120 approx.
3.	C-O-C stretch	1260
4.	C-F stretch	1100-1000
5.	C=N stretch	1750-1600
6.	Si-O-Si stretch	940-910
7.	OH bonding	3590-3750
8.	CF_3 stretch	1200-1100
9.	Zn-O stretch	Near about 650 cm^{-1}

4.6.5. Corrosion resistance of nano-ZnO modified sol-gel coatings:

Fig. 4.44 shows potentiodynamic polarisation curves of etched aluminium and different percentage of nano-ZnO (1, 2, 3 and 5wt %) modified sol-gel coatings in 3.5 % NaCl solution at scan rate 2 mV/s. The etched Al, as discussed earlier showed active dissolution due to pitting behavior with corrosion density of about $2 \times 10^{-4} \text{ A/cm}^2$. Whereas, nano-ZnO modified sol-gel coatings offered a pathway of lower current densities than the bare material. The i_{corr} value of optimised 2wt% nano-ZnO modified coating was about 9.18×10^{-7} which is of the same order in magnitude from 30wt% FE modified coating ($9.83 \times 10^{-7} \text{ A/cm}^2$) and two orders less in magnitude from neat sol-gel ($2.85 \times 10^{-5} \text{ A/cm}^2$). The corrosion potential (E_{corr}) showed a positive shift for all the concentrations of nano-ZnO from $-1.3V_{\text{SCE}}$ for bare Al to $-0.78V_{\text{SCE}}$ for 2wt% nano-ZnO modification, providing the anodic protection to the coated substrate. This increase in corrosion resistance is attributed to increase in water-repellency achieved after modification with nano-ZnO and the barrier properties of nano-ZnO particles that provides tortuous diffusion pathway to the corrosive species such as oxygen, hydroxide and chloride ions [70, 107, 108]. Table 4.12 lists the electrochemical parameters obtained from the corrosion studies.

Table 4.12: Polarisation and EIS parameters of various ZnO modified sol-gel coatings

Concentration of nano-ZnO	E _{corr} (V)	i _{corr} (A/cm ²)	Impedance (ohm cm ²)
Bare Al	-1.30	2.83× 10 ⁻⁴	1.02× 10 ³
1wt% nano-ZnO	-1.08	7.35× 10 ⁻⁷	3.81× 10 ⁴
2wt% nano-ZnO	-0.93	7.94× 10 ⁻⁷	1.06× 10 ⁵
3wt% nano-ZnO	-0.959	1.95× 10 ⁻⁶	5.74× 10 ⁴
5wt% nano-ZnO	-0.876	1.56× 10 ⁻⁵	6.12× 10 ⁴

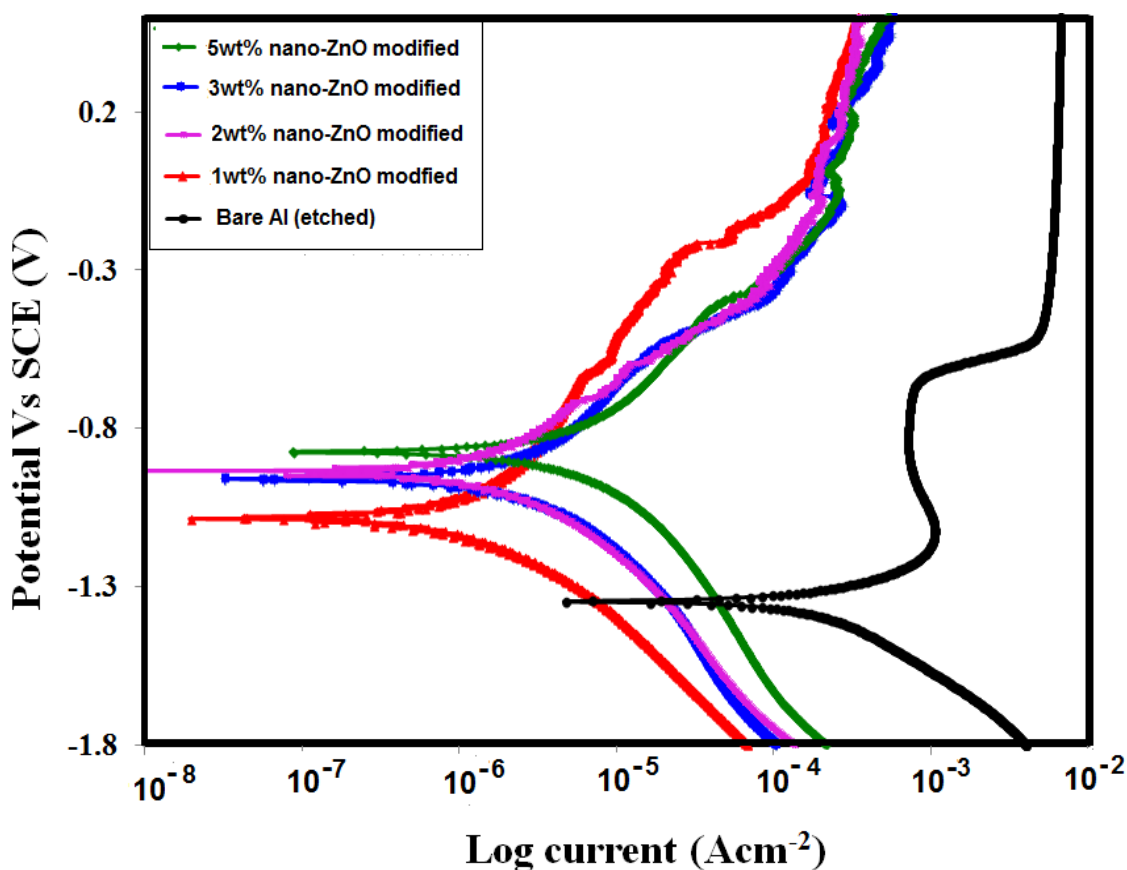


Figure 4.44: Potentiodynamic polarisation curves of bare Al and various wt % of nano-ZnO modified sol-gel coated samples

Fig 4.45 shows EIS plots of various nano-ZnO modified sol-gel systems. As per impedance spectroscopy analysis nano-ZnO coatings showed superior corrosion resistant properties as

compared to FE modified coatings. It was found that impedance increases with increase in nano-ZnO concentration upto 2wt% with value of $|Z|_{0.1\text{Hz}} \sim 1.06 \times 10^5 \Omega\text{cm}^2$ which is one order more in magnitude than FE modified sol-gel coatings and decreases with further addition. Hence incorporation of nano-ZnO after FE modification to GPTMS-MTMS-HMMM hybrid sol-gel coatings resulted in enhanced hydrophobicity both in terms of CA and SA leading to superior corrosion resistance properties. Improvement in corrosion resistance is attributed to dual scale roughness in form of peaks and valleys which allow partial entrapment of air making a barrier layer resisting the penetration of electrolytes [109]. Also the nano-particles itself provided tortuous path to the incoming electrolyte.

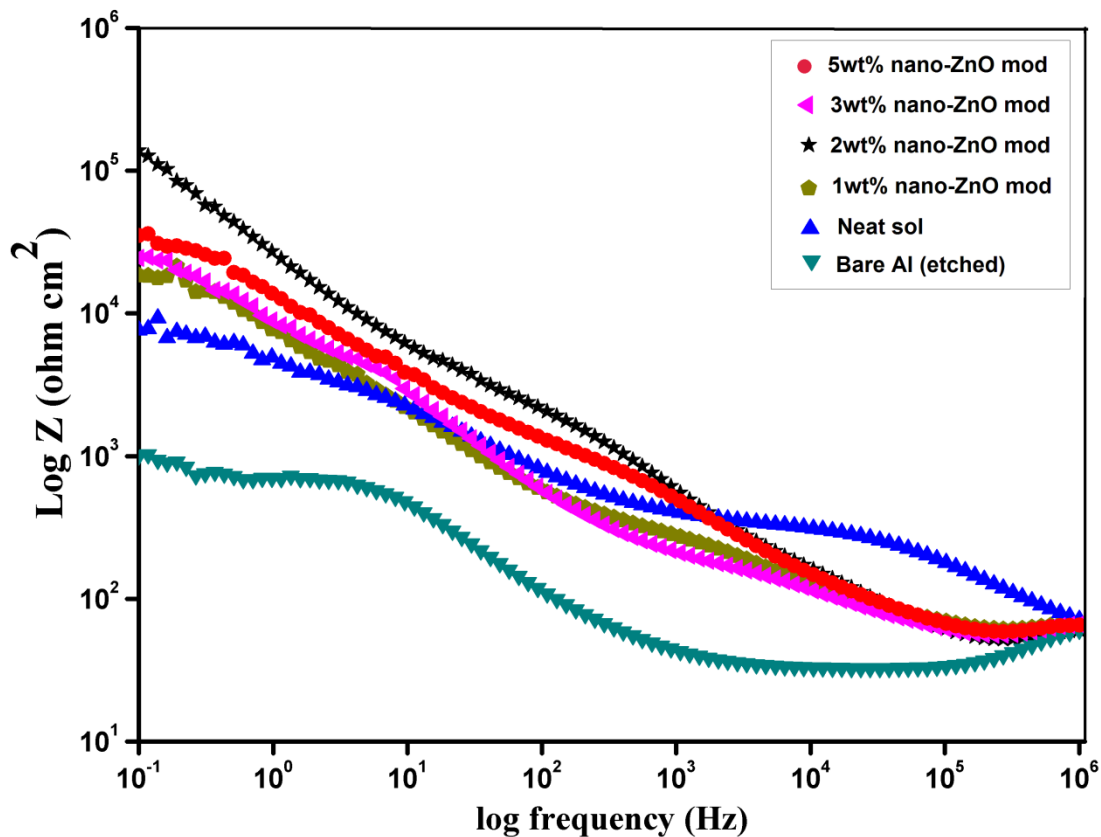


Figure 4.45: Bode plots of bare Al and various nano-ZnO modified sol-gel coatings

4.6.6. Mechanical properties of nano-ZnO modified sol-gel coatings

The indentation forces were plotted as function of the penetration depth for both neat and 2wt% nano-ZnO modified sol-gel coated substrate (Fig 4.46). Neat sol gel showed maximum penetration depth of 1000 μm for load of 1000 μN whereas 2wt% nano-ZnO modified sol-gel coating resulted in improved hardness with penetration depth of 480nm for load of 1000 μN .

Such improvement in coating harness could be attributed to the embedment of the coarser nano-ZnO particle aggregates within the sol-gel matrix offering more resistance to deformation as compared to neat sol.

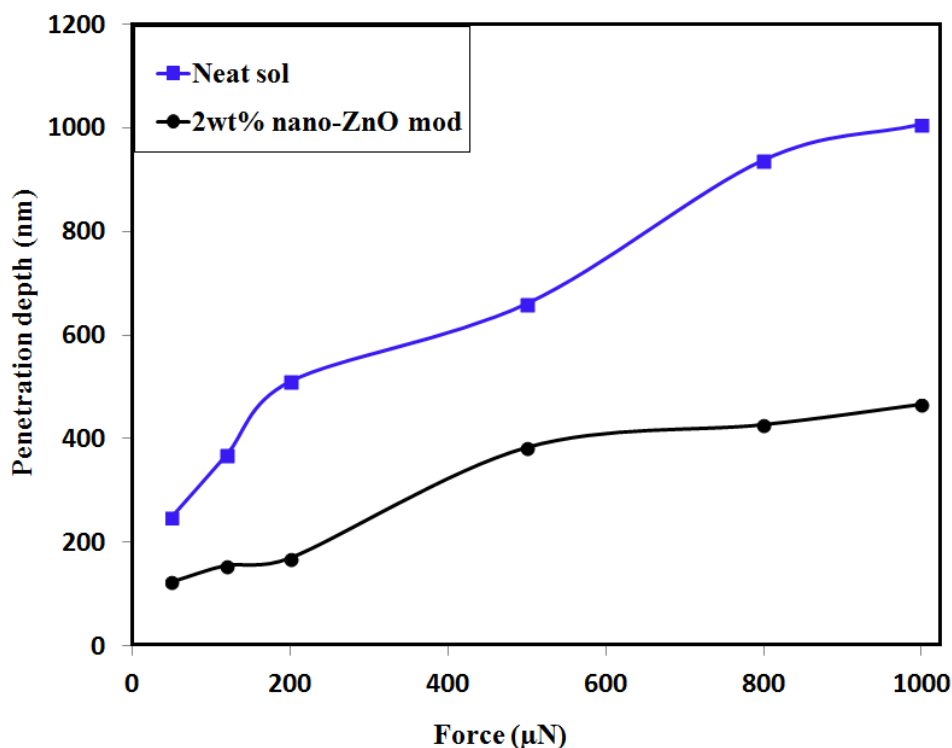


Figure 4.46: Load displacement curve of neat and nano-ZnO modified sol-gel coatings

Further, cross-hatch test was carried out to determine the adhesion of the various nano-ZnO modified coatings as listed in Table 4.13. It was found that 2wt% nano-ZnO modified formulation showed strong adhesion to the substrate with ASTM adhesion value of 5B and excellent pencil hardness of 5H. This indicates high resistance to indentations and deformations.

Table 4.13: Crosshatch adhesion and pencil hardness results of various wt % of nano -ZnO modified sol-gel coatings

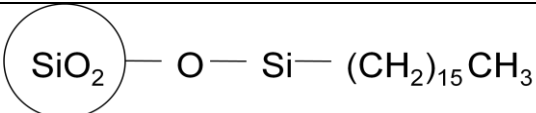
Wt% of nano-ZnO	Cross-hatch adhesion	Pencil hardness
1	5B	5H
2	5B	5H
3	5B	5H
5	3B	4H

4.7. Characterisation of HDTMS modified- fume silica sol-gel coatings:

4.7.1. TEM and BET Analysis

Fig 4.47 shows the TEM image of HDTMS nano-silica particles. The average particle size obtained from TEM investigation ranged from 15 to 25 nm which was lower than nano-ZnO particles (30nm). Also these particles showed high BET surface area of $85 \pm 20 \text{ m}^2/\text{g}$ due to smaller size and micro-pore structure of silica nano-particles (Table 4.14). Nano-silica particles, due to high thermodynamic surface energy tend to assemble together to obtain a stable state at higher concentrations. Hence, HDTMS modification resulted in reduced surface energy due to long hydrophobic non-polar chains [110, 111].

Table 4.14: Physical parameters of HDTMS nano-silica

Modified Silica	Average Particle size	Average BET surface area	Surface Chemistry
HDTMS nano-silica	15 to 25 nm	85 ± 20	 $\text{SiO}_2 - \text{O} - \text{Si} - (\text{CH}_2)_{15} \text{CH}_3$

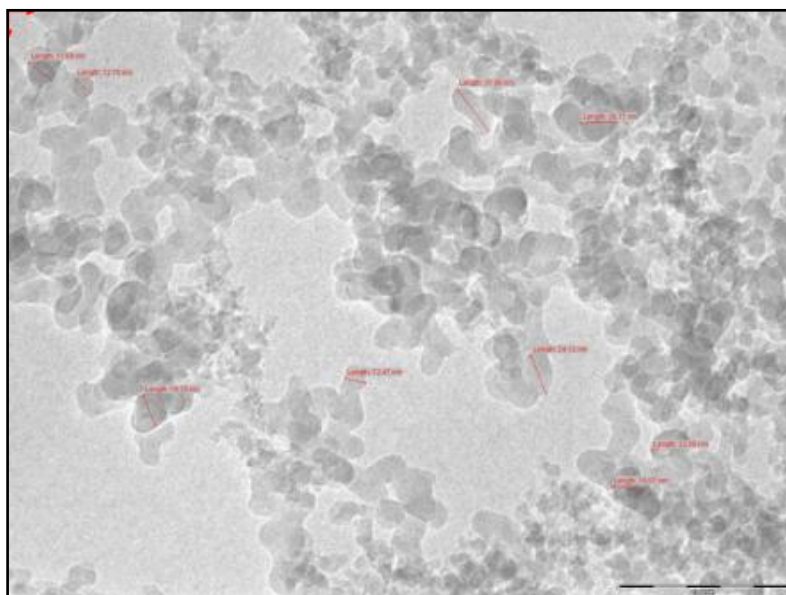


Figure 4.47: TEM image of HDTMS modified nano-silica particles

4.7.2 Contact Angle and Sliding Angle Analysis:

Fig 4.48 and Fig 4.49 shows average contact angle and sliding angle variation with various percentages of HDTMS modified fumed-silica, incorporated in FE sol-gel coating on aluminium samples. Ultrasonicing HDTMS-nano particles in the sol-gel matrix resulted in lowering of surface energy as the Hs from the OH groups on the silica surface were replaced by hydrolytically stable $-\text{Si}-\text{C}_{16}\text{H}_{33}$ groups [112, 113]. Secondly, high surface roughness was also achieved due to small size and high BET surface area of particles. In spite of favorable parameters, it was observed that there was not much effect on contact angle value on FE sol-gel coating after HDTMS-nano-silica modification. The maximum contact angle achieved was 118° for 1wt% concentration which was similar to FE coatings. The contact angle decreases with further loading of HDTMS nano-silica due to extensive agglomeration even at slightly higher percentage.

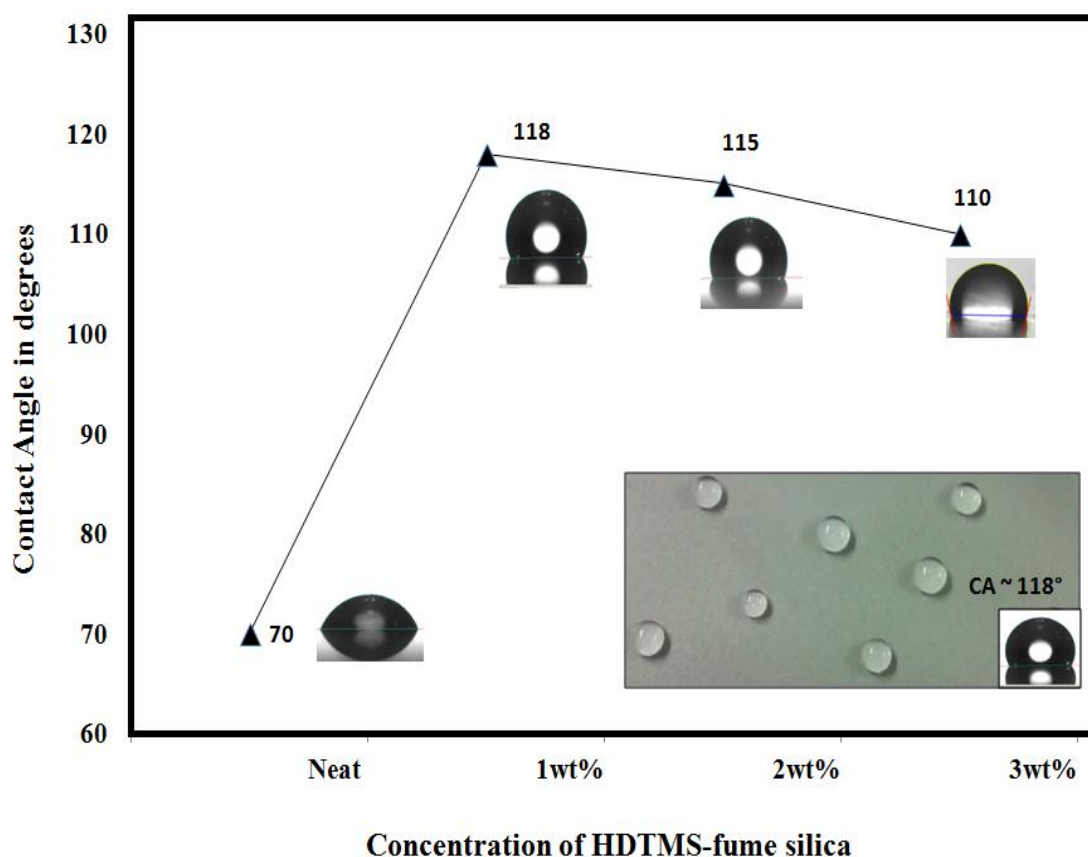


Figure 4.48: Variation of contact angle with concentration of HDTMS nano-silica particles

However improvement in hydrophobicity was achieved in terms of sliding angle. The 10 μ L water droplet displayed a sliding angle of $\sim 40^\circ$ at 1wt% concentration and increases with further addition of nano-silica. The probable reason for such behavior could be that hydrophobicity lied in mixed state where both Wenzel and Cassie regime are partially realised [59]. In this state large and smooth areas of the topography are filled with water (Wenzel), but the small nano-crevices allow sliding of water (Cassie-Baxter). Hence, the sliding angle becomes more significant than contact angle.

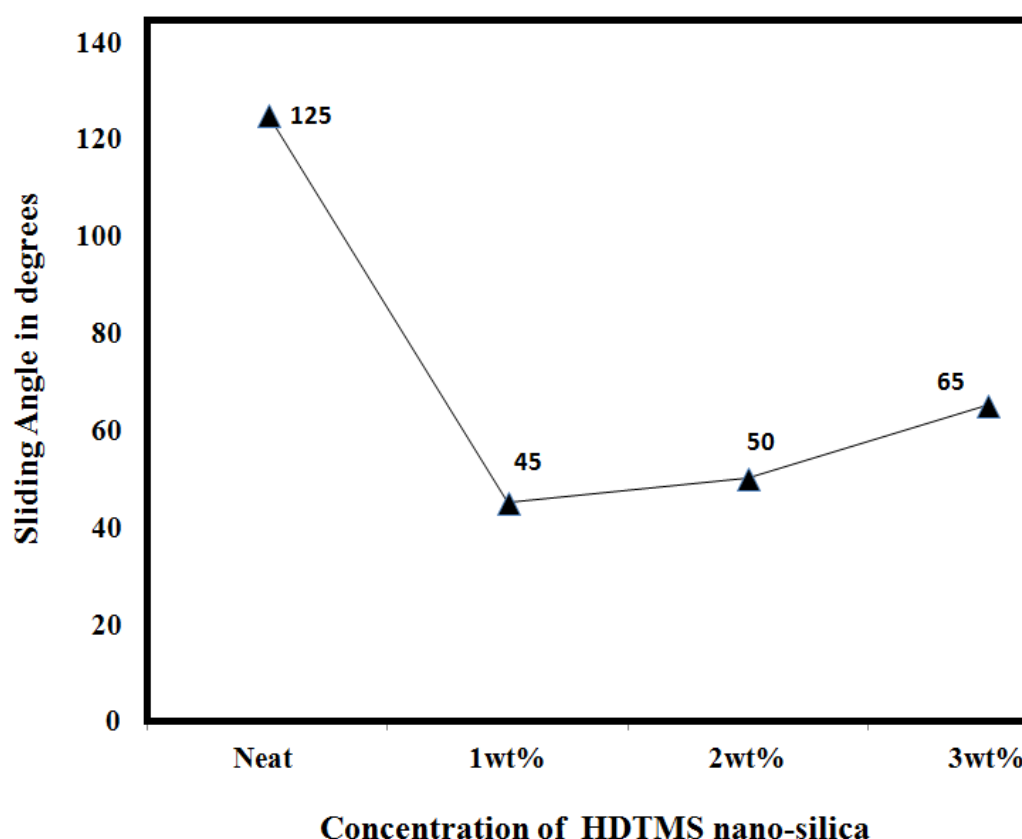


Figure 4.49: Variation of sliding angle with concentration of HDTMS nano-silica concentration

4.7.3 Morphological analysis of HDTMS modified FE-sol gel coatings:

Addition of the C-16 nano-silica particles to the FE system provoked significant morphology changes. Figs. 4.50 shows SEM images of Al panels coated with HDTMS fume-silica modified sol-gel coating at loading levels of 0.5wt%, 1wt%, 2wt% and 3wt%. According to SEM pictures HDTMS-nano-silica modification exhibits sheet-like layer with a uniform micro-nano pattern observed at 1wt% which diminishes at higher percentages due to

agglomeration of fumed-silica particles. Uniform distribution of silica particles was observed at 1wt% of HDTMS silica modification with micro-cavities and nano-filaments ranging from diameter of several nano-meters to $\sim 500\mu\text{m}$, resulting in dual scale roughness. Such hierarchical morphology supports the higher value of water contact angle of 118° at 1wt% and sliding angle of about 40° - 50° for $10\mu\text{L}$ water droplet. At higher concentrations, significant agglomeration of silica particles was observed, leading to flattening of surface topography, thereby decreasing the contact angle. The superior sliding behavior of water droplets indicated that the water droplet was not completely trapped as in Wenzel state and showed a significant shift from Wenzel state towards Cassie –Baxter state.

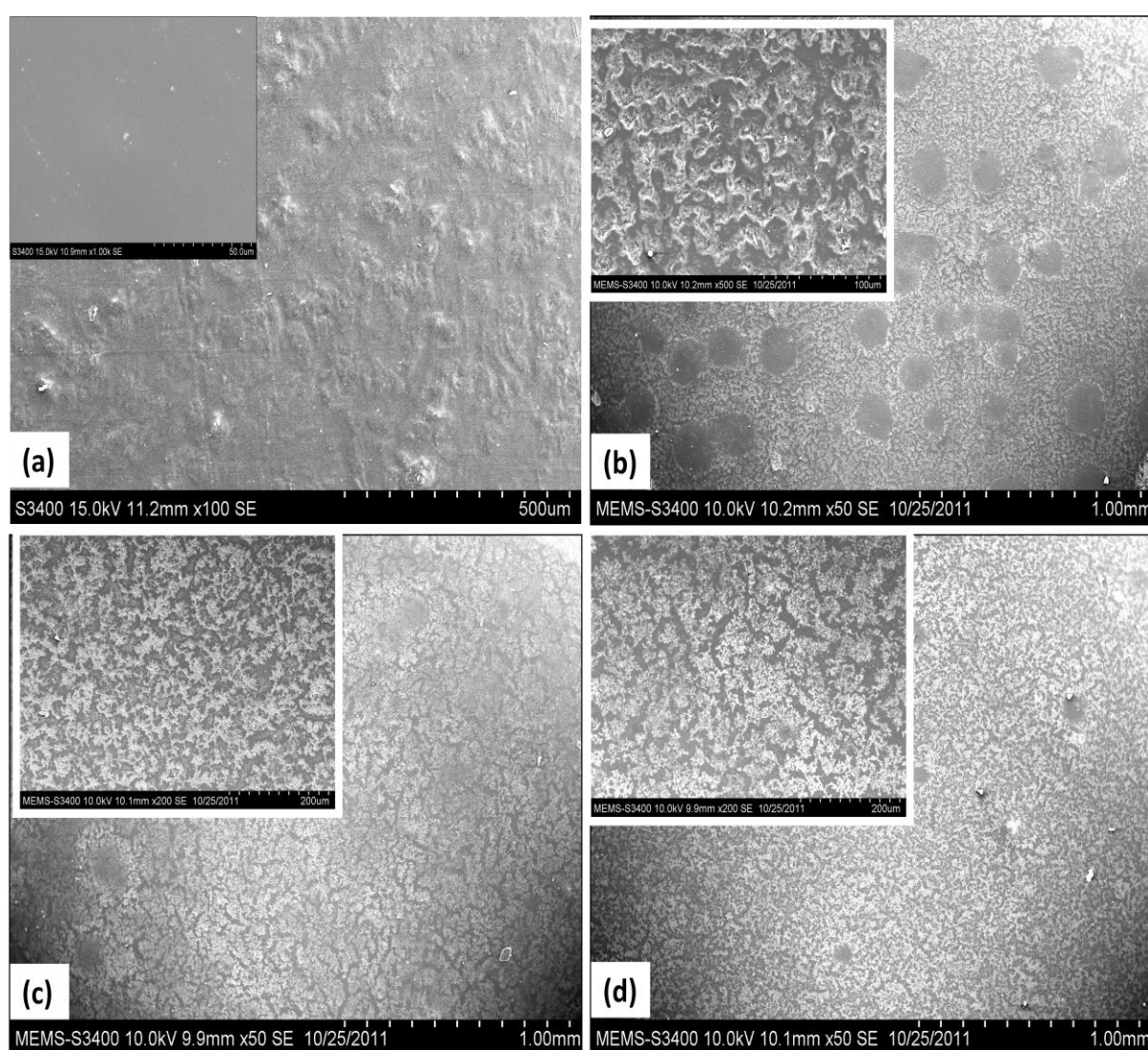


Figure 4.50: SEM images of a) 0.5wt%, b) 1wt%, c) 3wt% and d) 5wt% HDTMS nano-silica modified sol-gel coatings

In order to study the surface structure of the nano-aggregates that protrude above the smooth sol-gel film, AFM analysis was carried out. Fig 4.51 shows (ai) two dimensional height images, (bi) section profile and Fig 4.52 shows (ci) magnitude profiles and (di) three dimensional topographic images of various HDTMS modified fume silica sol-gel coatings at loading levels of 1wt%, 2wt% and 3wt%. The morphological features illustrated in 2D and 3D images of various concentrations of HDTMS nano-silica sol-gel coatings depicted randomly distributed protruding aggregates, implying that a two-length-scale hierarchical structure was formed on the surface. However 1wt% modification showed maximum number of peaks and cavities with “height” and “depth” of about 50nm and 100 nm respectively, value of around 75nm (Table 4.15). At higher percentages of HDTMS, roughness decreases to supporting relatively more hydrophobic character achieved for 1wt% concentration. Besides, quantitative roughness measurements were performed in several places of each sample. Maximum roughness was achieved for 1wt% of HDTMS modified formulation with RMS about 50nm, because of significant agglomeration of silica nano-particles. As per section profiles also, displayed in Fig 4.51 (bi) 1wt% HDTMS nano-silica coating showed maximum number of sharp peaks and valleys with respect to base line, whereas broadening was observed at higher percentages implying flattening of the hydrophobic profile. Similar trend was clearly observed from the magnitude images in Fig 4.52 (ci). As seen, the nano-silica small aggregates with magnitude of 10,000 nm were uniformly distributed and distinctly visible at 1wt% and goes on agglomerating with further addition upto magnitude of 14,000nm. Hence the HDTMS nano-silica incorporated coatings were rougher and displayed micro-nano structure as compared to 30wt% FE formulation thereby minimizing the adhesive interaction between the liquid drop and solid surface and making the drop to spontaneously slide down the inclined plane at lower angle of about 40-45°. Thus, it can be said that both Wenzel and Cassie regimes were partially resumed and dual scale roughness was achieved due to both perfluoro groups and HDTMS nano-silica particles [2].

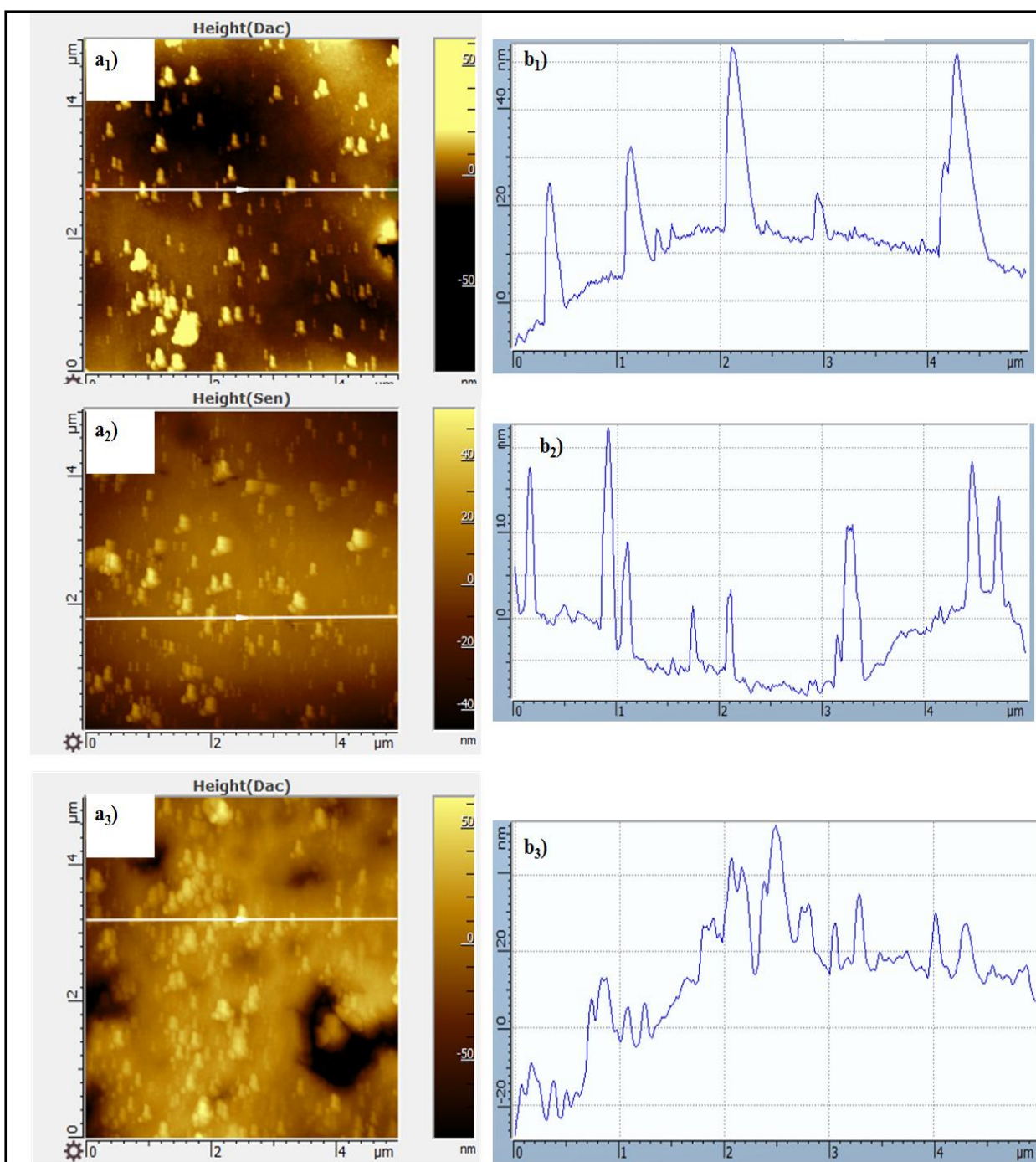


Figure 4.51: AFM images of (ai) 2D height and (bi) section profile of 1wt%, 2wt% and 3wt% HDTMS nano-silica modified sol-gel coatings respectively

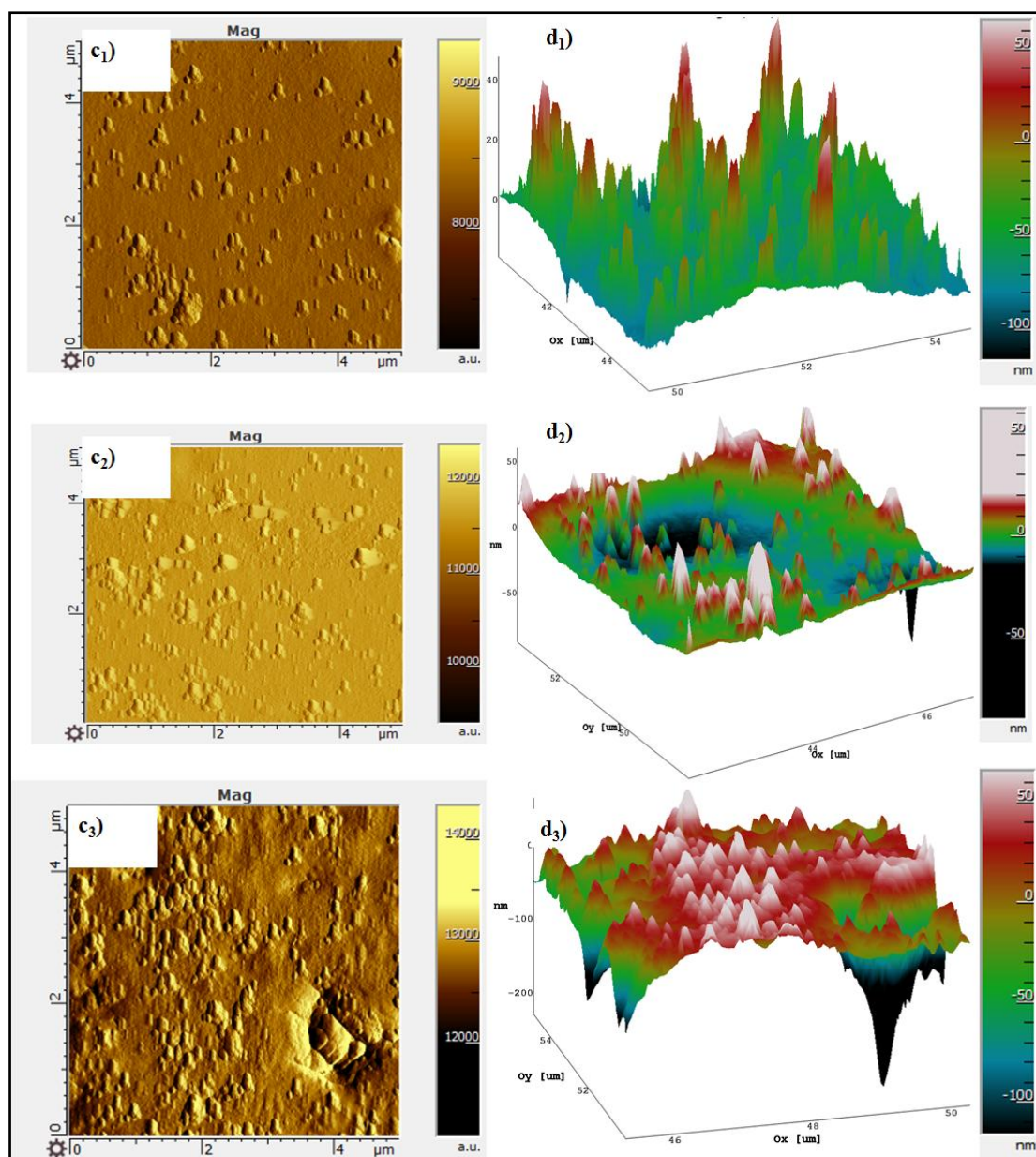


Figure 4.52: AFM images of (ci) magnitude and (di) 3-Dimensional height of 1wt%, 2wt%, and 3wt% HDTMS nano-silica modified sol-gel coatings respectively

Table 4.15: RMS values of various HDTMS-nanosilica modified sol-gel coatings

Concentration of HDTMS-nanosilica	Average RMS (nm)
1wt%	75
2wt%	63
3wt%	60
5wt%	50

4.7.4 Structural Analysis of HDTMS-nanosilica modified sol-gel coatings

As per FTIR spectroscopy (Fig 4.53), the absorption bands observed around 2942 and 2887 cm^{-1} in all neat, FE and 1wt% HDTMS modified sol-gel coating corresponds to symmetric and asymmetric stretching vibration modes of CH_2 bonds, respectively. The reduced intensity of CH_2 band though modified with long carbonated organic chain particles implied more of horizontal embedment of HDTMS nano-particle than vertical arrangement. The residual Si-OH groups which are the main source of hydrophilicity of the as developed coatings were found to decrease significantly due to replacement of the surface hydroxyl groups of nano-Silica with non-hydrolysable $-\text{Si-C}_{16}\text{H}_{33}$ groups resulting in significant broadening of $-\text{OH}$ peak in nano-modified spectra near 3423cm^{-1} [114]. The peaks around 1100, 800 and 470 cm^{-1} in nano-modified spectra arise due to asymmetric, symmetric and the bending modes of SiO_2 respectively [113].

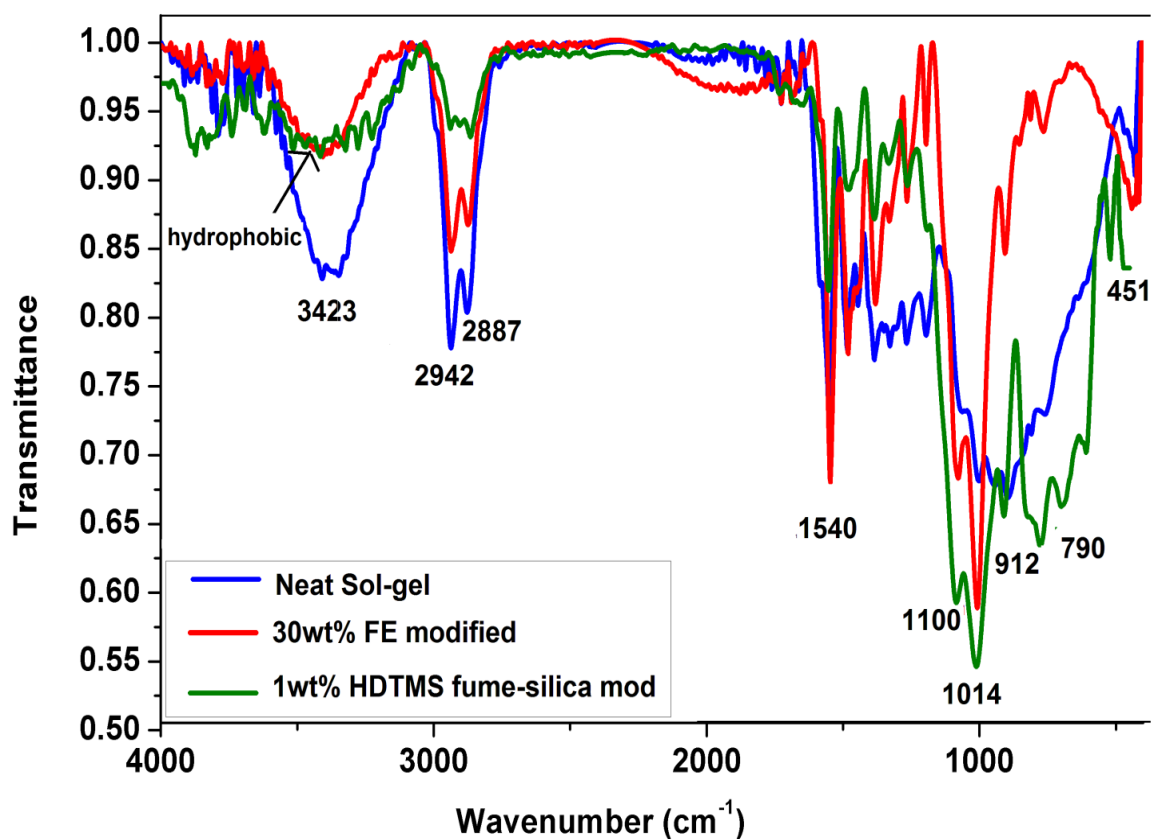


Figure 4.53: FTIR spectra of neat and HDTMS nano-silica modified sol-gel coating

4.7.5 Corrosion resistance of HDTMS-nano-silica modified sol-gel coatings

Effect of long chain organic silica nano-particles was also studied on corrosion resistance of the hydrophobic coatings. Fig 4.56 and Fig 4.57 displays potentiodynamic polarisation and electrochemical EIS plots of bare and various HDTMS nano-silica modified sol-gel coated samples. Table 4.16 lists various polarisation and EIS parameters for different sol-gel compositions. As discussed earlier, the polarisation curve of bare Al after etching in 10% NaOH solution has been included as reference data to compare the corrosion behavior of various modified systems. HDTMS nano-silica modified coatings showed a typical polarisation curve with lower polarisation current and hence better corrosion resistance as compared to bare and neat sol-gel coated Al sample. Though various HDTMS modified sol-gel coatings showed similar order of current densities of about $\sim 5.76 \times 10^{-6}$, corrosion potential showed a negative shift with the extent of nano-silica loading. Hence 1wt% HDTMS nano-silica coating showed better protection efficiency with E_{corr} of -0.84V than 2wt% and 3wt% formulation having E_{corr} value of -0.93V and -1.04V respectively.

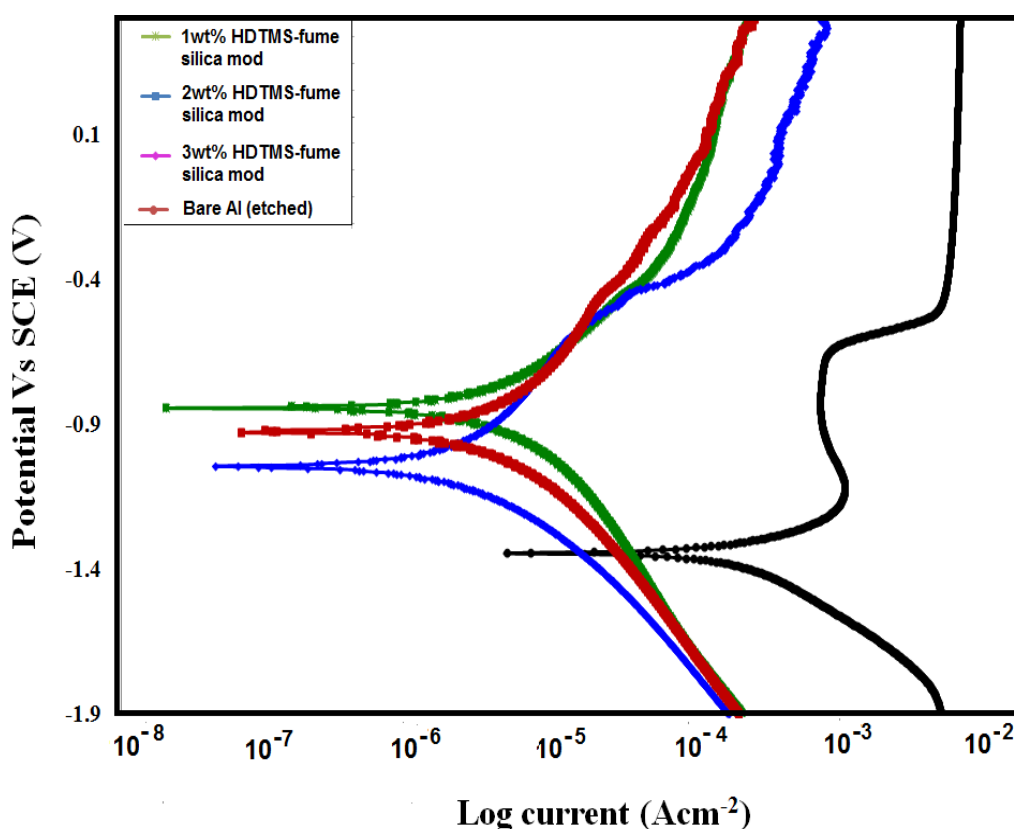


Figure 4.56: Tafel plots of etched Al and various HDTMS-nano-silica modified sol-gel coated Al samples

This trend in corrosion behavior again relates the hydrophobicity with the corrosion efficiency of the coatings supporting the superior water repellent character of the 1wt% modification, having higher contact angle and lower sliding angle than 2wt% and 3wt%. Overall, like contact angle, the HDTMS modification did not showed significant improvement in corrosion resistance when compared with 30wt% FE modified system. This implies that improvement in sliding behavior defiantly improves the hydrophobic character of the coatings, but is not sufficient for enhancing the corrosion resistance properties in submerged conditions. Since, the hydrophobicity achieved lied partially in Wenzel state; the nano-protrusions can act as pinning sites and allow penetration of electrolytes.

Fig 4.57 shows EIS plots of various HDTMS nano-silica modified sol-gel systems. As per impedance spectroscopy analysis these coatings showed superior corrosion resistant properties as compared to bare and neat sol-gel. It was found that impedance decreases with increase in HDTMS-nanosilica concentration with maximum value achieved for 1wt% of $|Z|_{0.1\text{Hz}} \sim 4.18 \times 10^4 \Omega\text{cm}^2$ and decreases with further addition. Hence incorporation of HDTMS-nano silica particles to FE-modified sol-gel system did not showed much improvement in corrosion resistance properties. The probable reason could be that HDTMS nano-particles due to their long chains might result in hindering of the formation of Si-O-Si covalent bonds during curing of the coating resulting in poor crosslinking of the sol-gel matrix thereby affecting the barrier properties of the coating. But at the same time, these long chains of HDTMS resulted in dual scale sheet like structure resulting in much improved sliding behavior as compared to FE-modified system.

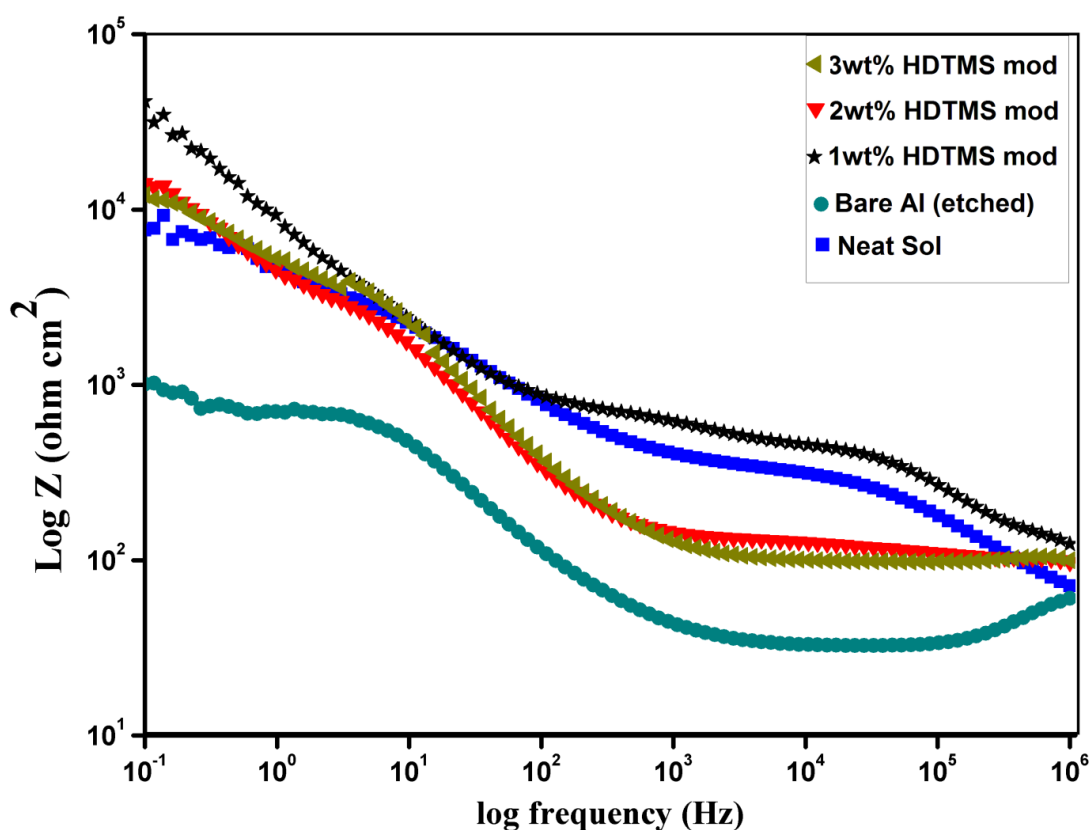


Figure 4.57: Bode plots of bare Al and various HDTMS nano-silica modified sol-gel coatings

Table 4.16: Polarisation and EIS parameters of HDTMS-nano-silica modified sol-gel coatings

Concentration (wt%)	E_{corr} (V)	i_{corr} (A/cm ²)	Impedance (Ωcm^2)
Bare Al	-1.33	2.58×10^{-4}	1.02×10^3
1wt% HDTMS-nano silica	-0.84	5.76×10^{-6}	4.18×10^4
2wt% HDTMS-nano Silica	-0.93	4.66×10^{-6}	1.32×10^4
3wt% HDTMS-nano Silica	-1.047	3.67×10^{-6}	1.17×10^4

4.7.6 Mechanical properties of HDTMS nano-silica modified sol-gel coatings:

Various mechanical tests were performed in order to determine the effect of HDTMS nano-silica particles on the hardness and adhesion of the coatings. As per force Vs penetration depth curve obtained from nano-indentation studies (Fig 4.58), maximum penetration depth

achieved for 1wt% HDTMS modification was about 600nm for force of 1000 μ N. Whereas FE modification resulted in penetration of 490nm under same force. Thus C-16 hydrocarbon chains of HDMTS decreased the hardness of the coatings attributed to steric hindrance to Si-O-Si bond formation which is responsible for the coating strength. Similar observation was made while performing cross-hatch adhesion and pencil hardness test on HDTMS-nano-silica modified coatings. Table 4.17 lists the pencil harness and crosshatch adhesion values of various percentages of nano-silica modified sol-gel coated samples with maximum value of 3H and 3B respectively for 1wt% modification. The significant decrease in adhesion is attributed to addition of solid fraction of long chain nano-silica aggregates leading to low bonding of sol-gel network with the substrate thereby resulting in poor mechanical properties as compared to FE sol-gel system.

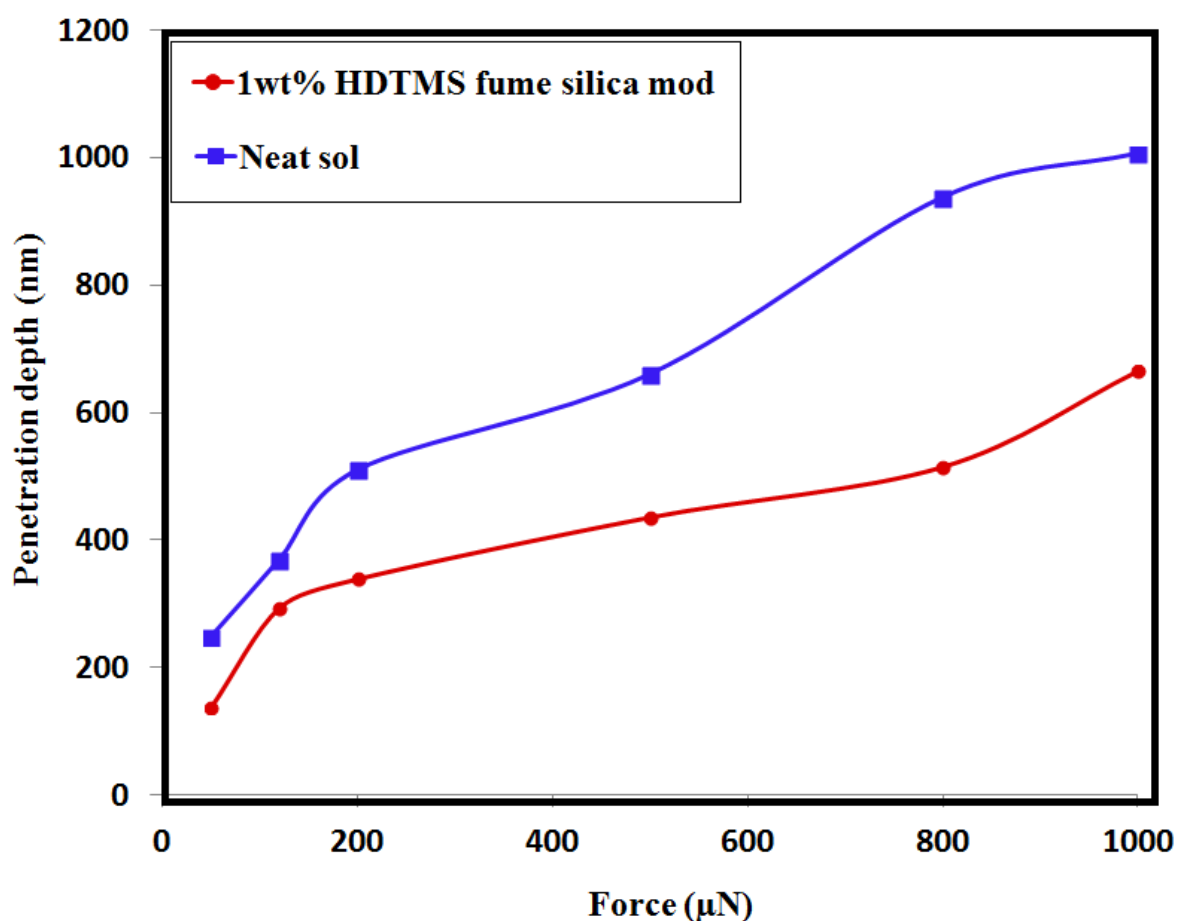


Figure 4.58: Nano-indentation curve of neat and 1wt% HDTMS nano-silica modified soll-gel coated sample

Table 4.17: Cross-hatch adhesion and pencil hardness of HDTMS-nano-silica modified sol-gel coatings

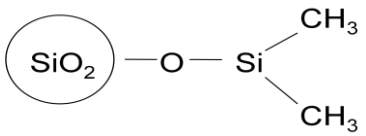
Wt% of nano-ZnO	Cross-hatch adhesion	Pencil hardness
1	3B	3H
2	3B	2H
3	2B	2H
5	2B	1H

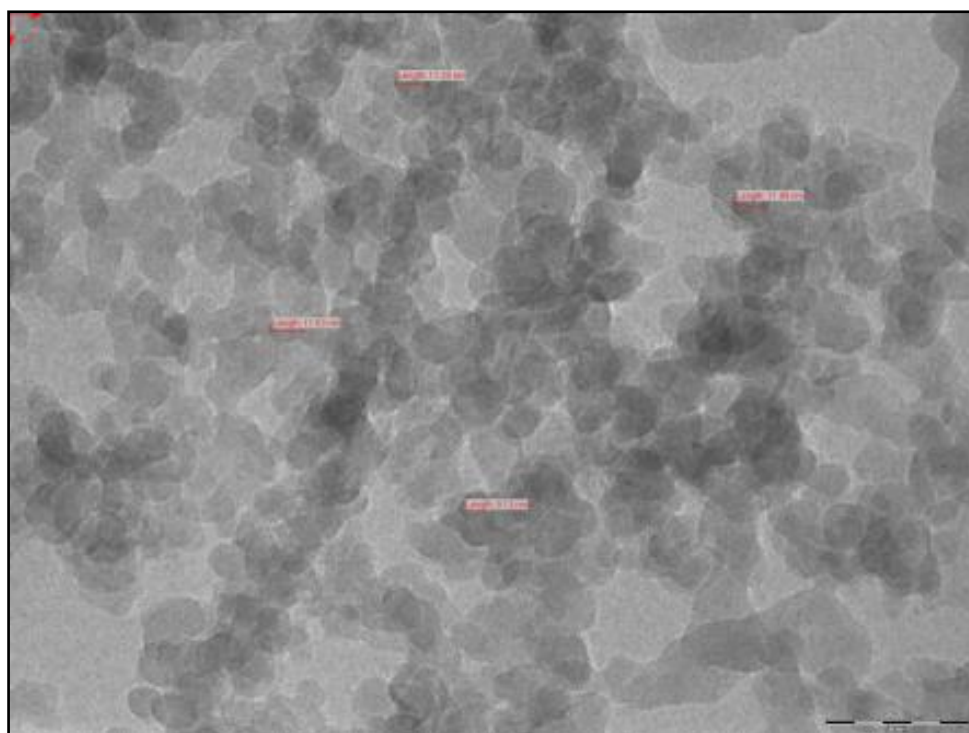
4.8 Characterisation of DDS nano- silica (Aerosil R-972) modified sol-gel coatings:

4.8.1 TEM and BET surface area analysis:

DDS modified hydrophobic nano-silica (Aerosil R972) procured from Evonik Degussa was subjected to TEM and BET surface area analysis. Accordingly, the particles were found to be spherical with particle size of about 10-15nm (Fig 4.59) and average BET surface area of $115 \pm 10 \text{ m}^2/\text{g}$. Table 4.18 shows the specifications and surface chemistry of hydrophobic DDS nano-particles used. In general, the ability of nano-particle to aggregate depends upon several factors such as size, mobility and end-group functionalities [115]. DDS modified nano-particles have di-methyl as end group which replaces hydrophilic surface $-\text{OH}$ groups of nano-silica and are responsible for the hydrophobic character when pointing upside [116] [66]. Also due to comparatively large surface area than nano-ZnO and HDTMS nano-silica, these particles showed better distribution and interaction with the sol-gel matrix leading to superior hydrophobicity and related properties.

Table 4.18: Particle size and surface area of DDS nano-silica particle

Modified Silica	Average Particle size	Average BET surface area m ² /g	Surface Chemistry
DDS nano-silica	10-15 nm	115±10	

**Figure 4.59:** TEM image of DDS nano-silica particles

4.8.2 Wetting properties of DDS nano-silica modified sol-gel coatings

The adsorption and desorption of water from silica depend on the concentration and the type of the surface functional groups, the specific surface area, the average particle size and the type of packing of the primary particles in aggregates [47]. DDS modified nano-silica particles were incorporated to optimised FE sol-gel system via ultrasonication at various concentrations of 1wt%, 2wt%, 3wt% and 5wt% of the total silane content. Table lists the details of contact angles and sliding angles at different concentrations of DDS-fume silica.

The maximum contact angle achieved for DDS modification was $\sim 122^\circ$ for 2wt% concentration which like nano-ZnO decreases on further addition (Fig 4.60).

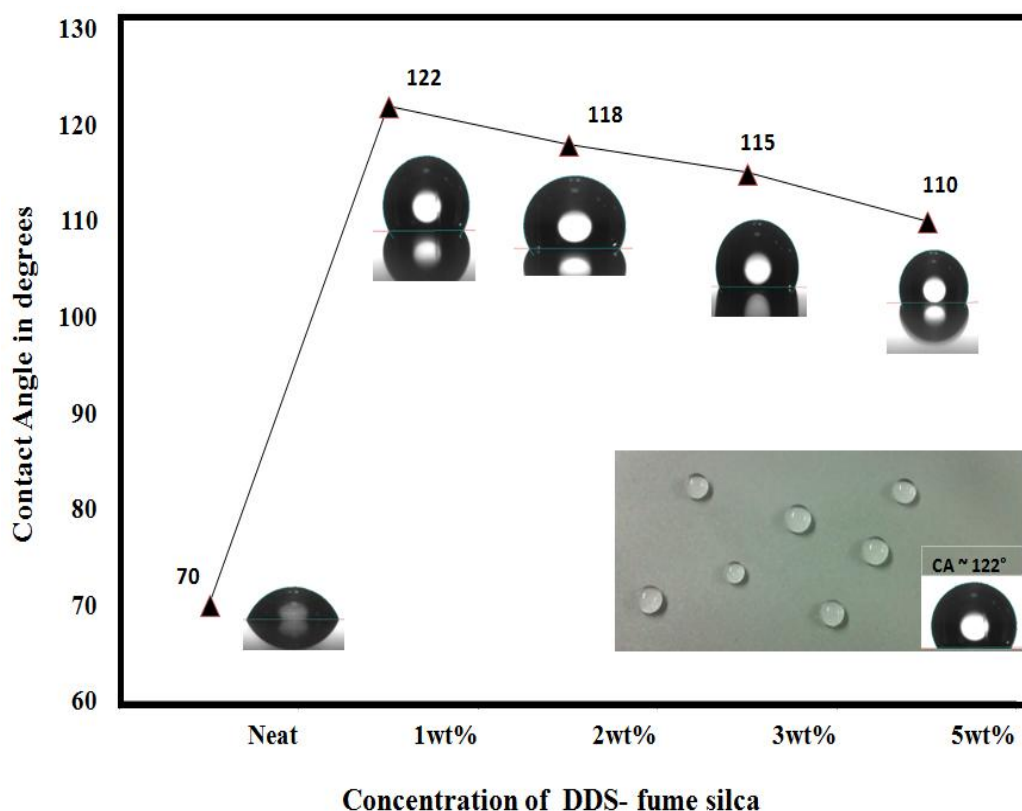


Figure 4.60: Variation of contact angle with concentration of DDS modified nano-silica particles

The increase in contact angle can be attributed to the orientation of methyl groups of silica nano-particles which are locally very mobile and can point into the air, rotating freely resulting in increased hydrophobicity [115]. This resulted in more effective lowering of energy as compared to other particles. Also due to small size and large surface area, DDS modified particles showed better distribution and enhanced surface roughness. DDS-fume silica resulted in extremely glossy finish with excellent improvement in sliding behavior of water droplet with minimum contact angle of about 35° for 2wt%. Decrease in sliding angle value from 70° for FE sol-gel to 35° for 2wt% DDS silica modified formulation indicated significant improvement in hydrophobicity resulting in low permeability of water (Fig 4.61). The SA started increasing on further addition due to lack of formation of air pockets offering more resistance to water droplet against moving down since, interfacial forces probably dominated the gravitational forces [117]. Hence the hydrophobic DDS silica nano-particles

embedded in sol-gel matrix increased the average contact angle of FE sol-gel system from 118° to 122° and improved SA from 70° to 35°.

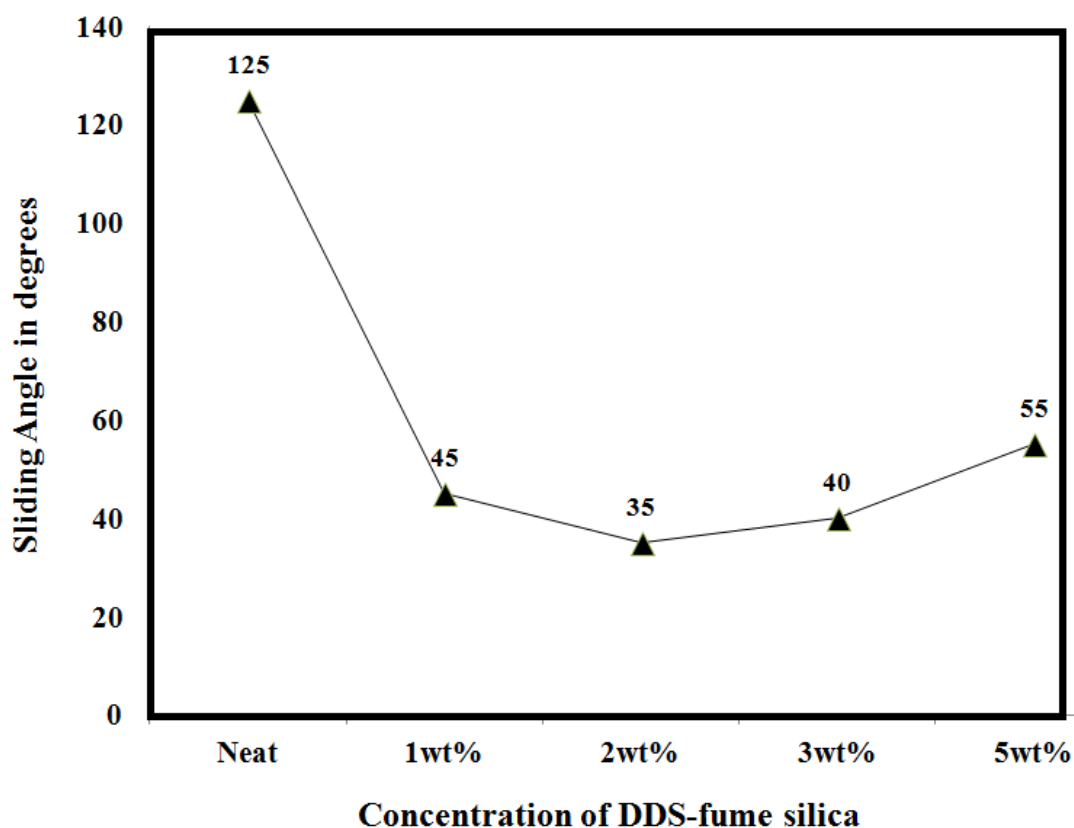


Figure 4.61: Variation of sliding angle with concentration of DDS nano-silica particles

4.8.3 Morphological analysis of DDS nano-silica modified sol-gel coatings

The SEM morphology of the deposited films was developed as a function of the DDS nano-silica particle concentration as shown in Fig 4.62. A highly porous structure was observed with spherical silica particles all over the surface. It was found that at low concentrations of 1wt% and 2wt% distinct particle aggregates were embedded in a continuous sol-gel matrix with diameter of about 1µm -5µm staked over FE profile having craters of about 30µm. Such dual scale nano/microstructure can easily trap large amount of air within the peaks and valleys and make the liquid droplets to rest on the layer of air [47]. As the DDS nano-silica concentration further increased, multilayer nano-particle absorption occurred. It resulted in large part of the micro-cavity created by FE modification filled up with the nano-particle aggregates of diameter ~ 20µm to produce a smoother surface, leading to decreased contact angle [118]. Furthermore, when the nano-silica concentration became very high such as

5wt%, extent of agglomeration increases further, resulting in loss of microsphere profile. Hence, dual scale roughness was achieved using optimum concentration of DDS nano-silica particles and as per Wenzel model, water contact angle of the surface increases with increasing surface roughness [110]. The less increase in contact angle and excellent sliding behavior supported the mixed regime where Wenzel drop interacts with many defects tends to remain stucked up within the roughness grooves, and Cassie state corresponds to non-sticking drops [119].

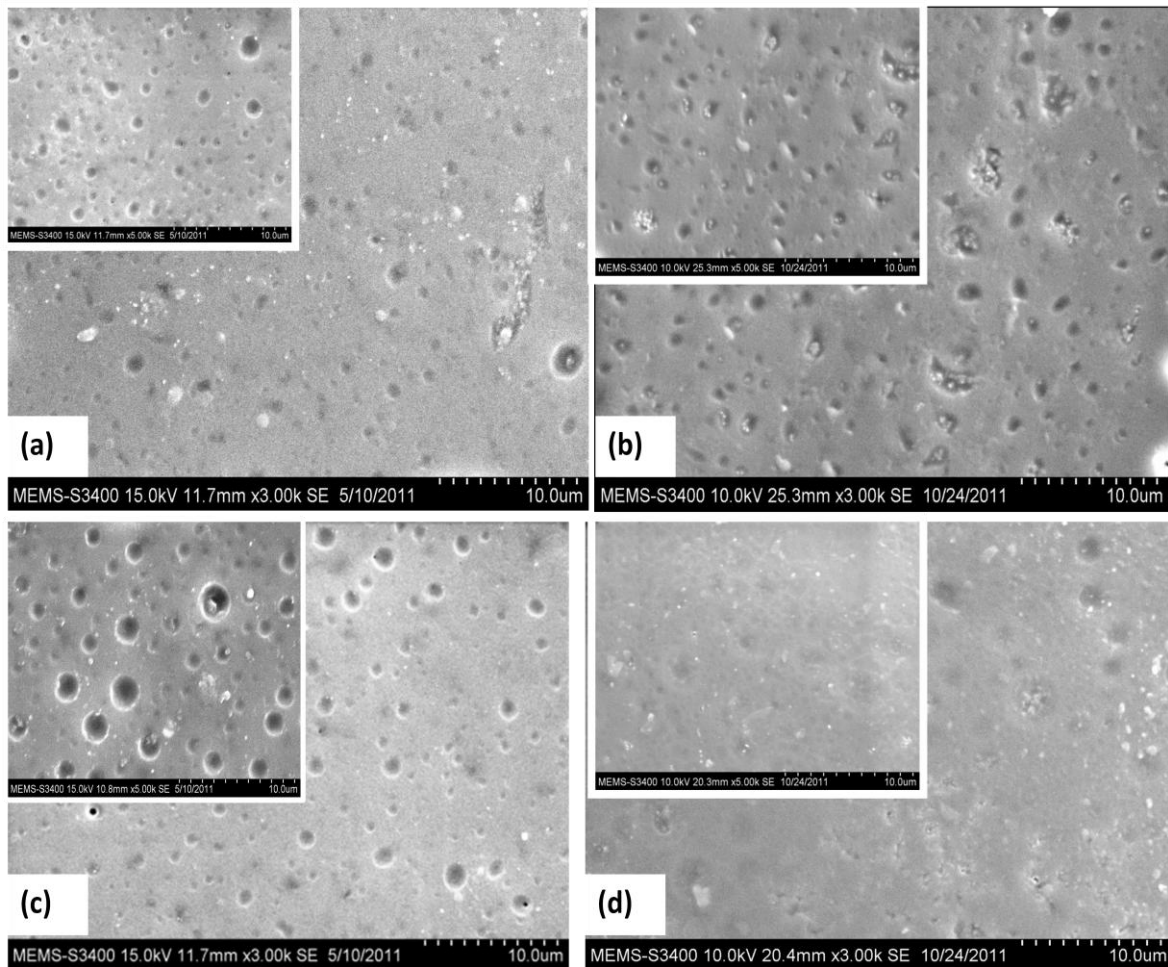


Figure 4.62: SEM images of a) 1wt%, b) 2wt%, c) 3wt% and d) 5wt% DDS Nano-silica modified sol-gel coated samples

To further study the dual scale structure of the nano-clusters formed by DDS nano-silica particles, AFM analysis was carried out. Fig 4.63 shows (ai) two dimensional height images, (bi) section profile and Fig 4.64 shows (ci) magnitude profiles and (di) three dimensional

topographic images of various DDS modified fume silica sol-gel coatings at loading levels of 2wt% ,3wt% and 5wt%. As per 2D and 3D images 2wt% nano-silica showed projections with maximum number of heights and depths which could trap sufficient air in the structure with RMS roughness of ~ 85nm with maximum height of 50nm. Conversely, 5wt% DDS modified formulation showed projections that were too low to trap sufficient air and had RMS of about 30 nm only with maximum height of 200nm (Table 4.19).

Such needle like structure may serve as a means of trapping sufficient air for high contact angles (122°) and low sliding angles (45°) to be exhibited. Water drop on such coating, only contacts the top of the protrusions resulting in a large water–air interface which prevents water droplets from penetrating into the valleys and troughs, leading to water repellent nature. Fig 4.63(bi) shows the section profiles of various samples. 2wt% modification showed maximum number of protrusions below and above the base line. As the percentage of DDS nano-silica was increased further, the section profile became broader with less number of protrusions due to agglomeration of nano-particles at higher concentration. It is therefore quite possible that the water does not penetrate the nano-crevices that exist among the closely packed protrusions (Cassie) or may fill the large, smooth areas that exist among the aggregates (Wenzel). The distribution of DDS nano-silica particles becomes more clear from Fig 4.64 (ci), displaying the magnitude of the agglomerated nano-particles. It is clearly seen that 2wt% modification resulted in uniform distribution of small clusters of magnitude ~ 5400 nm. Whereas at 5wt% extent agglomeration increases leading to loss of rough profile with large aggregates of magnitude ~ 10,000 nm. Hence, it can be said that hydrophobicity is a function of nano-particle concentration and depends upon their size, distribution and end group chemistry.

Table 4.19: Variation of surface roughness with concentration of DDS nano-silica particle

Concentration of DDS nano-silica (wt%)	Average Surface Roughness,Rms (nm)
1	55
2	85
3	62
5	30

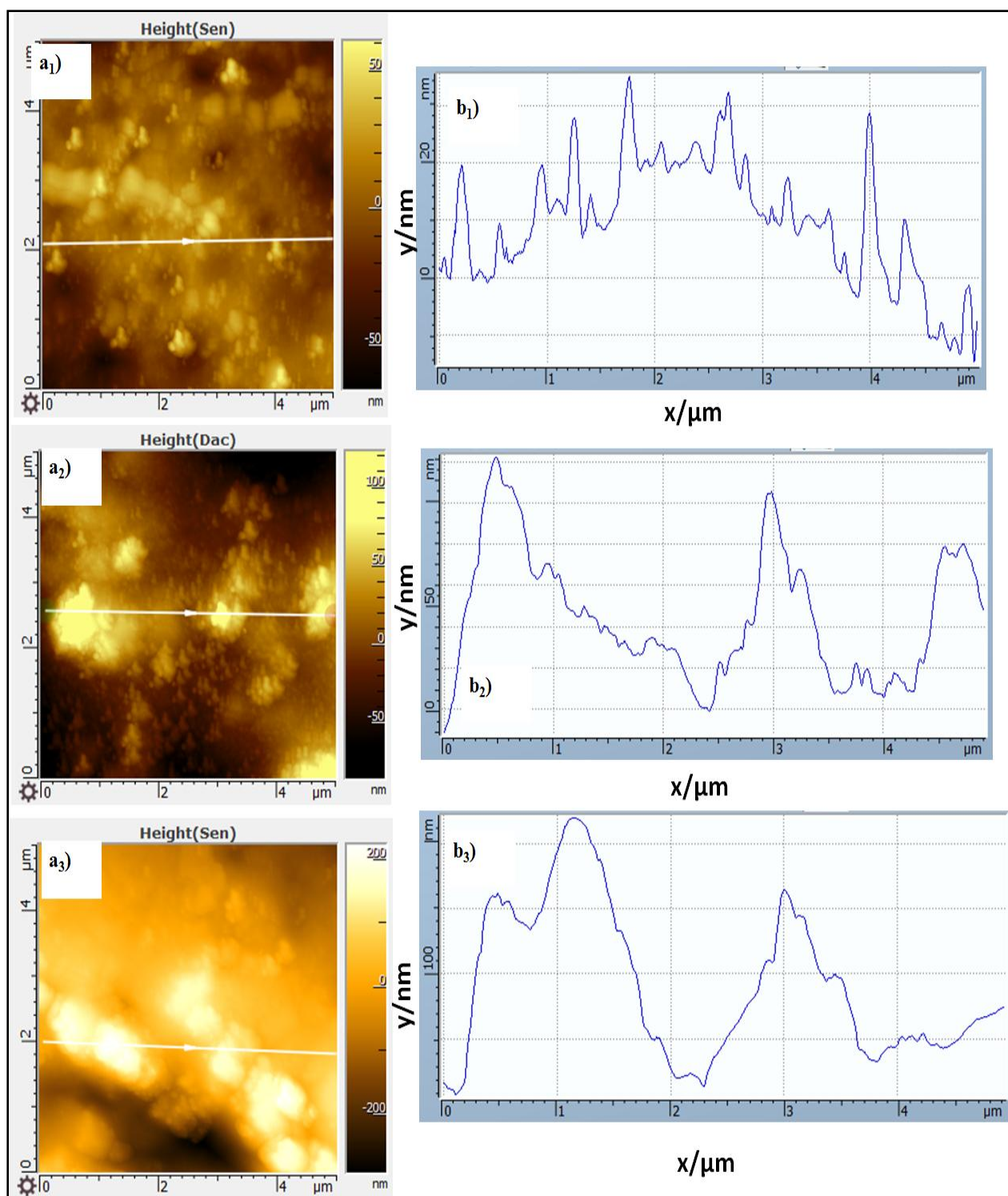


Figure 4.63: AFM images of (ai) 2D height and (bi) section profile of 2wt%, 3wt% and 5wt% HD DDS nano-silica modified sol-gel coatings

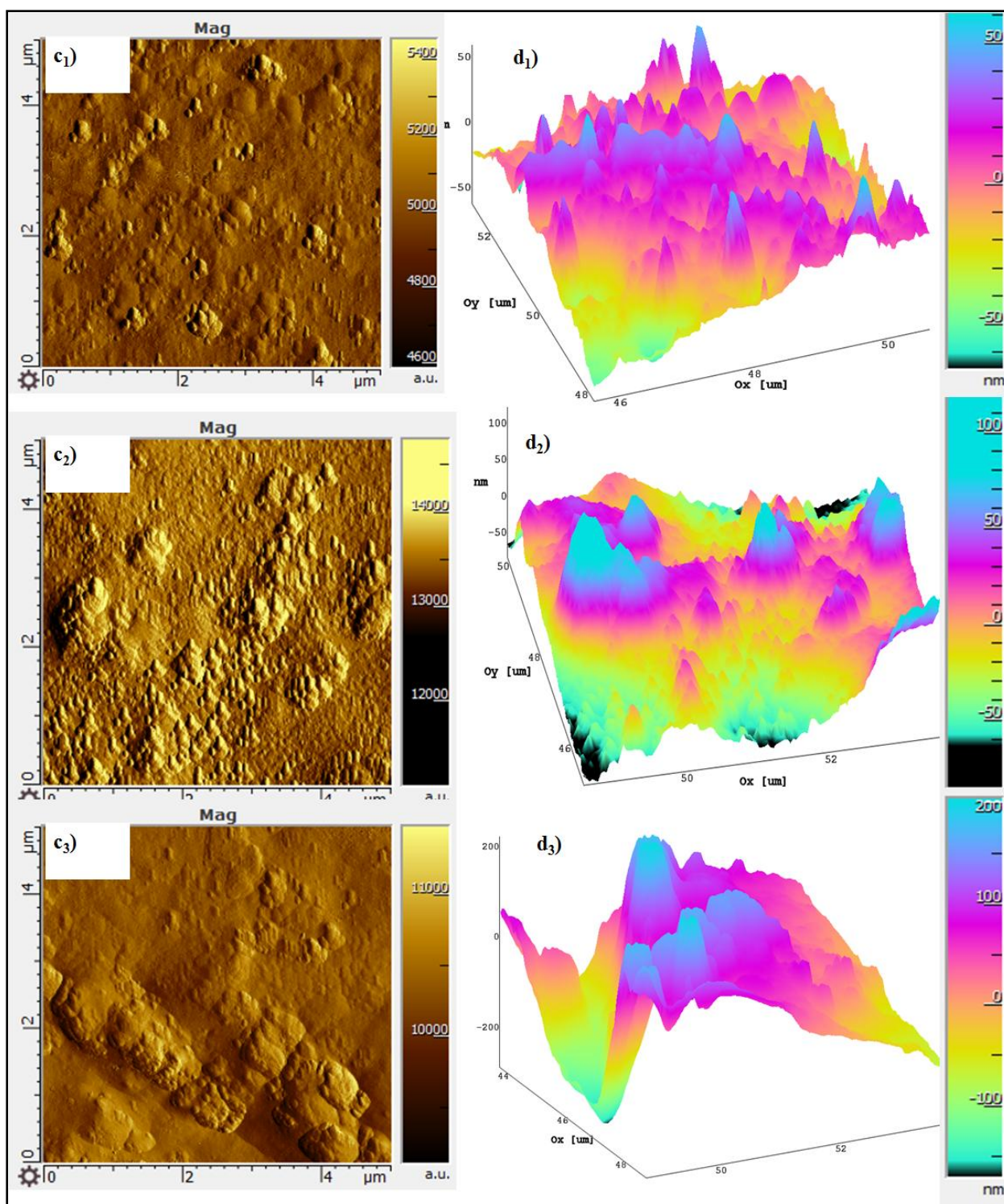


Figure 4.64: AFM images of (ci) magnitude and (di) 3-Dimensional height of 2wt%, 3wt%, and 5wt% DDS nano-silica modified sol-gel coatings respectively

4.8.4 Structural analysis of DDS modified sol-gel coatings:

It can be seen from Fig 4.65, after embedding of sol-gel matrix with DDS modified nano-silica particles, the intensity of -OH band about 3423 cm^{-1} was decreased as compared to neat sol-gel indicating the hydrophobic nature of the nano-modified coating. The peaks around 451 cm^{-1} and 790 cm^{-1} in DDS nano-silica modified spectrum correspond to symmetric stretching modes of SiO_2 and Si-CH_3 group moieties respectively [65]. Strong band due to Si-O-Si linkages was seen at 1100 cm^{-1} . The absorbance band at 1014 cm^{-1} corresponds to C-F bond probably coming from perfluoro group. The decrease in intensity of peaks around 2942 and 2887 cm^{-1} corresponding to CH_2 symmetric and asymmetric vibrations indicate the interaction of -CH groups with silica nano-particles [66, 115, 116].

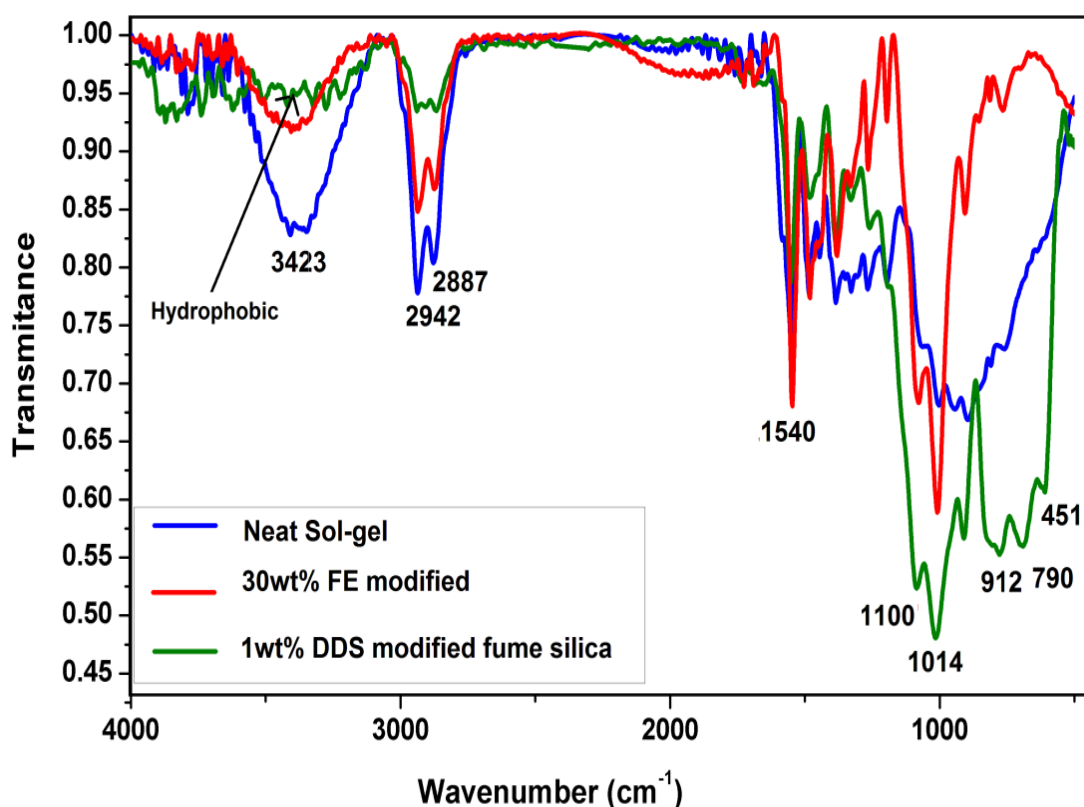


Figure 4.65: FTIR spectra of neat and DDS nano-silica modified sol-gel coating

4.8.5 Corrosion resistance of DDS nano-silica modified sol-gel coatings:

The corrosion resistance of the DDS nano-silica modified films was evaluated by electrochemical polarisation (Table 4.20). As mention earlier, in a typical polarisation curve,

the lower the polarisation current, the better is the corrosion resistance [59]. Fig 4.66 shows the polarisation curves of bare Al (etched) substrate and various DDS nano-silica sol-gel coated films. The curves were recorded after open-circuit exposure to 3.5% NaCl for 30 min. It was found that after coating the bare Al with modified coatings of different concentrations of DDS-nano-silica, the corrosion density (i_{corr}) was reduced by three orders of magnitude with minimum value of $7.12 \times 10^{-7} \text{ A/cm}^2$ achieved for 2wt% modification which was slightly more than 30wt% FE modified system ($i_{\text{corr}} \sim 9 \times 10^{-7}$). The maximum positive shift was observed in the corrosion potential (E_{corr}) value of -0.6V for 2wt% modification, whereas the higher concentrations of DDS nano-silica resulted in poor corrosion resistance both in terms of E_{corr} and i_{corr} . Table 4.20 lists polarisation parameters for various DDS-nano-silica modified coatings. Therefore 2wt% concentration was found to be optimum amount to achieve effective barrier to the transport of the aqueous species to the Al substrate. This can be explained due to entrapment of air within the micro-nano protrusions and thus restricting the penetration of the aggressive ions (in this case Cl^-) to the substrate, resulting in the improved anti-corrosion performance [70, 77, 93, 107]. Hence DDS nano-silica modification resulted in improved corrosion properties than FE modified system at 2wt% resulting in enhanced hydrophobicity with CA of about 122° and excellent sliding with SA of 35° .

Table 4.20: Polarisation and EIS parameters of DDS modified sol-gel coatings

Concentration (wt%)	E_{corr} (V)	i_{corr} (A/cm^2)	Impedance (Ωcm^2)
Bare Al	-1.33	2.58×10^{-4}	1.02×10^3
1wt% DDS-nano silica	-1.11	2.09×10^{-6}	2.7×10^4
2wt% DDS-nano Silica	-0.64	7.12×10^{-7}	3.5×10^4
3wt% DDS-nano Silica	-1.04	5.10×10^{-6}	2.9×10^3
5wt% DDS-nano-silica	-1.00	7.07×10^{-6}	-

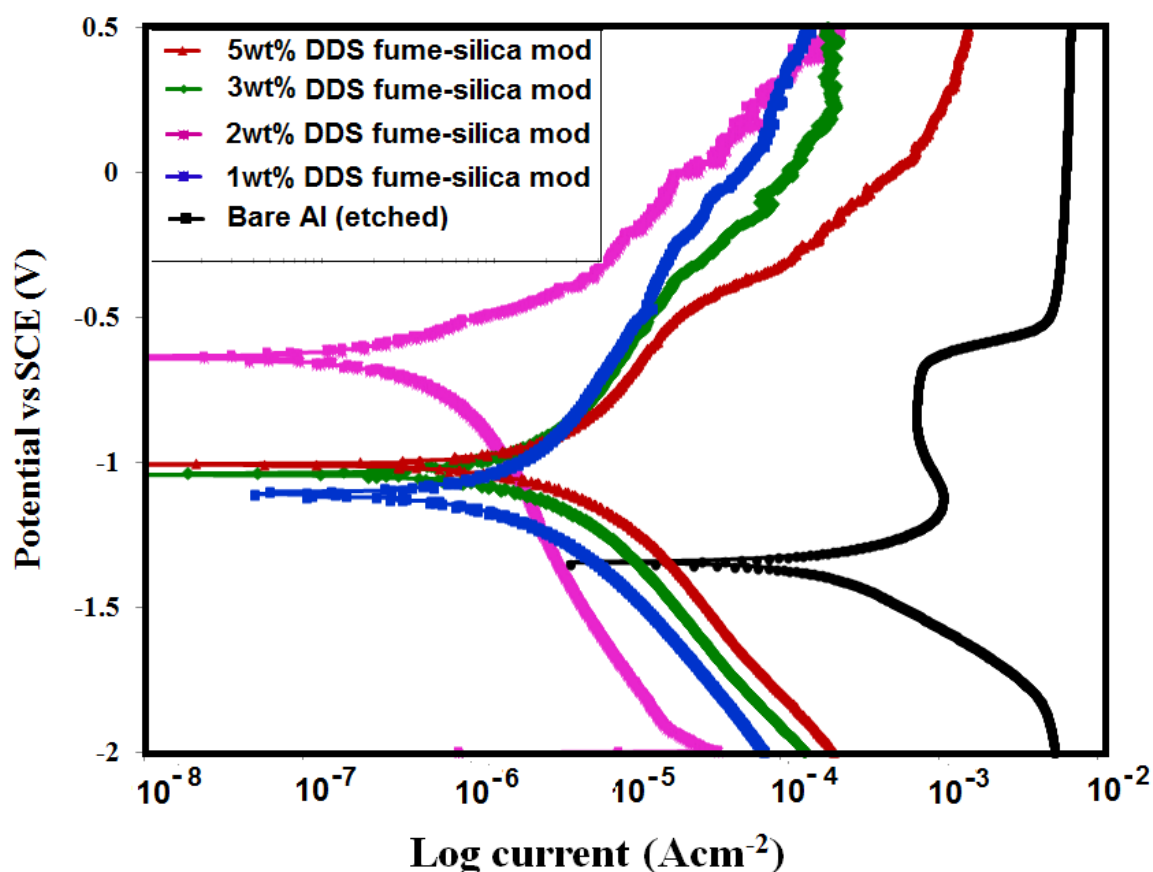


Figure 4.66: Tafel plots of bare Al and various DDS nano-silica modified sol-gel coated samples

Further electrochemical impedance spectroscopy was used to evaluate the corrosion activity of sol-gel coatings modified with different loading levels of DDS nano-silica. Fig.4.67 shows the impedance behaviour of bare Al, neat sol-gel and various DDS-nano-silica modified sol-gel coatings at initial period of immersion in 3.5% NaCl. The value of $|Z|_{0.1\text{Hz}}$ for bare alloy was found to be $1.02 \times 10^3 \Omega \text{ cm}^2$, whereas various DDS-modified sol-gel coatings showed $|Z|_{0.1\text{Hz}}$ of about 3×10^4 which is higher in magnitude by one order. The improvement in corrosion resistance was not significant in terms of EIS when compared with impedance of FE-modified system though the sliding angle was reduced to 35° from 65° indicating that improvement in sliding behavior does not affect the water repellence properties much in submerged conditions. Hence, further increase in water contact angle is required to achieve improved corrosion resistance.

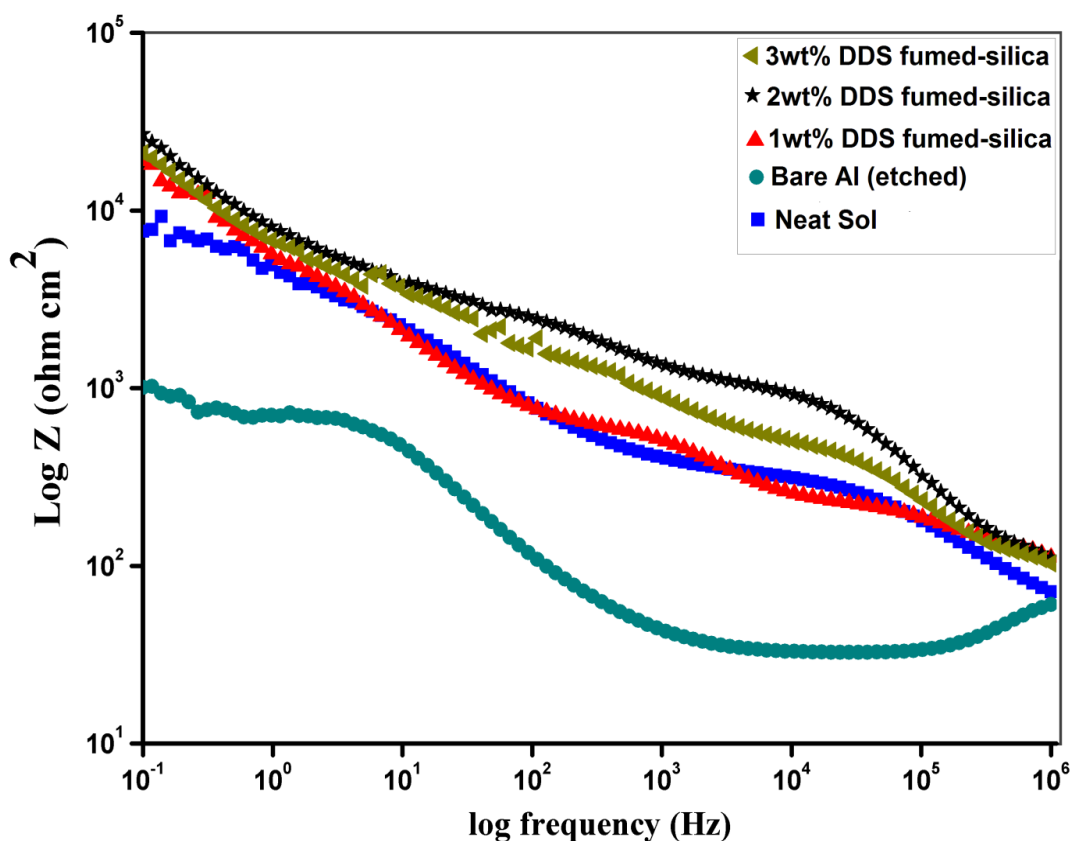


Figure 4.67: EIS plots of bare Al and various DDS nano-silica modified sol-gel coatings

4.8.6 Mechanical Properties of DDS nano-silica modified Sol-gel coatings

DDS nano-silica reinforced sol-gel coatings were then subjected to various mechanical tests in order to determine the strength of the modified coatings. Nanoindentation was performed on the 2wt% nano-silica modified formulation (Fig 4.68). The maximum penetration depth achieved for 1000 μ N force was 360 nm which is quite less than FE modified and neat sol with penetration depth of about 500 and 1000nm respectively. Such improvement in the hardness of the coatings can be attributed to the small size of the DDS nano-particles. Due to small filler size and large BET surface area, DDS nano-particles resulted in comparatively more homogeneous distribution within the sol-gel matrix. This resulted in improved resistance to deformation as compared to other systems. Further pencil hardness and crosshatch adhesion tests on various DDS nano-silica modified sol-gel coatings resulted in value of 5H and 5B respectively which indicated that the nano-particles did not interfere with the adhesion of the sol-gel matrix which could lead to debonding close to the particles. This resulted in non-fragile matrix around the particles and hence improved scratch resistance

and hardness [23, 106, 120]. However higher concentrations resulted in decrease in mechanical properties as the particles tend to aggregate which leads to poor adhesion and scratch resistance of the coatings.

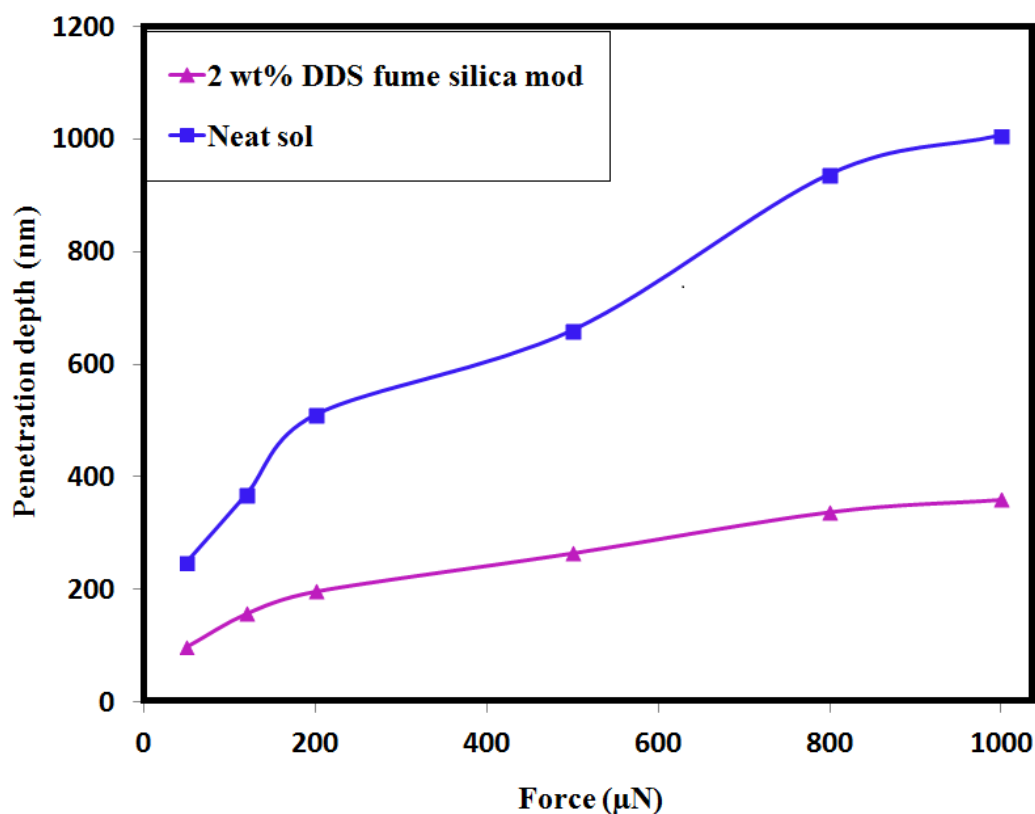


Figure 4.68: Nano-indentation curve of neat and 2wt% DDS nano-silica modified sol-gel coating

Table 4.21: Crosshatch adhesion and pencil hardness results of DDS nano-silica modified sol-gel coatings

DDS fume silica Concentration (Wt %)	1wt%	2wt%	3wt%	5wt%
Pencil hardness	5H	5H	5H	4H
Crosshatch adhesion	5B	5B	5B	3B

4.9 Characterisation of HMDZ nano- silica (Aerosil R8200) modified Sol-gel coatings:

4.9.1 TEM and BET surface area analysis of HMDZ nano-particles:

Particle Size and BET surface area of HMDZ modified nanosilica particles used are given in Table 4.22. HMDZ modified fume silica particles used had smallest particle size of 7 to 10 nm (Fig 4.69) and maximum surface area of $160 \pm 25 \text{ m}^2/\text{g}$ reported in the study. The surface chemistry of HMDZ silica surface consist of grafted non-polar methyl groups which imparts hydrophobicity to the nano-particles and also minimize inter-particle interactions between the silica particles and hence agglomeration [121].

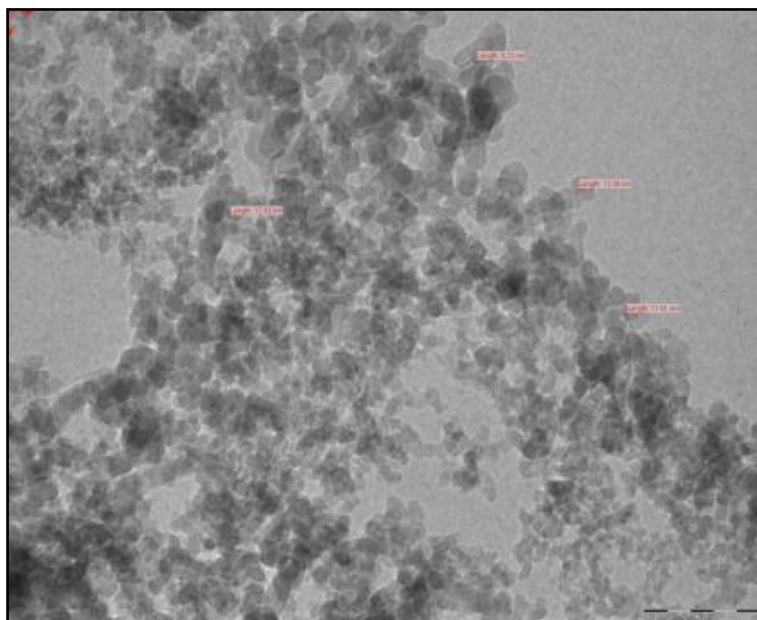


Figure 4.69: TEM image of HMDZ nano-silica particles

Table 4.22: particle size and BET surface area of various nano-particles

Nano-particle	Particle Size (nm)	BET surface area m^2/g	Surface chemistry
HMDZ fume-silica	7 to 10 nm	160 ± 25	$\text{SiO}_2 - \text{O} - \text{Si} \begin{matrix} \text{CH}_3 \\ \\ \text{CH}_3 \end{matrix}$

4.9.2 Wetting properties of various HMDZ nano-silica modified sol-gel coatings:

After modification with di-methyl substituted (DDS) nano-silica, tri-methyl substituted commercial grade hydrophobic silica particles were incorporated to 30wt% FE-sol-gel formulation. The highest contact angle of about 125° was obtained with HMDZ modification which resulted in improved water repellent properties, corrosion resistance and mechanical properties. Such behavior is related to both the rough morphology and the intrinsic low surface energy of the HMDZ-silica particles that stem from the chemical nature of the tri-methylated groups grafted onto the particle surface. These tri-methyl groups give rise to the asymmetric molecular forces responsible for water repellent properties [65, 66, 122]. Fig 4.70 shows the variation in contact angle with various percentages of HMDZ nano-silica addition. It was found that WCA enlarges from 0.5wt% to 3wt% with maximum value of about 125° and then further decreases at higher concentrations. This could be attributed to homogeneous distribution of nano-particles at lower percentages due to small size of 7-10nm and large BET surface area, creating effective roughness profile required for enhancing hydrophobic behavior. At higher percentages, agglomeration of nano-particles takes place due to particle – particle interaction of large number of methyl groups on the surface. This results in multi-layer absorption of nano-particles, which fill up the micro-cavities on the surface resulting in spreading of water and hence decreased contact angle. Another possible reason for low contact angle at higher concentrations could be sterically hindering of per-fluoro groups to come on surface by agglomerated tri-methyl groups and hence less perfect polymeric coating layer on the nano-particles [104, 118].

Fig 4.71 shows the variation in SA values with concentration of HMDZ nano-silica added. It was found that for neat sol, the water droplet firmly adhere to the coated Al substrate with SA more than 90° , whereas SA reduces to about 25° for 3wt% nano-silica modification. Hence, water droplets easily slide off the HMDZ nano-silica modified surface due to sufficient entrapment of air within micro-nano roughness hills indicating the significant shift towards Cassie Baxter state. The hydrophobicity was still observed in mixed state, as discussed in following sections.

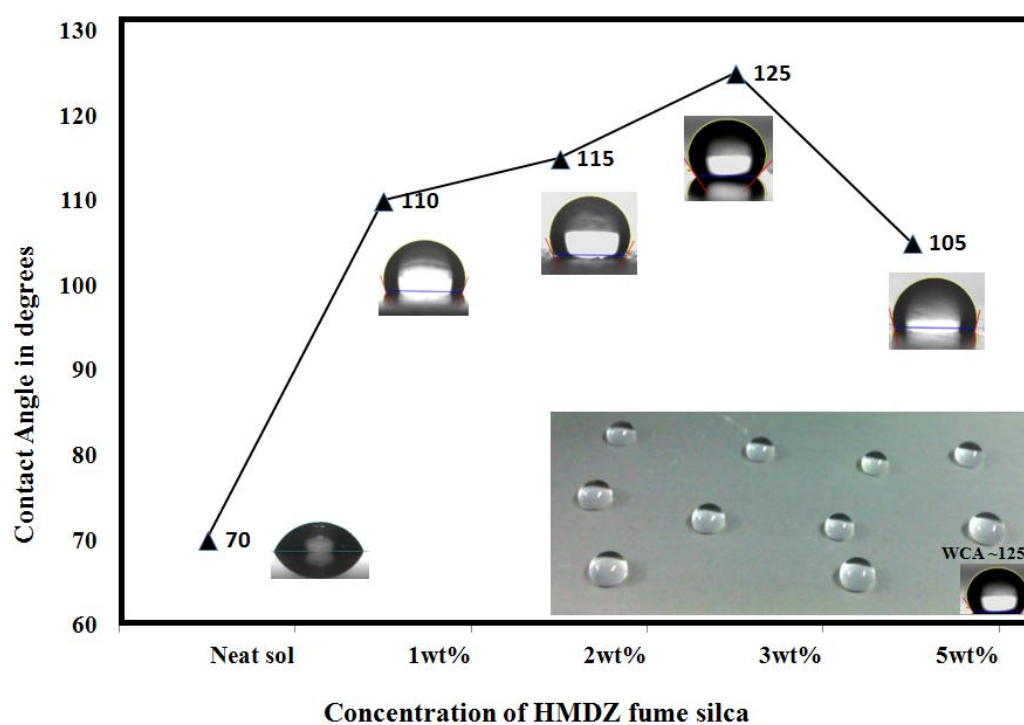


Figure 4.70: Variation of contact angle with concentration of HMDZ nano-silica particles

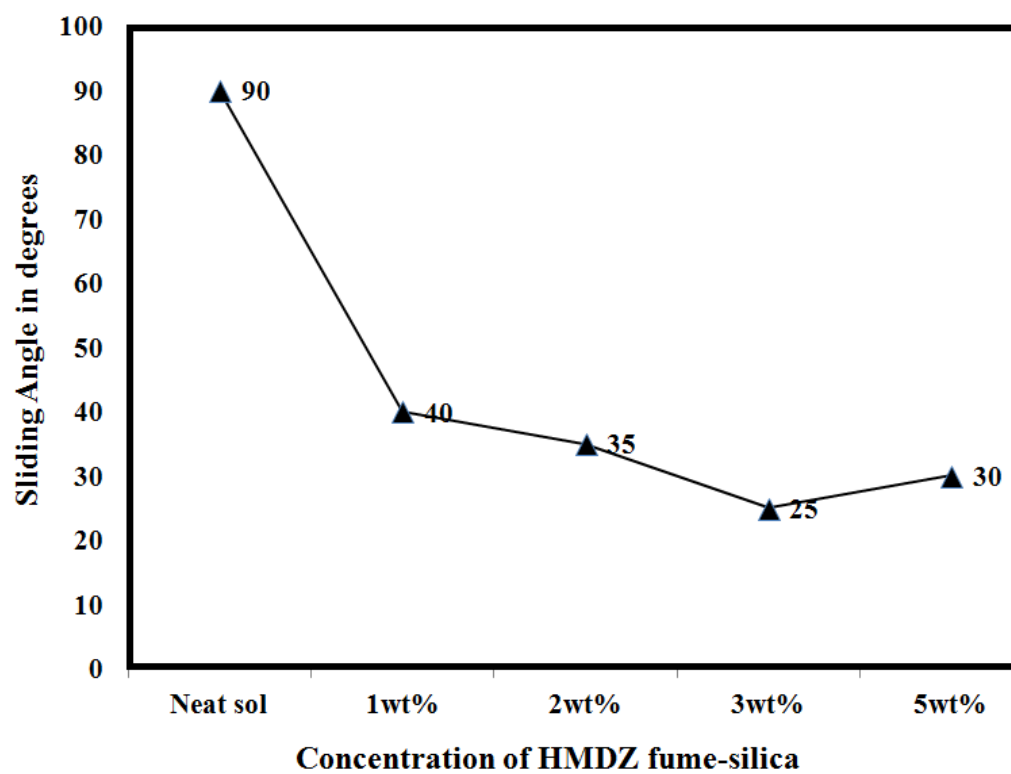


Figure 4.71: Variation of sliding angle with concentration of HMDZ nano-silica particles

4.9.3 Morphological analysis of HMDZ nano-silica modified sol-gel coatings:

The SEM images Fig 4.72 closely depict the 2wt%, 3wt%, 5wt% and 10wt% of HMDZ-nanoparticles incorporated in Fe-modified sol-gel coatings. The micrographs clearly showed a highly porous morphology with random network of microspheres over the entire surface. These spheres were present in form of clusters and tend to trap the air in the pores of the films, contributing to the higher water contact angle and easy sliding of water drop of the surface [123, 124]. For the low particle concentration of 1wt% the particle clusters formed are sparsely distributed and most parts of the film were relatively smooth. As the concentration increases upto 5wt% the clusters formed in film became larger in shape and closely packed with methyl groups residing on the nanocluster surfaces. Therefore, the formed surface become rougher, and the denser distribution of nano-particles make the surface more continuous in shape. At higher concentration of 10wt%, extent of agglomeration and SiO₂ particles are likely to be embedded completely in the dense crosslinked matrix derived from sol-gel process responsible for absorption of water and poor hydrophobicity. It was observed that an optimum roughness pattern was obtained at 3wt% concentration with microspheres ranging in diameter of 5µm to several nanometers. As mentioned earlier, the size of craters formed by FE modification was about 30µm in diameter. If we consider overlapping of both 30wt% FE profile and 3wt% HMDZ profile, a *micro-nano dual scale roughness* was obtained using small size HMDZ nano-silica particles resulting in trapping of air within the dual-scale, reducing the contact area between water drop and the surface. This is in accordance with *Hsieh et al.* who have proposed that rough surfaces with a high fraction of micropores enhance water repellency and therefore water droplets cannot penetrate easily into micropores on a repellent surface [125]. Also the combine effect of low surface energy due to electronegative perfluoro-groups and substitution of -Si-OH groups by low energy -Si-(CH₃) groups were responsible for obtaining much improved hydrophobicity in terms of both WCA and SA. Thus the microstructure of the coatings was found to depend on the nano-silica content and distribution pattern of nano-particles.

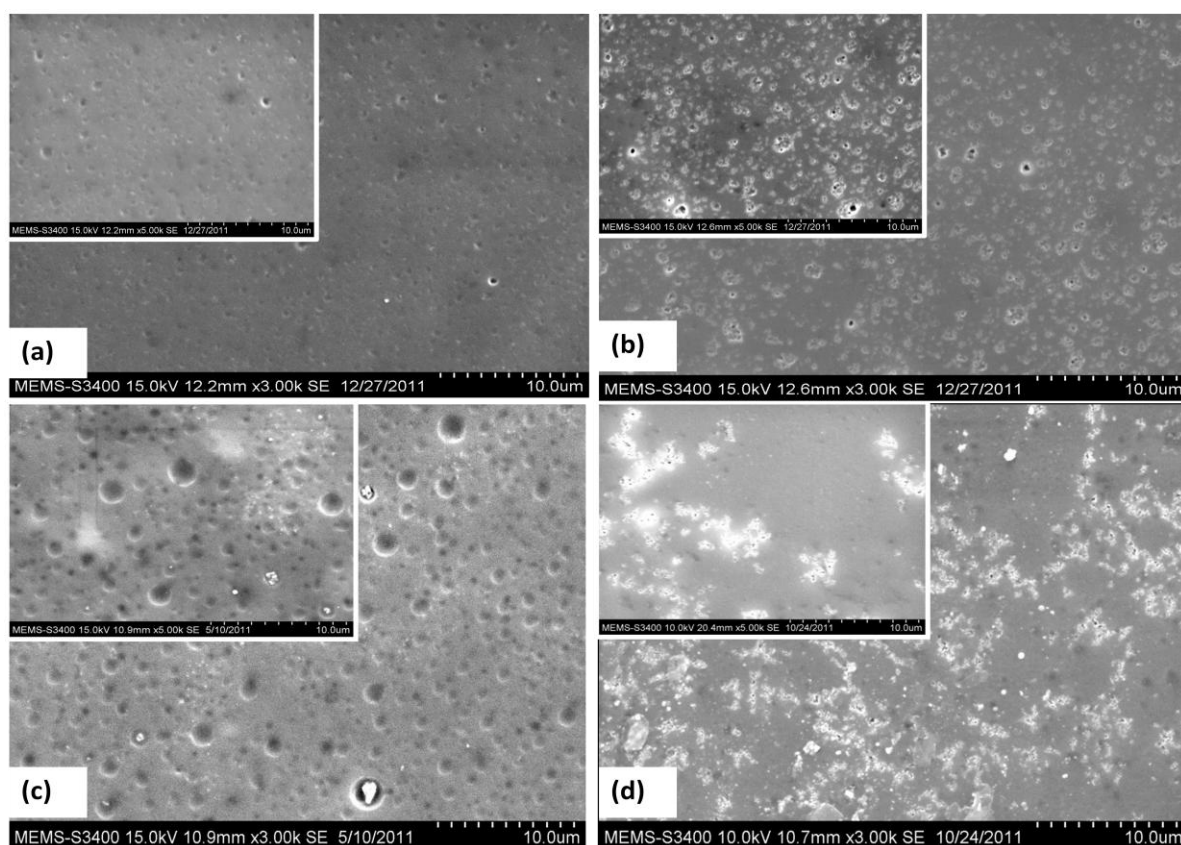


Figure 4.72: SEM images a) 2wt%, b) 3wt%, c) 5wt% and d) 10wt% of HMDZ nano-silica modified sol-gel coated samples

In order to further characterize the micro-nano structure of the HMDZ nano-silica modified sol-gel coatings, AFM analysis was performed. Fig 4.73 shows (ai) two dimensional height images and (bi) section profiles. Fig 4.74 shows (ci) magnitude profiles and (di) three dimensional topographic images. From both 2-d and 3-d AFM images of different samples the microscale and nano- scale roughness can be seen clearly. Number of peaks with maximum height increase with increase in concentration of nano-silica content, from 1wt% to 3 wt%, beneficial for the increase in hydrophobicity. Also the root mean square roughness (RMS) increases accordingly with value of 95 nm for 3wt% HMDZ nano-silica concentration with maximum peak found at $2.13\mu\text{m}$ and the minimum valley calculated at $2.17\mu\text{m}$ relative to average crossline. From the section profiles in Fig 4.73 (bi) the number of different protrusions, “hills” were increasing with increase in concentration of nano-silica upto 3wt% which implies that the surface of 3wt% HMDZ nano-silica modified sol-gel coated sample has more multiscale structures than that of lower concentrations attributing to uniform distribution of nano-clusters throughout the surface. Further 10wt% nano-silica concentration

showed broader section profile indicating enhanced agglomeration at higher loading level and hence decreasing the surface roughness. More importantly, the magnitude images, Fig 4.74 (ci), highlight the nano-cluster distribution. As seen from the images, magnitude of nano-clusters increase with increase in HMDZ nano-silica content with uniform and dense distribution of fume silica particles at 3wt% concentration. The smaller protrusions rest on the top layers, whereas the larger aggregations form the bottom layers. Thus, the multi-scaled roughness is created by the aggregations of nanoparticles resulting in protruding nubs covering the whole surface assures, in fact, that the surface contact area available to water was very low, while the hydrophobic nano-particles prevented penetration of water into the valleys resulting in excellent sliding behavior of water droplets with contact angle of 125° and SA of 25° for $10\mu\text{L}$ water droplet. However, at higher concentrations these aggregates are largely accumulated and make some area of protrusions smooth resulting in lowering of surface roughness and hence poor hydrophobic properties. Furthermore, the mixed state can better explain the results in which water droplet sits on the aggregates (Cassie State) or spreads out on the smooth areas between the aggregates (Wenzel) [47, 126].

Table 4.23: Variation of surface roughness with concentration of HMDZ nano-silica particles

Concentration of HMDZ nano-silica	Average Surface Roughness (nm)
1	45
2	78
3	95
5	60

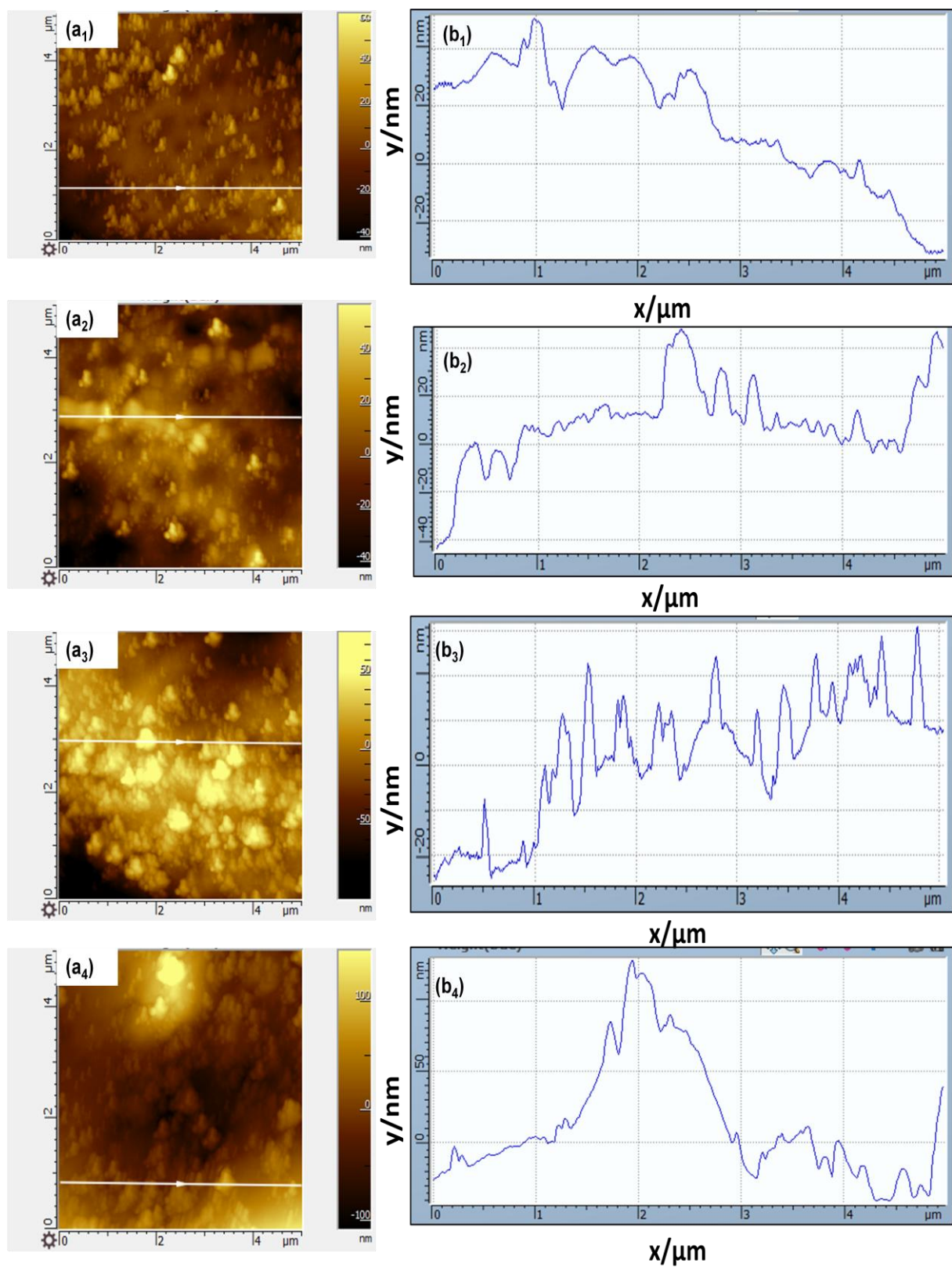


Figure 4.73: AFM images of (ai) 2D height and (bi) section profile of 1wt%, 2wt%, 3wt% and 5wt% HMDZ nano-silica modified sol-gel coatings

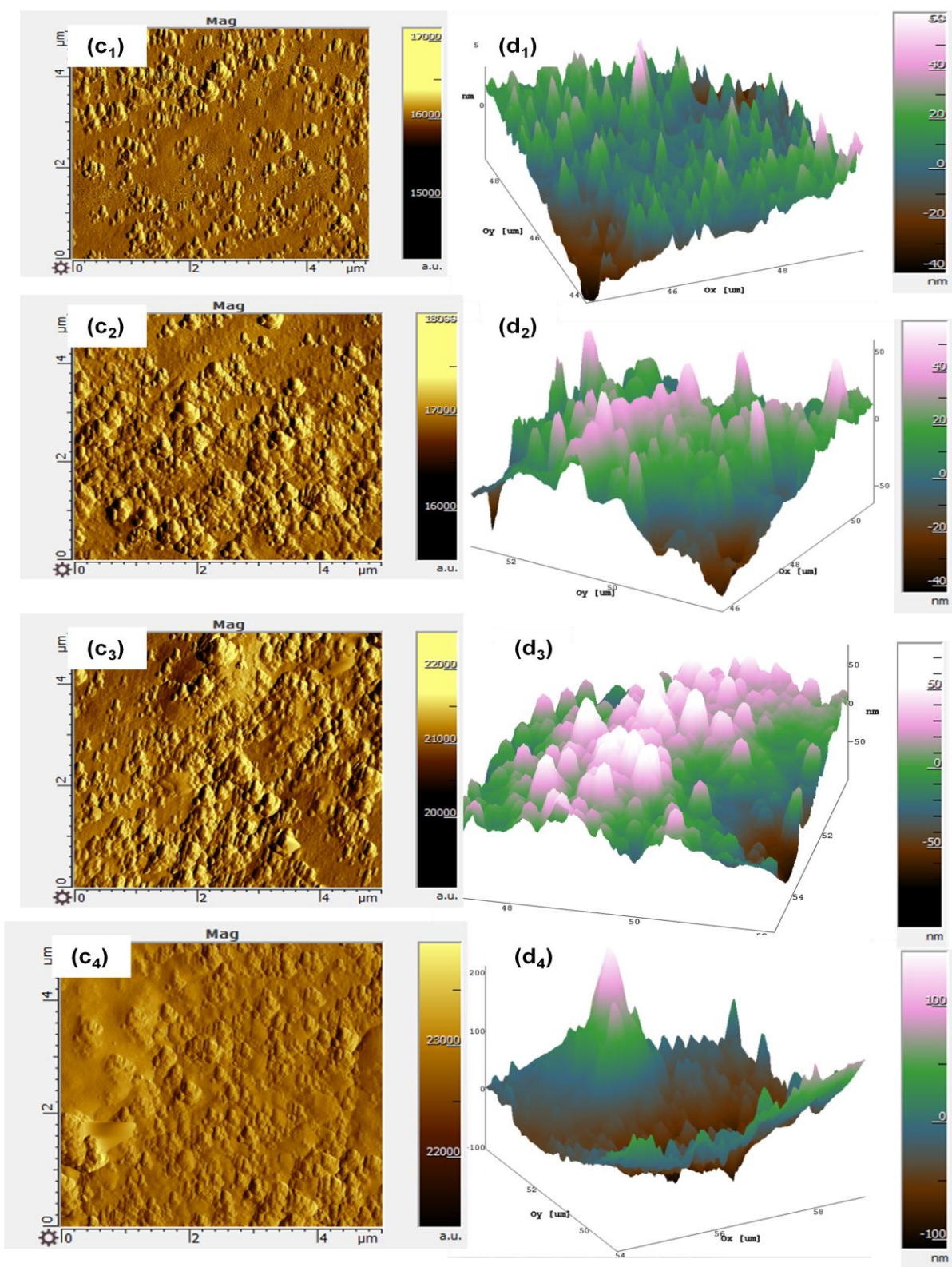


Figure 4.74: AFM images of (ci) magnitude and (di) 3-Dimensional height of 1wt%, 2wt%, 3wt% and 5wt% HMDZ nano-silica modified sol-gel coatings respectively

4.9.4 Structural Analysis of HMDZ modified sol-gel coated samples

As per FTIR analysis shown in Fig.4.75, all percentages of fume-silica particles modified formulations showed a broader OH-peak at 3423 cm^{-1} as compared to unmodified one indicating hydrophobic nature [25]. Strong peaks appearing at 1100 cm^{-1} and 790 cm^{-1} correspond to Si-O-Si linkage and Si-C bond respectively derived from Si-CH₃ group of HMDZ [47]. It was observed that intensity of both Si-O-Si and Si-C bonds increases with increase in nano-silica content upto 3wt% and further reduced at 5wt% indicating steric hindrance to bond formation due to agglomeration at higher loading level. Peaks appearing at 2942 and 2887 cm^{-1} are attributed to stretching vibration of C-H bonds in both neat and modified sols. Also the presence of absorption bands at 1540 cm^{-1} and 1014 cm^{-1} are attributed to N-H and C-F bonds coming from HMMM and per-fluoropolymer [89].

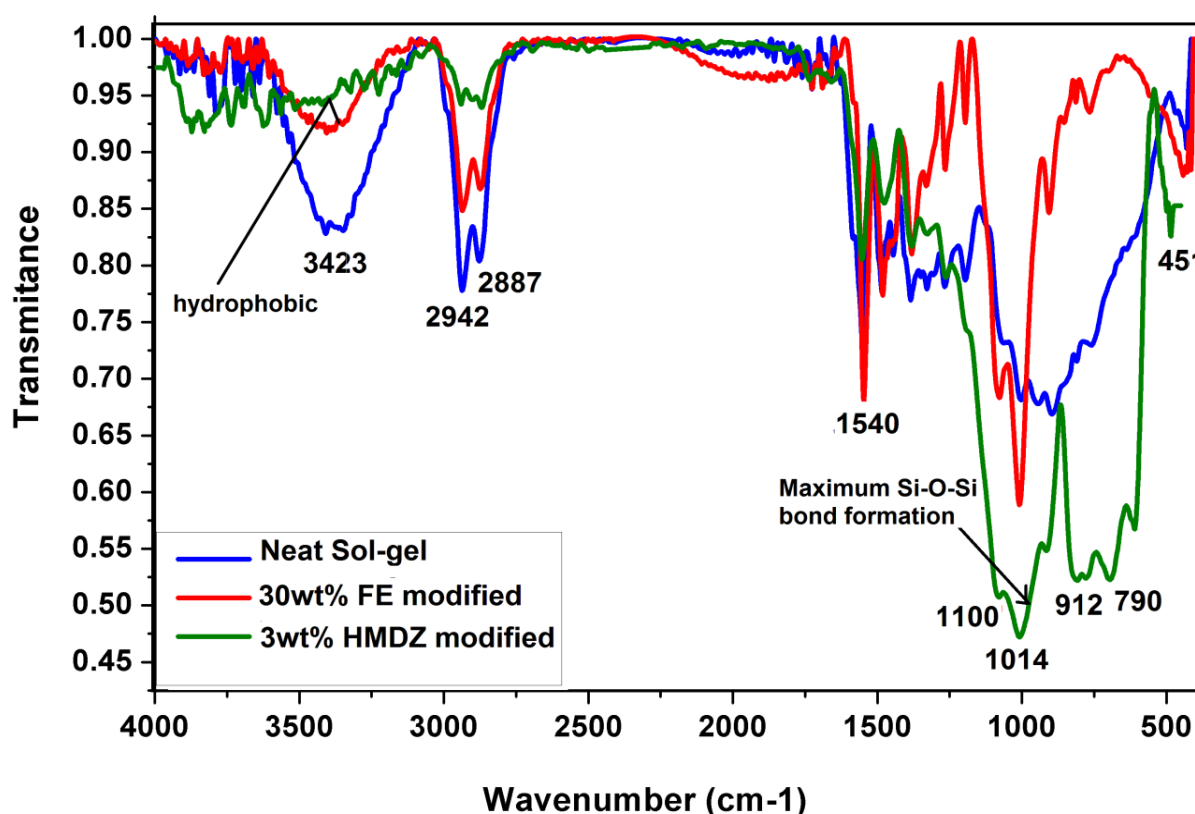


Figure 4.75: FTIR spectra of various HMDZ nano-silica modified sol-gel coated samples

4.9.4 Corrosion resistance of HMDZ nano-silica modified sol-gel coatings:

The potentiodynamic polarisation curves of bare Al (etched) and various concentrations of HMDZ nano-silica modified sol-gel coatings on Al in 3.5 % NaCl solution are given in Fig 4.76. The corrosion potential (E_{corr}) and the corrosion current density (i_{corr}) derived from the potentiodynamic polarisation curves are shown in Table 4.24. As clearly seen the corrosion potential positively increases from -1.3V for bare Al to -0.56V for 3wt% HMDZ nano-silica modified coating. The significant shift of the E_{corr} in the positive direction could be linked to improvement of the protective properties of hydrophobic coating formed on Al. The corrosion current density, i_{corr} of the 3wt% HMDZ nano-silica coating ($9.88 \times 10^{-8} \text{ A/cm}^2$) was decreased by four orders of magnitude as compared to that of the bare one ($2 \times 10^{-4} \text{ A/cm}^2$) and one order as compared to FE-modified system ($9.88 \times 10^{-7} \text{ A/cm}^2$). Such improvement in corrosion resistance can be attributed to water repellent profile generated due to combine effect of micro-nano hills of HMDZ silica nano-particles with protruding lower energy tri-methyl and perfluoro groups [87, 96], resulting CA of 125° and SA of 25° . Such morphology restricts the penetration of aggressive Cl^- to the substrate due to layer of entrapped air. Also the nano-particles provide a tortuous pathway to corrosive species due to large surface area to volume ratio enhancing the barrier properties of the sol-gel coating [30, 31, 76, 95].

As per impedance spectroscopy (Fig 4.77), HMDZ nano-silica modification resulted in significant improvement in protection efficiency against corrosion. It was found that the impedance increases with HMDZ-nano-silica concentration with value of $|Z|_{0.1 \text{ Hz}} \sim 4.6 \times 10^5 \Omega\text{cm}^2$ for 3wt% modification which was two orders higher than the bare substrate ($1.0 \times 10^3 \Omega\text{cm}^2$) and one order higher in magnitude from FE modified sol-gel system ($3.1 \times 10^4 \Omega\text{cm}^2$). However, the impedance value decreases at higher concentration of HDTMS nano-silica addition attributed to agglomeration of nano-particles leading smoothening of the spiky hydrophobic profile and restricting the migration of the per-fluoro groups on the surface. Thus the synergistic effect of micro-nano dual scale roughness and the lower energy perfluoro and tri-methyl groups resulted in superior anticorrosion properties of the GPTMS-MTMS based inorganic-organic hybrid coatings. The anticorrosion mechanism is discussed ahead.

Table: 4.24: Polarisation and EIS parameters of HDMZ nano-silica modified sol-gel coatings

Concentration	E_{corr} (V)	i_{corr} (Acm^{-2})	Impedance (Ωcm^2)
Bare Al (etched)	-1.34	2.27×10^{-4}	1.07×10^3
1wt% HMDZ nano-silica	-0.64	2.02×10^{-6}	1.07×10^5
2wt% HMDZ nano-silica	-0.63	7.02×10^{-7}	1.08×10^5
3wt% HMDZ nano-silica	-0.56	8.38×10^{-8}	4.50×10^5
5wt% HMDZ nano0silica	-0.68	6.74×10^{-6}	3.20×10^4

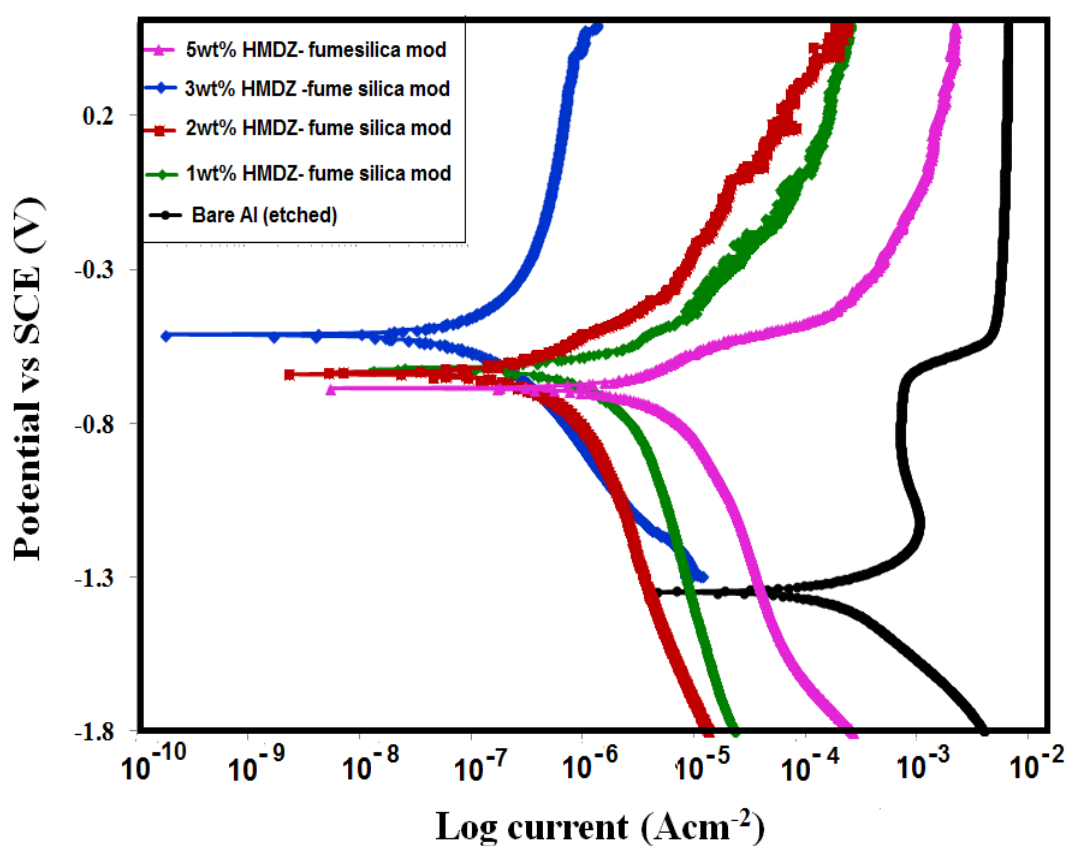


Figure 4.76: Tafel plots of bare Al and various HMDZ nano-silica modified sol-gel coated samples.

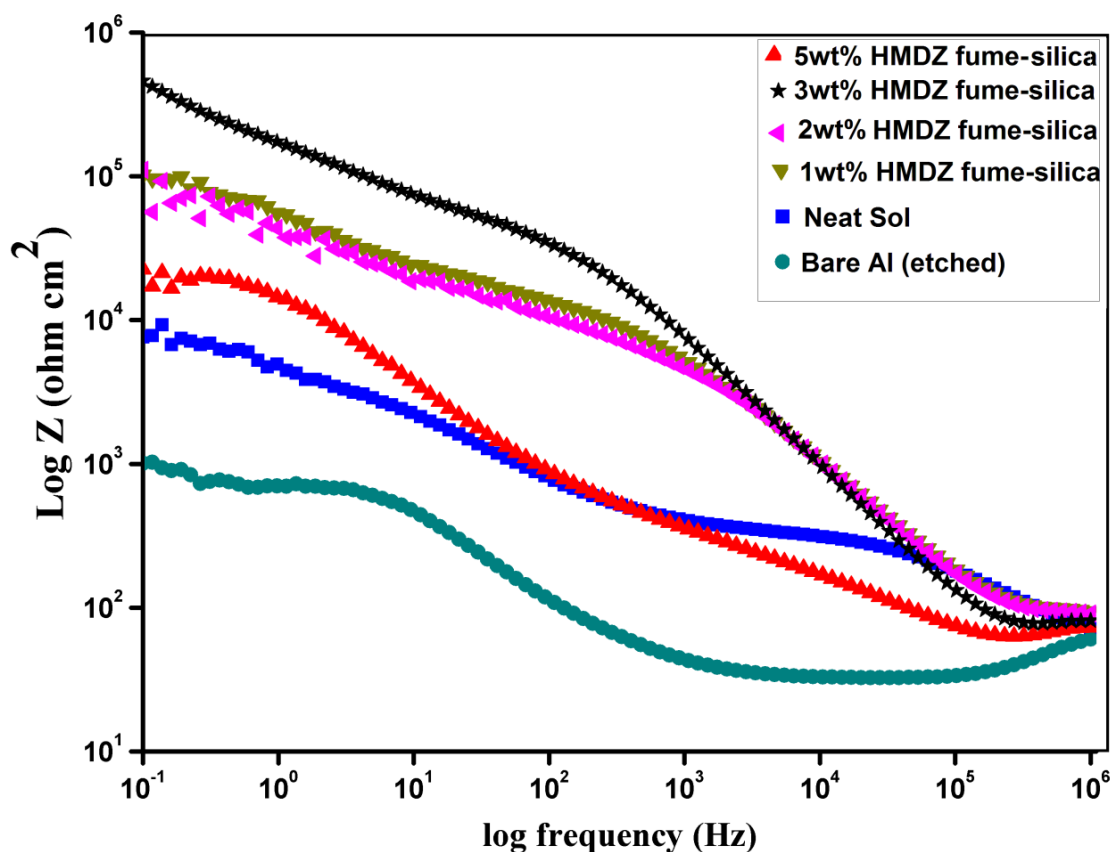


Figure 4.77: EIS plots of bare Al and various HMDZ nano-silica modified sol-gel coated samples

4.9.6 Mechanical Properties of HMDZ nano-silica modified sol-gel coatings:

Effect of trimethyl terminated nano-silica addition to the sol-gel system was studied by analysing mechanical properties of the as developed coatings. It was observed that the HMDZ silica nano-particles contributed to the hardness of the film determined using nano-indentation technique. Fig 4.78 shows a typical load-displacement curve of neat and 3wt% HMDZ nano-silica modified sol-gel coating. The modification resulted in minimum penetration of only 200 nm with load of 1000 μ N which was much less than penetration depth achieved for FE modification of 490 nm. This drastic improvement in hardness and flexibility was attributed to small size and narrow width of the HMDZ nano-silica particles (7-10nm). Due to smaller special dilatation distribution of particles was assumed to have less mechanical interaction with the surrounding coating. Thus, they can pass only a small amount of inducted deformation, which leads to higher flexibility and strength [106, 120]. Further

Maximum value of 5H and 5B of pencil hardness and crosshatch adhesion were obtained respectively for 3wt% modification. It was found that pencil hardness and adhesion of HMDZ nano-silica modified sol-gel coatings decreases at higher loading level of 5wt% and above (Table 4.25). Two causes could explain this. First, the addition of more filler leads to agglomeration which creates high stress around the particles. This makes the sol-gel matrix more fragile near the particles. Second, because of an imperfect adhesion attributed to hindrance in Si-O-Si bond formation due to solid fraction of nano-silica agglomerates added [119]. These two phenomena could probably lead to debonding, resulting in loss of mechanical properties at higher concentrations.

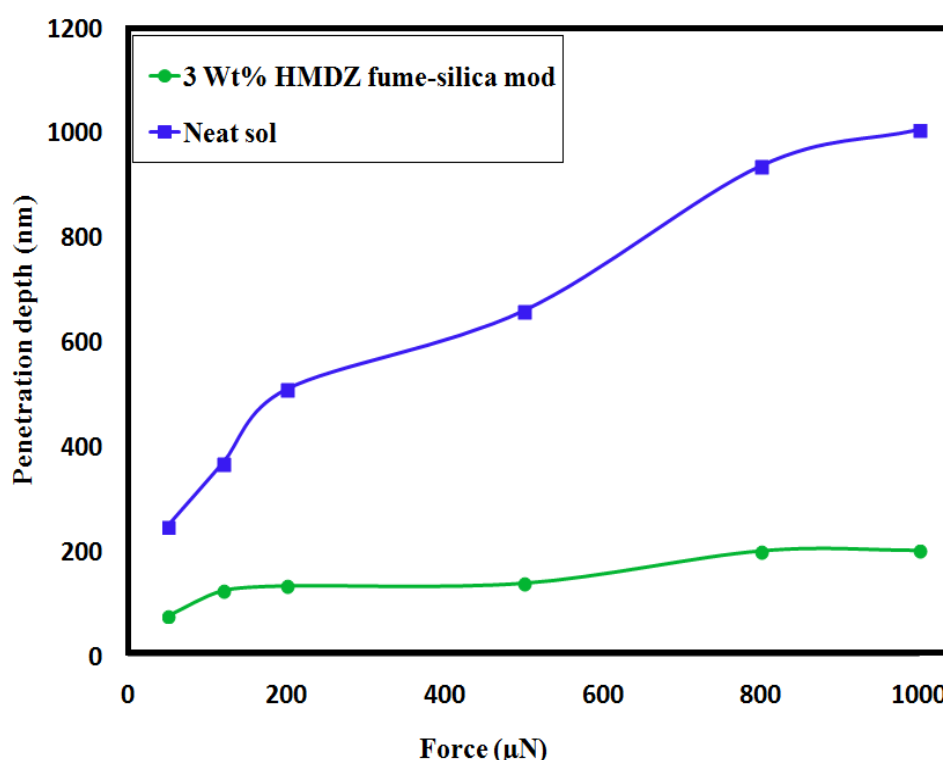


Figure 4.78: Nano indentation curves of neat and 3wt% HMDZ nano-silica modified sol-gel coating

Table 4.25: Pencil hardness and crosshatch adhesion results of various HMDZ modified sol-gel coated samples

Fumed silica concentration	1wt%	2wt%	3wt%	5 wt%
Pencil hardness	5H	5H	5H	4H
Crosshatch adhesion	5B	5B	5B	3B

4.10 Comparative experimental results of all nano-particle incorporated sol-gel coatings:

A hydrophilic (CA $\sim 75^\circ$) inorganic-organic sol-gel system based upon GPTMS, MTMS and HMMM, developed by *Pathak et al.* was modified further for enhancing its hydrophobic characteristics on Al. There are two important requirements to achieve enhanced hydrophobic properties- a) low surface energy and b) high surface roughness. Low surface energy was achieved by terminating –OH groups of the hydrophilic neat sol-gel with low energy fluoro alkyl silanes of different chain length i.e. 3-FAS-3 and 17-FAS and commercial perfluoro additives. Out of which 30wt% FE-2000 (FE) showed maximum improvement in hydrophobicity and was chosen as co-precursor along with GPTMS and MTMS to develop hydrophobic low energy sol with CA $\sim 118^\circ$ and S.A $\sim 70^\circ$. Further, the increase in surface roughness was achieved by incorporating nano-particles such as nano-ZnO, HDTMS-nanosilica, DDS-nanosilica and HMDZ nano-silica. Out of these, 3wt% HMDZ nano-silica showed maximum improvement in surface roughness resulting in CA $\sim 125^\circ$ and SA $\sim 25^\circ$. Following are the comparative results of various optimised amount of nano-particles incorporated in 30wt% FE –modified sol-gel coating. Table 4.34 compiles the results of contact angle and sliding angle of various nano sol-gel systems.

Table 4.34: Comparative values of contact angle and sliding angle of various sol-gel systems

Nano-particle	Contact angle ($^\circ$)	Sliding angle ($^\circ$)
Neat Sol	70°	$>90^\circ$
FE sol	118°	70°
Nano-ZnO	120°	65°
HDTMS-nano-silica	118°	45°
DDS nano-silica	122°	35°
HMDZ nano-silica	125°	25°

Surface chemistry plays an important role in, nano-particle distribution, interaction with sol-gel matrix and extent of agglomeration. Four different nano-particles with different surface chemistries were used to enhance the surface roughness of the fluorinated sol-gel coatings.

Firstly, nano-ZnO particles used consisted of surface –OH groups which were hydrophilic in nature. These polar hydroxyl groups have large affinity for water molecules because of which the expected enhancement in hydrophobicity due to increased roughness was not much effective and resulted in SA of 65° only. Various hydrophobically modified fumed-silica particles were further used to achieve the improved hydrophobic properties. The surface of HDTMS modified nano-silica particles consisted of hydrophobic long chains (C-16) which resulted in improved hydrophobicity with SA of about 45°. The limitation of HDTMS nano-particle was that the modified sol tend to become extremely viscous (wax like) due to progressive inter-penetration of long alkyl chains and steric hindrance which resulted in poor adhesion and scratch resistance [127]. Hence, di-methyl and tri-methyl modified silica particles were used further. Fig 4.79 depicts condensation reactions of DDS and HMDZ with –OH group of unmodified nano-silica particles. In case of DDS modification, the two terminal Si-OH groups on one DDS molecule link with two unmodified nano-silica particles, resulting in hydrophobically modified structure with –OH groups still remaining on the surface. These remaining –OH groups give rise to secondary and tertiary level clusters resulting in wide agglomerates which restrict the orientation of perfluoro groups on the surface responsible for lowering surface energy. Whereas the tri-methyl groups from HMDZ is capable of replacing all the four –OH groups from the unmodified nano-silica particles and surround them. Once the methyl groups covered the particle surface, the agglomeration among particles would become more difficult. Hence the tri-methyl-modified particles were better mono-dispersed in sol [65, 71, 116]. As a result, the surface morphology of film was composed of uniform small particles which differ considerably from DDS nano-particles, and hence allow maximum enrichment of perfluoro groups on the surface. Some researchers have mentioned that methyl groups of silica nano-particles are locally very mobile and they can point into the air resulting in an increase of hydrophobicity [128]. The orientation of methyl groups is totally random and silica particles are completely ordered at nano-composite coating, freely rotating to the air after curing [115]. Hence, incorporation of both DDS and HMDZ modified nano-silica particles showed less agglomeration and improved distribution within the sol-gel matrix at optimum levels, out of which HMDZ modified sol-gel coating, showed maximum improvement in hydrophobicity.

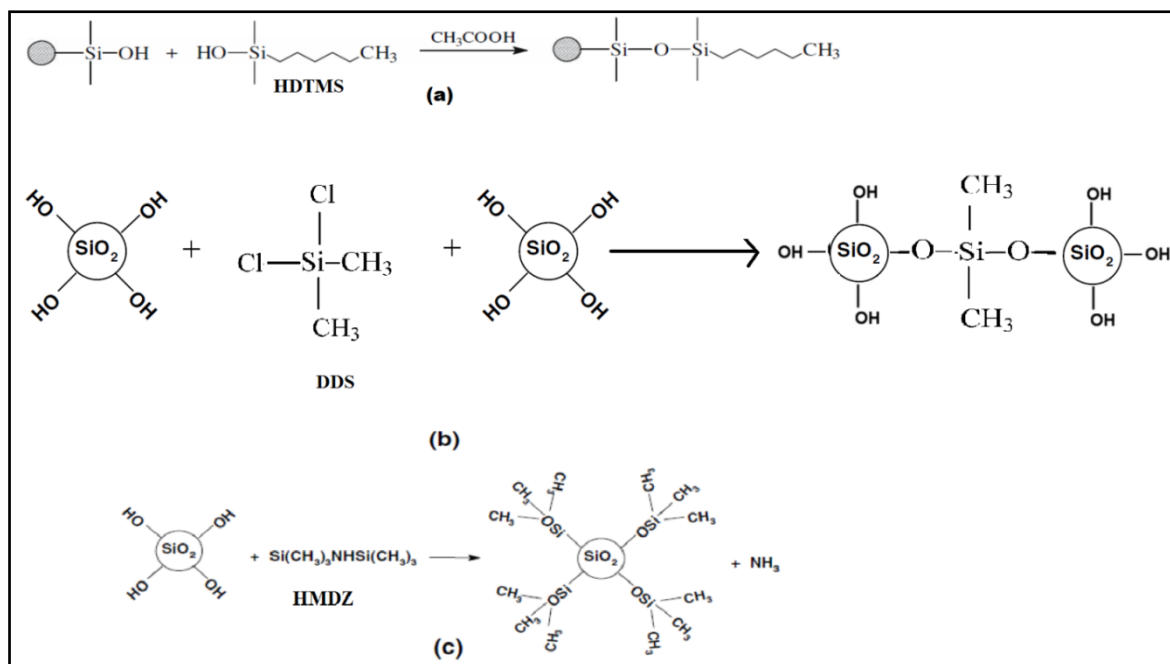


Figure 4.79: The condensation reaction between (a) HDTMS and fume silica silanol group on the silica surface, (b) DDS and fume silica silanol group on the silica surface and (c) HMDZ and fume silica silanol group on the silica surface [116, 128]

Furthermore, the behavior of the coatings with different particles type can be explained by considering the particle size and their BET surface area (Table 4.25). Due to comparatively large size (30-40nm) and small surface area (45g/m²), nano-ZnO particles were less uniformly dispersed as compared to various hydrophobic nano-silica particles and showed more agglomeration resulting in non-uniform hydrophobic profile and decrease in average contact angle and sliding angle. Moreover, amongst various hydrophobic silicas, the particle size varies as HDTMS nano-silica>DDS nano-silica>HMDZ nano-silica and BET surface area varies as HMDZ nano-silica> DDS nano-silica> HDTMS nano-silica (Table 4.25). Therefore small size (7-10nm) and high surface area (160g/m²) of HMDZ nano-silica particles supported large value of contact angle (125°) and small sliding angle (25°) indicating more uniform and less agglomerated state of nano-particles in dispersed form.

Table 4.25: Comparative particle size and surface area

Nano-particle	Particle size (nm)	BET surface area (g/m²)
Nano-ZnO	30-40nm	45±20
HDTMS-nano-silica	15 -25 nm	85±20
DDS nano-silica	10-15 nm	115±10
HMDZ nano-silica	7 to 10 nm	160± 25

The dispersal state of various nano-particles was further characterised by SEM. Table 4.26 lists parameters obtained from SEM micro-graphs of various sol-gel systems. As seen from the comparative SEM images (Fig 4.80), neat sol-gel showed a smooth morphology responsible for its hydrophilic behavior (WCA ~70°). Further, 30wt% FE modification to neat sol-gel resulted in micro-scale roughness with large craters of about 30µm in diameter and considerable improvement in hydrophobicity (WCA ~ 118°) attributed to low surface tension and surface roughness generated due to per-fluoro groups. Furthermore, various nano-particles were embedded in the FE-modified sol-gel matrix resulting in dual scale roughness. Out of all, HMDZ nano-particles due to extremely small size resulted in pores ranging from few microns to several nanometers in diameter at 3wt% concentration, whereas nano-ZnO, HDTMS-nano-silica and DDS-nano-silica resulted in comparatively bigger micropores (table 4.26) which largely fills the craters formed by FE-modification and also restrict fluoro migration to the surface. Hence HMDZ-nanosilica particles resulted in micro-nano dual scale roughness, which was best, required for entrapping air within it, promoting beading and sliding of water droplets over the nano-crevices.

Table 4.26: Comparative SEM parameters of various nano-modified sol-gel coatings

Nano-particle	Diameter of the micro-sphere (µm)
Neat sol	No spheres
FE-sol	30µm
Nano-ZnO	5-10µm
HDTMS-nano-silica	Sheet like
DDS nano-silica	1-5µm
HMDZ nano-silica	1-2µm-several nm

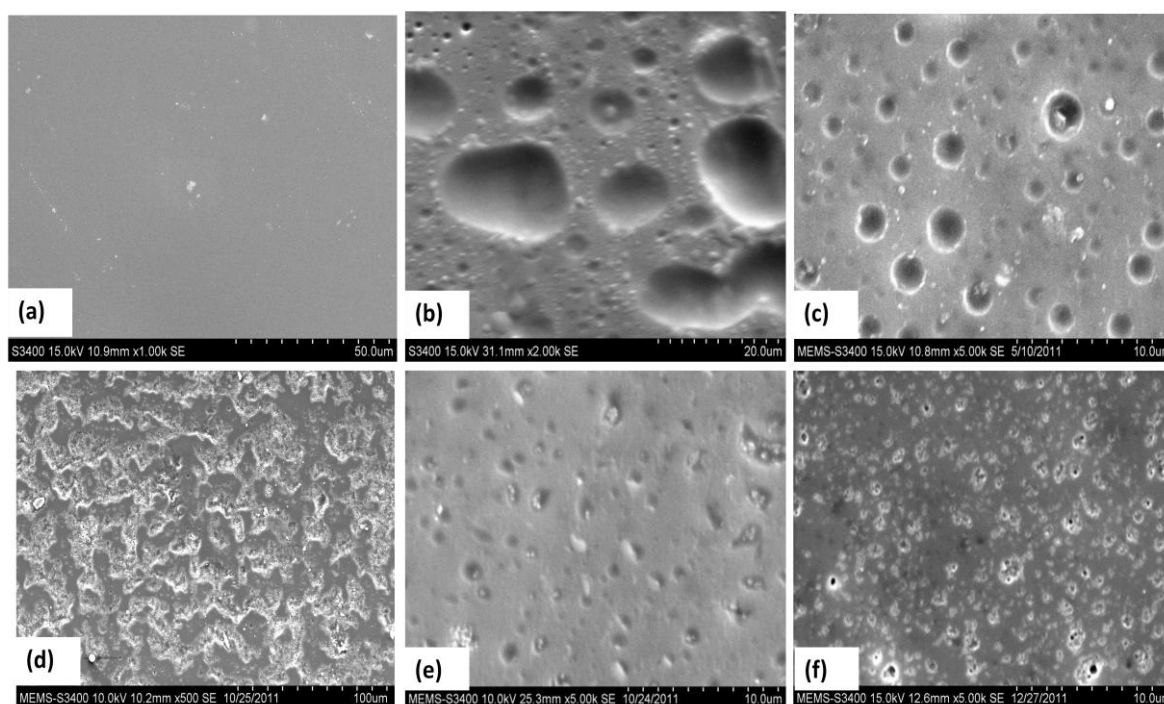


Figure 4.80: Comparative SEM images of a) neat sol, b) FE modified sol, c) nano-ZnO sol, d) HDTMS nano-silica modified sol, e) DDS nano-silica modified sol and f) HMDZ nano-silica modified sol

While comparing the surface topography obtained from AFM analysis of various sol-gel systems, it was found that HMDZ nano-silica particles showed maximum roughness of about 95 nm (Table 4.27). According to 2D images (Fig 4.81), neat sol exhibited smooth topography with extremely small roughness of 3nm, ranging in height from 0-2nm, attributed to GPTMS-MTMS-HMMM sol-gel species. After using 30wt% FE as co-precursor, the roughness increases to 37nm with maximum height of about 100nm. Further embedment of nano-ZnO particles resulted in enhanced surface roughness of about 35nm with maximum height of about 200nm resulting in dual scale roughness. In spite of significant improvement in surface roughness, the increase in hydrophobicity was not much due to hydrophilic surface hydroxyl groups surrounding the nano-ZnO particles. Furthermore, as we move from HDTMS nano-silica to HMDZ nano-silica modified sol; the nano-particles became more and more dispersed with minimum agglomeration resulting in more compact and uniform topography with maximum height of 50nm and surface roughness of about 95nm. Similarly, according to 3D images (Fig 4.82), the spiky structure increases from neat sol to FE-modified sol and increases more with further nano-particle addition. As we move from nano-ZnO to nano HMDZ nano-silica the number of peaks and valleys with maximum “height” and “depth” increases resulting in micro-nano dual scale

roughness like lotus leaf required for superhydrophobicity. Hence HMDZ nano-silica modification resulted in uniform distribution of nano-clusters (2D) and bumpy structure (3D) throughout the surface allowing maximum number of perfluoro-groups coming on the surface with possible orientation of tri-methyl groups in upward direction. Hence both lower energy and high surface roughness were achieved resulting in maximum hydrophobicity reported in the study with WCA of 125° and SA of 25° for a 10μL of water droplet. Improvement in hydrophobic properties resulted in superior corrosion resistance and mechanical properties which are compared and discussed in following section.

Table 4.27: Comparative RMS of various nano-modified sol-gel coatings

Sol-gel composition	RMS (nm)
Neat Sol	3nm
30wt% FE	37nm
2wt% nano-ZnO	105nm
1wt% HDTMS nano-silica	65nm
2wt% DDS nano-silica	75nm
3wt% HMDZ nano-silica	93nm

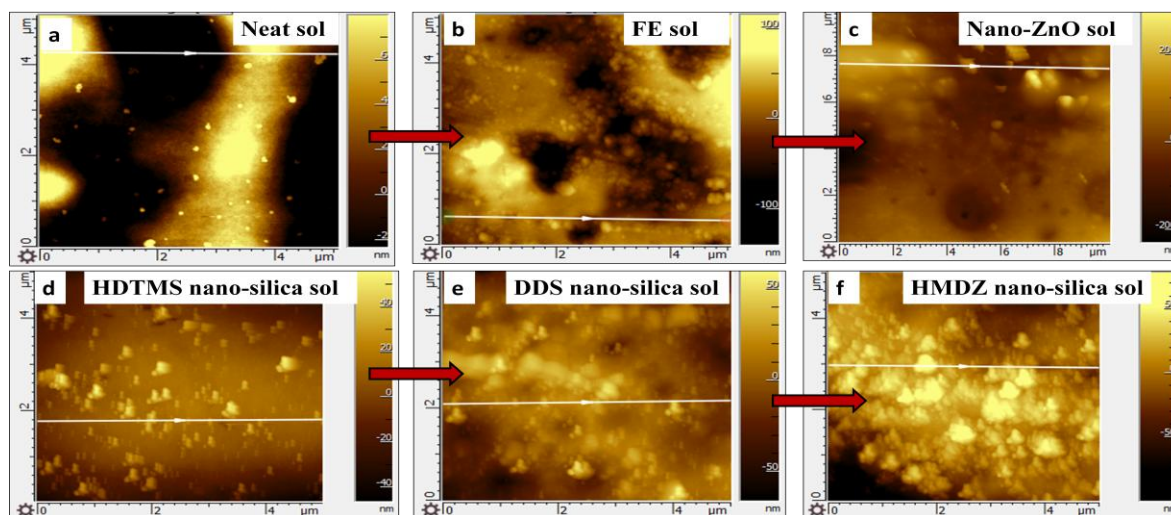


Figure 4.81: Comparative 2D AFM images of various sol-gel systems

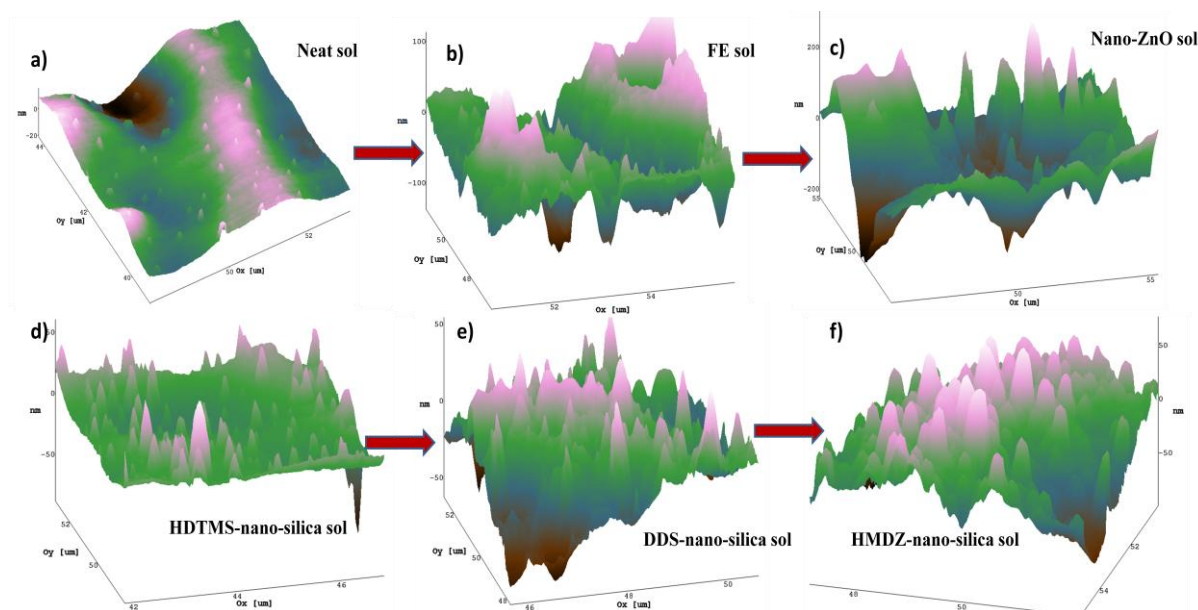


Figure 4.82: Comparative 3D AFM images of various sol-gel systems

Results of potentiodynamic polarisation and EIS were compared in order to study the effect of various nano-particles on corrosion resistance of the modified coatings. Table 4.28 list polarisation and EIS parameters at optimised concentrations of different sol-gel systems. As discussed previously, bare Al in etched condition showed pitting behaviour with i_{corr} value of $2.27 \times 10^{-4} \text{ Acm}^{-2}$ and E_{corr} of -1.34 V . After coating the etched specimen with hydrophilic neat sol-gel the current density was reduced by one order of magnitude ($2.87 \times 10^{-5} \text{ Acm}^{-2}$), indicating the barrier effect of inorganic-organic sol-gel network. Further, modification with low energy FE polymer introduced water repellency to the neat sol gel and resulted in improved corrosion resistance with decrease in current density by three orders of magnitude ($9.37 \times 10^{-7} \text{ Acm}^{-2}$). The water repellent properties of the fluorinated system were further enhanced by increasing the surface roughness using various nano-particles. As seen from the fig 4.83, incorporation of nano-ZnO, HDTMS-nano silica and DDS nano-silica did not showed much improvement on corrosion resistance and the current densities lied in almost same range of FE-sol. However, HMDZ nano-silica modification resulted in decrease of current density further by one order i.e. four orders less in magnitude than bare Al ($8.38 \times 10^{-8} \text{ Acm}^{-2}$). Various modifications resulted in stifling of the anodic reaction kinetics with a positive shift in E_{corr} values from -1.34 V for bare Al to -0.51 V for HMDZ nano-silica modification. Finally according to impedance data (Fig 4.84), the value of $|Z|_{0.1 \text{ Hz}}$ for bare alloy was found to be $1.02 \times 10^3 \Omega \text{ cm}^2$ which increased upto $3.42 \times 10^4 \Omega \text{ cm}^2$ for FE sol and

$4.50 \times 10^5 \Omega \text{ cm}^2$ for HMDZ nano-silica modified sol thus indicating that the synergistic effect of fluoro-emulsion and HMDZ nano-silica particles resulted in considerable improvement in corrosion resistance properties attributed to superior hydrophobicity and water repellent properties.

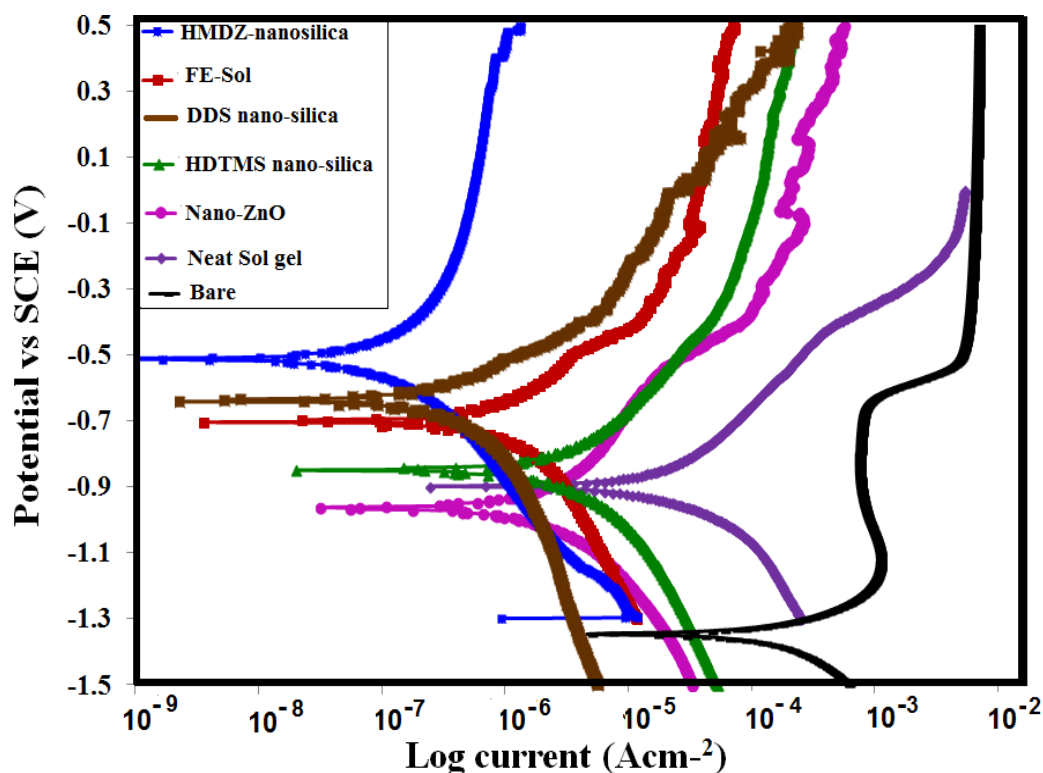


Figure 4.83: Comparative Tafel plots of various sol-gel systems

Table 4.28 Comparative corrosion resistance results of various sol-gel systems

Sol-gel composition	E _{corr} (V)	i _{corr} (Acm ⁻²)	Impedance (Ωcm ²)
Bare Al (etched)	-1.34	2.27×10^{-4}	1.07×10^3
Neat Sol	-1.19	2.87×10^{-5}	5.12×10^3
30wt% FE	-0.70	9.34×10^{-7}	3.42×10^4
2wt% nano-ZnO	-0.93	7.94×10^{-7}	1.47×10^5
1wt%HDTMS nano-silica	-0.84	5.76×10^{-6}	3.99×10^4
2wt% DDS nano-silica	-0.64	5.95×10^{-7}	2.6×10^4
3wt% HMDZ nano-silica	-0.51	8.38×10^{-8}	4.50×10^5

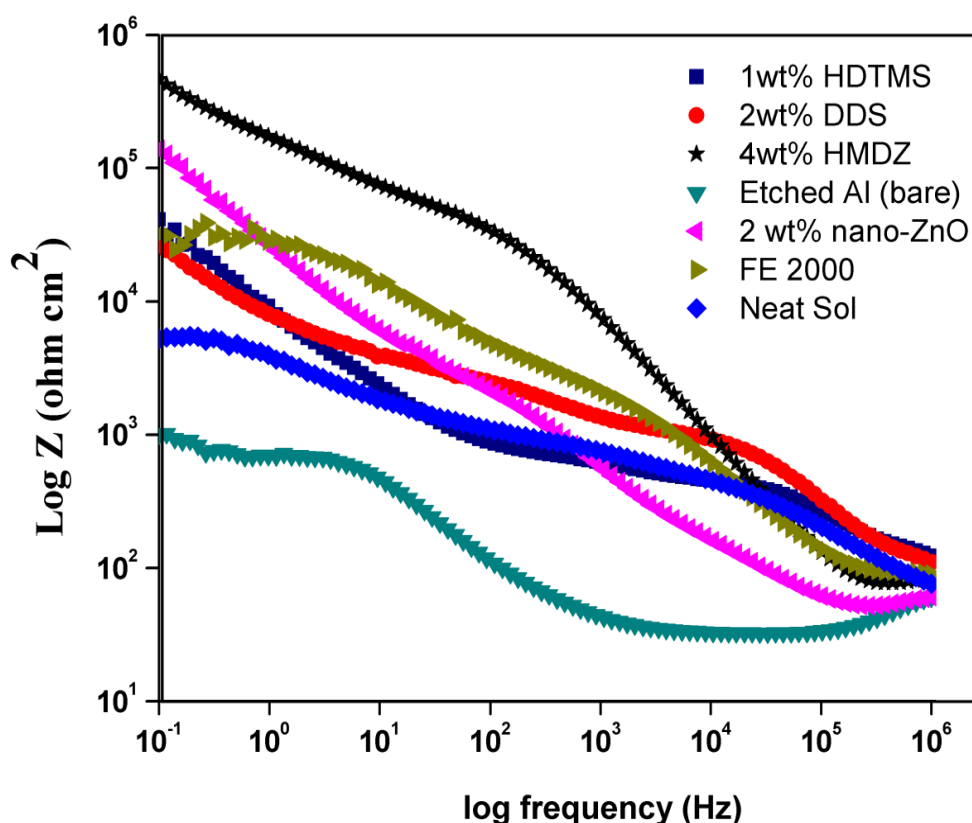


Figure 4.84: Comparative bode plots of various sol-gel systems

The specific surface area, primary particle size and the corresponding order of aggregation are the key parameters affecting the mechanical properties of the inorganic-organic nano composite coatings [129]. Regardless of the type of nanopowder, its addition to the sol increased the compactness of the coatings in comparison to neat coatings. As per comparative load-displacement curve obtained from nano-indentation study (Fig 4.85), a general trend can be stated: The lower the particle size, the lower the penetration depth made by particular indentation force (Table 4.29). This trend was however not reflected by HDTMS nano-silica particles due to its loosely anchored long chain structure. The most pronounced difference was found between the neat sol and HMDZ nano-silica modified coatings. In case of neat sol-gel, for an indent force of 1000 μ N, the penetration depth of about 1000nm was achieved, whereas for HMDZ nano-silica incorporation, the penetration depth was reduced to about 200 nm which was much insignificant in comparison with the coating thickness (2 μ m). Other sol-gel systems viz nano-ZnO, HDTMS-nano-silica and FE modified showed medium penetration depths. Fig 4.86 shows the variation of coating strength with various modified sol-gel systems which followed the similar trend as penetration depth: HMDZ-nano-silica

(0.68Gpa)>DDS-nano-silica (0.48Gpa)> Nano-ZnO (0.28Gpa)>HDTMS-nano-silica (0.18Gpa)>FE-sol (0.16Gpa)>neat-sol-gel (0.05Gpa) supporting the fact that as the primary particle size decreases, compactness of the coating increases resulting in enhanced hardness of the sol-gel coatings. Since smaller particles have less mechanical interaction with the surrounding coating, they can pass only a small amount of induced deformation.

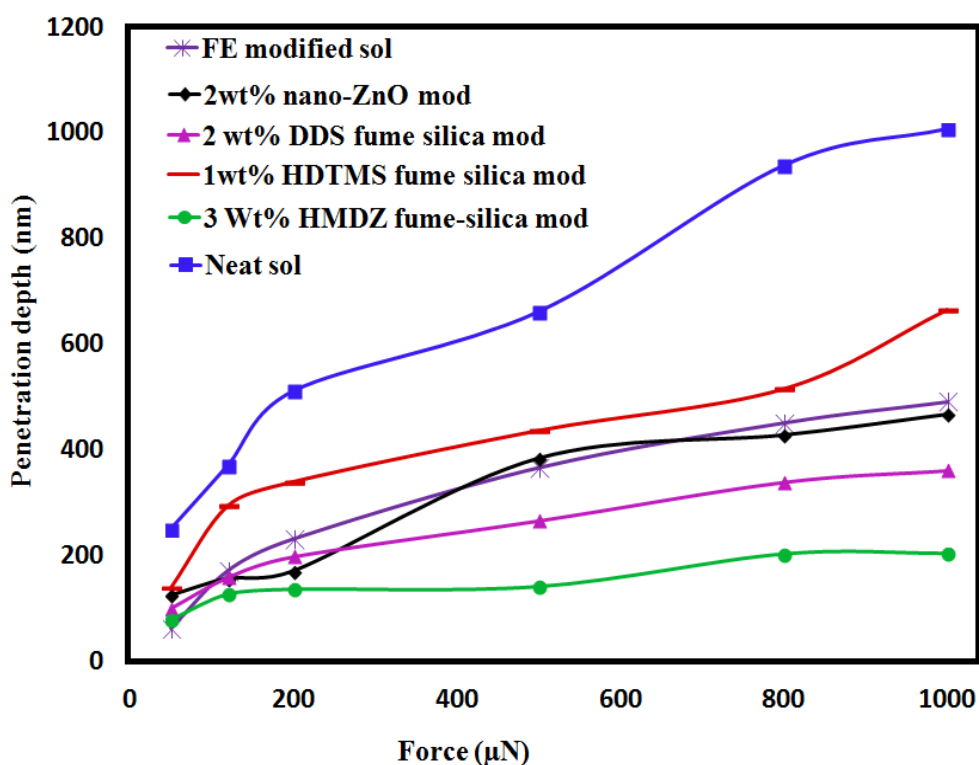


Figure 4.85: Comparative nano-indentation curves of various sol-gel systems

Table 4.29: Comparative mechanical properties of various sol-gel systems

Sol-gel composition	Maximum penetration depth (nm)	Strength (GPa)	Pencil hardness	Cross-hatch adhesion
Neat Sol	1006	0.05	5B	5H
30wt% FE	500	0.16	5B	5H
2wt% nano-ZnO	466	0.18	5B	5H
1wt%HDTMS nano-silica	665	0.28	4B	4H
2wt% DDS nano-silica	360	0.48	5H	5H
3wt% HMDZ nano-silica	202	0.68	5H	5H

Further the effect of reinforcement of various nano-particles on micromechanical properties such as adhesion and pencil harness was compared. Both neat sol-gel and various modified coatings (except HDTMS nano-silica) exhibited cross-hatch adhesion measure of 5B which indicated that Si-OH groups of highly crosslinked neat sol-gel coating were covalently bonded with metal-OH groups and were not interfered by addition of optimised amount of nano-particles. However, it was found that above optimised concentrations, adhesion value decreases and that can be attributed to interference of Si-O-Si as well as Si-O-M bond formation due to addition of solid fraction of large agglomerates of nano-particles. Further the pencil of 5H hardness made no scratch on various modified sol-gel coatings and the films remained intact. HDTMS nano-silica addition showed poor nano and micro-mechanical properties due to its loosely held wax like structure.

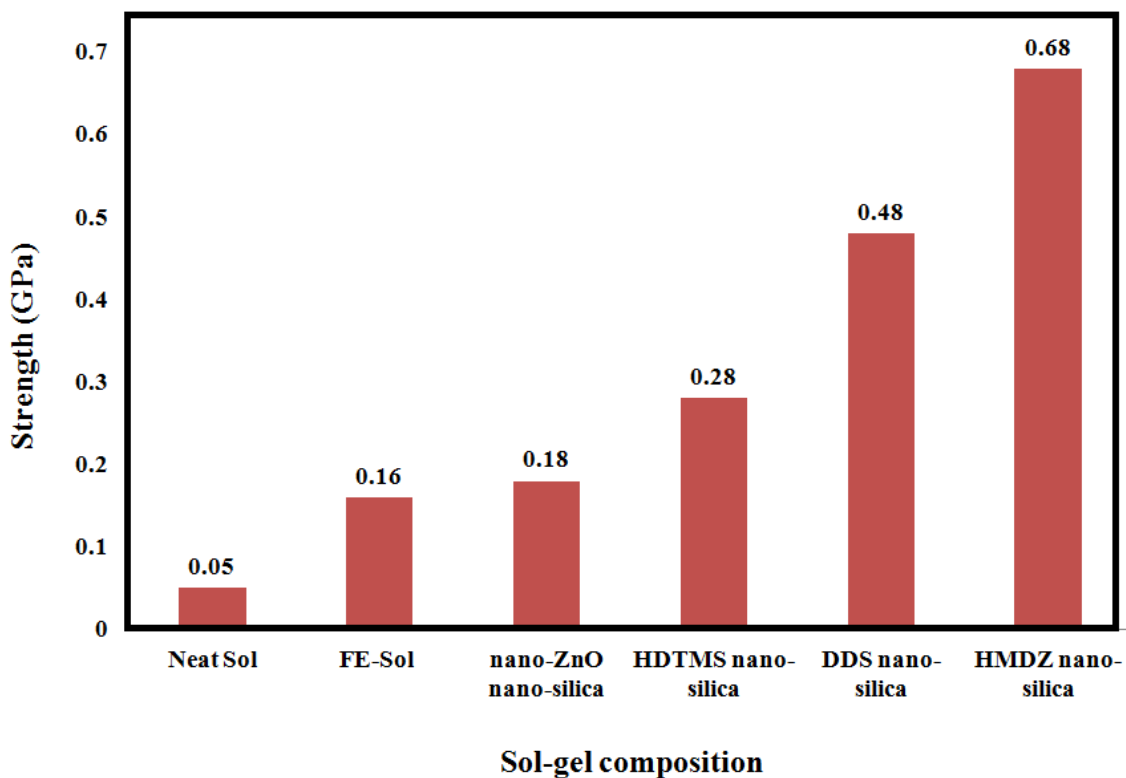


Figure 4.86: Comparative coating strength of various sol-gel systems

4.11 Accelerated lifetime study of HMDZ-FE composite nano-sol gel coatings:

The durability of the hydrophobic sol-gel layer is a crucial requirement for the practical use. The finally formulated HMDZ-FE composite hydrophobic sol-gel coatings were tested for their accelerated lifetime properties.

4.11.1 Self-Life:

The HMDZ-FE composite sol-gel coating solution can be stored as two pack system. Pack one consist of GPTMS-MTMS-FE crosslinked primary sol followed by ultrasonication with HMDZ-nano-silica particles. This nano-modified primary sol can be stored in refrigerator for about six months which may give superior hydrophobicity after prolong time due to aging of the sol-gel. Pack two consists only of the organic polymer HMMM. Hence, both the packs are blended under high shear in required ratio to obtain the desired coating for application. Hence, the coating solution once prepared can be preserved for six months and can be reused. This is called shelf life of the coating.

4.11.2 Gel Time or Pot life:

The time available for application of coating after mixing packs one and two is called pot life of the coating. After mixing, the coating solution can be applied within 12 hours. After 12 hours the HMMM starts undergoing self-condensation reactions resulting in gelling of sol and also leads to phase separation at times.

4.11.3 Salt Spray Exposure:

Al samples coated with final HMDZ-FE sol gel formulation were exposed in salt spray conditions as per ASTM B117 specifications i.e. the coated substrates were exposed to a salt fog chamber having 3.5wt% aqueous NaCl solution at temperature of 35 ± 1.7 °C. Salt spray test provides information about the nature of failures like blisters, rusting or cracking and delamination of film. It was found that the coating passed 400 hrs of salt spray exposure and started corroding above 500 hrs and finally delaminated at 1000 hrs of salt spray exposure (fig 4.89). The coating efficacy in such conditions can be directly related to the degree of

hydrophobicity. As the vigorous conditions increases inside the salt spray chamber, the contact angle decreases upto 95° for 400 hours. The coating became hydrophilic with contact angle of about 65° after 500 hours resulting in loss of hydrophobic profile and leading to penetration of corrosive environment and hence resulting in corrosion. Further after 1000 hrs of exposure the coating was found to be completely corroded and delaminated due to extremely small thickness of the coating with CA of about 15° . Thus it can be said that as developed hydrophobic coatings though resulted in loss of hydrophobicity (CA, 95°) were found to be intact and free from any defects like peeling or blisters and was capable to withstand the corrosive environment of salt spray chamber after 400 hrs. Figure 4.87 shows variation of contact angle of HMDZ-FE composite coating upon salt spray exposure

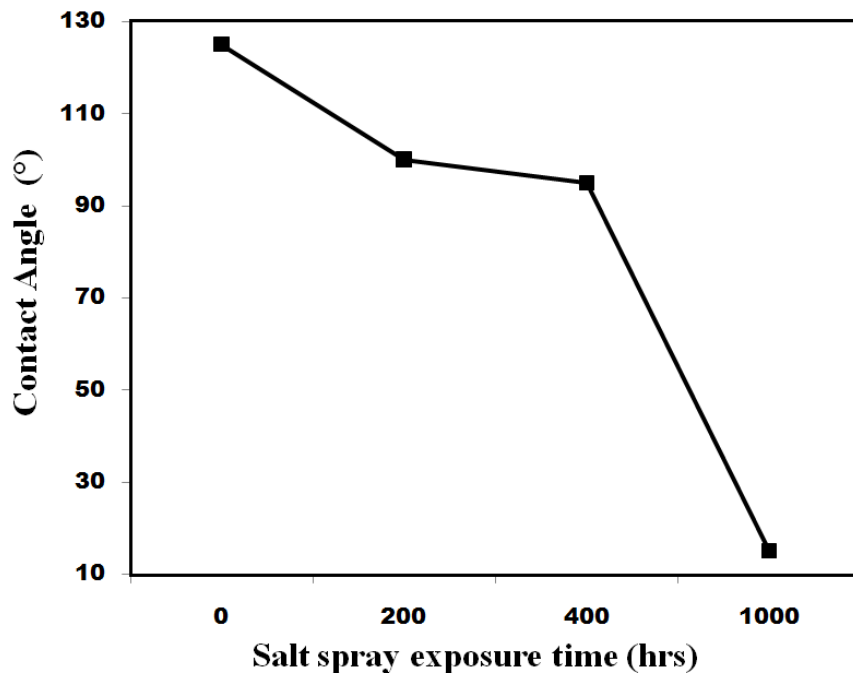


Figure 4.87: Variation of contact angle of HMDZ-FE composite coating upon salt spray exposure

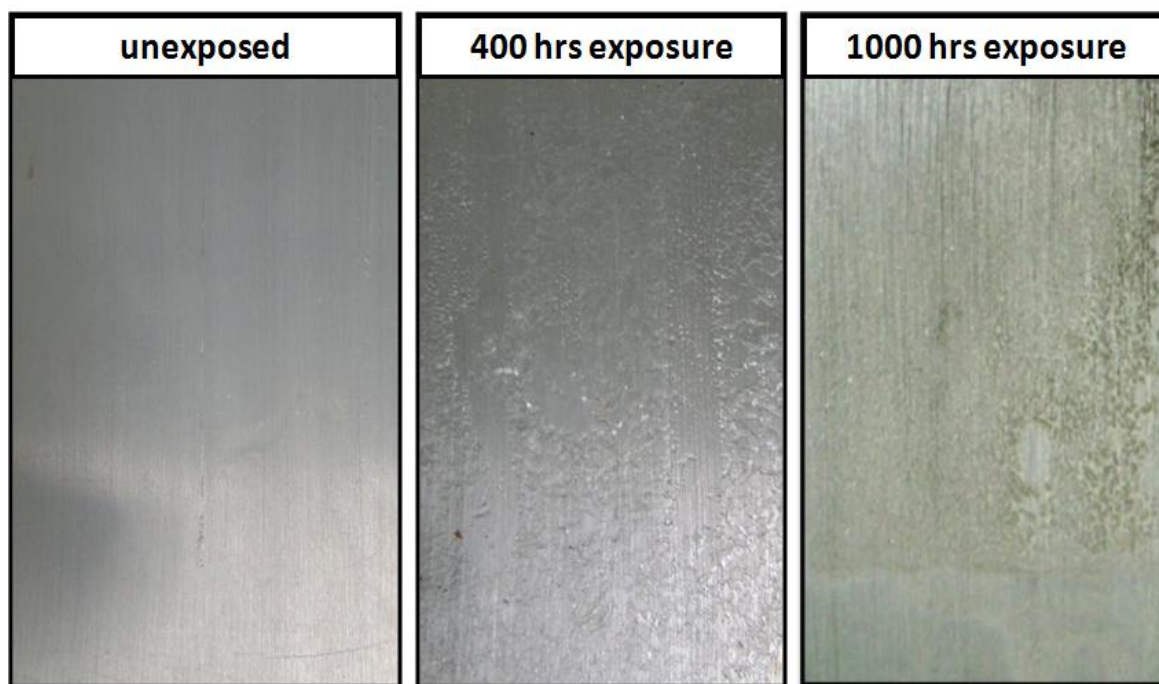


Figure 4.89: Image of unexposed and salt spray exposed HMDZ-FE composite sol-gel coated Al panels

4.11.4 U.V. exposure:

To study the durability of the as developed hydrophobic coatings for the outdoor applications, coated substrates were exposed to accelerated UV environment as per ASTM 4329 for 100 hours (Fig 4.90). It was found that the coated substrates showed significant loss of hydrophobicity (CA, 105°) after 2 cycles i.e. after 8 hours of UV irradiation and 8 hours of condensation. However, the coating was retained on the surface even after 100 hrs of U.V. exposure with no chalking or blistering observed, but showed hydrophilic behaviour with CA of about 45° (Fig 4.91). As shown in fig, the hydrophobic films fabricated in this study modified by nano-ZnO and HMDZ nano-silica showed much improved UV stability both in terms of change in energy (ΔE) and gloss retention (ΔG) relative to that of neat sol-gel (Fig 4.92)

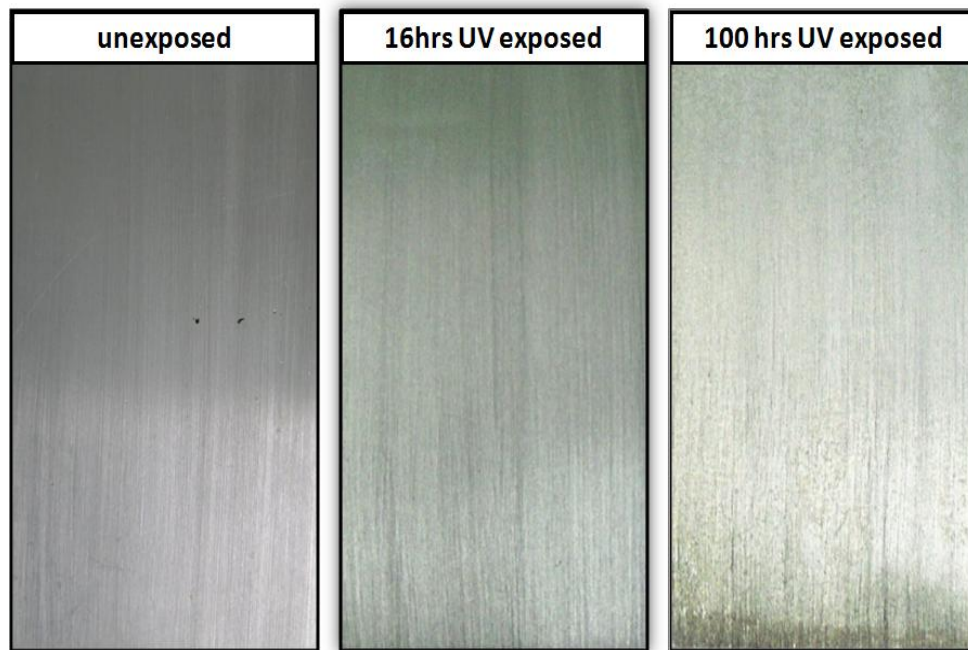


Figure 4.90: Image of unexposed and UV exposed HMDZ-FE composite sol-gel coated Al panels

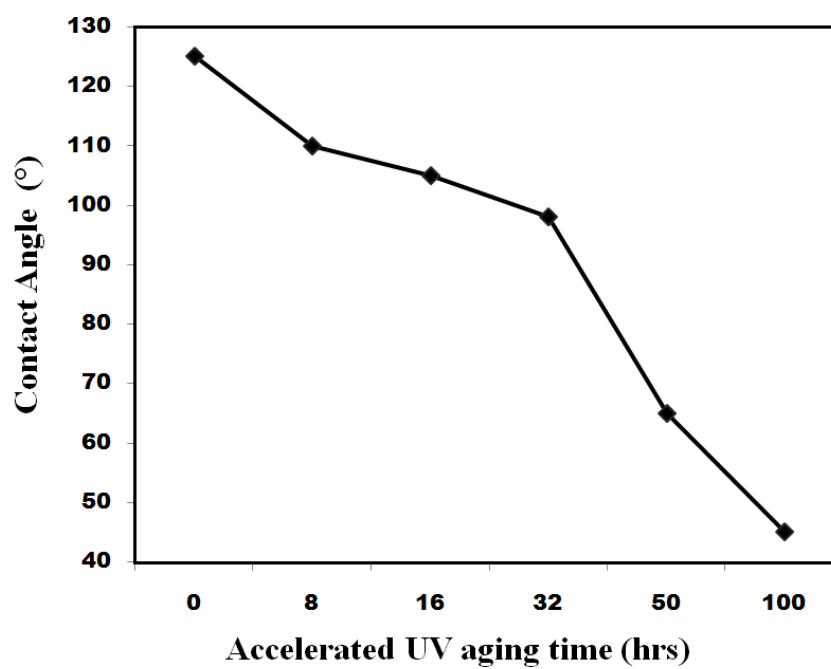


Figure 4.91: Variation of contact angle of HMDZ-FE composite sol gel coated Al substrate upon UV exposure

Nano-ZnO showed superior U.V. resistance than HMDZ fume silica particles, as the band gap energy and wavelength of nano-ZnO is 3.3eV and 375nm respectively, which provide U.V. protective properties, whereas the band gap energy and wavelength of nano-silica is 8.9eV and 138 nm respectively resulting in highly transparent and reflective properties [104]. Another probable reason for effectively higher UV resistance for nano-modified hydrophobic coatings as compared to neat sol-gel coating could be presence of non UV-labile perfluoro groups that exist on the material surface. These groups are more UV stable than simply Si-O-Si moieties due to strong $(-\text{Si}-(\text{CF}_2)_5\text{CF}_3)$ bonds. However the decrease in hydrophobic properties on prolong UV exposure can be attributed to presence of UV-labile segments or UV-absorbing groups (Epoxy group) that establish sites where the polymer can undergo photo-oxidation to form carbonyl or hydroxyl groups in the bulk polymer as well as on the surface leading to degradation (i.e., unzipping) into smaller chains. The introduction of these hydrophilic groups on the surface leads to significant loss of hydrophobicity [48].

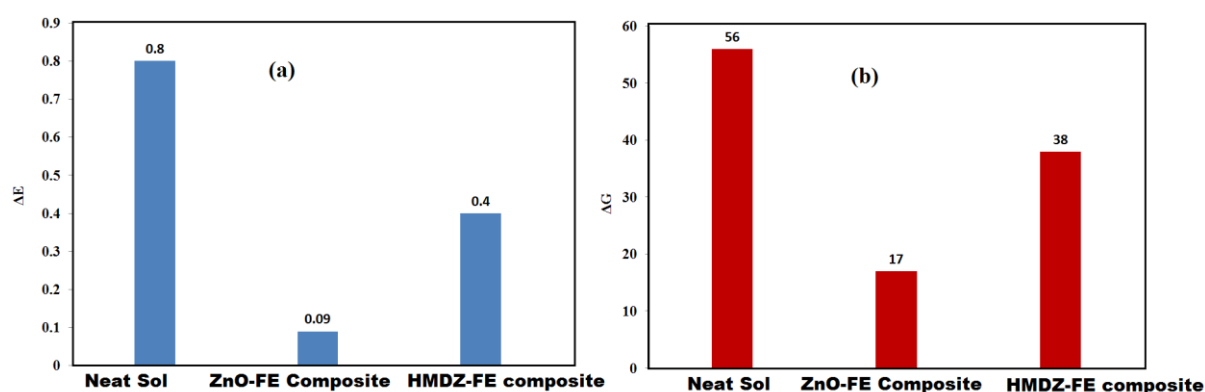


Figure 4.92: Variation of a) change in color (ΔE) and (b) change in gloss (ΔG) after modification with nano-ZnO and HMDZ nano-silica particles

4.11.5 Humidity exposure:

The effect of humidity on the wetting properties of the as deposited HMDZ-FE composite coatings was carried out at relative humidity of 85% at 30°C for a period of 30 days. It was found that the water repellent capability of HMDZ-FE composite sol-gel coated substrate gradually degraded during long term humidity exposure test. The neat sol gel showed a drastic decrease in contact angle of about 10° after 5 days only. This is due to hydrophilic surface $-\text{OH}$ groups that react with the moisture created in the humidity chamber resulting in

deterioration of the coating structure. However, it was observed that there was no significant change in contact angle value of HMDZ-FE composite films even upto 20 days (CA, 112°). This is attributed to presence of non-polar tri-methyl groups from HMDZ nano-silica and perfluoro groups from FE polymer resulting in improved water repellency in extremely humid conditions [26]. However, after 30 days of exposure the hydrophobicity of the as deposited coatings was completely lost resulting in hydrophilic contact angle of about 85°.

4.11.6 Mechanical Strength:

HMDZ-FE composite sol-gel coatings were found to be stable for more than six months when stored under ambient conditions. The mechanical stability and robustness of the HMDZ-FE composite coatings are previously discussed. The coatings showed excellent adhesion and scratch resistance of 5H and 5B after HMDZ-nano-silica incorporation and hence can be scale up for various industrial applications.

4.12 Effect of various surface roughness methods:

After studying the effect of various nano-particles on surface roughness it was observed that surface roughness is a dominating factor for enhancing hydrophobicity. Hence roughening of the substrate itself prior to the application of hydrophobic coating was explored using various roughening methods on aluminium surface, like chemical etching; mechanical etching, spraying, sand blasting and plasma etching. Table 4.30 lists the water contact angle values achieved on aluminium surface after roughening with various methods followed by as deposited hydrophobic coatings.

4.12.1 Effect of Chemical Etching:

The key to the etching technique was the use of a dislocation etchant that preferentially dissolves the dislocation sites in the grains [73, 130]. To study the effect of chemical etching on hydrophobicity three chemical etchants namely the Krolles etchant, Becks Etchant and 10% NaOH were used followed by coating with 17- FAS formulation. The objective of chemical etching of the aluminium metal prior to the application of hydrophobic coating was the removal of metal atoms from the surface in forms which are soluble in the etching solution resulting in micro-scale roughness. The etching rate bears a relationship to the defects present in the material,

its crystallographic orientation and the surface finish [131]. As discussed earlier the maximum contact angle achieved for 17-FAS formulation on 10% NaOH etched aluminium surface was about 110° , whereas the contact angle was found to increase upto 117° using Krolles reagent and decrease upto 100° using becks reagent. Hence chemical etching successfully supported the fact that roughening or patterning the metal substrate followed by application of hydrophobic coating can result in enhanced hydrophobicity.

4.12.2 Effect of Mechanical Roughening:

However, vigorous chemical etching may result in inferior corrosion resistance properties due to entrapment of corrosive species within the etched grain boundaries. Further various mechanical roughening methods were explored viz. grinding using sand paper of different grit sizes, sand blasting using fine alumina sand particles at different pressure conditions followed by application of FE-sol formulation. As reported the maximum contact angle achieved for FE-sol was 118° for combination of 400 and 600 grit sandpaper, whereas a higher contact angle of about 128° was obtained on sand blasted aluminium surface at pressure of 5psi coated with FE-sol. However, such high angle achieved was not repeatable as the roughness obtained by sand blasting cannot be controlled each time to get concordant results. Therefore, it can be said if aluminium surface could be uniformly patterned using sand-blasting, much high contact angle values could be obtained [132].

4.12.3 Effect of Plasma etching:

Plasma etching was done on aluminium samples at various DC voltages. Plasma-etching process is one of the important techniques to produce patterns from the nanometer to the micrometer range on various substrates [133]. In plasma etching process plasma is produced by the dissipation of electrical power to the medium. Electrons, to which most of the power is transferred, gain enough energy to initiate under collisions with atoms and molecules, processes such as excitation, ionisation and dissociation. Atoms, radicals and ion species, which are produced in this way, are at the origin of further reactions. Ultimately, the plasma species interact with the walls and the sample surface. Adsorption of species will occur depending on the chemical affinity and surface temperature. Adsorbed species may react with the surface to form a product or desorbed without or before reaction. If the product is volatile, it will desorbed into the plasma phase and, thus, cause etching of the material. If the product is non volatile, it will

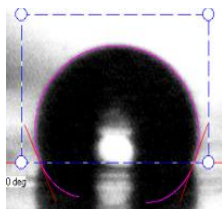
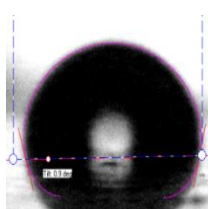
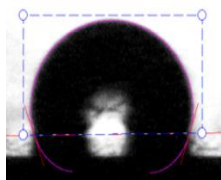
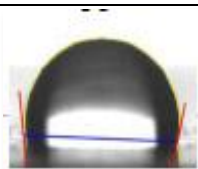

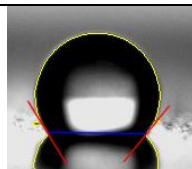

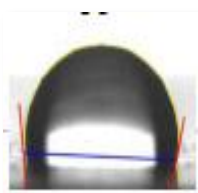
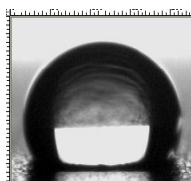
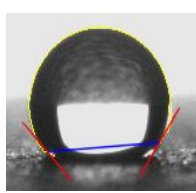
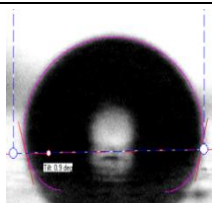

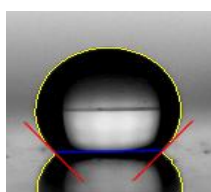

participate to the formation of a thin film at the surface of the material [134]. In present work the plasma environment was simulated by ion beam (Ar⁺). Aluminium substrate was placed inside the plasma chamber and subjected to DC pulsed plasma etching for various time intervals followed by coating with FE-sol. The maximum contact angle achieved was 123° by passing pulsed DC voltage for 60 min.

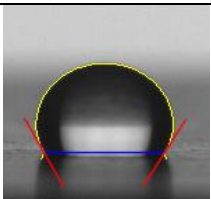
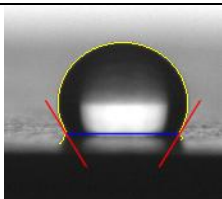
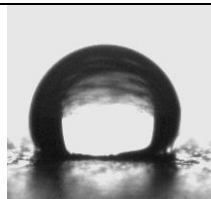
4.12.4 Effect of spraying:

In order to introduce roughness into the coating, HDTMS modified fumed silica particles with a size of 50 nm to 100 nm were dispersed into the FE sol-gel using ultrasonicator. After spraying the solution onto the substrate a defined roughness was generated by a random arrangement of the hydrophobic silica particles in the coating [135]. The particle size and particle amount were varied and the surface roughness was evaluated. All the coatings investigated in this study were produced by keeping the spray pressure constant (100psi). The applied coatings were annealed at 120° C for one hour to remove residual solvent and achieve complete curing. A maximum contact angle of 130° was obtained, but the result was not reproducible due to non-uniform random arrangement of particles each time.

All these techniques resulted in effective increase in root mean square roughness of more than 100nm, but the profile obtained was not uniform and results were not frequently reproducible. Hence it can be concluded that as developed hydrophobic sol-gel coatings were hydrophobic and capable of lowering enough surface energy to produce high contact angles >130°, if adequate and uniform surface roughness was achieved by various roughness methods.

Table 4.30: Effect of various surface roughness methods prior to hydrophobic sol-gel coating

Composition	Roughness Method			
Sol+ 2wt% 17-F.S	Chemical Etching			
	Krolls Reagent	Becks reagent	NaOH reagent	
				
	115°-117°	100°	105°	
Sol + 30wt% FE	Mechanical roughening- Sand Paper Grinding			
	100 + 400	200 +600	400 + 600	600+800
				
	95°-98°	110°- 115°	115°-118°	>100°
Sol + 30wt% FE	Mechanical Roughening- Sand Blasting			
	1 psi	3psi	5psi	7psi
				
	95°	110°	115°-128°	105°
Sol+ 30wt% FE+ HDTMS modified fumed-silica	Spraying			
	First Batch	Second Batch	Third and successive batches	
				
	118°	125° -130°	110°-115°	

Sol + 30wt% FE	Plasma Etching		
	15 min (DC voltage)	30 min (DC voltage)	60 min (DC voltage)
	 118°	 121°	 123°

4.13 Effect of as developed hydrophobic coating on various non-metallic porous substrates:

The effect of as developed coatings on hydrophobicity was studied using non-metallic substrates apart from Al metal which have inherent surface roughness. Table 4.31 and Fig 4.93 shows contact angle values obtained on various rough substrates like wood, cotton, cardboard, glass, paper and concrete after application of HMDZ-FE composite sol-gel coating. The contact angles achieved ranged between 130°-140° indicating that as developed coatings were capable of exhibiting super-hydrophobicity required a uniform roughness pattern was obtained prior to coating application.

Table 4.31: Contact angle values on various non-metallic substrates

Substrate	Contact angle (degrees)
Glass	115
Paper	145
Cardboard	130
Wood	135
Cotton	140
Concrete	145
Epoxy base coat	145
PU base coat	127

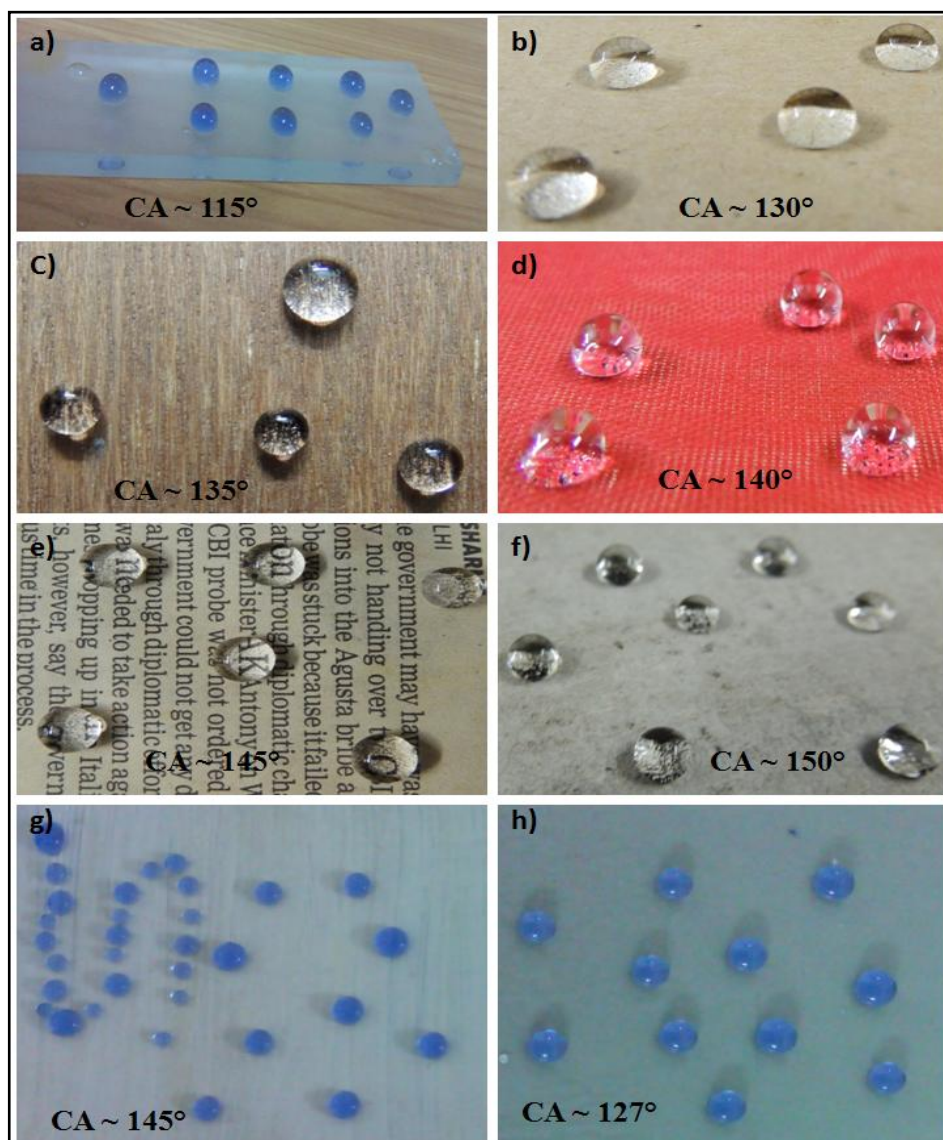


Figure 4.93: Contact angle image on hydrophobically coated a) glass, b) cardboard, c) wood, d) paper, f) concrete, g) epoxy coated surface and e) polyurethane coated surface

Hence, it can be concluded that Al metal has a flat surface and very high surface energy. The maximum contact angle reached after application of the HMDZ-FE modified coating on 10% NaOH etched Al substrate was 125° only with SA of 25° . However, a high contact angle of about 130° was obtained after mechanically roughening the panels using sand blasting technique, but the hydrophobicity lied in perfect Wenzel state i.e. the water droplet was completely stucked up within the blasted profile and did not slide down even if tilted with $SA > 90^\circ$. This can be attributed to high surface roughness obtained, above an optimum level, resulting in wider distance between peaks and valleys and hence restricting the sliding of the

water droplet. Further the same formulation when sprayed on different non-metallic rough surfaces resulted in superhydrophobicity with CA of about 135° - 150° and SA of 15° . Therefore, it can be said that that in present work, the developed hydrophobic inorganic-organic hybrid sol-gel coating was capable of exhibiting super-hydrophobicity lying in Cassie-Baxter state attributed to the fact that coating is applied on uniformly patterned rough surface. Superhydrophobicity can also be obtained on present Al alloy provided it is also uniformly roughened using sophisticated techniques like laser lithography, ion beam etching, anodization, molding and stamping etc [136].

Result and Discussion- Part III

4.14 Characterisation of non-fluoro sol-gel coatings:

4.14.1 Wetting properties of non-fluoro sol-gel coatings

Sol-gel coated aluminium substrates, without any modification were found to be hydrophilic with contact angle of around 65-70°. After modifying the same with various HDTMS formulations, the surface turned hydrophobic with contact angle ranging from 95° to 100°. It was found that the hydrophobicity increases with increase in concentration of HDTMS. Since, HDTMS is long chain alkyl precursor, responsible for lowering the surface energy, contact angle increases with increase in its amount, but gelling time is another important factor, which actually decreases drastically after substantial increase in HDTMS concentration. Hence, only small amount of HDTMS was required for introducing hydrophobicity and for longer pot life. Sol D with GPTMS: HDTMS: TEOS volume ratio of 2:2:6 was found to be the optimum formulation to achieve a reasonable contact angle of about 95° with a long gel time of 15 days. Table 4.31 lists gel-time and contact angle of various sols coated on un-etched aluminium substrate.

Table 4.31: Gel-time and contact angle of various sols coated on un-etched aluminium substrate

Formulation	Gel Time	Contact angle on un-etched flat substrate
Sol A	1 month	95°
Sol B	7 days	97°
Sol C	1 day	100°
Sol D	15 days	95°
Sol E	15 days	98°

Table 4.32: Water contact angle of various formulations of non-fluoro sol-gel coatings developed on differentially etched aluminium specimens

Formulation	C.A on coated Krolles reagent etched specimen	C.A on coated NaOH reagent etched specimen	C.A on coated Becks reagent etched specimen
Uncoated	45°	65°	55°
Sol A	105°	110°	120°
Sol B	105°	110°	125°
Sol C	107°	115°	135°
Sol D	107°	115°	130°
Sol E	102°	110°	128°

In order to achieve higher value of water contact angle, aluminium substrates were further etched using various chemical etchants. Fig 4.94 and Table 4.32 shows the variation of contact angle achieved on aluminium samples, etched with various etchants, followed by coating with various sols. It was found that irrespective of the kind of roughening method was used, hydrophobicity on etched surfaces increases when compared to un-etched surface. All hydrophobic formulations showed similar trend for a particular surface roughness. The surface of bare specimens etched with Krolles reagent, 10% NaOH and Becks reagent, showed hydrophilic behavior with contact angles of about 45°, 65° and 55° respectively. However, after coating with various HDTMS sols the average contact angle increased to 105° for Krolles etching, 115° for 10% NaOH etching and about 130° for becks etching.

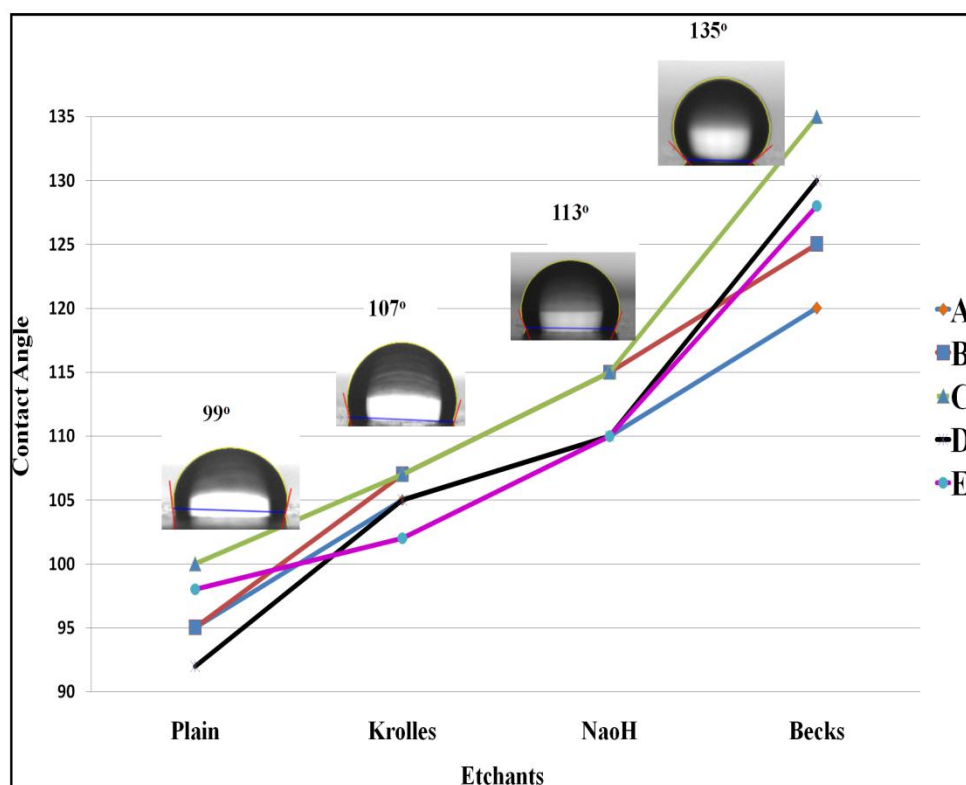


Figure 4.94: Variation of contact angle of different non-fluoro formulations coated aluminium samples etched with various reagents

Table 4.33 shows the sliding angle behavior of optimised sol D formulation, coated various etched surfaces. It was found that sliding angle decreases with increase in severe nature of etchant with minimum value of about 15°- 25° for becks etched coated sample. This shows that both long chain hydrophobic HDTMS sol-gel coating and roughening due to etching were synergistically responsible for achieving hydrophobic aluminium surface.

Table 4.33: Variation of sliding angle with different kind of etching on aluminium after coating with various hydrophobic sol-gel formulations

Etched surface coated by various formulations	Sliding Angles of 10 μ L water droplet
Flat Surface	>90°
Krolles reagent	75° -65°
NaOH reagent	55° -45°
Becks reagent	15° - 25°

4.14.2 Morphological analysis of non-fluoro sol-gel coatings:

Fig 4.95(a) shows Scanning electron Microscopic (SEM) image along with Energy Dispersive X-ray analysis (EDAX) spectra of un-etched flat aluminium substrate, followed by application of sol D, according to which the surface is covered by large number of silica particles also confirmed from EDAX responsible for initial hydrophobic behavior with contact angle $>90^\circ$ due to lower energy HDTMS components.

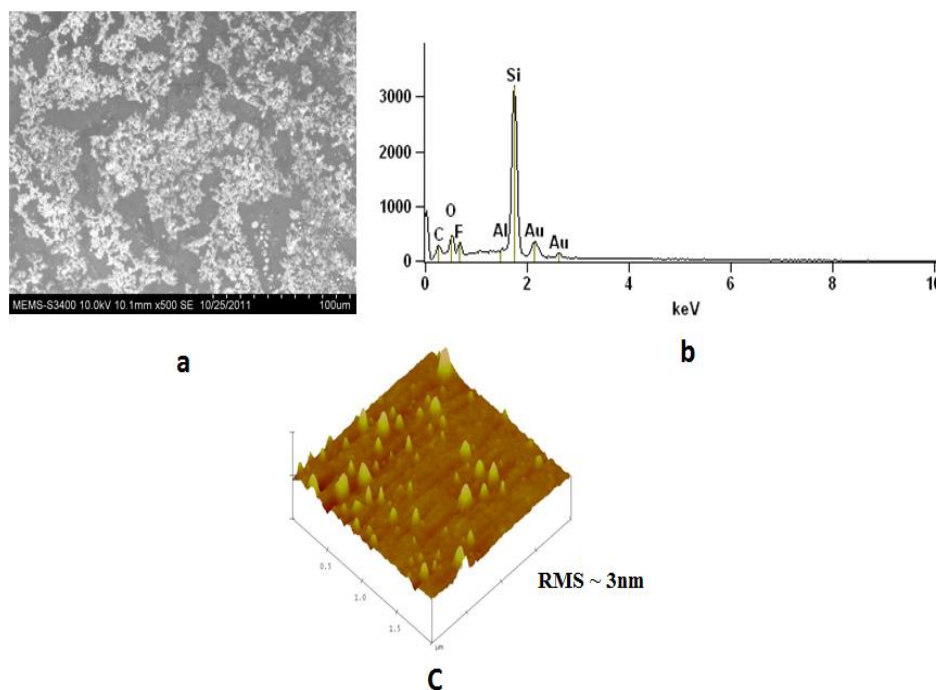


Figure 4.95: a) SEM image, b) EDAX Spectra and c) AFM image of flat aluminium substrate coated with sol-gel formulation having GPTMS: HDTMS: TEOS ratio 2:2:6

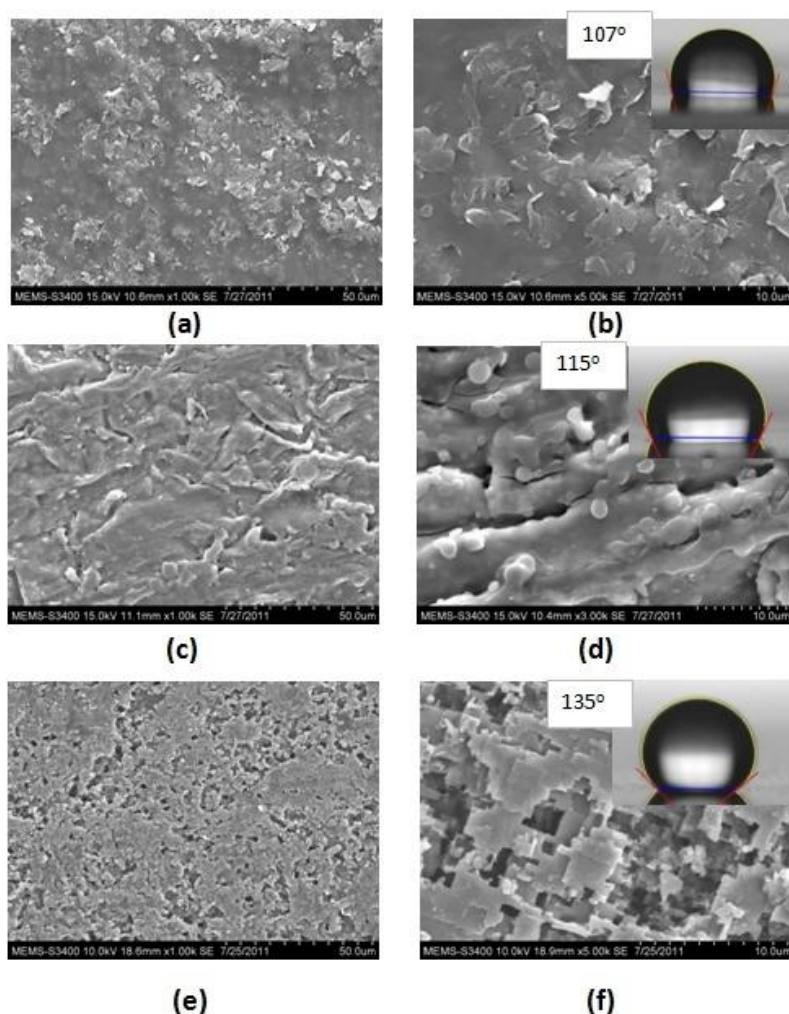


Figure 4.96: SEM images of specimens coated with sol-gel formulation having GPTMS:HDTMS:TEOS ratio of 2:2:6 after a) Kroll's etching at magnification of 1000X and b) 5000 X , c) 10% NaOH etching at magnification of 1000X d) 5000 X and e)Becks etching at magnification of 1000X and(f)5000X

The microstructures formed on the substrates after etching of aluminium surface by various methods followed by application of formulation sol D using SEM are shown in Fig 4.96. These images clearly indicate that the formation of micro-scale hillocks on the surface due to etching of grain boundaries enhance surface roughness. Extent of roughness increases with the severity of the etchant, with maximum roughness being achieved with becks etchant. According to *Quin et al.* [73], one of the major constituent of Becks reagent is HCl which helps in revealing grain boundaries and polycrystalline microstructure of aluminium substrate, resulting in wider and deeper pits as compared to other etchants. Further,

hydrophobisation with HDTMS based sol-gel coatings resulted in superhydrophobicity with contact angles of about 130° . Also average coating thickness was measured using field emission scanning electron microscope (FE-SEM) and was found to be about 2 microns (Fig 4.97). Hence, chemical etching is one of the effective methods for introducing desired amount of surface roughness, which is the key factor combined with low surface energy responsible for developing superhydrophobic coatings

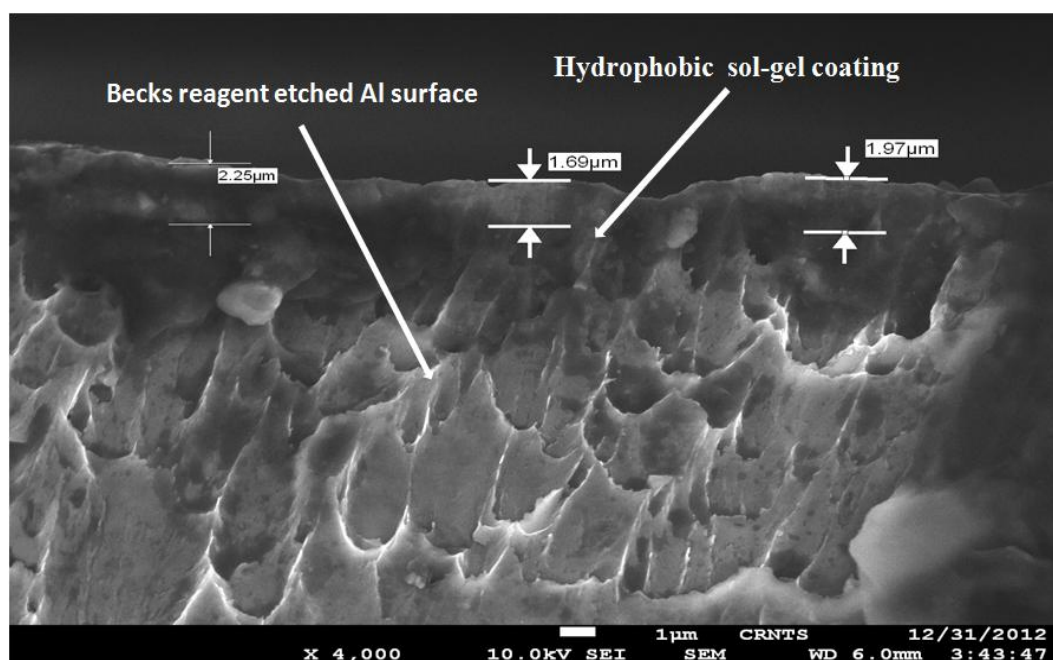


Figure 4.97: FE-SEM image of thickness of Sol gel coated (GPTMS: HDTMS: TEOS ratio 2:2:6) becks reagent etched aluminium sample

Atomic Force Microscopic (AFM) analysis was further carried on sol-gel coated un-etched and various etched specimens in the tapping mode to evaluate surface morphology of various specimens. Fig 4.98(c) shows the AFM topography of un-etched aluminium substrate followed by coating with sol D having small protruding nubs due to long chains of HDTMS on surface with root mean square roughness (RMS) value of about 5nm. The AFM images and RMS values of aluminium specimens, etched with various etchants, followed by application of formulation C and D are shown in Fig 4.98. The average RMS values of Krolls, 10% NaOH and Becks etched sol-gel coated samples were found to be 30nm, 60nm

and 120nm respectively for all the five formulations which is significantly high as compared to coated un-etched substrate. The surface of the films showed many dispersed islands that were distributed on the film surface with Becks etched sample, having maximum height of the protruding islands which supports high value of contact angle of 130° the low value of sliding angle of about 25° attributed to increased fraction of air entrapped below the roughness grooves leading to lowering of friction between the surface and water droplet. Hence the similar trend was observed from AFM analysis as from SEM studies, thereby indicating that chemical etching along with HDTMS modification is one of the effective approaches to obtain hydrophobic surface.

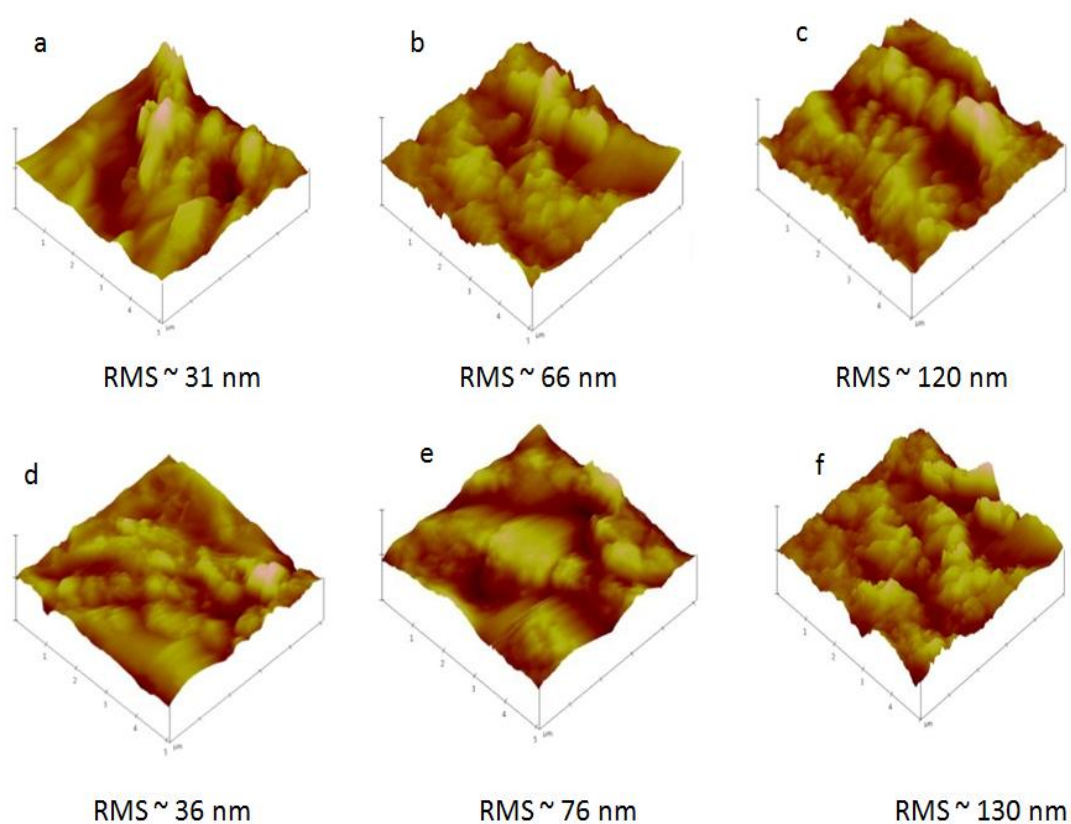


Figure 4.98: AFM images and RMS values of aluminium samples etched with a),d) Krolls reagent, b),e) 10% NaOH and c),d) Becks reagent followed by coating with sol-gel formulation having GPTMS:HDTMS:TEOS ratio 2:2:6 and ratio 1:3:6 respectively

Hence, eco-friendly hydrophobic sol-gel coatings were synthesised for aluminium substrates by non-fluoro approach, using long chain alkyl HDTMS, GPTMS and TEOS precursors.

Application of these coatings on smooth and clean aluminium substrates resulted in hydrophobic surface with contact angle of about 95° . Further, pre-treating the aluminium substrate, using various etchants, helped in enhancing the hydrophobicity substantially by creating suitable roughness of about 120 nm. This resulted in contact angle of about 130° . Hence, chemical etching, combined with HDTMS modification, resulted in an effective water repellent surface.

Chapter 5

General Discussion

The successful formation of a hydrophobic interface in the present work is believed to be the interplay between the presence of electronegative perfluoro groups which migrate towards the air/film interface to minimise the interfacial energy and the roughness of the sol-gel coating due to incorporation of nano-particles [87]. The surface tension of typical substituent end group decreases in the following order: CH_2 (36 dyn/cm) > CH_3 (30 dyn/cm) > CF_2 (23 dyn/cm) > CF_3 (15 dyn/cm). Therefore, $-\text{CF}_3$ groups are the ideal building blocks to develop hydrophobic coatings. However, the maximum contact angle that can be reached by coating fluorinated methyl groups onto a flat solid surface is only 110° [2]. In the present work firstly, FAS-3 and FAS17 were blended with GPTMS-MTMS based neat sol –gel. Further a short chain water based perfluoro polymer (FE) of six carbon atoms was used as hydrophobic precursors along with other two inorganic silane precursors viz. GPTMS and MTMS to form a primary sol. This primary sol was further crosslinked with organic resin HMMM to achieve three dimensional crosslinked inorganic-organic hybrid sol-gel coatings with enhanced low surface energy on etched aluminium substrate. Fig 5.1 shows the proposed reaction mechanism of the as developed fluorinated sol-gel coating using FE as co-precursor.

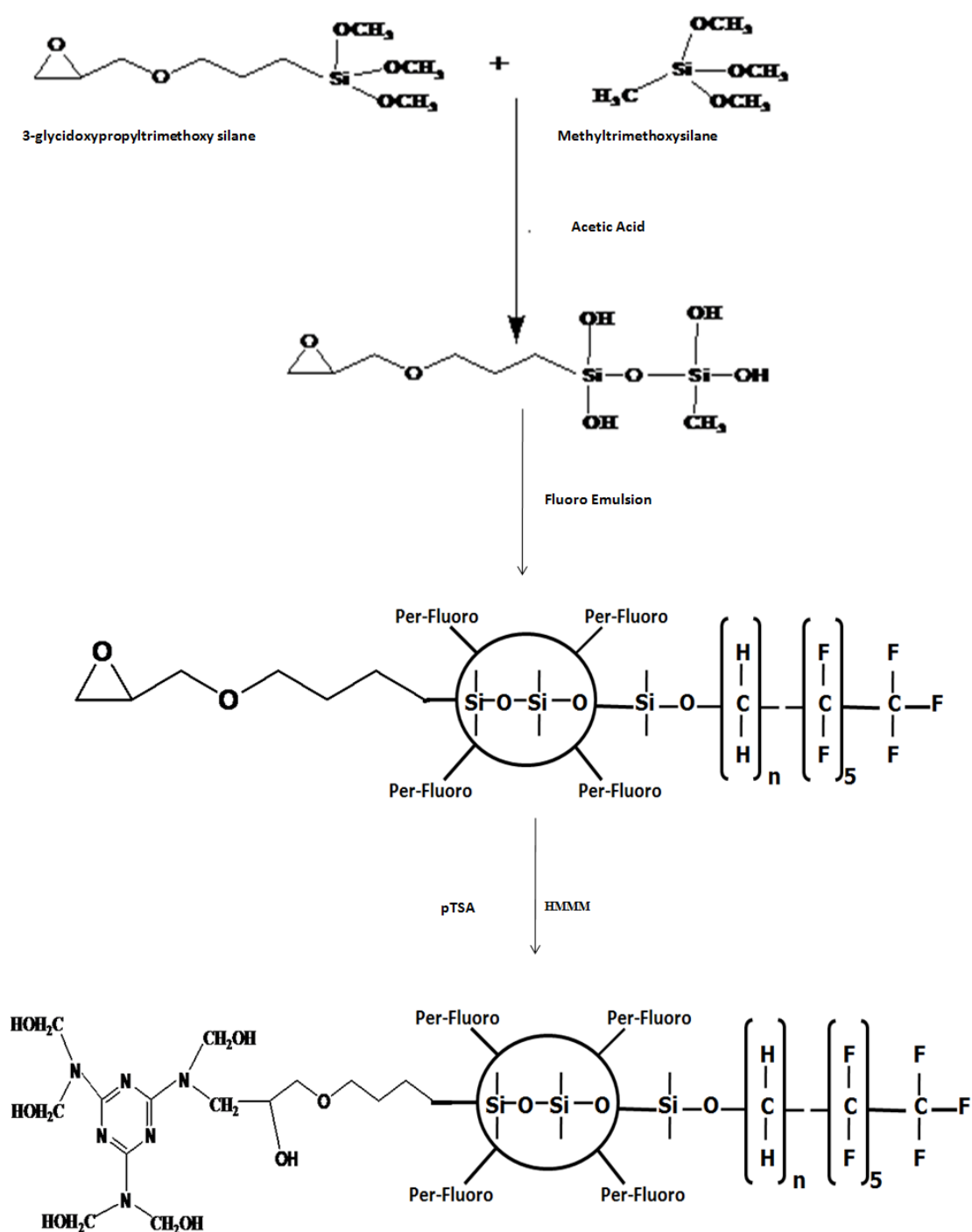


Figure 5.1: Probable reaction mechanism of as developed hydrophobic sol-gel coating

Hydrolysis of GPTMS and MTMS takes place in the presence of acetic acid initially, followed by subsequent condensation reactions with loss of water and alcohol as by product,

to form a sol-gel network with significant amount of Si-OH groups above and below the matrix, which contribute to strong adhesion to metal as well as enhance overall hydrophilic character [32, 33, 137, 138]. Addition of HMMM as cross linker opens the epoxy ring by simple nucleophilic substitution reaction on OH group, which further releases O-H groups, leading to both enhanced adhesion and hydrophilicity [32]. Hence, the initial primary sol-gel formulation had excellent hardness and adhesion but poor water repellency due to highly hydrophilic precursors (W.C.A. 70°). Further, perfluoro emulsion (FE) was used as co-precursor and added in various percentages to achieve enhanced hydrophobicity due to low surface tension end-groups. Modified coatings resulted in excellent water repellent properties with increased water contact angle of 118° , in accordance with the Wenzel's model i.e. the water droplets still stick to the surface when tilted with large angles (65°) [81, 82, 90, 139]. Further, various nano-particles were incorporated to fluorinated sol-gel system to enhance surface roughness resulting in sliding of water droplets. The wetting phenomena responsible for sticking or sliding of water droplets due to interfacial interactions between the liquid and solid in the presence of air is discussed as follows. The nature of the wetting interaction is defined by the balance between the cohesive forces within the liquid and solid and its adhesion to the surrounding environment as shown in Fig 5.2

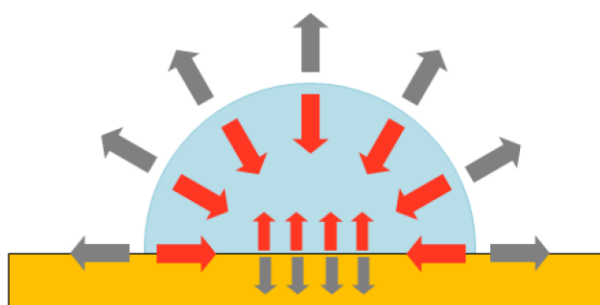


Figure 5.2: The shape of a liquid droplet resting on a surface (yellow) is governed by the balance between liquid cohesion (red arrows) and interfacial adhesion (grey arrows)

A fluid will wet and spread across the surface, if the adhesion between the liquid and the surface is greater than the cohesion within the liquid. Conversely, a droplet is formed if liquid cohesion exceeds adhesion to the surface. According to Young and Laplace, the wetting behaviour of a liquid droplet on a smooth homogeneous surface is described by the angle of contact it makes with the surface at the three phase contact point as shown in Fig 5.3.

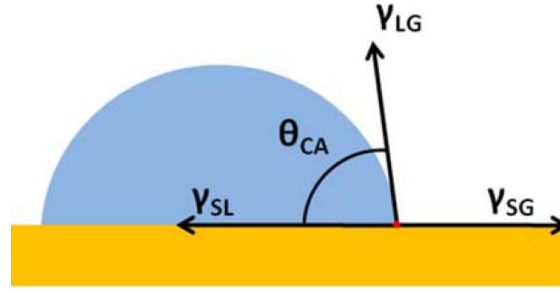


Figure 5.3: The contact angle of a droplet at the triple phase contact point (red dot)

The correlation between the surface roughness and contact angle was first examined by Wenzel. According to Wenzel, the increase in contact angle depends upon surface energy and surface roughness. With an increase in roughness, a higher intensity of surface energy is observed and thus a water droplet can occupy a smaller area to achieve the equilibrium interfacial energy as shown in Fig 5.4.

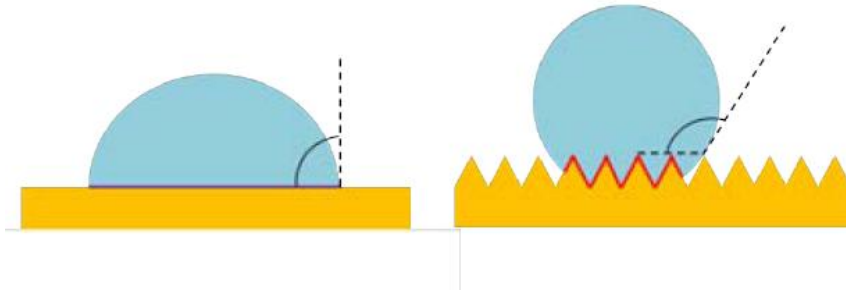


Figure 5.4: A droplet can occupy less geometric area on a surface with increased roughness

Therefore the measured contact angle (θ_{CA}) is proportional to the apparent contact angle ($\theta_{apparent}$) of a surface by a factor of roughness as shown in equation. It should be noted that Wenzel model assumes a completely wetted interface between the fluid and the surface.

$$\theta_{CA} = \frac{\text{actual roughness}}{\text{geometric roughness}} \theta_{apparent} \quad (5.1)$$

However, if chemical heterogeneity (such as air) is present at the liquid-solid interface, Wenzel and previous models are no longer valid. This unique de-wetted state was described

by Cassie and Baxter [10]. Cassie and Baxter demonstrated that, for a droplet resting on a porous surface without wetting it, a composite interface of air and solid is observed at the traditional liquid-solid interface as shown in Fig 5.5.

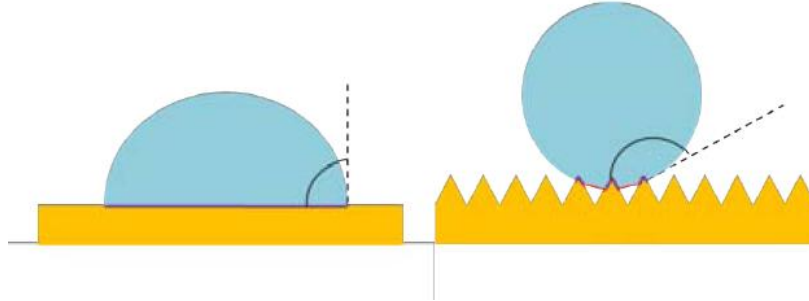


Figure 5.5: A water droplet resting on a composite interface resulting in increased contact angle due to the presence of entrapped air

The measured contact angle (θ_{CA}) of a liquid drop on a surface shown in equation is now the average of the contact angle of solid (θ_1) and air, weighted based on their respective fractional contact areas (f_1, f_2)

$$(\theta_{CA}) = f_1 \cos(\theta_1) + f_2 \cos(\theta_2) \quad (5.2)$$

According to the Cassie-Baxter model, a surface could theoretically be engineered to exhibit static contact angles approaching that of air (180°), the ultimate hydrophobe, by creating a roughness regime such that the water droplet makes minimal contact with the surface.

The hydrophobic modification in the present work is further discussed on the basis of Wenzel and Cassie models discussed above.

Fig 5.6 shows the surface morphology (SEM) and nano-particle distribution of various modified sol-gel systems. In the present system, modification of hydrophilic neat sol-gel (CA $\sim 70^\circ$, RMS ~ 3 nm) with FE as a co-precursor resulted in lowering of energy (CA $\sim 118^\circ$) and increase in surface roughness with RMS ~ 15 nm with craters of about 30 microns. Various nano-particles viz. nano-ZnO(30nm), HDTMS-fume silica(20nm), DDS-fume silica(15nm) and HMDZ(7nm) fume silica, were further incorporated to FE-modified sol-gel system to enhance surface roughness. As seen from SEM insets, as the nano-particle size decreases the distribution of nano-particles became more compact and distinguished. Nano-ZnO resulted in microspheres of about 10-20 μ m, HDTMS nanosilica particles resulted in sheet like structure, DDS-nanosilica particles resulted in further smaller and dense microspheres of

about 5nm. However, HMDZ nano-silica particles resulted in most compact and mono-dispersed morphology with nano-clusters (less than 1µm) resulting in micro-nano dual scale roughness. Hence, FE modification followed by HMDZ nano-particle incorporation resulted in desired hydrophobic sol-gel formulation.

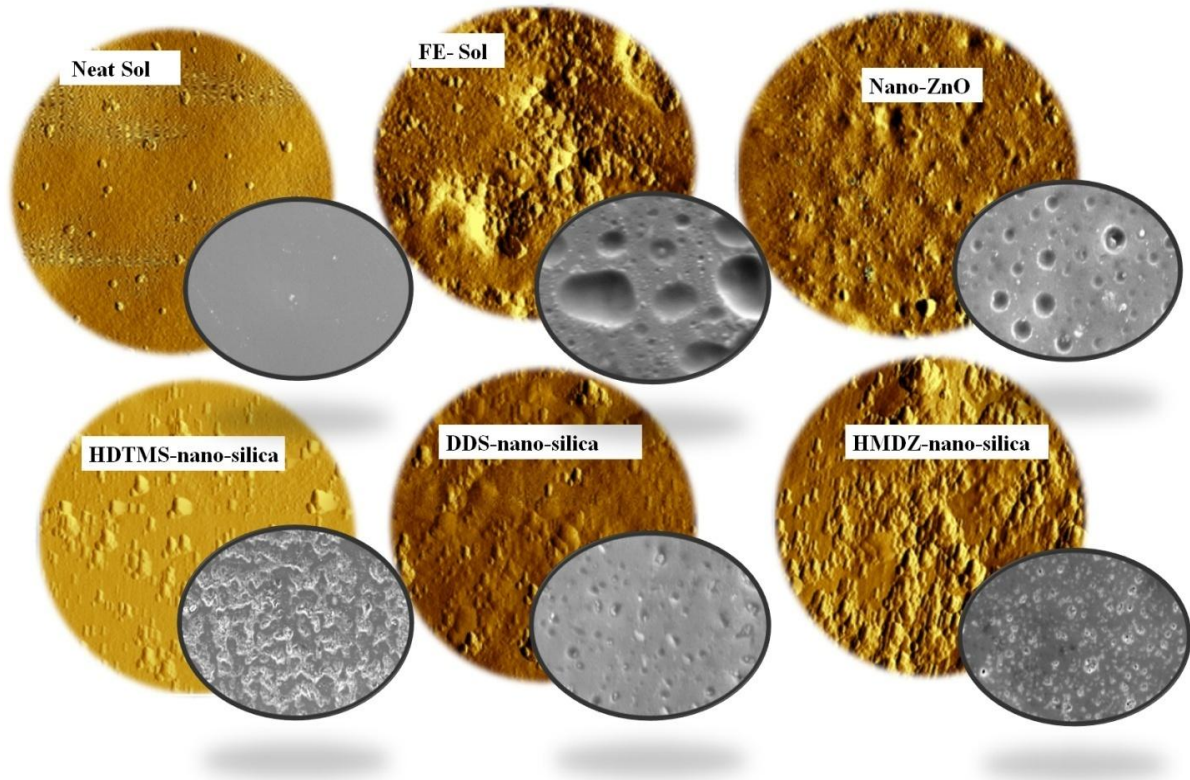


Figure 5.6: Surface morphology and nano-particle distribution of various sol-gel systems

For a better understanding of the wettability of the as developed hydrophobic HMDZ-FE composite sol-gel coating, the CA described in terms of the Wenzel equation can be considered,

$$\cos\theta_r = r\cos\theta_s \quad (5.3)$$

This equation is used to describe the WCA for a liquid droplet at a rough solid surface. Here, r is the roughness factor and θ_r and θ_s are the WCA values on a rough surface and smooth surface made of the same material respectively. In this regime, water is assumed to follow the

roughness of the underlying surface. Here, the actual water-solid contact area is much larger than the apparent contact area. Water drops on neat sol-gel showed a hydrophilic contact angle of about 70° and hydrophobic contact angles >90° for the various nano-composite sol-gel coatings. In case of HMDZ modification, the surface exhibited self-cleaning property with wca of 125°, and sliding angle of 25°. This is due to the transition from Wenzel regime to cassie regime. The roughness created on the surface due to small size of nano-HMDZ silica might be sufficient to trap air inside the voids of the surface. This causes a heterogeneous surface composed of both air and solid, which reduces the adhesive force between the water and solid surface. Contact angle in terms of Cassie-Baxter equation is described as,

$$\cos\theta_r = f(\cos\theta_s + 1) - 1 \quad (5.4)$$

Where θ_r and θ_s are the WCA of the roughened and smooth surfaces respectively. Here θ_s is 70° for neat sol-gel and θ_r are 120°, 118°, 122° and 125° for 2wt% nano-ZnO, 1wt% HDTMS nano-silica, 2wt% DDS nano-silica and 3wt% HMDZ nano-silica modification respectively. The area fraction f , of solid surface was calculated to be 0.37, 0.39, 0.35, and 0.31 for nano ZnO, HDTMS nano silica, DDS nano-silica and HMDZ nano silica respectively. This implies that HMDZ nano-silica modification resulted in exposure of water droplets to comparatively larger portion of air that offers a high resistance against wettability and hence favor the movement of water droplets resulting in low sliding angle of 25°. This can also be studied by considering the *work of adhesion* (W) on the surface. Work of adhesion basically estimates the ease with which the water drops move on the surface. The W for smooth coatings is given by the young-dupre's equation

$$\cos\theta = \frac{\gamma_{SA} - \gamma_{SL}}{\gamma_{LA}} = \frac{W}{\gamma_{LA}} - 1 \quad (5.5)$$

Where γ_{LA} is the liquid-air interfacial surface tension, which is 72.99 mN/m for water. W for the neat sol-gel coating was calculated to be 97.95 mN/m. Nano-modified composite coatings will have the water droplets partially sitting on the solid surface and hence W depends on the surface fraction (f) and in turn on the size of the nano-particle used. Equation (5.5) thus becomes

$$W = \gamma_{LA} f (1 + \cos\theta) \quad (5.6)$$

W, for the HMDZ-FE composite coating was calculated as 11.31mN/m. The decline of W from 97.95mN/m for neat sol-gel to 11.31mN/m for HMDZ-FE composite sol-gel coating indicates that the water droplets are partially suspended on a layer of air decreasing the interaction between the solid and liquid phases. Furthermore, mixed state can better explain the results because the contact angle of 125° achieved cannot be rationalised by the cassie-baxter scenario (in which a water droplet completely reside on a layer of air producing large contact angles) and small sliding angle of 25° which cannot be explained by wenzel scenario (in which water droplet gets stuck up within the roughness grooves and did not move even if tilted at 90° angle.). At higher concentrations of nano-silica particles extensive agglomeration results in smoothening of the topography. It is therefore quite possible that water does not penetrate the nano-cervices that exist on the surface of the protruding aggregates due to Laplace pressure or water may fill the large, smooth areas that exist among the aggregates. In summary it is speculated that large, smooth areas are filled with water (wenzel) but not the small nano-crevices that exist on the surface of the particle aggregates (Cassie). This is called mixed regime [59].

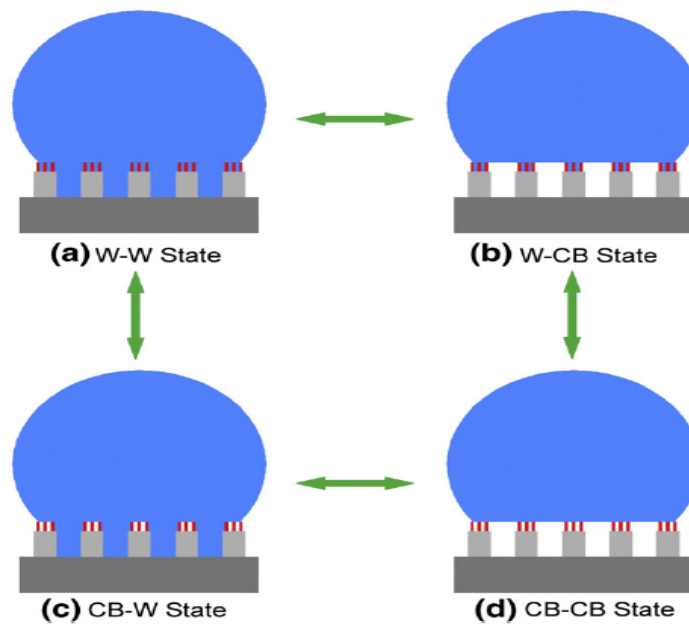


Figure 5.7: Transition between various mixed states on a rough surface [59]

Mixed state can be further explained on the basis of relation between contact angle and sliding angle on a rough surface. According to Wenzel state a water drop can have a high contact angle $> 150^\circ$, but simultaneously sliding angle would be high for a Wenzel state as the water penetrates the asperities. But in the present case, the sliding angle achieved is much lower i.e about 35° for Al substrate which indicates that the sol-gel composite films partially lay in Cassie –Baxter state. Fig 5.7 depicts transition of a water droplet within various mixed states on a rough surface. Hence, surface roughness plays an important role in desciding the hydrophobic state of the surface.

Further, the proposed distribution mechanism is explained which relates the size of the nano-particles and particle clusters with the physical properties of the as developed nano-composite coating Fig. 5.8 a,b shows the schematic illustration of distribution of nano-particles at a) lower and b) higher concentration of silica nano-particles in sol-gel matrix [44]. At low concentration nano-particles tend to distribute uniformly without effecting the Si-O-Si bond formation during curing as well as Si-O-M bond required for adhesion with substrate. At higher concentrations large agglomerates leads to low bonding of sol-gel network to the substrate thereby resulting in poor mechanical properties. Fig 5.8(c) shows a multi-scaled sol-gel coating with a low energy perfluoro film with small nanoclusters of fumed silica embedded on top of the protrusions and large agglomerates embedded inside the dense sol-gel matrix, giving rise to several peaks and cavities required for hydrophobicity. However, at higher concentrations the orientation of perfluoro-groups on the surface may be restricted, resulting in decrease in hydrophobicity.

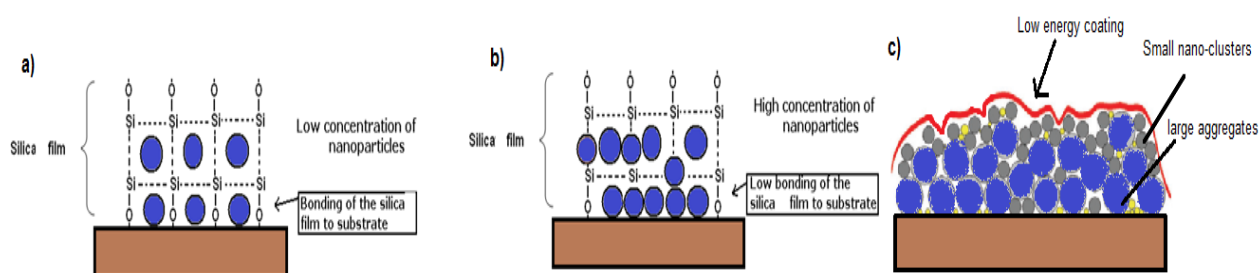


Figure 5.8 Distribution of nano-particles at a) low concentration, b) high concentration and c) fluoro-composite nano-coating at optimised concentration

The highest contact angle reported on Al in present work was saturated upto 125° which is not superhydrophobic. The major reason for this saturation is the high energy of the Al metal and hydrophilic surface –OH groups which remained unreacted. As majority of surface –OH groups comes from nucleophilic reaction of HMMM and epoxy ring of GPTMS, improvement in hydrophobicity can be expected if the epoxy sol-gel precursor was replaced by a low surface energy silane precursor [118]. Another reason for the saturation of contact angle could be that, at higher concentration of nano-particles, multi-layer nano-particle absorption cause larger part of the micro-cavity filled up with the particle aggregates and produce a smooth surface, leading to a decreased contact angle. Furthermore, when the nano-silica concentration became very high, the nano-particle surface would not be sufficiently covered with the sol-gel coating layer and restrict the effective amount of perfluoro-groups to migrate on the surface.

The distribution of per-fluoro groups on HMDZ nano-silica modified surface was further confirmed by EDX analysis which was carried out at different locations was on the HMDZ-FE composite sol-gel coated surface - in the flat region and on the bump. The results are shown in Fig 5.9. The flat region had fluorine count of 167 whereas fluorine count of 1207 was present on the bumps. The fact was confirmed by the EDX spectra shown in fig 5.9 c) and d). The flat region (point 2) showed less intense fluorine peak as compared to bump (point 1) respectively. The Si concentration was found to be nearly the same at both the areas. Thus it was evident that fluorine accumulation was more on the peak or aggregates of silica particles as compared to flat region. Hence, it can be inferred that FE had more affinity towards silica particles. A similar observation was also made by *Hsieh et al.* [125]. Thus EDX analysis confirmed that FE-adsorbed HMDZ-silica moieties were responsible for enhanced hydrophobicity of the coating at optimum concentration of 3wt%. However at higher percentages hydrophobicity decreases which can be attributed to the agglomeration of silica particles which inhibit the migration and enrichment of fluorine-containing segments towards the coating surface [47].

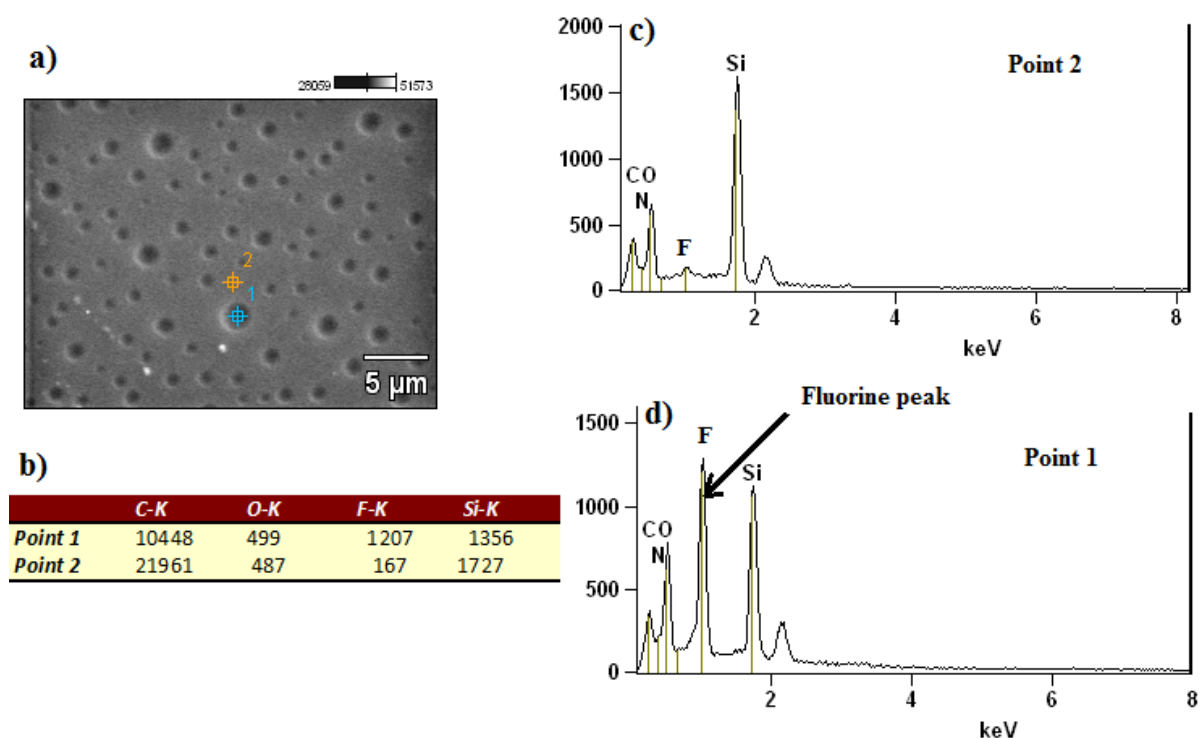


Figure 5.9: EDX analysis of HMDZ-FE composite coating at planner and bumpy surface

In order to qualitatively study the chemical bonding in FE-HMDZ composite coating, FTIR characterisation was done. The strong bands observed at $1100\text{--}1300\text{ cm}^{-1}$ indicate the presence of Si-O-Si moieties confirming the interaction of nano-silica particles. The peaks at around 470 and 870 cm^{-1} correspond to the symmetric stretching and bending modes of SiO_2 respectively. The peaks at 750 and 1276 cm^{-1} are due to Si-CH₃ groups. Finally, Decrease in the absorption peak intensity of -OH groups around 3800 cm^{-1} in case of FE-HMDZ composite sol-gel coating confirms the termination of hydrophilic -OH groups by perfluoro non-hydrolysable groups inducing the hydrophobic character. The hydrophobicity of the coatings was thus confirmed by the FTIR spectra.

Finally the proposed models were linked with the corrosion –preventive ability of the coating which depends upon three aspects: (1) the water sorption performance of the coating, (2) the transport of water in the coating and (3) the accessibility of the coating/surface interface to water. Since HMDZ-FE composite coatings showed low wettability, it is reasonable to assume that these coatings effectively prevent water from permeating the substrate and can exhibit superior corrosion resistance in wet environments. A schematic illustration of the

liquid-solid interface between an ideal superhydrophobic surface and the aqueous electrolyte solution is shown in Fig. 5.10, as reported by *Liu et al.* and *Ishizaki et al.* [109, 140] where the hydrophobic surface consists of peaks and valley surface profile allowing entrapment of air within these protrusions, resulting in reduced area of rough surface in contact with water. This results in preventing Cl^- ions coming in contact with the metal substrate resulting in enhanced corrosion resistance [141].

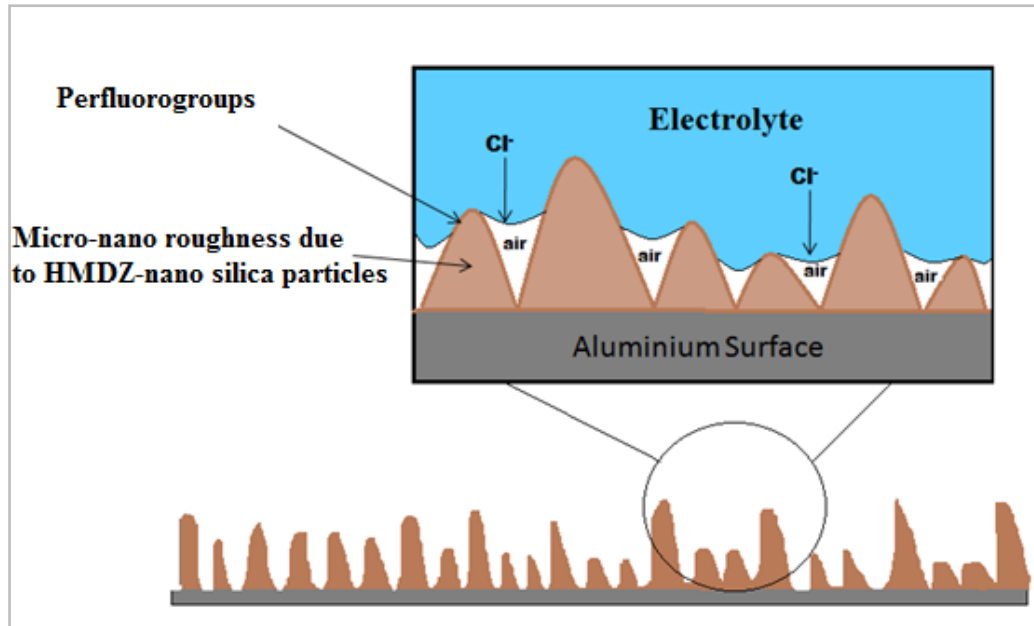


Figure 5.10: Proposed anti-corrosion mechanism of HMDZ-FE nano-composite sol-gel coating

As developed coatings consisted of similar kind of rough profile and could be well related to above-mentioned mechanism resulting in effective corrosion resistance due to obstructive effect of layer of air entrapped [109, 140] within several peaks and valleys attributed to combined effect of HMDZ-nanosilica clusters and protruding low energy perfluoro-groups which are largely accumulated on the micro-nano bumps. Another possible reason for superior corrosion resistant properties of such coatings could be dense, barrier network of epoxy-HMMM hybrid structure due to condensation of silanols with hydroxyls of opened epoxy ring resulting in strong adhesion with the aluminium metal oxide with hydrophobic perfluoro groups pointing outwards and hence making water molecules and Cl^- difficult to permeate [138, 142, 143].

Furthermore, hydrophobic *non-fluoro* thin films were developed using long chain HDTMS, GPTMS and TEOS as silane precursors over chemically etched aluminium surface. Presence of large number of polar Si–OH groups on the surface imparts hydrophilicity. Replacement of the H's from the Si–OH groups by the hydrolytically stable non hydrolysable Si–R (where, R = alkyl or aryl) groups, prevent the adsorption of water, resulting in the dehydroxylation of the film surface, leading to hydrophobicity [26]. Hence condensation reactions of TEOS and GPTMS followed by hydrophobisation with HDTMS layers of long chain alkyl groups imparting both hydrophobicity and roughness could be a possible sol-gel mechanism. In a similar work reported by *Mahadik et al.* [89], trimethylchlorosilane (TMCS) was used in the sol-gel processing to replace the –OH group by hydrolytically stable –O–Si–(CH₃)₃ groups, producing superhydrophobic films. Fig 5.11 shows the probable reaction of GPTMS, TEOS and HDTMS that may result in grafting of surface Si–OH groups with non polar Si–(C₁₆H₃₂) groups of HDTMS forming a non-hydrolysable and hence hydrophobic layer on the surface with C.A. >90 [10]. Sol D with GPTMS: HDTMS: TEOS ratio of 2:2:6 was found to have optimum hydrophobicity with C.A. of 95° on un-etched aluminium sample with gel time of 15 days. At higher concentrations, long chain structure of HDTMS may contribute to the decrease in the reaction rate due to steric hindrance, leading to poor adhesion and other mechanical properties [144].

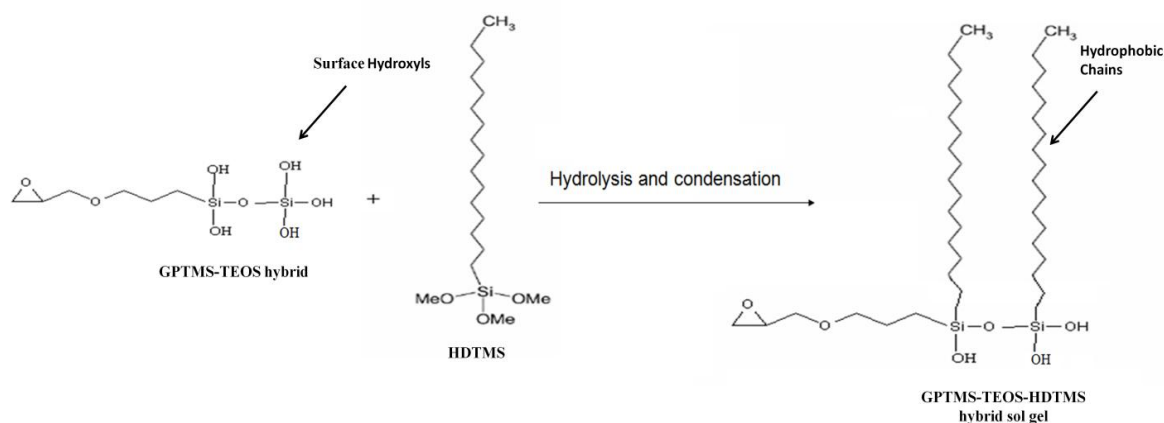


Figure 5.11: Probable mechanism of reaction of GPTMS, TEOS and HDTMS

Moreover, the extent of hydrophobicity was found to increase with enhanced surface roughness of the Al metal. It is well known that contact angles of long chain hydrocarbon

and fluorocarbon self-assembled mono-layers generally do not exceed 112° and 115° respectively on smooth hydrophobic surface. However, the situation is quite different when the surface is rough. The effect of chemical etching with various etchants prior to coating application, resulted in enhanced roughness. It was observed that surface roughness increases with severity of the etchant with maximum contact angle achieved for Becks reagent of about 130° and RMS of about 100 nm. According to *Qu et al.*[73], etching of aluminium revealed grain boundaries, cavities and island structures. Such a rough surface plays an essential role in trapping air between the substrate surface and the liquid droplets, leading to lowering of forces of friction and hence enhancing the hydrophobic and sliding behavior of the water droplets. Other techniques such as sand blasting, spraying and plasma etching also resulted in substantial increase in micron scale roughness and contact angle of about 130°

It has also been established that the height and width of the textures, as well as the distance between textures, are determining factors to achieve a Cassie–Baxter state [86]. It is also evident that the size and shape of textures created have a significant impact on the resulting wetting properties [132]. Hence, the as developed coatings were further applied on various non-metallic substrates like cotton, wood, paper, concrete, cardboard, glass etc with varying height, width, and spacing of the textures. Therefore, application of HMDZ-FE composite coating on various substrates with inherited roughness resulted in thin transparent superhydrophobic films with contact angles of about 140° and sliding angles of about 5° .

Therefore, it can be said that in present work, various hydrophobic sol-gel systems were developed on aluminium surface, the maximum contact angle achieved lied between 120 - 125° only. Further extending the application of as developed hydrophobic coatings on other rough substrates, superhydrophobicity was achieved with contact angle of about 140 - 145° and sliding angle of about 5° indicating that the Cassie regime was completely resumed. Hence, a detailed study on development of superhydrophobic sol-gel coatings on non-metallic substrates lays down the future aspects of research work.

Chapter 6

Conclusion

The research presented in this dissertation was undertaken to fabricate hydrophobic inorganic-organic coatings on aluminium alloy using water based sol-gel technique. The coatings were based upon epoxy silane GPTMS and MTMS as starting precursors, crosslinked with HMMM polymer. In order to introduce hydrophobicity, low energy fluoro-alkylsilanes and fluoro polymers were incorporated to the hydrophilic neat sol-gel followed by addition of various nano-particles. As developed coatings were subjected to various characterisation techniques viz. contact angle and sliding angle analysis; SEM, AFM, FTIR and XPS analysis; polarisation and EIS analysis; nano-indentation and scratch resistance analysis. Results further highlight the importance of distribution mechanism of nano-particles in achieving hydrophobic properties and establishing subsequent relation to Wenzel, Cassie and intermediate states. Further, non-fluoro sol-gel coatings were also developed on in order to obtain non-toxic fluorine free coatings.

Following are the summarised results:

1. GPTMS-MTMS-HMMM based sol-gel coating was deposited on aluminium surface and designated as neat sol-gel. The neat sol gel coated Al surface exhibited contact angle of about 70-75° with RMS value of 3nm
2. The neat sol-gel was hydrophobically modified with fluoro silanes of three and seventeen fluorine atoms followed by addition of commercial fluoro emulsion (FE). The 30wt% FE modified sol-gel system resulted in maximum improvement in hydrophobicity out of all with contact angle of 118° and sliding angle of 70°. The surface roughness achieved in this case was about 37nm.
3. FE modified sol gel coatings when applied on various rough aluminium surfaces using techniques like sand blasting, plasma etching and chemical etching resulted in extremely high roughness >100nm and contact angle of about 130°. Though the

contact angle achieved was high, the state of hydrophobicity resumed was completely Wenzel.

4. Incorporation of nano-ZnO in FE modified sol-gel resulted in surface roughness of 105nm and this resulted in marginal increase in hydrophobicity due to hydrophilic nature of nano-ZnO particles. The contact angle achieved was 120° with sliding angle of 65°. Further modification was achieved by using various functionally modified nano-silica particles out of which hexamethyldisilazane (HMDZ) nano-silica particles resulted in maximum surface roughness of 95nm with contact angle of 125° and sliding angle of 25°. Hence, HMDZ-FE composite sol-gel coatings were realised as finally formulated hydrophobic coatings for Al metal in present study. These coatings resulted in improved corrosion resistance with current density lower in 4 orders of magnitude as compared to bare substrate and improved mechanical properties.
5. HMDZ-FE sol-gel coatings when applied on non-metallic substrates viz. cotton, wood, paper, concrete and cardboard, resulted in superhydrophobicity with contact angle >135° and sliding angle <5°.
6. HMDZ-FE composite sol-gel coating lays in mixed state where both Wenzel and Cassie Baxter regimes were partially resumed and a suitable mechanism was proposed for nano-particle distribution.
7. At last, HDTMS based non-fluoro sol-gel coatings were obtained on differentially etched Al surface resulting in contact angle of 130° for becks reagent etched surface.

Hence it can be concluded that in present work, as developed coatings successfully resulted in hydrophobicity on aluminium metal and are capable of resulting superhydrophobicity on porous and textured surfaces. This lays down the future aspects of the present research work.

List of Publications

1. Ruchi Grover Wankhede, Shantaram Morey, A.S. Khanna and N. Birbilis, “Development of water-repellent organic–inorganic hybrid sol–gel coatings on aluminium using short chain perfluoro polymer emulsion”, *Applied Surface Science* 283 (2013) 1051– 1059
2. Ruchi Grover Wankhede, Shantaram, Karan Thanawala, Anand Khanna and Nick Birbillis, “ Development of Hydrophobic Non-Fluorine Sol-Gel Coatings on Aluminium Using Long Chain Alkyl Silane Precursor”, *Journal of Materials Science and Engineering A* 3 (4) (2013) 224-231
3. Ruchi Grover Wankhede, N. Birbillis, A.S.Khanna, poster and oral presentation on “Development of hydrophobic inorganic-organic waterborne coatings on aluminium via sol-gel route” at Gordon Research Conference on Corrosion-Aqueous held July, 2012, NH United States.
4. Ruchi Grover Wankhede, N. Birbillis, A.S.Khanna, oral presentation on "Development of ultra-hydrophobic non- fluorine sol-gel films on aluminium alloy” in 33rd Australasian Polymer Symposium at Hobart, Australia. This paper was published in the 33rd Australasian Polymer Symposium proceedings, ISBN number: 978-0-646-57205-5
5. Ruchi Grover Wankhede, Karan Thanawala, Anand Khanna and Nick Birbillis, poster presentation on “Nano-modified self cleaning sol-gel coatings”, in FAPS-Macro 2013, Bangalore, India. The extended abstract was published in conference proceeding under section Blends and composite page no. 20
6. Published article, “Superhydrophillic coatings: The next generation approach”, *Chemical World* (2010)
7. Published article, “Floor coatings: Protective to the core”, *Chemical World* (2008)

References

1. Scardino, A., et al., *Microtopography and antifouling properties of the shell surface of the bivalve molluscs mytilus galloprovincialis and pinctada imbricata*. Biofouling, 2003. **19**(sup1): p. 221-230.
2. Nakajima, A., K. Hashimoto, and T. Watanabe, *Recent Studies on Super-Hydrophobic Films*. Monatshefte für Chemie / Chemical Monthly, 2001. **132**(1): p. 31-41.
3. Kulinich, S.A. and M. Farzaneh, *Effect of contact angle hysteresis on water droplet evaporation from super-hydrophobic surfaces*. Applied Surface Science, 2009. **255**(7): p. 4056-4060.
4. Yue-Kun Lai, Z.C., and Chang-Jian Lin, *Recent Progress on the Superhydrophobic Surfaces with Special Adhesion: From Natural to Biomimetic to Functional*. Journal of Nanoengineering and Nanomanufacturing, 2011. **1**: p. 18-34.
5. Jafari, R. and M. Farzaneh, *Fabrication of superhydrophobic nanostructured surface on aluminium alloy*. Applied Physics A, 2011. **102**(1): p. 195-199.
6. Chao-Hua, X., et al., *UV-durable superhydrophobic textiles with UV-shielding properties by coating fibers with ZnO/SiO₂ core/shell particles*. Nanotechnology, 2011. **22**(41): p. 415603.
7. Jafari, R., R. Menini, and M. Farzaneh, *Superhydrophobic and icephobic surfaces prepared by RF-sputtered polytetrafluoroethylene coatings*. Applied Surface Science, 2010. **257**(5): p. 1540-1543.
8. Ma, M. and R.M. Hill, *Superhydrophobic surfaces*. Current Opinion in Colloid & Interface Science, 2006. **11**(4): p. 193-202.
9. Zhang, X., et al., *Superhydrophobic surfaces: from structural control to functional application*. Journal of Materials Chemistry, 2008. **18**(6): p. 621-633.
10. Li, X.-M., D. Reinhoudt, and M. Crego-Calama, *What do we need for a superhydrophobic surface? A review on the recent progress in the preparation of superhydrophobic surfaces*. Chemical Society Reviews, 2007. **36**(8): p. 1350-1368.
11. Xue, C.-H., et al., *Large-area fabrication of superhydrophobic surfaces for practical applications: an overview*. Science and Technology of Advanced Materials, 2010. **11**(3): p. 033002.
12. Bahners, T., et al., *Recent approaches to highly hydrophobic textile surfaces*. Journal of Adhesion Science and Technology, 2008. **22**(3-4): p. 285-309.
13. Yin, B., et al., *Preparation and properties of super-hydrophobic coating on magnesium alloy*. Applied Surface Science, 2010. **257**(5): p. 1666-1671.
14. Balu, B., V. Breedveld, and D.W. Hess, *Fabrication of "Roll-off" and "Sticky" Superhydrophobic Cellulose Surfaces via Plasma Processing*. Langmuir, 2008. **24**(9): p. 4785-4790.
15. Pathak, A.K.a., *Advances in Sol-gel hybrid Membrane & Materials*.
16. Coclite, A.M., Y. Shi, and K.K. Gleason, *Super-Hydrophobic and Oleophobic Crystalline Coatings by Initiated Chemical Vapor Deposition*. Physics Procedia, 2013. **46**(0): p. 56-61.
17. Chen, T., M.-S. Chiu, and C.-N. Weng, *Derivation of the generalised Young-Laplace equation of curved interfaces in nanoscaled solids*. Journal of Applied Physics, 2006. **100**(7): p. 074308-074308-5.

18. Nosonovsky, M. and B. Bhushan, *Superhydrophobic surfaces and emerging applications: Non-adhesion, energy, green engineering*. Current Opinion in Colloid & Interface Science, 2009. **14**(4): p. 270-280.
19. Cassie, A.B.D., *Contact angles*. Discussions of the Faraday Society, 1948. **3**(0): p. 11-16.
20. Johnston, E., et al., *Networks from α,ω -Dihydroxypoly(dimethylsiloxane) and (Tridecafluoro-1,1,2,2-tetrahydrooctyl)triethoxysilane: Surface Microstructures and Surface Characterization*. Macromolecules, 1999. **32**(24): p. 8173-8182.
21. Miwa, M., et al., *Effects of the Surface Roughness on Sliding Angles of Water Droplets on Superhydrophobic Surfaces*. Langmuir, 2000. **16**(13): p. 5754-5760.
22. Mahadik, S.A., et al., *Transparent Superhydrophobic silica coatings on glass by sol-gel method*. Applied Surface Science, 2010. **257**(2): p. 333-339.
23. Ji, H., et al., *Hydrophobic fluorinated carbon coatings on silicate glaze and aluminium*. Thin Solid Films, 2002. **405**(1-2): p. 104-108.
24. Monde, T., et al., *Preparation and surface properties of silica-gel coating films containing branched-polyfluoroalkylsilane*. Journal of Non-Crystalline Solids, 1999. **246**(1-2): p. 54-64.
25. Valtola, L., et al., *Tailored surface properties of semi-fluorinated block copolymers by electrospinning*. Polymer, 2009. **50**(14): p. 3103-3110.
26. Venkateswara Rao, A., et al., *Preparation of MTMS based transparent superhydrophobic silica films by sol-gel method*. Journal of Colloid and Interface Science, 2009. **332**(2): p. 484-490.
27. Xu, X., Z. Zhang, and W. Liu, *Fabrication of superhydrophobic surfaces with perfluorooctanoic acid modified TiO₂/polystyrene nanocomposites coating*. Colloids and Surfaces A: Physicochemical and Engineering Aspects, 2009. **341**(1-3): p. 21-26.
28. Schultz, M.P., C.J. Kavanagh, and G.W. Swain, *Hydrodynamic forces on barnacles: Implications on detachment from fouling-release surfaces*. Biofouling, 1999. **13**(4): p. 323-335.
29. Bormashenko, E., et al., *Wetting Properties of the Multiscaled Nanostructured Polymer and Metallic Superhydrophobic Surfaces*. Langmuir, 2006. **22**(24): p. 9982-9985.
30. Pathak, S.S., A. Sharma, and A.S. Khanna, *Value addition to waterborne polyurethane resin by silicone modification for developing high performance coating on aluminum alloy*. Progress in Organic Coatings, 2009. **65**(2): p. 206-216.
31. Pathak, S.S. and A.S. Khanna, *Synthesis and performance evaluation of environmentally compliant epoxysilane coatings for aluminum alloy*. Progress in Organic Coatings, 2008. **62**(4): p. 409-416.
32. Pathak, S.S., A.S. Khanna, and T.J.M. Sinha, *HMMM cured corrosion resistance waterborne ormosil coating for aluminum alloy*. Progress in Organic Coatings, 2007. **60**(3): p. 211-218.
33. Pathak, S.S. and A.S. Khanna, *Investigation of anti-corrosion behavior of waterborne organosilane-polyester coatings for AA6011 aluminum alloy*. Progress in Organic Coatings, 2009. **65**(2): p. 288-294.
34. Daoud, W.A., J.H. Xin, and X. Tao, *Superhydrophobic Silica Nanocomposite Coating by a Low-Temperature Process*. Journal of the American Ceramic Society, 2004. **87**(9): p. 1782-1784.
35. Hoefnagels, H.F., et al., *Biomimetic Superhydrophobic and Highly Oleophobic Cotton Textiles*. Langmuir, 2007. **23**(26): p. 13158-13163.

36. Xu, L., et al., *Superhydrophobic cotton fabrics prepared by one-step water-based sol-gel coating*. Journal of The Textile Institute, 2011. **103**(3): p. 311-319.
37. Gao, Q., et al., *Formation of Highly Hydrophobic Surfaces on Cotton and Polyester Fabrics Using Silica Sol Nanoparticles and Nonfluorinated Alkylsilane*. Industrial & Engineering Chemistry Research, 2009. **48**(22): p. 9797-9803.
38. Li, Z., Y. Xing, and J. Dai, *Superhydrophobic surfaces prepared from water glass and non-fluorinated alkylsilane on cotton substrates*. Applied Surface Science, 2008. **254**(7): p. 2131-2135.
39. Bae, G.Y., et al., *Superhydrophobicity of cotton fabrics treated with silica nanoparticles and water-repellent agent*. Journal of Colloid and Interface Science, 2009. **337**(1): p. 170-175.
40. Lathe, S.S., et al., *Superhydrophobic silica films by sol-gel co-precursor method*. Applied Surface Science, 2009. **256**(1): p. 217-222.
41. Wang, H., et al., *One-step coating of fluoro-containing silica nanoparticles for universal generation of surface superhydrophobicity*. Chemical Communications, 2008(7): p. 877-879.
42. iop, large scale.
43. Yang, S.H., et al., *Preparation of super-hydrophobic films using pulsed hexafluorobenzene plasma*. Surface and Coatings Technology, 2009. **203**(10-11): p. 1379-1383.
44. Bravo, J., et al., *Transparent Superhydrophobic Films Based on Silica Nanoparticles*. Langmuir, 2007. **23**(13): p. 7293-7298.
45. Xu, W., et al., *Fabrication of Superhydrophobic Surfaces with Hierarchical Structure through a Solution-Immersion Process on Copper and Galvanized Iron Substrates*. Langmuir, 2008. **24**(19): p. 10895-10900.
46. Sheen, Y.-C., et al., *New approach to fabricate an extremely super-amphiphobic surface based on fluorinated silica nanoparticles*. Journal of Polymer Science Part B: Polymer Physics, 2008. **46**(18): p. 1984-1990.
47. Lakshmi, R.V., et al., *Fabrication of superhydrophobic and oleophobic sol-gel nanocomposite coating*. Surface and Coatings Technology, 2012. **206**(19-20): p. 3888-3894.
48. Yonghao Xiu , D.W.H.C.P.W., *UV-Resistant and Superhydrophobic Self-Cleaning Surfaces Using Sol-Gel Processes*. Journal of Adhesion Science and Technology, 2008. **22**(15): p. 1907-1917.
49. Brassard, J.-D., D.K. Sarkar, and J. Perron, *Fluorine Based Superhydrophobic Coatings*. Applied Sciences, 2012. **2**(2): p. 453-464.
50. Kulinich, S.A. and M. Farzaneh, *Alkylsilane self-assembled monolayers: modeling their wetting characteristics*. Applied Surface Science, 2004. **230**(1-4): p. 232-240.
51. Sheen, Y.-C., et al., *Non-fluorinated superamphiphobic surfaces through sol-gel processing of methyltriethoxysilane and tetraethoxysilane*. Materials Chemistry and Physics, 2009. **114**(1): p. 63-68.
52. Daoud, W.A., J.H. Xin, and X. Tao, *Synthesis and characterization of hydrophobic silica nanocomposites*. Applied Surface Science, 2006. **252**(15): p. 5368-5371.
53. Sanjay S Lathe, H.H.a.V.R., *TEOS based water repellent silica films obtained by a co-precursor sol-gel method* Journal of Smart Material and Structures, 2009 **18**: p. 05017.
54. Textor, T. and B. Mahltig, *A sol-gel based surface treatment for preparation of water repellent antistatic textiles*. Applied Surface Science, 2010. **256**(6): p. 1668-1674.

55. Bergbreiter, D.E. and K.-S. Liao, *Covalent layer-by-layer assembly—an effective, forgiving way to construct functional robust ultrathin films and nanocomposites*. Soft Matter, 2009. **5**(1): p. 23-28.
56. Ming, W., et al., *Superhydrophobic Films from Raspberry-like Particles*. Nano Letters, 2005. **5**(11): p. 2298-2301.
57. Roach, P., N.J. Shirtcliffe, and M.I. Newton, *Progress in superhydrophobic surface development*. Soft Matter, 2008. **4**(2): p. 224-240.
58. Steele, A., I. Bayer, and E. Loth, *Inherently Superoleophobic Nanocomposite Coatings by Spray Atomization*. Nano Letters, 2008. **9**(1): p. 501-505.
59. Manoudis, P.N., et al., *Superhydrophobic Composite Films Produced on Various Substrates*. Langmuir, 2008. **24**(19): p. 11225-11232.
60. Kamps, S., et al., *Processes and structures for generation of hydrophobic surfaces for large-scale and industrial operations*. Applied Surface Science, 2009. **256**(3, Supplement): p. S92-S95.
61. Xue, L., et al., *Super-hydrophobicity of silica nanoparticles modified with vinyl groups*. Colloids and Surfaces A: Physicochemical and Engineering Aspects, 2009. **338**(1-3): p. 15-19.
62. Dhoke, S.K., N. Rajgopalan, and A.S. Khanna, *Effect of Nanoalumina on the Electrochemical and Mechanical Properties of Waterborne Polyurethane Composite Coatings*. Journal of Nanoparticles, 2013. **2013**: p. 11.
63. Dhoke, S.K., A.S. Khanna, and T.J.M. Sinha, *“Effect of nano-ZnO particles on the corrosion behavior of alkyd-based waterborne coatings”*. Progress in Organic Coatings, 2009. **64**(4): p. 371-382.
64. Dhoke, S.K. and A.S. Khanna, *Electrochemical behavior of nano-iron oxide modified alkyd based waterborne coatings*. Materials Chemistry and Physics, 2009. **117**(2-3): p. 550-556.
65. Xu, Y., et al., *Comparative study on hydrophobic anti-reflective films from three kinds of methyl-modified silica sols*. Journal of Non-Crystalline Solids, 2005. **351**(3): p. 258-266.
66. Jeevajothi, K., R. Subasri, and K.R.C. Soma Raju, *Transparent, non-fluorinated, hydrophobic silica coatings with improved mechanical properties*. Ceramics International, 2013. **39**(2): p. 2111-2116.
67. R. Jafari, M.F., *A Simple Method to Create Superhydrophobic Aluminium Surfaces*. Material Science Forum, 2012. **706-709**: p. 2874-2879.
68. Gao, N., et al., *Superhydrophobic Composite Films Based on THS and Nanoparticles*. Journal of Bionic Engineering, 2010. **7**, **Supplement**(0): p. S59-S66.
69. Basu, B.J. and V.D. Kumar, *Fabrication of superhydrophobic nanocomposite coatings using polytetrafluoroethylene and silica nanoparticles*. ISRN Nanotechnology. **2011**.
70. Schem, M., et al., *CeO₂-filled sol-gel coatings for corrosion protection of AA2024-T3 aluminium alloy*. Corrosion Science, 2009. **51**(10): p. 2304-2315.
71. Bharathibai J. Basu , V.H., S. T. Aruna ,R. V. Lakshmi ,J. Manasa and B. S. Shruthi, *Effect of microstructure and surface roughness on the wettability of superhydrophobic sol-gel nanocomposite coatings*. Journal of Sol-Gel Science and Technology 2010. **56**: p. 278-286.
72. Xu, Y., et al., *Antireflective silica thin films with super water repellence via a solgel process*. Applied Optics, 2003. **42**(1): p. 108-112.

73. Qu, M., et al., *Fabrication of Superhydrophobic Surfaces on Engineering Materials by a Solution-Immersion Process*. Advanced Functional Materials, 2007. **17**(4): p. 593-596.
74. Qian, B. and Z. Shen, *Fabrication of Superhydrophobic Surfaces by Dislocation-Selective Chemical Etching on Aluminum, Copper, and Zinc Substrates*. Langmuir, 2005. **21**(20): p. 9007-9009.
75. Fukuda, K.T., J.; Nobunaga, T.; Iwasaki, T.; Kunitake Y. J. , *Nature -inspired superhydrophobic surfaces*, in *Soci. Naval Architects Japan* 1999: Japan.
76. Barkhudarov, P.M., et al., *Corrosion inhibition using superhydrophobic films*. Corrosion Science, 2008. **50**(3): p. 897-902.
77. Fir, M., et al., *Corrosion Studies and Interfacial Bonding of Urea/Poly(dimethylsiloxane) Sol/Gel Hydrophobic Coatings on AA 2024 Aluminum Alloy*. Langmuir, 2007. **23**(10): p. 5505-5514.
78. He, T., et al., *Super-hydrophobic surface treatment as corrosion protection for aluminum in seawater*. Corrosion Science, 2009. **51**(8): p. 1757-1761.
79. Sheffer, M., A. Groysman, and D. Mandler, *Electrodeposition of sol–gel films on Al for corrosion protection*. Corrosion Science, 2003. **45**(12): p. 2893-2904.
80. Xu, Q.F. and J.N. Wang, *A superhydrophobic coating on aluminium foil with an anti-corrosive property*. New Journal of Chemistry, 2009. **33**(4): p. 734-738.
81. Liu, L., et al., *Fabrication of superhydrophobic surface by hierarchical growth of lotus-leaf-like boehmite on foil*. Journal of Colloid and Interface Science, 2011. **358**(1): p. 277-283.
82. Wang, F., et al., *Preparation of Superhydrophobic Polymeric Film on Aluminum Plates by Electrochemical Polymerization*. Molecules, 2009. **14**(11): p. 4737-4746.
83. Wang, Q., et al., *Fabrication of superhydrophobic surfaces on engineering material surfaces with stearic acid*. Applied Surface Science, 2008. **254**(7): p. 2009-2012.
84. Wang, H., et al., *Fabrication and anti-frosting performance of super hydrophobic coating based on modified nano-sized calcium carbonate and ordinary polyacrylate*. Applied Surface Science, 2007. **253**(22): p. 8818-8824.
85. Musante, L., et al., *Synthesis and Characterization of New Organic–Inorganic Hybrid Nanosilica Fillers Prepared by Sol–Gel Reaction*. Composite Interfaces, 2010. **17**(5-7): p. 467-479.
86. Masashi Miwa , A.N., Akira Fujishima , Kazuhito Hashimoto , and Toshiya Watanabe *Effect of the Surface Roughness on Sliding Angles of Water Droplets on Superhydrophobic Surfaces*. Langmuir, 2000. **16**(13): p. 5754-5760.
87. Zheng, S. and J. Li, *Inorganic–organic sol gel hybrid coatings for corrosion protection of metals*. Journal of Sol-Gel Science and Technology, 2010. **54**(2): p. 174-187.
88. Akram Raza, M., et al., *Superhydrophobic Surfaces by Anomalous Fluoroalkylsilane Self-Assembly on Silica Nanosphere Arrays*. Langmuir, 2010. **26**(15): p. 12962-12972.
89. V.G. Paralea, D.B.M., S.A.Mahadika, M.S.Kavalea, P.B.Waghb, SatishC.Guptab, A. VenkateswaraRaoa, *OTES modifiedtransparentdipcoatedsilicacoatings*. Journal of Ceramics International, 2012.
90. Brassard, J.-D., D.K. Sarkar, and J. Perron, *Synthesis of Monodisperse Fluorinated Silica Nanoparticles and Their Superhydrophobic Thin Films*. ACS Applied Materials & Interfaces, 2011. **3**(9): p. 3583-3588.

91. Wu, L.Y.L., A.M. Soutar, and X.T. Zeng, *Increasing hydrophobicity of sol–gel hard coatings by chemical and morphological modifications*. Surface and Coatings Technology, 2005. **198**(1–3): p. 420-424.
92. Guo, Z., et al., *Effects of system parameters on making aluminum alloy lotus*. Journal of Colloid and Interface Science, 2006. **303**(1): p. 298-305.
93. Weng, C.-J., et al., *Corrosion resistance conferred by superhydrophobic fluorinated polyacrylate–silica composite coatings on cold-rolled steel*. Journal of Applied Polymer Science, 2012. **126**(S2): p. E48-E55.
94. Liu, W., et al., *Fabrication of the superhydrophobic surface on aluminum alloy by anodizing and polymeric coating*. Applied Surface Science, 2013. **264**(0): p. 872-878.
95. Yuan, S., et al., *Superhydrophobic fluoropolymer-modified copper surface via surface graft polymerisation for corrosion protection*. Corrosion Science, 2011. **53**(9): p. 2738-2747.
96. Conde, A., A. Durán, and J.J. de Damborenea, *Polymeric sol–gel coatings as protective layers of aluminium alloys*. Progress in Organic Coatings, 2003. **46**(4): p. 288-296.
97. Liu, H., et al., *Preparation of Superhydrophobic Coatings on Zinc as Effective Corrosion Barriers*. ACS Applied Materials & Interfaces, 2009. **1**(6): p. 1150-1153.
98. Yin, Y., et al., *Structure stability and corrosion inhibition of super-hydrophobic film on aluminum in seawater*. Applied Surface Science, 2008. **255**(5, Part 2): p. 2978-2984.
99. Hasnah Mohd Zaid, N.Y., Majid Niaz Akhtar, Ahmad Badruzzaman Ahmad Sallehim, *Synthesis and Characterizations of ZnO Nanoparticles for Application in Electromagnetic Detectors*. Journal of Nano Research, 2011. **13**: p. 93-98.
100. Chakradhar, R.P.S., et al., *Fabrication of superhydrophobic surfaces based on ZnO–PDMS nanocomposite coatings and study of its wetting behaviour*. Applied Surface Science, 2011. **257**(20): p. 8569-8575.
101. Qingping Ke, W.F., Huile Jin, Lei Zhang, Tiandi Tang, Jingfeng Zhang, *Fabrication of mechanically robust superhydrophobic surfaces based on silica micro-nanoparticles and polydimethylsiloxane*. Surface & Coatings Technology, 2011(205): p. 4910-4914.
102. Roe, B. and X. Zhang, *Durable hydrophobic textile fabric finishing using silica nanoparticles and mixed silanes*. Textile Research Journal, 2009. **79**(12): p. 1115-1122.
103. Yokogawa, H. and M. Yokoyama, *Hydrophobic silica aerogels*. Journal of Non-Crystalline Solids, 1995. **186**(0): p. 23-29.
104. Hikita, M., et al., *Super-Liquid-Repellent Surfaces Prepared by Colloidal Silica Nanoparticles Covered with Fluoroalkyl Groups*. Langmuir, 2005. **21**(16): p. 7299-7302.
105. Ebert, D. and B. Bhushan, *Transparent, Superhydrophobic, and Wear-Resistant Coatings on Glass and Polymer Substrates Using SiO₂, ZnO, and ITO Nanoparticles*. Langmuir, 2012. **28**(31): p. 11391-11399.
106. Douce, J., et al., *Effect of filler size and surface condition of nano-sized silica particles in polysiloxane coatings*. Thin Solid Films, 2004. **466**(1–2): p. 114-122.
107. Zhou, S. and L. Wu, *Development of Nanotechnology-Based Organic Coatings. Composite Interfaces*, 2009. **16**(4-6): p. 281-292.

108. Zhang, F., et al., *Fabrication of oriented layered double hydroxide films by spin coating and their use in corrosion protection*. Chemical Engineering Journal, 2008. **141**(1–3): p. 362–367.
109. Ishizaki, T., et al., *Corrosion resistance and chemical stability of super-hydrophobic film deposited on magnesium alloy AZ31 by microwave plasma-enhanced chemical vapor deposition*. Electrochimica Acta, 2010. **55**(23): p. 7094–7101.
110. Sanjay S Latthe, H.H.a.A.V.R., *TEOS based water repellent silica films obtained by a co-precursor sol–gel method*. Smart Materials and Structures, 2009. **18**: p. 095017.
111. Walid A. Daoud, J.H.X.a.X.T., *Superhydrophobic Silica Nanocomposite Coating by a Low-Temperature Process*. Journal of American Ceramic Society, 2004. **87** (9): p. 1782–1784.
112. Xu Huang, X.F., Zhen Lu and Su Chen, *Reinforcement of polysiloxane with superhydrophobic nanosilica*. Journal of Material Science, 2009. **44**: p. 4522–4530.
113. Rao, N.D.H.a.A.V., *Organic modification of TEOS based silica aerogels using hexadecyltrimethoxysilane as a hydrophobic reagent*. Applied Surface Science 2006. **253**: p. 1566–1572.
114. M. Messaoud , M.H., S. Briche , F. Roussel and M. Langlet, *Hydrophobic functionalization of cotton-based textile fabrics through a non-fluorinated sol–gel route*. Journal of Sol-gel Science and Technology, 2010. **55**: p. 243–254.
115. Gashti, M.P., F. Alimohammadi, and A. Shamei, *Preparation of water-repellent cellulose fibers using a polycarboxylic acid/hydrophobic silica nanocomposite coating*. Surface and Coatings Technology, 2012. **206**(14): p. 3208–3215.
116. Venkateswara Rao, A. and R.R. Kalesh, *Comparative studies of the physical and hydrophobic properties of TEOS based silica aerogels using different co-precursors*. Science and Technology of Advanced Materials, 2003. **4**(6): p. 509–515.
117. Jung, B.B.a.Y.C., *Wetting study of patterned surfaces for superhydrophobicity*. Journal of utramicroscopy, 2007. **107** p. 1033–1042.
118. Zhe Cui , L.Y., Qingjun Wang, Jianfu Ding and Qingmin Chen *A facile dip-coating process for preparing highly durable superhydrophobic surface with multi-scale structures on paint films*. Journal of Colloid and Interface Science, 2009. **337**: p. 531–537.
119. Lakshmi, R.V., T. Bharathidasan, and B.J. Basu, *Superhydrophobic sol–gel nanocomposite coatings with enhanced hardness*. Applied Surface Science, 2011. **257**(24): p. 10421–10426.
120. Ballarre, J., et al., *Mechanical characterization of nano-reinforced silica based sol–gel hybrid coatings on AISI 316L stainless steel using nanoindentation techniques*. Surface and Coatings Technology, 2009. **203**(20–21): p. 3325–3331.
121. Ma, X.-k., et al., *Surface modification and characterization of highly dispersed silica nanoparticles by a cationic surfactant*. Colloids and Surfaces A: Physicochemical and Engineering Aspects, 2010. **358**(1–3): p. 172–176.
122. K. Jeevajoithi , D.C.a.R.S., *Non-fluorinated, room temperature curable hydrophobic coatings by sol–gel process*. Journal of Ceramics International 2012. **38**: p. 2971–2976.
123. Sarkar, M.K., et al., *Design of an outstanding super-hydrophobic surface by electro-spinning*. Applied Surface Science, 2011. **257**(15): p. 7003–7009.
124. Tolnai, G., et al., *Preparation and Characterization of Surface-Modified Silica-Nanoparticles*. Langmuir, 2001. **17**(9): p. 2683–2687.
125. C.T. Hsieh, J.M.C., R.R. Kuo, T.S. Lin, C.F. Wu, *journal of applied surface science*, 2005. **240**: p. 318–326.

126. Lakshmi, R.V. and B.J. Basu, *Fabrication of superhydrophobic sol–gel composite films using hydrophobically modified colloidal zinc hydroxide*. Journal of Colloid and Interface Science, 2009. **339**(2): p. 454-460.
127. M. Messaoud , M.H.S.B., F. Roussel and M. Langlet, *Hydrophobic functionalization of cotton-based textile fabrics through a non-fluorinated sol–gel route*. Journal of Sol-Gel Science and Technology 2010. **55**: p. 243-254.
128. Barthel, H., *Surface interactions of dimethylsiloxy group-modified fumed silica*. Colloids and Surfaces A: Physicochemical and Engineering Aspects, 1995. **101**(2–3): p. 217-226.
129. Jacek Grzegorz Chełmanowski, B.S., *Effect of nanosilica type on protective properties of composite ceramic coatings deposited on steel 316L by sol–gel technique*. Journal of Non-Crystalline Solids, 2008. **354**: p. 1786-1795.
130. Fu, X. and X. He, *Fabrication of super-hydrophobic surfaces on aluminum alloy substrates*. Applied Surface Science, 2008. **255**(5, Part 1): p. 1776-1781.
131. Shen, B.Q.a.Z., *Fabrication of Superhydrophobic Surfaces by Dislocation-Selective Chemical Etching on Aluminum, Copper, and Zinc Substrates*. Langmuir 2005. **21**: p. 9007-9009.
132. S. Kamps, et al., *Processes and structures for generation of hydrophobic surfaces for large-scale and industrial operations*. Journal of applied surface science, 2009. **256**(3): p. S92-S95.
133. Daniele C.Bastos, A.E.F.S., MonicaL.V.J.daSilva and RenataA.Simao, *Hydrophobic corn starch thermoplasticfilms produced by plasmatreatment* journal of ultramicroscopy.
134. Shih-Hsien Yang , C.-H.L., Chun-Hsien Su and Hui Chen, *Atmospheric-pressure plasma deposition of SiO_x films for super-hydrophobic application*. Journal of thin solid films, 2009. **517** p. 5284-5287.
135. Rosa Taurino , E.F., Massimo Messori , Francesco Pilati , Doris Pospiech and Alla Synytska, *Facile preparation of superhydrophobic coatings by sol–gel processes*. Journal of Colloid and Interface Science Contents lists, 2008. **325**: p. 149-156.
136. Michael Thieme, R.F., Sylvia Schmidt, Frank Simon, Anja Hennig,Hartmut Worch, Klaus Lunkwitz, and Dieter Scharnweber, *Generation of Ultrahydrophobic Properties of Aluminium - A first Step to Self-cleaning Transparently Coated Metal Surfaces*. Journal of Advanced Engineering Materials 2001. **2**: p. 9.
137. Latthe, S., et al., *Ultrahydrophobic silica films by sol–gel process*. Journal of Porous Materials, 2010. **17**(5): p. 565-571.
138. Metroke, T.L., O. Kachurina, and E.T. Knobbe, *Spectroscopic and corrosion resistance characterization of GLYMO–TEOS Ormosil coatings for aluminum alloy corrosion inhibition*. Progress in Organic Coatings, 2002. **44**(4): p. 295-305.
139. Lu, S., et al., *Controlled growth of superhydrophobic films by sol–gel method on aluminum substrate*. Applied Surface Science, 2010. **256**(20): p. 6072-6075.
140. Liu, T., et al., *Corrosion behavior of super-hydrophobic surface on copper in seawater*. Electrochimica Acta, 2007. **52**(28): p. 8003-8007.
141. Wang, P., et al., *Super-hydrophobic film prepared on zinc as corrosion barrier*. Corrosion Science, 2011. **53**(6): p. 2080-2086.
142. Pirhady Tavandashti, N., S. Sanjabi, and T. Shahrabi, *Corrosion protection evaluation of silica/epoxy hybrid nanocomposite coatings to AA2024*. Progress in Organic Coatings, 2009. **65**(2): p. 182-186.

143. Zhang, S.Y., et al., *Mechanism of the significant improvement in corrosion protection by lowering water sorption of the coating*. Corrosion Science, 2000. **42**(12): p. 2037-2041.
144. Qinwen Gao, Q.Z., and Yuliang Guo, *Formation of Highly Hydrophobic Surfaces on Cotton and Polyester Fabrics Using Silica Sol Nanoparticles and Nonfluorinated Alkylsilane*. Journal of Industrial Engineering and chemical research 2009. **48**: p. 9797-9803.